Stability and Applications of Model Membranes

by

Alex Ashenden

Thesis
Submitted to Flinders University
for the degree of

Doctor of Philosophy

College of Science and Engineering

4 November 2022

Overview

Whilst biological membranes act as a barrier between the inside and outside cell environment ubiquitously across all organisms, there is a high degree of architectural complexity inherent in the structure. This makes systematic studies in areas such as protein functionality and antibiotic efficacy difficult to perform. Various model systems have been developed to mimic biological membranes using only essential components.

This thesis focuses on one specific type of model system, tethered-bilayer lipid membranes. In a tethered-bilayer lipid membrane a solid supporting structure is used as a base to which anchoring tether lipids bind to form a monolayer, with additional lipids added to complete the bilayer. Spacer lipids are also utilised to bind to the substrate at different ratios to increase bilayer fluidity and sub-membrane hydration. As a planar surface-based model a variety of techniques can be used to analyse these systems such as electrochemical impedance spectroscopy and neutron scattering, which will be the techniques showcased through this thesis.

This thesis is split into three distinct parts. Chapter 1 acts as an introduction to biological membrane systems and the various models that have been utilised to mimic their structure and capabilities, as well as discussing the various pros and cons of each system in order to explain why tBLMs have been utilised for the work showcased in this thesis. This is followed by chapter 2, a discussion of the methods utilised through the thesis.

The second part of the thesis, chapter 3, focuses on improving the understanding of how the functionality of tBLMs is affected by removal from the aqueous solution they are usually situated in. This is important as a case study for determining the feasibility of these model systems in future biosensor devices where they may be subject to such dehydration, as well as to determine their capacity for transport. Hence, studies were undertaken to determine the quality of tBLMs before and after being dried out and rehydrated at different levels of tethering density. Additionally, the improvement of this rehydration process was investigated using polyelectrolytes to coat the bilayers before dehydration. Finally, complexity of the bilayers was increased through addition of cholesterol, ubiquitous across mammalian cell membranes, to the outer leaflet of the bilayer before the dehydration process to determine if behaviour was similar with a more realistic membrane model.

The final part of this thesis, chapter 4, focuses on the biomedical applications of tBLMs designed to replicate bacterial membranes. Firstly, the use of tBLMs mimicking gram-negative bacteria as a screening tool to improve the efficacy of colistin, a last line antibiotic, is discussed. Colistin's damaging of the bacterial membrane was shown to be improved when functionalised gold nanoparticles were introduced to the bilayer initially, before addition of colistin afterwards. Secondly, the formation of novel tBLMs from bacterial lipid extracts is discussed. Lipids were extracted directly from *A. baumannii* cultures and used to form tBLMs with and without the inclusion of DHA, to help determine that membrane potential loss is not a likely antimicrobial mechanism of DHA.

Contents

Overview ii
List of Abbreviations vi
Acknowledgements viii
Declaration x
Chapter 1 - Model Membranes 1
1.1 Biological Membranes 1
1.2 Model Membrane Systems 6
1.3 Patch-clamp Membranes 7
1.4 Black Lipid Membranes 9
1.5 Vesicles and Liposomes 13
1.6 Solid-supported Lipid Bilayers 16
1.7 Polymer-supported Lipid Bilayers 21
1.8 Tethered-Bilayer Lipid Membranes 26
Chapter 2 - Methods 34
2.1 Electrochemical Impedance Spectroscopy 34
2.1.1 Methods for Fitting and Interpreting EIS Data 39
2.2 Neutron Reflectometry 41
2.2.1 Methods for Fitting and Interpretation of Neutron Reflectometry Data 45
2.3 Protocols for Experimental Methods 47
2.3.1 Electrochemical Impedance Spectroscopy 49
2.3.2 Neutron Scattering 51
Chapter 3 - Air Stability of Tethered-Bilayer Lipid Membranes 52
3.1 Introduction 52
3.2 Methods 62
3.2.1 Standard EIS Methods 62
3.2.2 Neutron Reflectometry Methods 63
3.2.3 Polyelectrolyte Methods 63
3.2.4 Cholesterol Incorporation Methods 64
3.3 Effect of Dehydration and Rehydration on DPhyPC Lipid Bilayers 65
3.3.1 100%-Tethered Lipid Bilayers 66
3.3.2 80%-Tethered Lipid Bilayers 72
3.3.3 60%-Tethered Lipid Bilayers 79
3.3.4 40%-Tethered Lipid Bilayers 83
3.3.5 10%-Tethered Lipid Bilayers 88
3.3.6 Neutron Reflectometry of DPhyPC tBLMs 89
3.4 Effect of Polyelectrolyte on Dehydration and Rehydration on DPhyPC Lipid Bilayers 96
3.4.1 80%-Tethered Lipid Bilayers with Polyelectrolyte 98
3.4.2 60%-Tethered Lipid Bilayers with Polyelectrolyte 108

3.4.3 40%-Tethered Lipid Bilayers with Polyelectrolyte 115
3.5 Effect of Cholesterol on Dehydration and Rehydration on DPhyPC Lipid Bilayers ... 123
3.5.1 80%-Tethered Lipid Bilayers with 10% Cholesterol in DPhyPC Outer Layer 124
3.5.2 60%-Tethered Lipid Bilayers with 10% Cholesterol in DPhyPC Outer Layer 131
3.6 Summary 139
Chapter 4 - Biomedical Applications of tethered-Bilayer Lipid Membranes 140
4.1 The Use of Cationic Gold Nanoparticles in Gram-Negative Bacterial Membrane Models 141
4.1.1 Introduction 141
4.1.2 Materials and Methods 147
4.1.2.1 Chemicals 147
4.1.2.2 Cationic Gold Nanoparticle Synthesis 147
4.1.2.3 Bilayer Formation 148
4.1.2.4 Electrochemical Impedance Spectroscopy 149
4.1.2.5 Neutron Scattering 149
4.1.3 Results and Discussion 150
4.1.3.1 Addition of Gold Nanoparticles to the Membrane 150
4.1.3.2 Simultaneous Addition of Colistin and Gold Nanoparticles 152
4.1.3.3 Pre-treating with Gold Nanoparticles before Colistin Addition 155
4.1.4 Conclusions 160
4.2 Analysis of the Effects of DHA Incorporation on Model *A. baumannii* Membranes 161
4.2.1 Introduction 161
4.2.2 Chemicals 165
4.2.3 Materials and Methods 165
4.2.4 Results and Discussion 167
4.2.5 Conclusion 174
Chapter 5 - Conclusions and Future Directions 175
Reference List 180
Appendix 192

List of Abbreviations

AC – Alternating current

AFM – Atomic force microscopy

AuNP – Gold nanoparticle

BLM – Black lipid membrane

CM – Contrast match

CPE – Constant phase element

DC – Direct current

DHA – Docosahexanoic acid

DNA – Deoxyribonucleic acid

DPhyPC – 1,2- di-O-phytanoyl-sn-glycero-3-phosphocholine

DPhyTL – 2,3-di-O-phytanyl-sn-glycerin-1-tetraethylenglycollipoic acid ester

EIS – Electrochemical impedance spectroscopy

GC-MS – Gas chromatography mass spectroscopy

GUV – Giant unilamellar vesicle

HC – Hydrocarbon chain

HG – Head group

LB – Lysogeny broth

LPS – Lipopolysaccharides

LUV – Large unilamellar vesicle

MCMC – Markov chain Monte Carlo

MLV – Multilamellar vesicle

MUV – Medium unilamellar vesicle

MVV – Multivesicular vesicle

NR – Neutron reflectometry

OLV – Oligolamellar vesicle

PBS – Phosphate buffered saline

PDADMAC – Polydiallyldimethylammonium chloride

PEG – Polyethylene glycol

POPC – 1-palmitoyl-2-oleyl-sn-glycero-3-phsophocholine

PSS – Polystyrene-4-sulfonate

PUFA – Polyunsaturated fatty acid

QCM – Quartz crystal microbalance

RC – Resistive-capacitive

Rc-LPS – Rc-strain lipopolysaccharides

RND – Resistance-nodulation division

RSE – Rapid solvent exchange

SLB – Solid-supported lipid bilayer

SLD – Scattering length density

SUV – Small unilamellar vesicle

tBLM – Tethered bilayer lipid membrane

ULV – Unilamellar vesicle

UV – Ultra-violet

Acknowledgements

I would like to acknowledge several people who have been central to the completion of my PhD thesis, both in terms of its contents and the fact that I was able to complete it at all throughout the many unexpected twists and turns the world has taken over the last few years.

Firstly, to my primary supervisor Associate Professor Ingo Koeper, I would offer a great deal of thanks for providing me with a clear head and calm presence to help navigate through the many ups and downs of the project, providing advice where needed but also allowing for this to very much be my own project as well.

I would also like to thank my co-supervisor Dr Jason Gascooke and others at the ANFF facilities for providing me with support throughout my PhD, especially with regards to clean room access and sputter coating instrumentation teaching.

To Dr Jakob Andersson, I extend a great deal of thanks for support and assistance with learning how to make the bilayers used throughout this project, and teaching with regards to use of EIS and neutron reflectometry instrumentation.

To Dr Stephen Holt, I am deeply thankful not only for your support with learning how to use the neutron reflectometry instrumentation at ANSTO and coordinating experiments there with myself and others from the Koeper group, but also for stepping in and performing experiments with our samples where the coronavirus pandemic stopped us from always being able to attend in person. To Andrew Nelson of ANSTO as well for providing the Motofit software used for neutron data analysis and the technical support he has provided alongside that.

To Dr Shinji Kihara, Ashley Carey and Brodie Parrott, I am thankful to have been able to work alongside you in both teaching and learning capacities, as well as in friendship too. Thanks also to others who have been a part of the Koeper group and our wider multi-disciplinary Supergroup and Membrane group for providing a wonderful platform for inclusivity and learning from each other throughout my time at Flinders University.

To the Australian Government, I would like to mention my appreciation for the Research Training Scholarship that has allowed me to focus on my research throughout its tenure.

And finally, I would like to thank my family and friends who have provided me with encouragement and support where needed. To my parents, for providing me with a stable base from which to focus on myself and my work throughout the early period of my PhD. To Simon, Nick, Kaili and others who have provided an escape to clear my head when the going got tough. And most of all to my partner who has provided me with everything else I needed to get through the last few years, including no shortage of motivation and a positive attitude to allow me to believe in myself and my accomplishments.

Declaration

I certify that this thesis does not incorporate without acknowledgement any material previously submitted for a degree or diploma in any university; and to the best of my knowledge and belief, does not contain any material previously published or written by another person except where due reference is made in the text.

Alex Ashenden, 4 November 2022

Chapter 1 - Model Membranes

Parts of this chapter have been published as a part of:

Model architectures for bacterial membranes, Ashley B. Carey, Alex Ashenden, Ingo Koper, Biophysical Reviews 2022

1.1 Biological Membranes

All organisms rely on the presence of biological membranes that act as selectively permeable barriers. Membranes separate the intra- and extra-cellular environments of the cell whilst facilitating movement of ions and molecules in and out. They are involved in many vital processes such as cell-cell signalling and energy generation through ion gradients. The functionality of cell membranes is dictated by the types of lipids and other molecules such as carbohydrates and proteins that make up the membrane structure.[1, 2]

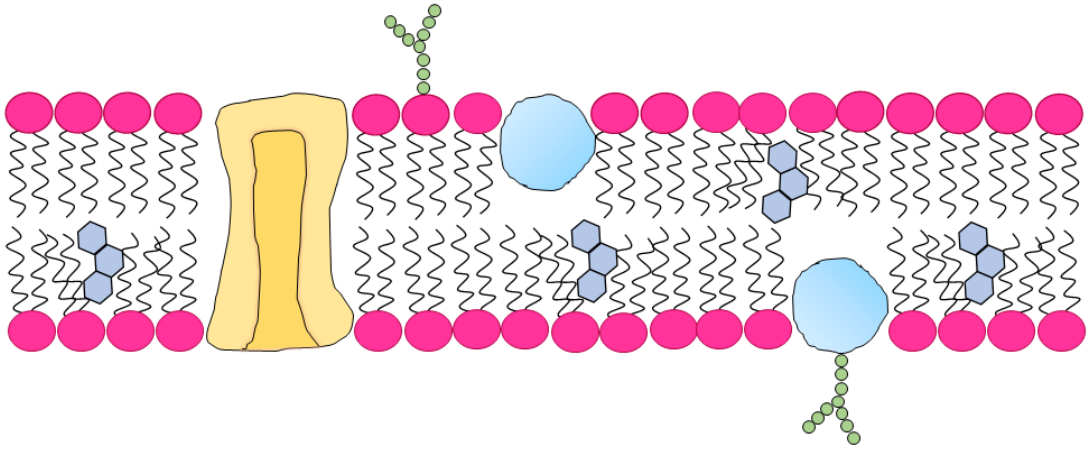

Figure 1-1: Schematic depicting the lipid bilayer of a cell membrane with phospholipids interspersed by cholesterol, proteins, glycolipids, and carbohydrates.

The primary structure of eukaryotic membranes consists of an amphiphilic lipid bilayer interspersed with other molecules (figure 1-1). The two lipid layers of the bilayer are often referred to as the inner and outer leaflet. Asymmetry across the two halves of

the lipid bilayer is important for many aspects of cell functionality, with certain proteins and lipids only present in one leaflet, or more often in one leaflet than the other.[3]

The lipids that make up the backbone of the bilayer are not rigid. According to the fluid mosaic model of the membrane initially proposed by Singer and Nicholson, individual lipids that make up a bilayer move around constantly to create a highly dynamic structure.[4] In eukaryotic cells, enzyme proteins bound to the endoplasmic reticulum synthesise lipids inside the cell that are then transferred to its bilayer. Flippase enzyme proteins inside the bilayer are then able to provide the necessary energy for some lipids to 'flip-flop' and move from the bilayer's inner leaflet to its outer leaflet. Selectivity of flippases can result in different types of lipids in each leaflet.[5]

Phospholipids are the most common form of lipid found in cell bilayers. These lipids have a hydrophilic charged head group with long hydrophobic hydrocarbon tails (figure 1-2). The primary driving forces of bilayer formation are the entropic interactions between the hydrocarbon tails and water. When hydrocarbons are present in an aqueous solution, water must re-arrange itself around the hydrocarbons to maintain hydrogen bonding. This entropically disfavoured state can be reversed by the tight packing of hydrocarbons into a bilayer. This nonpolar substance aggregation is known as the hydrophobic effect.[6, 7]

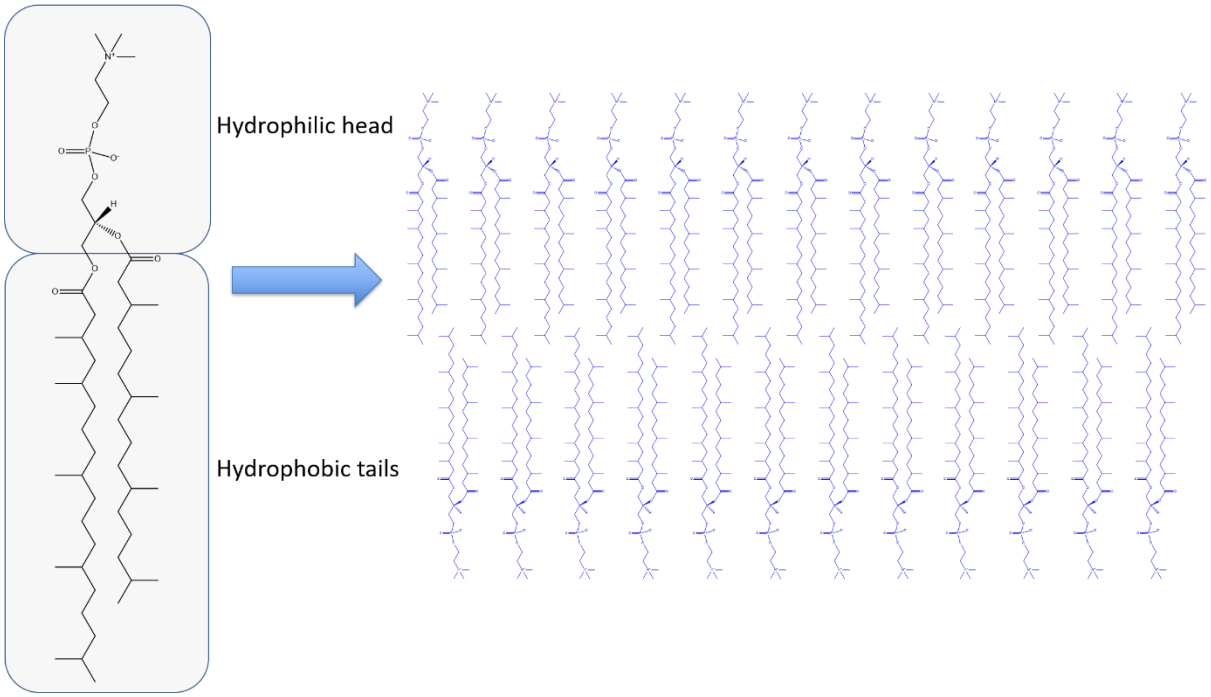

Figure 1-2: Structural depiction of DPhyPC as an example of an amphiphilic lipid. Hydrophobic carbon chains make up the inside of the lipid bilayer whilst hydrophilic charged head groups make up the outer parts of each leaflet.

Unlike eukaryotic membranes, prokaryotic membranes often contain a more complicated barrier called a cell envelope. In Gram-negative bacteria the cell envelope contains a peptidoglycan cell wall and periplasmic space between two different lipid bilayers – the outer membrane and the cytoplasmic membrane. Gram-positive bacteria meanwhile do not have an outer membrane. Despite these differences with eukaryotic cells, bacterial cytoplasmic membranes are otherwise structurally very similar, with phospholipids making up the majority of lipid components.[8] The main point of difference occurs in the outer membrane of Gram-negative bacteria in which lipopolysaccharides consisting of lipid A, polysaccharides and O antigen help to make up the outer leaflet.[9]

Much of the functionality of cell membranes is enabled by the embedding of proteins in the lipid bilayer. These proteins can open pathways that allow for selective ion transport, cell-cell communication, and stimuli response systems. Embedded proteins

can be peripheral or integral, with peripheral proteins binding indirectly with the bilayer surface by interacting with the polar phospholipid head groups or with other integrated proteins. Integral proteins embed directly into the bilayer through interactions with the long carbon chains in the tails of the phospholipids. Most integral proteins extend the entire width of the bilayer across both leaflets. These are known as transmembrane proteins.[1, 10]

The fluid structure of the lipid bilayer provides an ideal environment for protein functionality. Lipid-protein interactions can result in the formation of annular lipid shells - lipids that bind to the surface of membrane proteins. This can have a lubricating effect on the proteins within the bilayer, giving them the freedom to rotate and diffuse much more freely within the bilayer.[11]

Some molecules can naturally diffuse across membrane bilayers. Small, hydrophobic molecules are most readily able to diffuse across the membrane without assistance as they do not greatly alter the packing density of the lipids and are not repulsed by the hydrophobic hydrocarbon tails making up a majority of the membrane structure. However, most other atoms and molecules require some form of assistance due to selective permeability of the membrane. Charge, size and other properties all play a role in successful diffusion across the bilayer.[5]

Integral transmembrane proteins that facilitate such movement are referred to as transport proteins (figure 1-3). These proteins engage in passive and active transportation through formation of electrochemical gradients.[1, 12]

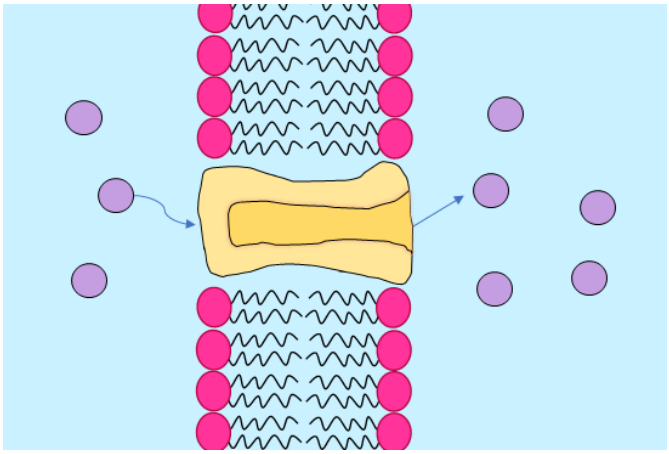

Figure 1-3: Depiction of ion transport through a membrane-spanning channel protein. The individual charged ions (purple) can cross the bilayer through the charged ion channel which counteracts the hydrophobic behaviour of the uncharged carbon tails that make up the middle of the lipid bilayer.

Passive transport involves the movement of charged species through a protein channel from a region of high concentration of that species to a region of lower concentration. Such channels are hydrophilic to counteract the hydrophobic nature of the inner structure of the bilayer. Channel selectivity, which limits the types of ions that can be transported, comes from their size and shape as well as the charge of the amino acids lining the channel wall.

Active transport provides a mechanism for charged species to move against the electrochemical gradient from a region of low concentration to high concentration. This requires an input of energy. Most commonly energy is derived from adenotriphosphate hydrolysis. Another source of energy for this process is secondary active transport where passive movement of one species provides the free energy necessary for the active moment of another species.[1, 12, 13]

1.2 Model Membrane Systems

As described above, biological membrane bilayers have a high degree of architectural complexity. This makes it difficult to assess properties associated with specific aspects of their structure, such as the functionality of specific ion channels or embedded proteins. A variety of different model systems have been designed to mimic the structure and functionality of these bilayers in a controlled environment using only the most essential components.[14, 15]

It is possible to create model systems from a top-down approach by modifying existing cell membranes through genetic engineering methods. Whilst this is highly analogous to the use of true cell membranes it does little to solve the issue of over-complexity.[16, 17] This is because even though such techniques might provide more control over a membrane's structure, there are still too many different components present to be able to analyse each one individually without the potential for other components to interfere. Isolating the effects of singular proteins in particular can be difficult to achieve through a top-down approach.[18]

Model techniques that utilise a bottom-up design approach involve formation of a bilayer system from individual building blocks. This results in a simplified system that can be altered depending on the specific requirements of a given investigation. The makeup of the bilayer and any incorporated molecules are both key aspects of the system that can be varied.[19, 20] The mechanical properties and structural organisation of such bilayers are also highly tuneable.[21, 22] Most model systems utilise electrochemical techniques to study lipid bilayer properties, with different signals

depending on the bilayer stability able to showcase changes in structure and permeability.[23, 24]

Model systems designed to mimic cell membranes will be discussed in the following sections. These include patch-clamp membranes, black lipid membranes, free-standing systems such as vesicles and liposomes, and solid-supported systems including polymer-supported and tethered-bilayer lipid membranes.

1.3 Patch-clamp Membranes

One of the earliest developed electrophysiological methods of cell membrane analysis is the patch clamping technique, first reported by Neher and Sakmann.[25] An electrical signal is isolated through a small patch of membrane tissue connected to the opening of a pipette tip. The tip is filled with an electrolyte solution, as well as an electrode. A grounding reference electrode is also used in a bath surrounding the cell tissue. By creating what was in effect a continuous electric circuit, this was one of the first techniques to allow for determination of the isolated current flow through a singular membrane ion channel embedded in a membrane patch.[25, 26]

The use of micrometre-wide pipette tips allows for the analysis of micro-sized patches of membrane tissue, likely to contain only a couple of different ion channels. Channels can be studied under different ionic conditions by changing ions present in the bath and electrolyte solutions. Membrane tissue is partially drawn into the tip and forms a seal with resistances of up to 100 giga ohms. This level of resistance allows for high resolution measurements of current flow across the membrane tissue.[27]

The patch clamp technique allows for analysis using a multitude of different setups including cell-attached, whole cell, inside-out and outside-out. These techniques vary based on whether pulling or suction of the pipette occurs after bringing the pipette into contact with the membrane surface (figure 1-4).

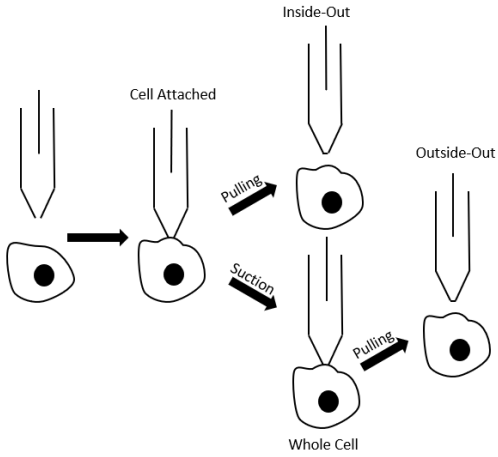

Figure 1-4: Schematic of the different ways that patch-clamp membranes can be attached to the pipette. Once the cell is attached to the pipette pulling, suction or a combination of the two can be applied to provide different methods of analysis.

In the cell-attached method the pipette attaches to the surface of an intact cell patch and utilises compounds in electrolyte solution that directly react with the surface of the patch. This method allows for accurate concentration-response analysis and is often used to study ligand-gated ion channels.[28, 29] The whole cell method involves the application of suction to rupture the cell membrane. A voltage clamp is then used to perform simultaneous measurement of multiple ion channels. This method increases electrical access to the inside of the cell however it quickly contaminates the cell with the electrolyte solution so can only be performed for short periods.[28]

The inside-out method involves pulling the pipette from the cell after forming a seal, ripping out the attached membrane patch. This technique is used for analysis of intracellular ligand components of ion channels. Finally, in the outside-out method the

pipette is pulled from the surface after applying the whole cell method.[28, 30] Antibiotics have also been used to perforate sealed membrane patches to allow analysis of small ions with greater stability than other patch setups.[31] The effects temperature and mechanical stress have on channel proteins has also been investigated.[32-34]

Whilst patch clamping of membranes is an incredibly useful and versatile technique there are many drawbacks as well. Membranes must be fully exposed for it to be utilised which can cause them to become unstable. Because of the lack of stabilisation, patch clamping experiments can only be performed over periods of hours at most, and so such systems are not conducive to long-term experiments. It is also a highly labour-intensive process that can be complex to perform.[27] Automated systems have been developed to counteract this issue, however they decrease the quality control as well. Thus, cell samples used for automated experiments must be of exceptional quality and uniformity. For these reasons automated techniques are of limited use for most research purposes.[28, 35]

1.4 Black Lipid Membranes

Black lipid membranes were the first true bottom-up models of cell bilayers created. Initially developed by Mueller et al., these membranes are made up of a free-standing lipid bilayer suspended in the aperture of a hydrophobic material acting as a supporting substrate.[36, 37] The bilayer connects to the substrate, usually teflon, via a solvent annulus (figure 1-5), with two distinct chambers of aqueous solution on either side of the bilayer.[38] The name ‘black lipid’ membrane comes from the opacity caused by interference of reflected light by the bilayer making it appear black.[39] Electrical measurements can be performed on BLMs using electrodes to provide resistive and capacitive markers for bilayer quality.[37]

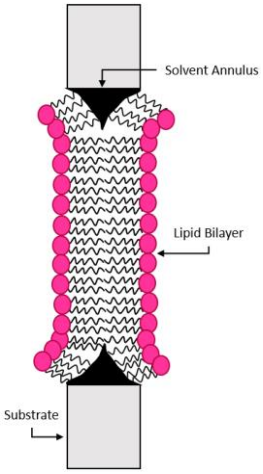

Figure 1-5: Structural design of a typical BLM. The lipid bilayer is formed in the gap between two substrates and held via a solvent annulus.

BLMs are most commonly formed using either the Montal-Mueller method or the manual painting method. In the Montal-Mueller method a bilayer is formed through lipid monolayers in two chambers combining at the substrate aperture by increasing the solution levels in each chamber from below to above the aperture opening.[40, 41] The manual painting method involves submerging the aperture in aqueous solution and wiping across it with a lipid mixture dissolved in organic solvent. The use of an organic solvent in an aqueous solution creates an interface at which a bilayer can form.[42]

The bilayer of a BLM is able to be formed with a thickness of only a few nanometres due to suction exerted by the Plateau-Gibbs border. The border is the edge of the gap where the membrane ends. The concave interface of the bilayer results in a decreased pressure at the border, with resulting suction causing membrane thinning. BLM formation can be mapped with second-harmonic generation imaging, a coherent optical technique in which two photons combine to emit a single photon. The bilayer produces no SHG signal whilst the annulus region produces a signal due to the presence of solvent between lipids.[43]

Electrical characterisation of BLM systems can provide important information about their structural quality. An electrode can be placed in each chamber with electrical measurements then performed to determine resistance and capacitance of the system. A high-quality BLM will have a similar capacitance to that of a biological membrane. Differences in capacitance can be due to bilayer rupture or a build-up of organic solvent residue pushing apart the lipid tails, particularly in the annulus region. Solvent build-up or trapping of solvent within the bilayer can be a major factor in BLM disruption.[37] This can be minimised by using volatile solvents such as chloroform that can paint the lipids whilst the substrate is out of solution. The substrate is then immersed once the solvent has evaporated.[41]

Incorporating ion channel proteins into BLMs can be difficult as it cannot be done during bilayer formation. Exposure to organic solvents used in the formation would result in protein denaturation. Micelle-coated proteins can be introduced after bilayer formation, however. Proteins will spontaneously insert themselves into the bilayer in a manner approximated by the Saffman-Delbrück model that describes the membrane as a thin layer of viscous fluid.[44, 45] Electrophysiological measurements can be performed on BLMs by applying a voltage across the membrane. The resulting current flow through the ion channel can then be detected with a current-voltage amplifier connected to an oscilloscope or computer.[39] BLMs make for excellent tools in the study of singular ion channels, however there is a more limited scope for other types of characterisation due to their vertical architecture meaning the use of surface techniques is not possible.[46]

Similar to patch-clamping experiments BLMs have very short lifespans, typically hours at most. This makes long-term studies difficult. Structural stability is primarily maintained by weak non-covalent interactions. Solid-supported systems can be used to improve stability of BLMs, however they tend to reduce BLM capacitive quality due to interactions between the bilayer and supports causing further defects.[39]

The lifespan of BLMs has been increased by creating well-defined and clean holes in the supporting substrate using wet-etching and a focused ion beam.[47] BLM lifespan has also been extended through chemical crosslinking of the lipids that make up the bilayer or by adding further mechanical supports such as gels.[48] BLMs have been successfully created, frozen and transported before use for ion channel measurements with no noticeable drop in membrane quality.[49] Progress has also been made to minimise human input required for this process, and to make the process more readily scalable.[50, 51]

Highly crosslinked hydrophilic polymers called hydrogels have been used to protect BLMs outside of an aqueous environment. Hydrogels do not dissolve in water so are able to be applied to membranes in aqueous solution before the dehydration process. Hydrogel encapsulated membranes have shown that stability of up to 10 times as long as typical planar bilayers is possible. Such membranes were still able to functionally incorporate proteins. Using poly(ethylene glycol) dimethacrylate monomers that were formed into a hydrogel through UV-initiated polymerisation to encapsulate a BLM, Jeon et. al. were able to measure the single ion channel currents of α-hemolysin for several days. They were also able to measure the delivery of DNA strands to the

channel protein with the only difference from non-hydrogel encapsulated membranes being a decrease in translocation speed caused by the presence of the gel.[52]

A major disadvantage of BLMs is the difficulty in creating them in a sufficiently reliable and flexible manner with conventional techniques. The Montal-Mueller method's requirements limit integration with many analytical techniques, whilst the manual painting method is difficult to execute consistently. Methods for automating BLM formation include PDMS extraction and application of hydrostatic pressure across a micro-aperture.[40, 53]

1.5 Vesicles and Liposomes

Similar to cell membranes, liposomal vesicles are spherical shells made up of lipid in a bilayer formation. The encapsulated solvent within their structure is separated from the solvent outside. Vesicles will spontaneously form in water due to energetic favourability.[54] The size of vesicles can vary dramatically from the nanometre to micrometre scale (figure 1-6). They can also be multi-layered or have other vesicles inside them. Techniques such as extrusion or sonication can be used to form vesicles as well as to control their size by breaking them down into smaller unilamellar structures.[55]

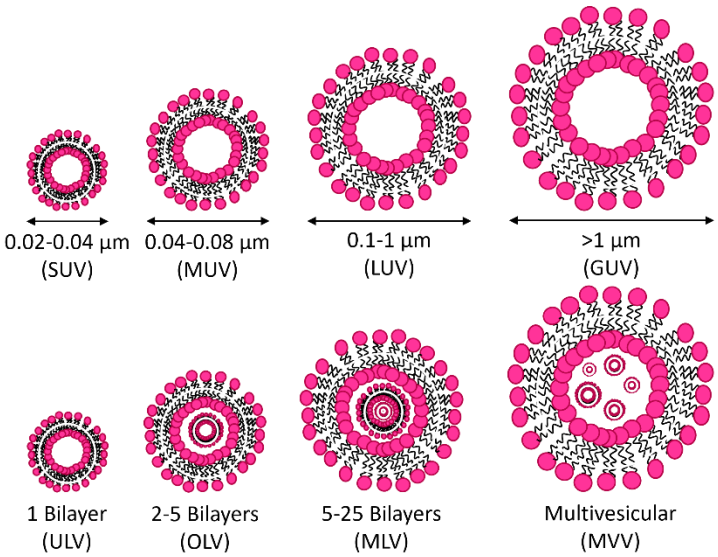

Figure 1-6: Vesicles and liposomes can come in a variety of sizes. Small unilamellar vesicles (SUVs) and medium unilamellar vesicles (MUVs) are vesicles under 100 nm in size, whilst giant unilamellar vesicles (GUVs) are typically more than 1 micrometre in size, with large unilamellar vesicles (LUVs) between the two. They can also have multiple layers to their structure with unilamellar (ULV), oligolamellar (OLV) and multilamellar (MLV) variations, as well as being multivesicular (MVV) where smaller vesicles are compartmentalised inside larger vesicles.

In the extrusion process a suspension of lipids is pushed through pores typically between 50 and 200 nm in size.[56] This process can be used to produce monodisperse vesicle solutions. Dispersity of the vesicles is dependent on factors such as number of extrusions and pore size.[57] The amount of pressure exerted on the lipids as they are pushed through the pores can also have an effect on the overall dispersity.[58]

Artificial vesicles can be produced in large quantities which makes them ideal for bulk material studies. It is also possible to use them for studies of the membrane damaging effects of peptides and other chemicals.[59] Small unilamellar vesicles (SUVs) also play an important role in the formation of other bottom-up membrane mimicking systems. Liposomal vesicles have also been explored as drug delivery candidates. Hydrophobic drugs could be carried into the middle of a phospholipid bilayer, whilst hydrophilic ones could be transported inside the vesicle core.[60]

SUVs have minimal intracellular space, causing concentrations of any transported components to build up quickly. This makes studies of steady-state mechanics difficult. In such situations giant unilamellar vesicles (GUVs) can be utilised. GUVs are on the micrometre scale in size and are much more readily able to be studied through techniques like fluorescence microscopy.[61, 62]

GUVs can be prepared through electroformation. This involves hydrating a lipid solution with a small amount of water before subjecting it to an electric field at constant temperature.[63] Electroformation can also be performed by first forming SUVs through extrusion or rapid solvent exchange.[61, 64] Rapid solvent exchange is the process of quickly changing from a non-polar solvent to water to force the formation of vesicles through the hydrophobicity of lipid tails. An alternative method of GUV formation is gentle hydration, whereby a lipid film is formed in a test tube and incubated under nitrogen in an aqueous salt sucrose solution.[65]

GUVs are a useful tool in the study of electroporation. Short high voltage electric pulses have been shown to increase the permeability of GUV bilayers without compromising their integrity.[66] However, in general GUVs are quite fragile. They are also time-consuming to produce and there is often difficulty in obtaining high yield as readily as SUVs.[67]

Whilst some types of vesicles can maintain stability in the right conditions for long periods, phospholipid vesicles are easily broken apart by surfactant-like materials and can also be disrupted through hydrolysis in aqueous solution. Whilst the degree of ease of hydrolysis varies from lipid to lipid, it can make long-term usage of

phospholipid vesicles difficult in aqueous solution.[67] Phospholipid vesicles are also highly sensitive to changes in temperature, ionic concentration and pH of the solution they are suspended in. Changing these parameters can affect the scope of vesicle lipid aggregation.[68]

The polydispersity of vesicles formed from lipids such as DPhyPC has been investigated and determined to have different aggregation behaviour depending on temperature of storage. The addition of cholesterol to DPhyPC vesicles has been shown to improve their stability and minimise increases in polydispersity over long periods of time. However, this improved resilience to changes in vesicle size variation required the keeping of vesicles at temperatures well below (4 °C) or above (50 °C) room temperature.[69]

1.6 Solid-supported Lipid Bilayers

Many more contemporary artificial membrane models utilise a solid substrate to stabilise bilayer formation and structure. Supported lipid bilayers, first described by Tamm and McConnell[70], are planar structures that sit directly on top of a supporting substrate (figure 1-7). One side of the lipid bilayer is continuously in close proximity to the supporting structure, with only a nanometre thick hydration layer separating them.[70] Direct substrate-substrate contact can cause issues with protein incorporation and flow of solution to both sides of the membrane. However, when compared to BLMs the stability of solid-supporting systems is far superior.[70, 71]

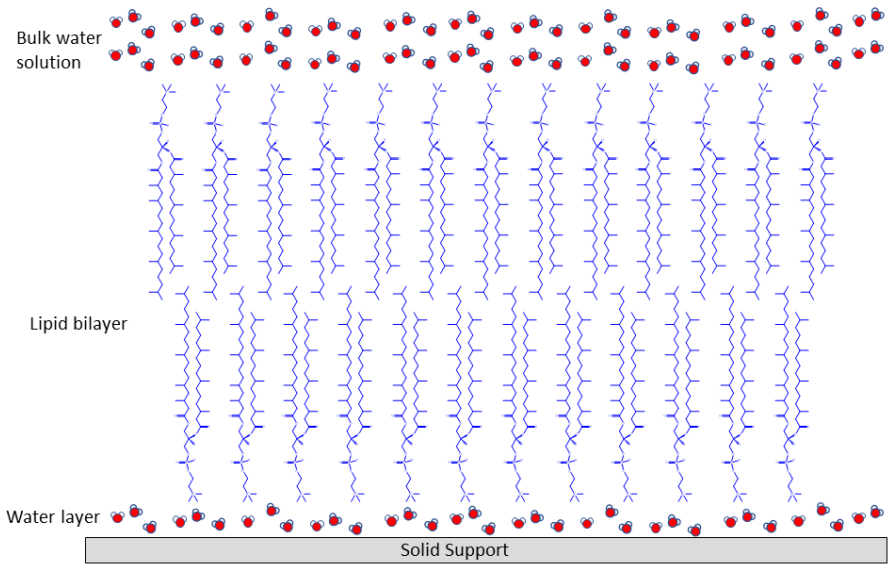

Figure 1-7: Example of solid-supported lipid bilayer structure formed from DPhyPC lipid. A small water layer exists between the bottom layer of lipids and the solid support whilst a bulk solution is situated above the top lipid layer.

SLBs provide greater scope for chemical manipulation and the use of surface techniques that is not possible with free floating bilayers. Techniques such as surface plasmon resonance and atomic force microscopy are well-adapted methods of surface analysis for planar systems in aqueous solution.[72-74] The kinetics of binding events at the bilayer surface can also be characterised using quartz crystal microbalance systems with resonant frequencies sensitive to nanogram-level changes in mass.[75] Bulk solvent on top of the bilayer can also be readily exchanged through flushing of the system the bilayer is situated within.[76]

SLB formation is most commonly achieved through deposition and rupturing of SUVs on a solid substrate surface via vesicle fusion (figure 1-8). Whether rupturing occurs is determined by a combination of intra-vesicle, inter-vesicle and vesicle-substrate interactions. These interactions are governed by a number of different aspects; surface charge, structure and roughness of the substrate, composition, charge osmotic pressure and size of the vesicle as well as the pH, ionic strength and temperature of the surrounding solution.[77, 78]

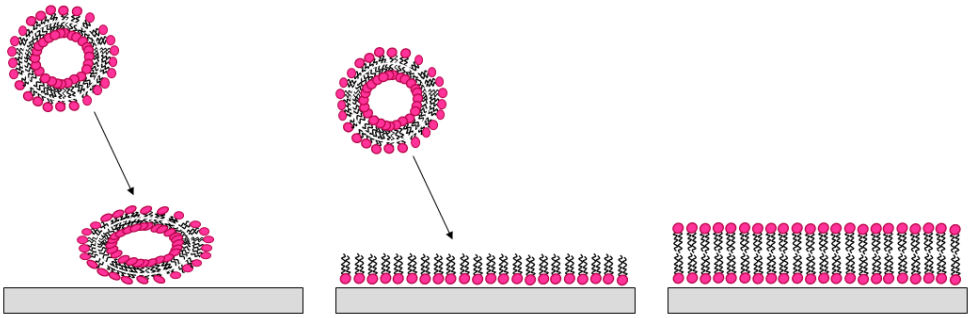

Figure 1-8: Steps in the formation of a SLB using vesicle formation. Initially vesicles rupture on the surface of a hydrophilic substrate to form a monolayer before the rupturing of further vesicles on top of the now-hydrophobic monolayer forms a bilayer.

QCM studies have shown that charge can have an especially strong effect. Rupturing of vesicles is much less likely to occur if the substrate surface and vesicles have the same charge.[79] Vesicles will also often fuse together to form larger ones before bilayer formation. In the case of neutrally charged surfaces, a critical concentration of vesicles is required on the surface of the substrate before rupture occurs.[77] The presence of ions such as calcium is also known to aid this process. This is due to their effects on the polarity and charge of lipids present in solution.[80]

SLBs can also be formed through Langmuir-Schaefer/Blodgett techniques. A hydrophilic solid surface acting as the substrate is dipped into solution containing lipids at the air-liquid interface. The substrate is then slowly lifted out of solution. Affinity of the lipids for the surface over the solution causes them to stick to the surface and form a monolayer. The process can be repeated to add a secondary layer of lipids to form a bilayer.[81] It is also possible to combine this technique with vesicle fusion by using it for formation of the monolayer before using vesicle fusion for the addition of the second layer.[71]

The type of substrate used depends on what SLB properties are required. Electrical or plasmon spectroscopy measurements require the substrate to be made of conductive material, whilst transparency and reflectivity can also be important factors.[76] Substrates are most commonly silicon and silicon dioxide based.[78] Other materials such as gold, quartz and titanium oxide are also often used. Each material has different parameters which need to be adhered to for vesicle fusion to successfully occur.[77] A balance of van der Waal attraction and hydration repulsion is important for the effective adsorption of vesicles. If the substrate is too hydrophilic then binding of surface hydroxide groups with water molecules becomes too strong and blocks adsorption.[78]

SLBs have been utilised to model and image protein adsorption, function and localisation on membrane surfaces.[82] In one study, phospholipase A_2 was shown through AFM imaging to form narrow channels through the membrane surface due to its hydrolysis of ester linkages in the phospholipid bilayers.[83] AFM imaging has also been used to visualise the introduction of proteins into the membrane, and the effect the presence of cholesterol in the bilayer has on binding and insertion rates.[84] Fluorescence spectroscopy has also been used to probe protein insertion mechanisms.[85, 86] Microfluidic systems have been created using arrays of SLBs that greatly increase efficiency, especially for biosensing applications.[87] Patterning of SLBs has been achieved through various printing processes including the use of UV illumination for membrane photolithography.[88, 89]

In SLBs the insertion of functional channels has been achieved for variety of proteins such as Na^+/K^+ ATPase[90, 91], Ca^+ ATPase[92], Na^+[93] and K^+ channel proteins.[42, 94]

Incorporation of channel proteins such as gramicidin D is verified through electrochemical impedance spectroscopy measurements. Successful incorporation results in large electrical resistance changes when the bilayer medium contains the cations relevant to the selectivity of the channel proteins.[94-96]

Many of the first SLBs formed were only able to maintain stability with no defects for periods of a few hours, however more recently SLBs have been formed that remained stable for over a week. For SLBs to maintain this high level of stability it was important to treat glass slides used as substrates carefully to maximise hydrophilicity and cleanliness.[97]

SLBs are not ideal systems for membrane protein analysis for several reasons. The minimal space between the bilayer and the substrate causes decreased membrane diffusion, undesirable substrate interaction and denaturation of incorporated channel proteins.[71, 98] Movement of proteins embedded within the membrane is also minimised due to the proximity of the substrate. This affects the inner leaflet of the bilayer considerably more than the outer leaflet. It also reduces the ability of the bilayer to self-heal any defects.[99] To solve some of these issues, systems that incorporated polymers, hydrogels and tethering lipids between the substrate and the bilayer have been developed.

Traditional SLBs are also unable to maintain their structure when exposed to an air-water interface. Delamination readily occurs due to the interface acting as an interfacial support ripping the bilayer away from its supporting substrate structure. Addition of biomolecules such as disaccharides and proteins on top of the bilayer have

been utilised to form protective layers over the top of lipid bilayers to minimise the effects of delamination. Holden et. al. were able to minimise bilayer delamination through the attachment of streptavidin to the SLB outer leaflet, whilst Chiantia et. al. were able to maintain a stable bilayer structure as viewed through AFM using sucrose or trehalose coatings.[100, 101] However, such solutions permanently alter the membrane species environment, and have the potential to cause steric hinderance to potential interactions between membranes and proteins or other introduced chemical species.[102]

Other methods that have been investigated include the use of physical confinement mechanisms to keep the bilayer in place without altering membrane properties or accessibility. This involved the addition of phospholipase A_2 to form a branching obstacle network within which bilayer segments would form and remain stabilised even after exposure to the air-water interface. Due to the uneven height of the created obstacles it was suggested that thin pockets of water were retained within the network that helped to facilitate bilayer stability.[102]

1.7 Polymer-supported Lipid Bilayers

The space between the lipid bilayer and solid substrate surface can be increased significantly through the introduction of a polymer cushion bonded to the substrate (figure 1-9). These cushions act similar to the protein-based cytoskeletons found in many cells that provide bilayer support.[103, 104] The use of a polymer spacer can minimise the negative effects of substrate proximity, and also allows greater mobility and activity of transmembrane proteins.[105-108] The films used for supporting bilayers are usually produced as polymer-lipid composites. Their properties must be carefully managed to balance system stability and membrane fluidity, as well as avoiding

polymer blistering.[109] If the binding adsorption of the bilayer to the polymer cushion is too weak then it may become detached.[99] Charged polyelectrolyte multilayers have been used to create a more porous substrate space for SLBs that allows for more effective analysis of lipophilic biomolecules.[110, 111]

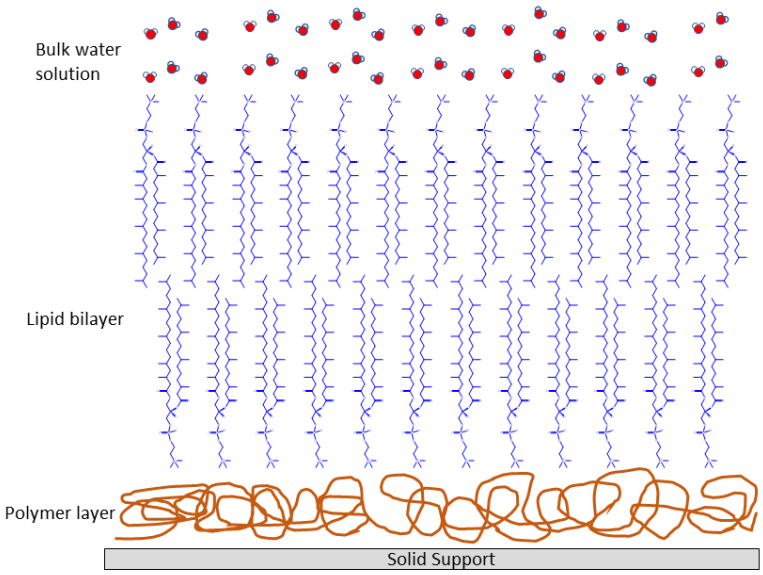

Figure 1-9: Example of solid-supported lipid bilayer structure using DPhyPC with a polymer supporting layer. This layer provides more of a cushion than the small water layer present in other SLBs.

There are several ways that polymer-supported bilayers can be formed through similar methods to SLBs. A solid substrate can be immersed in polymer solution before being dried and then exposed to a solution of vesicles. Adding polymer solution after exposure to vesicles has been found to produce similar results, as the polymer crawls through defects in the bilayer. The Langmuir-Blodgett technique combined with vesicle fusion has also been shown to provide reasonable bilayers by dipping the substrate into polymer solution before exposure to vesicles.[112]

An alternative approach to formation of polymer-SLBs involves covalent tethering between the substrate and polymer cushion, and also between the cushion and

bilayer. The former can be achieved through photobleaching, which forms crosslinks between polymers and a functionalised substrate. Langmuir-Blodgett/Schaeffer techniques are then used to transfer a lipopolymer-phospholipid mixture to form the bilayer.[99] Attachment can also be achieved between metal surfaces and lipopolymers through high-strength bonding between the substrate and sulphur groups on the polymer.[113, 114] Other methods of substrate-polymer bonding include epoxy and silane chemistry.[71]

Lipopolymers can act as anchors that bind substrate and polymer together. Their use allows for greater control of important parameters such as chain conformation within the cushion, cushion thickness, and the interaction strengths between each component. A decreased reliance on electrostatic interactions also minimises importance of ionic salt presence and solution pH. However, the tethering process can reduce bilayer fluidity.[71, 99]

Alongside lipopolymers, polyelectrolytes are also often used in polymer-SLBs.[111, 115] They can ease the use of functionalised metallic substrates such as mercaptoundecanoic acid-coated gold by absorbing through electrostatic charge interactions.[115] Layer-by-layer deposition of differently charged polyelectrolytes allows for well controlled film thickness. The layered method of film formation is well controlled because as each layer deposits on the substrate it will repel addition of similarly charged polyelectrolyte due to charge build-up. This minimises polymer clumping.[71] As the process is well-controlled, the relationship between thickness and number of layers is considered linear.[116]

Polyelectrolytes bind to the lipid bilayer through a combination of van der Waal, hydrogen bonding and electrostatic interactions. This electrostatic reliance means that pH and ionic strength of the solvent is of great important. Electrostatic absorption of lipid mixtures with polymers such as poly(amino acid methacrylate) have resulted in a high level of mobility within the bilayer, with no additional anchoring required.[117]

Other materials such as polyethylene glycol have also been used as the polymer spacer (figure 1-10). The use of PEG can result in bilayer systems with large and well-hydrated sub-membrane spaces.[118] This makes them well suited to the incorporation of transmembrane proteins that may otherwise have unfavourable spacer or substrate interactions.

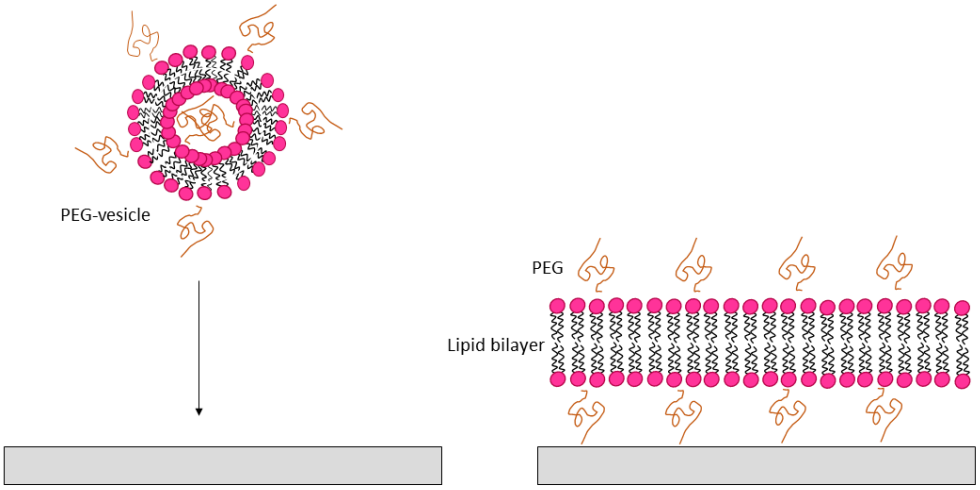

Figure 1-10: Example of the formation of a solid-supported lipid bilayer structure a PEG polymer supporting layer. This type of polymer cushion can provide more room under the bilayer for protein incorporation.

Hydrogels provide an alternative supporting structure to provide space between the substrate and lipid bilayer. Hydrogels are networks of cross-linked polymer chains that can form a colloidal solution with water. The hydrophilic polymer backbone provides a high level of water absorptivity. When in an aqueous solution the high level of water content results in a flexible structure that can swell without dissolving.[119]

Controlling the mesh size of hydrogels can block embedded proteins from migrating out of the bilayer. The downside is that they can also cause the proteins to become immobilised in the lipid structure.[120] The use of hydrogels has also been shown to enable greater flow speed resistance when exchanging solvent solutions.[121]

Polymer spacers have also been found to decrease alternating current signal noise in impedance measurements by reducing local defect density.[122] Despite this, it is rare for polymer-supported membranes to have strong electrical sealing properties, limiting their usefulness in ion transport studies.[123] The electrical sealing properties of most SLBs are inferior to those of other systems like BLMs. Whilst BLMs can have electrical resistances of greater than 10 mega ohms, most SLB systems have resistances below 1 mega ohm.[124] The use of hydrogels has provided some membranes with resistances of 1-5 mega ohms.[120] However, this is still well below what BLMs are capable of.

Despite the lower levels of resistance in many polymer-supported bilayers, systems have still been designed that were able to remain stable for weeks at a time. Förtig et. al used lipopolymers with lipid head groups and silanol coupling end groups to form dense brush-like monolayers before completing the bilayer through vesicle fusion. The bilayers formed through this method were shown through fluorescence microscopy to have no observable changes to appearance or mobility of lipids.[125]

1.8 Tethered-Bilayer Lipid Membranes

The stability and flexibility of SLBs has been further enhanced through the creation of tethered-bilayer lipid membranes. The tBLM architecture involves the use of tethering anchor lipids binding the bilayer to a substrate, increasing the reservoir space between them. Advantages of tBLMs over other model systems include the high amount of flexibility afforded to their design[126, 127] as well as the long-term stability they provide without compromising on strong electrical sealing properties.[128, 129] Vockenroth et. al were able to form tBLMs with electrical impedance measured to be greater than 10 gigaohms, by using photoresist patterned electrode substrates.

In the most common tBLM systems, a silicon substrate coated with gold is bound through strong gold-sulphur bonding interactions to lipids that terminate with a thiol or disulphide group. This self-assembly process creates a tethered monolayer of lipids on the substrate. A secondary lipid layer is then self-assembled on top to create a bilayer (figure 1-11).[130, 131]

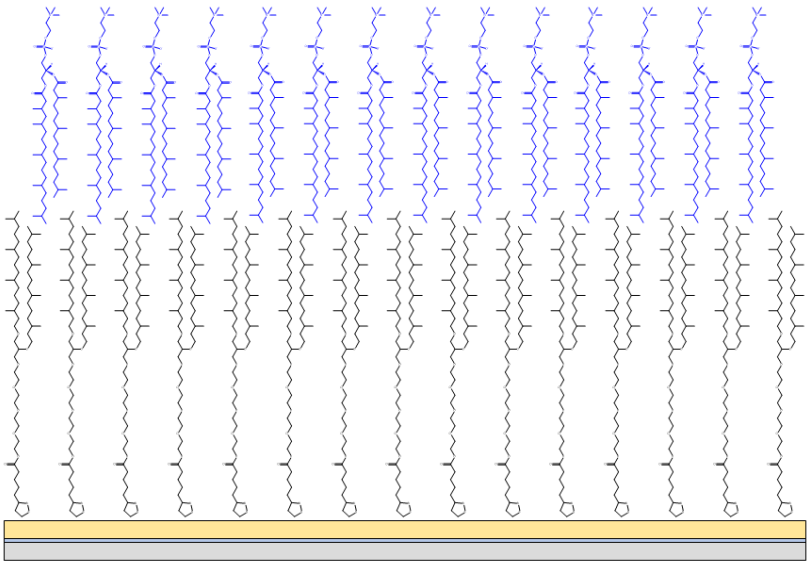

Figure 1-11: Schematic of the structure of a fully tethered tBLM using DPhyTL (black) and DPhyPC (blue). Silicon is coated in a thin layer of chromium and a layer of gold. Sulphur bonds in the tethering lipid form a strong bond with gold to create a monolayer which can then be added to with additional lipids to complete the bilayer.

The secondary layer can be added through one of two methods: vesicle fusion and rapid solvent exchange. Which method is used depends on the steric bulk of the lipid molecules involved in bilayer formation.[132] In the vesicle fusion process phospholipids are extruded through membrane pores to create vesicles that can then be introduced to the existing monolayer. This process can also readily allow for incorporation of proteins into the phospholipid mixture.[133] The rapid solvent exchange process involves incubation of the tethered system in an ethanol-lipid solution. When the solution is rapidly exchanged for a buffer a bilayer will spontaneously form.[134]

The processes for producing tBLMs are relatively simple and reproducible compared to other model systems, but the quality of the resulting membrane is dependent on a number of factors. The roughness of the surface can be easily affected by any contamination in the formation process. The chemical composition and tethering density of the anchor lipids is also important.[135] A greater density of tethering lipids on the surface results in a stronger membrane. This is especially true in terms of electrical resistance, which in tBLMs is comparable to or greater than in traditional BLMs. In some cases tBLMs with GΩ-level resistances have been recorded.[129]

Fully tethered bilayers are disadvantageous for the incorporation of proteins. They can also result in levels of stability and resistance that are unrealistic when compared to biological membranes. To solve this, sparsely tethered systems can be used which utilise smaller spacer molecules to increase the space underneath the bilayer (figure 1-12). This can have minor detrimental effects on the electrical sealing properties of the tBLM, but with dramatically increased ion transport capabilities.[136, 137]

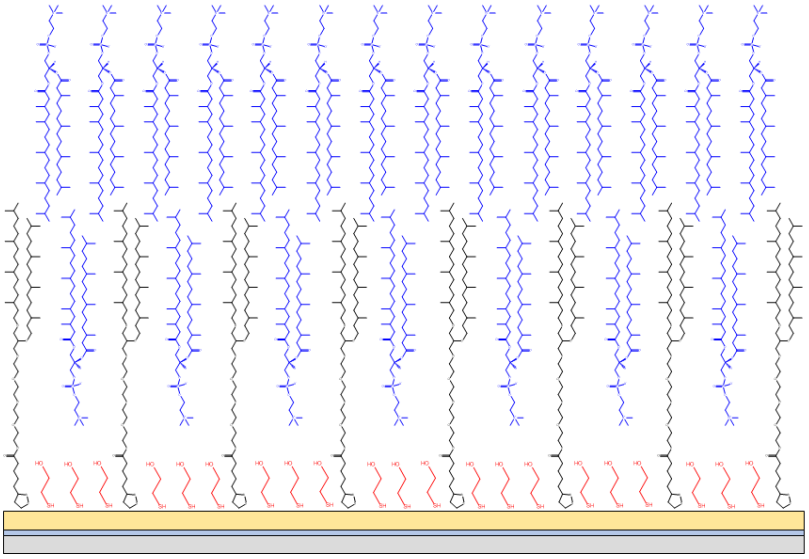

Figure 1-12: Schematic of the structure of a partially tethered tBLM using DPhyTL (black), 2-mercaptoethanol (red) and DPhyPC (blue). Addition of the mercaptoethanol spacer creates more space beneath the bilayer, improving realism and ability for the bilayer to incorporate other molecules. Some DPhyPC will flip and fill spaces in the inner leaflet.

The area between the bilayer and the substrate is referred to as the sub-membrane space. By increasing the number of short spacer molecules that attach to the substrate, the hydration of this sub-membrane area can be increased. Greater hydration allows more room for embedded proteins that may have intra-cellular functional domains. It also allows for smoother transport of ions from one side of the membrane to the other.[133] Hydration levels in fully tethered systems can be as low as 5%, whilst levels of over 60% have been achieved with sparsely tethered tBLMs.[126, 130]

A sparsely tethered makeup fundamentally changes the structure of the bilayer. In a fully tethered system where no spacing molecules are used the anchoring lipid also acts as one half of the bilayer. When sparsely tethered, the gaps in the inner leaflet of the bilayer are filled in with additional lipids from the bilayer formation process.[137]

Electrical resistance of tBLMs can be adversely affected by tethering too sparsely. In typical tBLM systems, the resistance of bilayers decreases with tethering density due to a decrease in stability of the bilayer structure.[136] The high level of hydration observed in these systems can make them useful for testing other membrane properties as an increased level of hydration results in greater membrane fluidity.[138]

The chemical structure of the tethering anchor lipids can also have a significant effect on the membrane. In the case of membranes formed using gold as the substrate, thiol bonding with disulphide groups is optimal. This is due to the increased electrical resistance provided by the additional sulphur bonding a disulphide provides.[130] Diphytanoyl-based lipids are commonly used in tBLM structures.[139] These lipids have two long hydrophobic carbon chains with some additional carbon branching.[140] In anchoring lipids such as 2,3-di-O-phytanyl-sn-glycerin-1-tetraethylenglycollipoic acid ester the disulphide and carbon chains are separated by a polar tethering region made up of a combination of ester and ethylene glycol groups.[136, 141]

A major advantage of tBLMs is the tunability of the different parts of their structure for a variety of different uses. The choice of lipid that forms the bilayer is dictated by the desired type of membrane that it is meant to mimic. For an approximation of eukaryotic cells, 1,2- di-O-phytanoyl-sn-glycero-3-phosphocholine and 1,2-dioleoyl-sn-glycero-phosphocholine are often used. Both of these lipids have low melting points and are able to form relatively fluid bilayers.[138, 142] The choline group moiety present in these structures is also highly prevalent in the phospholipid structures of the eukaryotic cells being mimicked.[143]

It is also possible to mimic bacterial membranes with tBLMs. Lipopolysaccharides are found in the outer membrane of gram-negative bacterial cells, making up their outer bilayer in combination with phospholipids. LPS can be used in combination to DPhyPC to mimic this structure in a tBLM system (figure 1-13).[137]

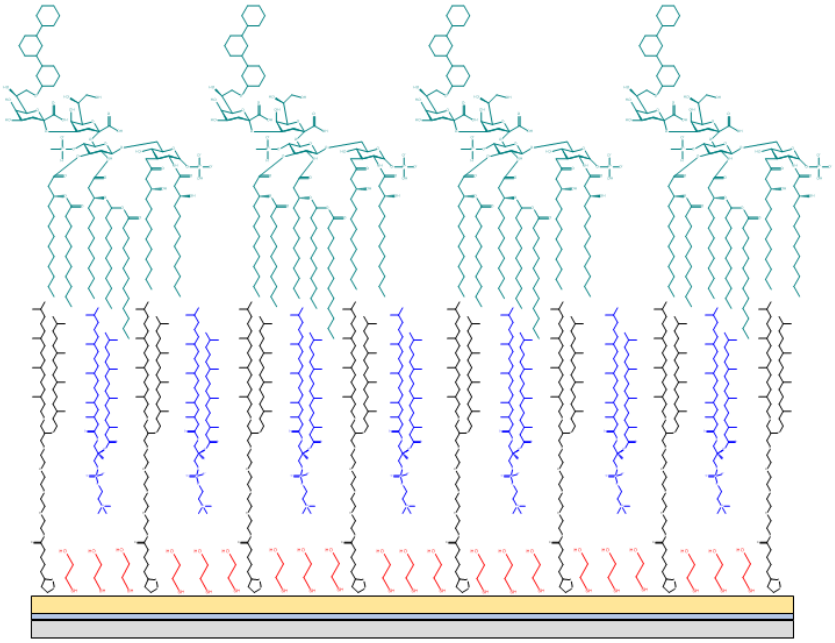

Figure 1-13: Schematic of the structure of a partially tethered tBLM using DPhyTL (black), 2-mercaptoethanol (red), DPhyPC (blue) and LPS (green). LPS is used to mimic the outer membrane of gram-negative bacteria. Some DPhyPC is used to fill spaces in the inner leaflet as LPS has too much steric bulk to do so.

LPS is made up of an O antigen region, a hydrophobic oligosaccharide core and a 'Lipid A' region. LPS has a strong negative charge due to the phosphate present in the Lipid A region.[144] This can be balanced through the use of positively charged ionic salts in solution. The presence of the O antigen region dictates whether the LPS is smooth or rough.[137] Without this region, rough LPS is more hydrophobic and thus more penetrable by hydrophobic antibiotics.[145] Whilst SLBs can also be used for such studies[146], they do not provide as good a simulation of the bacterial environment due to the lack of a hydrated sub-membrane space.

Ion transport can be carried out with tBLMs using ionophores. Ionophores are chemicals that reversibly bind ionic species. Many are lipid-soluble and can transport ions across membranes.[147] This relies on the cell membrane being fluid enough to allow such mobility.[148] The use of gramicidin (selective towards H+, Na+, K+ ions) and valinomycin (selective towards K+ ions) in the transport of ions across tBLM bilayers is well-documented (figure 1-14).[142, 149-151]

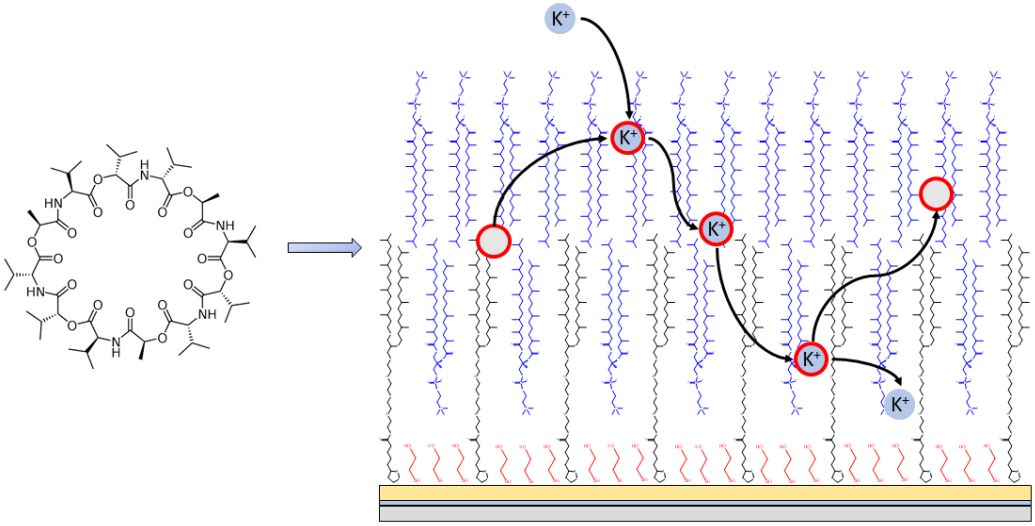

Figure 1-14: Schematic of the valinomycin ionophore and the process it uses to capture and transport potassium ions from one side of the bilayer to the other.

Selective transport of ions from one side of the bilayer to the other can be observed through changes in electrical alternating current measurements of bilayer resistance and capacitance using electrochemical impedance spectroscopy. A tBLM can be modelled with electrical circuits that use resistive and capacitive elements. When the matching ions are present in solution for an ionophore incorporated into the bilayer a decrease in bilayer resistance occurs as the ions can readily flow across the membrane.[152] The capacitance meanwhile will provide information about the changes in membrane thickness and water content. As such, a large resistance drop and minimal increase in capacitance in the presence of the requisite ions indicates successful channel formation.[153]

EIS has been combined with infrared absorption spectroscopy to study the mechanism of pore formation within the membrane.[149] The high level of stability and reproducibility of the tBLM means it has successfully been used for testing single channel ion currents.[154] EIS has also been combined with surface-enhanced infrared absorption spectroscopy to further characterise the presence of gramicidin in tBLMs.[150]

A variety of other different proteins have been successfully integrated into tBLMs. Ion transporting proteins such as melittin have been successfully incorporated both before and after formation of the bilayer.[155, 156] Pore-forming exotoxins such as α-hemolysin can also incorporated into the bilayer during formation. This has also been successful for ligand-gated ion channels such as OmpF, as well as synthetic channels.[157, 158]

The presence of additional molecules such as cholesterol in formation of the bilayer structure has been shown to allow more effective protein penetration. The formation of ion channels has also been determined to be influenced by pH in cases such as the insertion of lactophoricin. Improvement of protein incorporation has also been investigated with the use of protein tethers instead of anchor lipids.

This high compatibility of tBLMs with a number of proteins, ionophore and pore forming molecules means they have a wide variety of potential applications. These include as ion channel-based biosensor switches[128], stochastic sensors for single molecules[159], molecular characterisation[160] and as part of DNA sequencing devices.[161]

One form of molecular characterisation with increasing interest is that of synthetically engineered nanomaterials (ENMs). Understanding the interactions between ENMs and cell membranes is a vital step for their use in applications such as drug delivery and biosensing.[162] Silver nanoparticles in particular are well-known for their antibacterial properties[163, 164], however they can have unfavourable interactions with mammalian cells. Tethered-bilayer lipid membranes allow for better determination of the effects that these nanoparticles can have on cell membranes.[165] Similar experiments have been performed with silica and polystyrene particles.[166, 167]

A significant advantage of tBLMs is their high level of stability over time. Patch clamp and black lipid membrane systems only last for periods of time equivalent to hours. Solid-supported tBLMs have been shown to remain relatively stable for up to months at a time. This has been achieved at room temperature in an aqueous reservoir.[131] Not only is this long-term stability useful for studies of mechanisms such as aforementioned ionophore impact, but it also allows for multi-step procedures that can take longer periods of time to conduct. Beyond this, the repeatability of this level of stability means that thorough long-term studies can be undertaken.

Chapter 2 - Methods

2.1 Electrochemical Impedance Spectroscopy

Electrochemical impedance spectroscopy (EIS) is a well-established technique for electrical measurements of model membranes.[168] In a typical EIS measurement an AC voltage is applied across the membrane at different frequencies with the current output measured at each frequency. The phase angle is also determined as the difference between the output current and the original applied voltage potential. These measurements are typically performed over a range of frequencies between 2 mHz and 100 kHz.[136] The resistance that occurs in the electrical circuits that utilise this system is known as impedance.

Impedance is a complex quantity comprised of resistive and capacitive elements in an AC circuit system. It has both real and imaginary resistance components. The real resistance impedes movement of charges and is caused by resistive circuit elements. The imaginative resistance is caused by capacitive circuit elements and results in the phase shift between applied voltage and produced current that gives rise to the phase angle. Measured in ohms, impedance (Z) is given as;

$$Z = R + jX \qquad \textbf{(Equation 1)}$$

where the resistive elements are represented by R and the capacitive elements are represented by X, the reactance.[168, 169] The reactance is an imaginary component as represented by j.

Three types of circuit elements are used for modelling bilayers. Basic resistors have an impedance equivalent to resistance in a DC circuit. This is because their impedance is independent of frequency and effectively constant. There is no imaginary component to these elements, and they do not cause a shift in phase angle between the current and voltage.

Capacitors have impedance given by their reactance. The reactance is directly affected by the response of capacitive elements to different frequencies. The charging and discharging of capacitors in an AC system leads to an impeding effect on current flow. This is unique to AC systems. The reactance of a given capacitor is given as;

$$X_C = \frac{1}{2\pi f \mathrm{C}} \qquad \textbf{(Equation 2)}$$

where the capacitive of the specific element is C, and the f refers to the frequency at which a voltage is applied. Reactance is inversely proportional to frequency. This is due to there being less time for the capacitor to accumulate charge before the signal is switched at high frequencies. As a capacitor accumulates charge it will become more resistant to further electron input, thus increasing the reactance. Current flow through a charging capacitor also becomes phase shifted from the applied voltage, increasing the phase angle. Not all capacitors behave in an ideal manner. Constant phase elements (CPE) act as a series of infinite capacitors with impedance given as;

$$X_C = \frac{1}{(2\pi f)^{\alpha} \mathrm{C}} \qquad \textbf{(Equation 3)}$$

where the closer α is to 1 the closer the CPE is to an ideal capacitor. When α is equal to 1, the CPE acts as an ideal capacitor, whereas when α is equal to 0, the CPE acts instead as a resistive element.[168-170]

EIS measurements can be used to indicate the current-impeding quality of lipid bilayers by fitting with electrical circuit models using circuit elements analogous to the bilayer structure (figure 2-1). A higher level of measured impedance would indicate a more intact or well-sealed bilayer. It can also be used measure membrane disruption caused by small molecules or peptides. Measurements are performed using a reference electrode immersed in an electrolyte solution, a counter electrode and a working electrode.

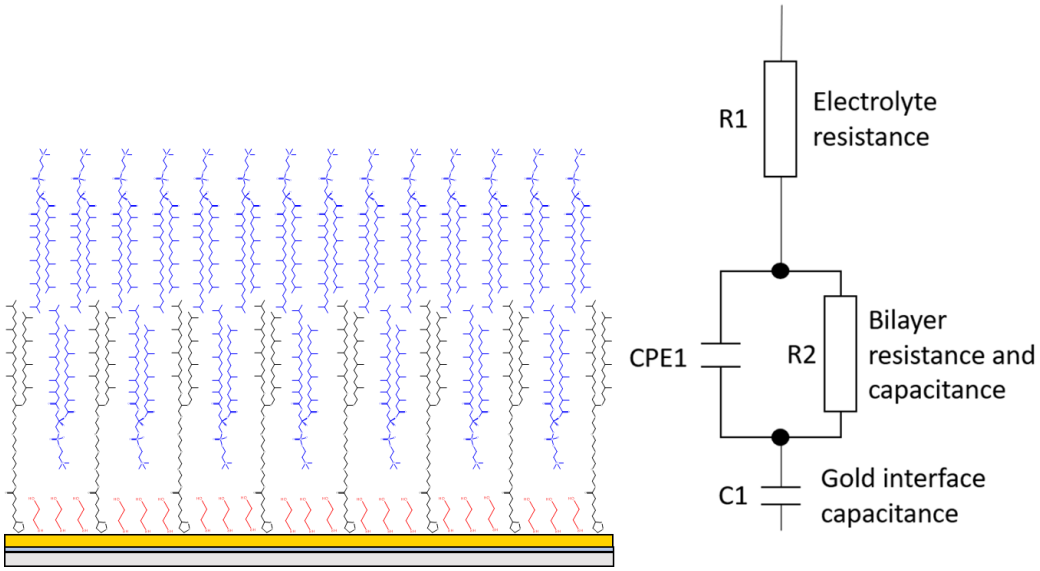

Figure 2-1: Schematic of a DPhyTL/DPhyPC sparsely tethered membrane with an equivalent circuit model used to determine electrochemical properties such as impedance and capacitance.

The resistance of the aqueous electrolyte solution can be modelled by a singular resistive element R_1. The resistance of a model bilayer can be modelled by a combined resistive and capacitive mesh element (R_2 and CPE_1). Sometimes an additional capacitive element C_1 is also required to model the sub-membrane region between the bilayer and the gold surface.[171-173]

One of the most common ways to present EIS results is in the form of a Bode plot (figure 2-2). In a Bode plot the log of the magnitude of the impedance Z and the phase angle θ are graphed against the log of applied frequencies. The impedance of the series at any given frequency is given by the element with the highest impedance at that frequency. At very high frequencies the impedance is initially governed by the resistance of the electrolyte solution, as its impedance is independent of frequency. This also results in a near-zero phase angle at high frequencies.[173, 174]

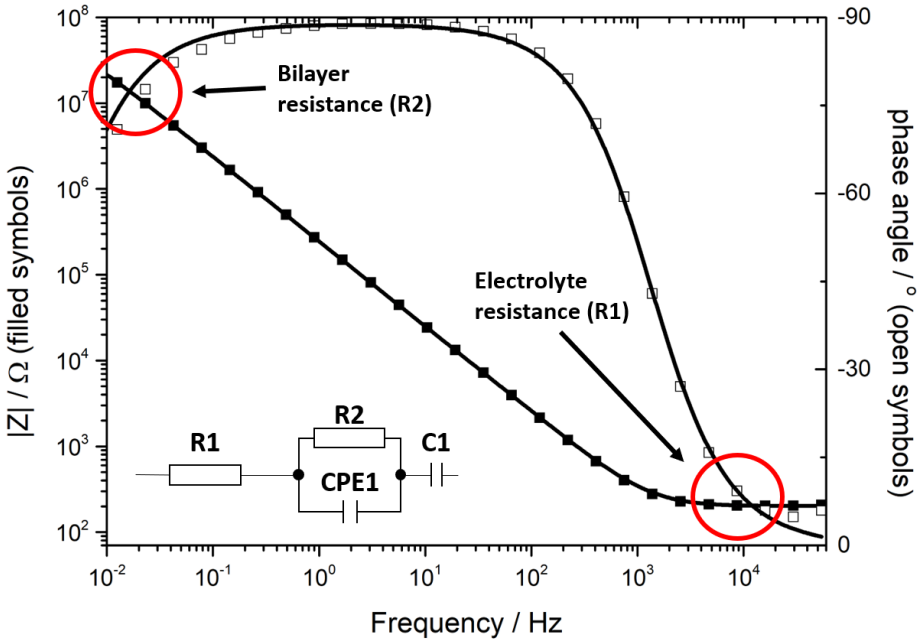

Figure 2-2: Example of a typical bode plot measurement of a tBLM. The electrolyte solution is modelled with resistive element R1 whilst the bilayer itself is modelled with resistive element R2 and capacitive element CPE_1.

The resistive and capacitive elements that model the bilayer are in parallel and as such the impedance of the combined mesh is determined by the element with the lowest level of impedance. At high frequencies the impedance is thus very low due to the low reactance of the CPE_1 element (see equation 2) which has a lower impedance than the R_2 element. As frequency decreases, the impedance of the series becomes dominated by the CPE_1 element.

With the series acting as a capacitor the plot of log $|Z|$ against log $|f|$ will thus have a slope in the vicinity of -1. The phase angle also increases throughout this frequency range. At lower frequencies the R_2 element dominates and the plot becomes independent of frequency once again. The phase angle tends to zero as the bilayer no longer acts as an ideal capacitor.[172]

At very low frequencies the additional C_1 element may cause the series to act in a capacitive manner again depending on the quality of the bilayer and the breadth of frequencies being measured. Additional factors such as defects in the bilayer and incorporation of ion carriers such as valinomycin can result in more complex measurements that require additional RC elements.[165, 172]

Figure 2-2 shows an example plot of a high electrical sealing-quality tBLM sample. A tBLM with defects, incomplete bilayer leaflets or molecules embedded that promote current flow will, when reading from right to left, have an impedance curve that flattens out with much lower impedance values at low frequencies, whilst the phase angle curve will not reach 90 degrees and will dip at higher frequencies (figure 2-3).

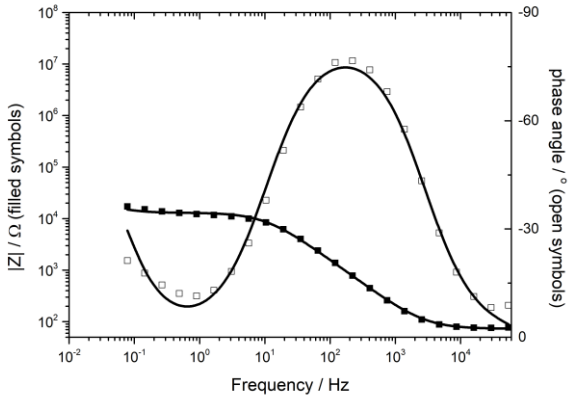

Figure 2-3: Example of a lower quality tBLM Bode plot, where the phase angle does not reach 90 degrees and impedance curve flattens at 10^4 Ω.

2.1.1 Methods for Fitting and Interpreting EIS Data

In this thesis, experimental data was interpreted using theoretical circuits generated in the ZView2 software, developed by Scribner Associates. This software allows for the generation of theoretical circuit models to model data gathered through EIS. The circuits were generated to fit data as accurately as possible with different resistive and capacitive elements representing the bilayer, substrate, and surrounding solution. The data is primarily showcased in the form of Bode plots throughout this thesis.

There are multiple different ways to approach the modelling of lipid bilayers with electrical circuits. Models can be so complex as to involve different circuit elements for different sections of the bilayer, such as treating the inner and outer leaflets separately. One could also consider the lipid bilayer as a perfectly resistant entity and model only the supposed defects within the bilayer. The more complex the model, the better it may fit to the bilayer in question, however for the sake of consistency and simplicity a set of simple generalised models were adhered to for this thesis. The studies described within focus mostly on the overall quality of the bilayer and changes in defect presence, so a simple model is adequate for extracting the relevant information to draw conclusions from. The different electrical circuits used to model the experimental data are shown in figure 2-4 and are an established series of fitting models established previously.[136, 137]

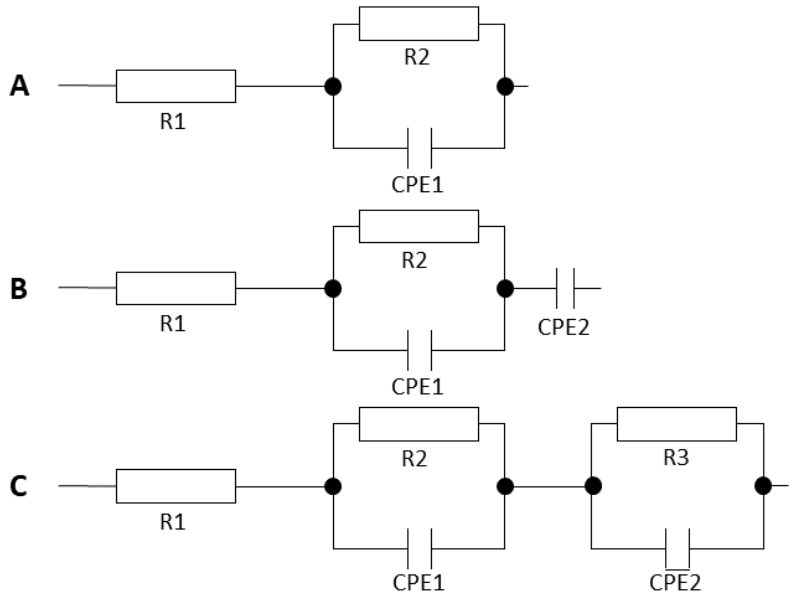

Figure 2-4: Different equivalent circuit models for determination of resistance and capacitance of various model membranes.

For high quality undamaged membrane models equivalent circuit A can be used. When a bilayer has sufficient impedance quality, the sub-membrane spacing region is not visible in the frequency spectrum the measurements are taken in. This is because the membrane resistance is too strong to allow a relevant population of ions to be present for capacitance to be measurable. If the bilayer quality is not at this level and there are enough ions in the sub-membrane region, then circuit B is utilised. This does not necessarily mean that the membrane is damaged, however – only that the resistance is below a certain threshold. This is experimentally more likely in a bilayer with lower tethering density. The third circuit, circuit C, can be used in a situation where the membrane is severely damaged or an ionophore such as valinomycin is incorporated and facilitating a large amount of ion transport across the bilayer.

2.2 Neutron Reflectometry

Neutron scattering allows for a detailed layer-by-layer characterisation of lipid bilayer samples. Samples for neutron reflectometry have a much higher surface area than EIS samples due to the staging requirements of the instrumentation. This means that a minor defect which could greatly decrease the impedance measurement of a bilayer in EIS will not have the same level of impact on the reflectometry data gathered from a NR bilayer as it is averaged out over the higher surface area. Whilst EIS can determine whether there are structural changes in a smaller sample, NR can allow the pinpointing of which specific parts of the bilayer structure are being affected (e.g. interface, head groups, hydrocarbon tails, tethering region). Crucially, NR does not require a vacuum unlike other techniques such as x-ray scattering and can be performed on lipid bilayer samples in solution.

Neutrons are sub-atomic particles. As subatomic particles they are subject to diffraction, refraction, and reflection. Scattering of neutrons occurs through interactions with atomic nuclei (known as nuclear scattering), or between the magnetic moments of the incident neutron and unpaired electrons (known as magnetic scattering). Whilst both forms of scattering can be utilised by neutron reflectometry, the former is commonly used for lipid bilayer experiments. Through nuclear scattering interactions, neutron reflectometry provides high resolution information about the bilayer structure perpendicular to the support.

The nuclear scattering that occurs when a neutron encounters an atomic nucleus is elastic, so whilst momentum remains constant the movement direction is changed. Scattering is dependent on the interaction potential V(r) that exists between a neutron

and nucleus with distance r between them. The nucleus acts as a point scatterer due to the interaction potential falling to zero at a shorter distance than the wavelength of the neutrons. This means that spherical isotropic scattering occurs.

A neutron beam can be represented by a wave function;

$$\varphi_i = e^{ikz} \qquad \textbf{(Equation 4)}$$

where k represents the wave number $k = \frac{2\pi}{\lambda}$ and z represents the distance propagated from the nucleus in a given direction, whilst λ represents the wavelength of the neutron beam. Due to the point scattering of the nucleus the wavefunction of the scattered wave can be given as;

$$\varphi_s = -\frac{b}{r} e^{ikz} \qquad \textbf{(Equation 5)}$$

where b represents the neutron-nucleus interaction in the form of nuclear scattering length. Whilst the scattering length has an imaginary component, it is only important for very specific nuclei and as such it is usually treated as a real quantity.

Neutron data can be shown in the form of reflectivity plotted against the momentum transfer vector Q. This vector is always perpendicular to the sample surface. The wave vectors k_i and k_f describe incident and reflected neutron waves with equal magnitude. Momentum transfer can thus be calculated as;

$$Q = \left|k_f - k_i\right| \qquad \textbf{(Equation 6)}$$

$$Q = \frac{4\pi \sin\theta}{\lambda} \qquad \textbf{(Equation 7)}$$

where Q is in units of $Å^{-1}$, θ is the grazing angle of incidence and λ is the wavelength of the incident neutron beam.[175, 176]

Fringes in the diffraction pattern can be predicted using Bragg's law. Constructive interference between particles occurs when the path length between diffracted particles differs by a multiple of the wavelength. Maxima fringes are highly dependent on the depth of each different layer of material in a sample. Multiple different grazing angles are used to observe scattering at different ranges of Q, typically between 0.4 and 4 degrees, with the exact numbers depending on the instrument. A schematic of the reflection process is shown in figure 2-5.

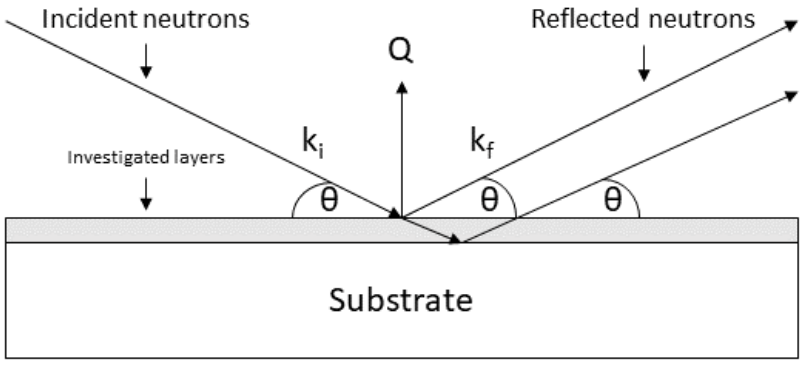

Figure 2-5: Schematic of the reflection process undergone by neutrons used in a neutron reflectometry experiment. Incident neutrons will interact with the various investigated layers of the substrate and reflect in a specular fashion. At different depth levels this will result in neutrons reaching the detector at different points that can be used to extrapolate details about the surface the neutrons were reflected from.

Sample surfaces for neutron scattering experiments must be flat enough for reflection to be specular. This means that the angle of surface reflection is identical to the angle of beam incidence. The reflectivity off a surface can be calculated as the ratio between the amount of incident neutron radiation versus the amount reflected by the sample. The perpendicular surface structure of the analysed sample can be determined using the neutron scattering patterns picked up by a detector.

Different materials that make up the layers of a lipid bilayer will reflect neutrons at different points, causing them to hit different areas of the detector. This allows for the creation of a scattering profile. A typical neutron data set involves plotting of the log of reflection intensity against Q.[175, 177]

The specific scattering profile of a bilayer sample depends on the scattering length density (SLD) of the molecules interacting with the neutron beam. The scattering length density of a molecule can be determined by dividing its scattering length by its volume, averaged over many nuclei;

$$\rho = \frac{\sum_i^n b_i}{V} \qquad \textbf{(Equation 8)}$$

SLD (presented in units of $\times 10^{-6}\text{Å}^{-2}$) is a constant value with no correlation to isotope or atomic number. Sample deuteration is widely utilised in soft matter studies. This variability of SLD values can be utilised to help create a layer by layer sample profile by manipulating solvent SLD through isotopic substitution.[175, 178] The SLD of water varies strongly between different isotopes, with H_2O's SLD of -0.56 compared to D_2O's SLD of 6.36.[179]. Different mixes of H_2O and D_2O allow the SLD of other compounds with an SLD between -0.56 and 6.36 to be matched, such as gold which has an SLD of 4.5.[180] This is known as contrast matching (CM) and allows parts of a lipid bilayer measurement to be hidden in the SLD of the solvent. The matching of an H_2O/D_2O solution with the SLD of gold is referred to as a CM 4.5 solution. Scattering experiments for the lipid bilayers discussed here are performed using three different contrasts – H_2O, D_2O and CM 4.5 that allow for the determination of more structural information than can be determined from only one type of solvent. If the solvent is changed and the SLD of any given part of the bilayer changes as well, then there is a direct correspondence to the hydration of that part of the bilayer.

2.2.1 Methods for Fitting and Interpretation of Neutron Reflectometry Data

Fitting neutron data for this thesis was performed using standalone co-refinement software developed by Andrew Nelson called MotoFit. A model system is used to approximate bilayer structure by generating theoretical fringe patterns. The accuracy of the fit is determined through minimisation of a chi-squared value which is calculated with the equation;

$$\chi^2 = \sum_{n=1}^{L} \frac{1}{L-p} \left(\frac{y_{obs} - y_{calc}}{y_{error}} \right)^2 \qquad \textbf{(Equation 9)}$$

where L represents the number of measured data points and p represents the fitting parameters. The y values y_{obs} and y_{calc} represent the observed and calculated values, whilst y_{error} is the standard deviation of the observed values. A perfect fit results in a χ^2 value of 1.[178] A greater number of parameters can increase the quality of the fit, however the number used should be kept only to ones that fit with a realistic theoretical membrane model.

The models used for lipid bilayers break the structure of the bilayer down into a variety of different layers with different values for size, SLD, hydration and surface roughness. Some of the parameters are fixed due to having specific known values, whilst others are allowed to change within a set of physically reasonable values determined and utilised in previous studies with similar tBLM samples (table 2.1).[136, 137]

Table 2.1: Typical SLD and thickness values for the theoretical model used as a base for neutron modelling analysis

	SLD (10^{-6} Å^2)	**Thickness (Å)**
Silicon substrate layer	2.07	infinite
Silicon oxide layer	3.03	3-15
Chromium layer	3.47	20-80
Gold layer	4.1-4.5	100-250
Tethering region	0.5-2	12-18
Inner & outer hydrocarbon chains	-0.4-0	12-18
Outer head groups	1-3.5	6-12

Modelling data in the MotoFit software generates a reflectivity plot (for examples of reflectivity plots, see figures 3-27 and 3-28) as well as an SLD profile showing variance in SLD at different distances from the interface (figure 2-6). Roughness in the bilayer, due to each layer of the model not being entirely discrete in a physical system, results in a smoothing of the SLD profile. This is more realistic than fitting each layer with a specific SLD that changes immediately between layers.[178] Roughness between each of the layers can vary depending on the quality of the sample, especially in cases where defects are present in the bilayer or introduced by sample preparation methods, however a good sample will typically have roughness values lower than 10 Ångstroms.[130]

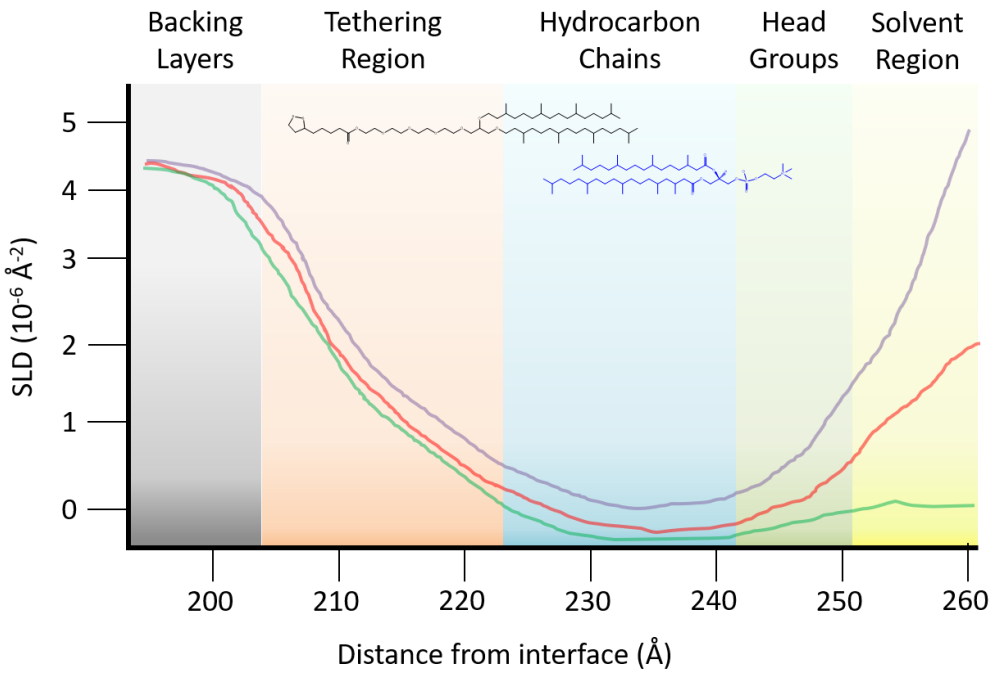

Figure 2-6: SLD diagram showing changes in SLD as distance from substrate interface increases with different layers of material. Initially high SLD due to the backing layers decreases to the relatively low SLD of the hydrocarbon chains with variable SLD at the furthest distance from the interface depending on deuteration of solvent.

2.3 Protocols for Experimental Methods

Sample preparation and measurement protocols for EIS and neutron scattering experiments followed a relatively standardised procedure for most experiments undertaken. Any variance for a particular data set will be specifically stated. Chemicals were acquired from Sigma Aldrich, ChemSupply, Avanti Polar Lipids and Celestial Synthetics and used without additional purification. All experiments were performed using ultrapure MilliQ water with 100 mM electrolyte solutions except where stated otherwise, and all experiments were performed at standard room temperature. No chemicals were added in quantities that could noticeably affect solution pH, and pH was not monitored during experiments, following standard practice from previous work.[136, 137]

Valinomycin (≥99%), sodium chloride (NaCl, ≥99%), potassium chloride (KCl, ≥99%) and calcium chloride ($CaCl_2$, ≥99%) were purchased from Sigma Aldrich, Australia. Ethanol (C_2H_5OH, 100%), hydrogen peroxide (H_2O_2, 30% w/w), and ammonia solution (NH_3, 30 wt%) were obtained from Chem-Supply, Australia. All purchased chemicals used were of analytical grade and utilised without further purification. Ultrapure water obtained from a WaterPro PS reverse osmosis system (18.2 MΩcm resistance, Labconco) was used for all aqueous solutions.

Lipids used in experiments are shown in figure 2-7. DPhyTL and 2-mercaptoethanol have been shown to provide a platform for creation of high quality tBLMs, hence their use in the experiments in following chapters.[136] DPhyPC was used for experiments in chapter 3 due to the high prevalence of PC lipids as a standard through many studies, including previous studies on membrane stability.[131, 142] LPS was used to mimic bacterial membranes in the first part of chapter 4.

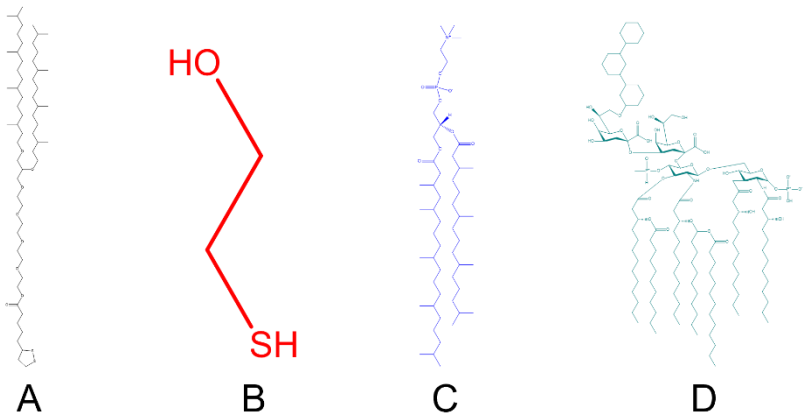

Figure 2-7: Chemical structure of the four main chemicals used for bilayer formation. A) DPhyTL anchorlipid used for all bilayers. B) 2-mercaptoethanol spacer used for all bilayers. C) DPhyPC lipid used for mammalian cell models. D) LPS used for bacterial cell models.

2.3.1 Electrochemical Impedance Spectroscopy

For all experiments, wet cells with 1 ml volume and 0.283 cm^2 area were used. Substrates were prepared by rinsing single-side polished silicon with ethanol and ultrapure water before being immersed into a 'basic piranha' solution for 1 hour at 70^oC. The piranha solution consisted of a 1:1:5 ratio of NH_3, H_2O_2 and ultrapure water. After being rinsed with ultrapure water and ethanol the samples were sputter coated with a 5 nm adhesion layer of chromium and then a 20 nm layer of gold. Samples were then rinsed with ethanol and immersed for approximately 18 hours in an ethanol solution containing either an anchorlipid or anchorlipid/spacer mix with total concentration 0.2 mM. After functionalisation samples were then rinsed with ethanol, dried under nitrogen and assembled as part of the wet cell. Further steps were dependent on sample type.

For samples using lipopolysaccharides in the outer leaflet and samples with 100% tethering density 20 µl/ml vesicle solution was added to the sample and left overnight before rinsing with 5 cell volumes of electrolyte solution the next day. Vesicles were prepared by mixing lipids in an aqueous solution. The lipid–water mixture was extruded 31 times through a track-etched polycarbonate filter membrane. The size of the filters was dependent on the size of the lipids being used for membrane formation. For LPS membranes 200nm filters were used, whilst for DPhyPC membranes 50 or 100nm filters were used. All vesicle solutions were extruded just prior to use.

For samples using only DPhyPC in the outer leaflet with tethering density of less than 100% rapid solvent exchange was used. 100 µl of 10 mg/ml DPhyPC in ethanol was added to the sample for 20 minutes before flushing quickly with 20 cell volumes of electrolyte solution. In some cases, additional time post-RSE and further flushing was required to form a good quality bilayer. A schematic of the cells used for EIS experiments is shown in figure 2-8.

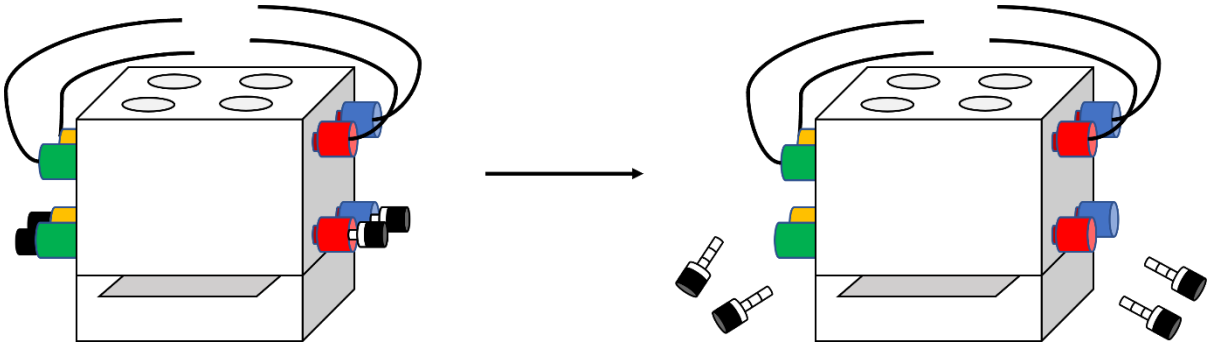

Figure 2-8: Schematic of the cell used for EIS spectroscopy. The coated silicon wafer is held between the two halves of the cell, with circular seals creating 4 distinct 0.283 cm^2 sample chambers. Each chamber has a coloured inlet (bottom) and outlet (top) for flow of electrolyte. Material can also be added into the top of each chamber. Solution can be drained completely by removing inlet stoppers.

EIS was performed using a Metrohm Autolab potentiostat with a three-electrode setup using platinum wire as a counter electrode as well as a Ag/AgCl reference electrode. For each sample data points were collected in the range from 100 kHz to 2 mHz with an amplitude of ± 10 mV. The default solution for all measurements was 100 mM NaCl except where specified otherwise.

The EIS data was analysed using ZView2 (Scribner Associates). All spectra were area-normalised using a surface area of 0.283 cm^2. Data was fitted to one of the equivalent circuits shown in chapter 2.2. The error is the range of values that can be fitted for the respective parameter without decreasing fit quality evaluated by least-squares fitting.

Data is presented in the form of graphs produced using OriginPro data analysis and graphing software with impedance and phase angle graphed against frequency.

2.3.2 Neutron Scattering

Substrate preparation was identical to that of EIS with the exception that the substrates used were silicon discs with a thickness of 1 cm. Bilayer quality was observed using three different sets of neutron measurements in D_2O, CM 4.5 and H_2O solutions with SLD for solutions adjusted accordingly depending on the solvent.

Chapter 3 - Air Stability of Tethered-Bilayer Lipid Membranes

3.1 Introduction

Model membrane systems such as tethered-bilayer lipid membranes are used to replicate the fundamental properties of cell membranes in a controlled environment. This chapter focuses on an exploration of whether these tethered systems can be dried and rehydrated and how this affects their structure and use in further applications. This work is important for better understanding the water retention properties of tBLMs to determine their suitability for use in biosensing, where they may not be able to be completely submerged in solution. It is also important to determine whether additional protective coatings may be necessary to improve bilayer quality through the drying and rehydrating process. Similar work has already been performed on other model systems, but only tentatively in the field of tBLMs.[131]

The structure of the lipid bilayer inherently relies on hydration. Whilst the degree of hydration can affect bilayer properties, complete dehydration would result in structural collapse. This is due to the amphiphilic nature of the bilayer and hence its reliance on the presence of water for the hydrophilic head groups to be attracted to and for the hydrophobic tails to be repulsed by. Water provides a hydration shell surrounding phospholipid head groups that plays an important part in stability of the bilayer.[181] A decrease in hydration can also greatly decrease lipid mobility.[182] The main goal of any attempt to protect lipid bilayers outside of solution would be to determine whether they are able to naturally retain enough water in their structure, and how to enhance water retention if necessary.

Black lipid membranes have been successfully created, frozen and transported before use for ion channel measurements with no noticeable drop in membrane quality. Jeon et. al achieved this using a high freezing point lipid-containing solvent mixture made from hexadecane and n-decane. Whilst decane is often used as a solvent during membrane formation, hexadecane is less common due to its higher viscosity. By using a mixture of the two, they were able to mitigate the viscosity of hexadecane whilst making use of its favourable freezing point of 18 ◦C, below room temperature but well above the freezing temperature of water. By freezing the solution prior to bilayer self-assembly occurring, ready-to-form bilayers were able to be shipped from one location to another before thawing out to finish the process. Functionality of membranes was verified using single channel measurements of embedded α-haemolysin molecules with an Axopatch amplifier. The membrane bilayers formed from these frozen precursors had similar qualities to conventional BLMs, raising the possibility for them to be stored indefinitely and shipped for commercial use.[49] Work has also been done to minimise the human input required for this process and to make it scalable for industrial applications.[50, 51]

Hydrogels and other gels have both been used to protect planar bilayers outside of an aqueous environment. Results from Axopatch amplifier experiments using hydrogel encapsulated membranes have suggested that stability of up to 10 times as long as typical planar bilayers is possible. After formation of BLMs, Jeon et. al were able to encapsulate them with polyethylene glycol dimethacrylate through polymerisation of monomers in solution.

They found that these hydrogel encapsulated membranes were not only able to maintain a high level of electrical sealing but were also able to confirm that the presence of a coating did not block diffusion of molecules of interest – an important factor to consider in membrane stabilisation studies – by verifying the functionality of pore protein alpha haemolysin. It was also determined that the coated samples were less prone to damage from mechanical stress caused by rough handling of samples that would typically damage planar lipid membranes, as shown through measurements of current movement through channels embedded in the membranes.[52]

Pre-cast agarose gels have also been used to increase bilayer stability, but had the side effect of creating too much signal noise for effective channel-current measurements.[183] Small agarose-gel based chips have also been created which involve using a small bilayer with a single pore such as α-hemolysin and encapsulating it in an agarose solution. These chips are stable for more than a week and can be readily accessed by analyte molecules due to the porous nature of the agarose gel.[184, 185]

Air stability of SLBs has also been investigated through attempts to decouple bilayer formation from the use of bulk solvents. Cisternas et. al have successfully formed lipid bilayers on silicon substrates without using solvents, and without any additional cushioning molecules. DPPC molecules were evaporated directly onto a silicon substrate with evidence from AFM and ellipsometric measurements that bilayer self-assembly had occurred. These samples also appeared to maintain stability for long periods of up to months at a time.[186]

A promising avenue for the enhancement of tBLM stability is through the addition of polymer-based coatings. Similar examples exist in nature in areas such as the human nose, where mucosal layers provide protection from external pathogens and drying out of nasal tissue. The nasal mucus is formed as a flexible network of hydrated mucin molecules, stabilised by disulphide bonds and secondary interactions between ions. Mucins are heavily glycosylated proteins able to hold large amounts of water. The hydration of mucin gives it gel-like properties, and its presence allows for protection of the nose's mucous membranes. It can prevent infections by blocking unwanted pathogens, and provides a process for cleaning air breathed in through the nostrils.[187]

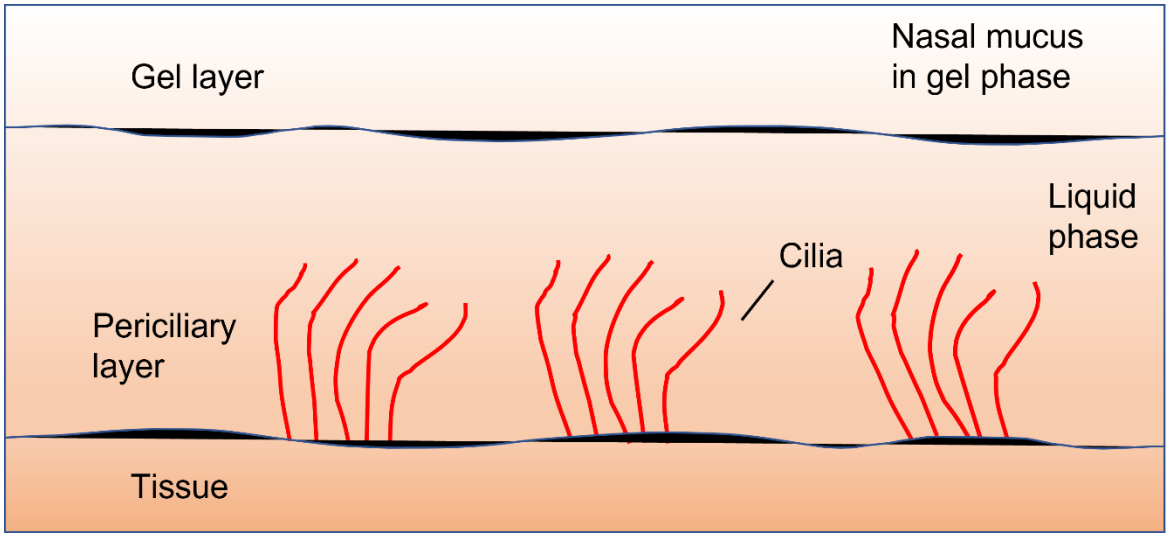

Figure 3-1: Schematic of the nasal mucous membrane. Cilia float within a liquid periciliary layer, with a gel layer on top providing protection.

This mucous layer is normally 10-15 μm thick, and divided into two layers (figure 3-1).[188] The lower layer that sits on the mucous membrane is more liquid-like and is known as periciliary liquid. On top of this is a more viscous gel phase given structure by the mucin embedded within it.[189]

90% of this structure is made up of water and glycoproteins, as well as large amounts of sodium and chloride ions, some potassium ions, and a small amount of calcium and magnesium ions.[187] Similar ionic salt solutions are used to help stabilise model membrane systems.

The nasal mucus acts as a diffusion barrier to drugs as well as pathogens. The size and charge of the drugs will affect how well they diffuse through the barrier. The nasal mucus is slightly acidic with a pH of 5.5-6.5 and has a negative electrical charge. The negative charge as well as the viscoelasticity and adhesiveness of the mucus are all predominantly governed by the oligosaccharide glycoprotein backbone of its structure.[187] Similar approaches have been utilised for protection of model membrane systems.[52, 131] The lipid bilayer in solution could be considered the periciliary layer and protective coatings act as the gel layer on top.

The protection of tBLM systems utilising coatings has briefly been investigated in the past using hydrogels by using impedance spectroscopy to measure the impedance of a bilayer sample after addition of a hydrogel, and then after dehydrating and rehydrating On addition of a poly(NIPAAM) hydrogel to the bilayer an initial decrease in impedance was observed before some recovery. The hydrogel structure was also able to retain some moisture after removal of the membrane from solution. After 24 hours the membrane's electrical sealing properties were intact when resubmerged, however impedance had decreased.[131]

This avenue requires a greater degree of exploration, however, as the results were limited to very few samples, and the membranes utilised not of high electrical sealing quality compared to what is possible with highly tethered BLM systems. The timeframe of drying out before rehydration was also limited to only 24 hours. In further development of bilayers for use in a biosensor-based application, it would be important to look at the effect of longer timeframes. There was also no investigation as to how the presence of a coating may affect the ability of ionophores to embed within a membrane and functional successfully. If a coating is able to protect a lipid bilayer but decreases its ability to function properly as a means of investigating ion channels or other molecules inserted into the bilayer, then that greatly limits the coating's scope of use.

The stability of tBLMs is naturally favourable compared to other systems such as BLMs or alternative SLBs[129], so it was thought that as long as a coating does not directly decrease the functionality of a tBLM, it should be able to enhance its ability to withstand the dehydration process without proving an impediment to further experiments.

The first part of this chapter focuses on the effects that drying out and then rehydrating tBLMs has on their structure, as determined through electrochemical impedance spectroscopy measurements. Experiments were performed with bilayers of varying tethering density.

The second part of this chapter describes the effects of the addition of polyelectrolytes to the electrolyte solution before drying out and rehydrating of tBLMs of varying tethering densities.

The final part of this chapter focuses on how the incorporation of cholesterol into tBLMs to increase their complexity and realism effects their recovery and function after being dried out and rehydrated.

It is important to note that the level of initial impedance between each of the bilayer samples was variable even at the same tethering density. This can make it difficult to show statistically significant differences between different sample types. As such, measurements across a series of different membrane samples were analysed in a semi-quantitative manner to determine general trends at different tethering densities for each of the studies showcased throughout this chapter. Such forms of tBLM sample analysis are not unique to this thesis, as variance between bilayer samples is a common factor that must be considered in studies of bilayer stability. This is especially prevalent in studies where bilayers are further analysed after being subjected to addition of molecules such as ionophores that can alter the structure of the bilayer.[131, 133]

The incorporation of functional membrane proteins is an essential parameter for the successful application of a tBLM in any kind of real-world capacity such as for use in biosensors. Thus, it is important to determine the ability of a bilayer to incorporate such proteins to make sure that it could be feasibly used in such scenarios in future cases.

Basic function of tBLMs can thus be assessed by the addition of an ionophore such as valinomycin. The structure of valinomycin resembles a cyclic peptide but can more accurately be described as a depsipeptide due to its alternating amino acid peptide and amino alcohol ester bonds. Inside the ring structure, 12 carbonyl oxygens can chelate a single K^+ ion, with no room for further ions. With an affinity for K^+ 1000 times greater than its affinity for sodium (Na^+) it can effectively transport potassium ions across even highly ordered lipid bilayers. Valinomycin's oily surface readily dissolves in the bilayer, allowing it to transport K^+ down its electrochemical gradient.[190]

The result of this is usually observed as a large decrease in the bilayer resistance and an increase in bilayer capacitance when valinomycin is successfully incorporated in the bilayer and in the presence of potassium ions. Such changes are reversible. An increase in resistance and decrease in capacitance would be expected when potassium ions are replaced in solution by sodium ions as the bilayer regains its resistive qualities.

The results from each section are outlined in table 1, as determined through modelling and analysis of EIS data for numerous tBLM samples. At high levels of tethering density (100%, 80%), there was no clear change in bilayer impedance after being dried out and rehydrated, with functionality to successfully incorporate valinomycin also intact. Addition of polyelectrolytes to these bilayers also did not appear to impede functionality, however it did not noticeably improve long-term bilayer stability either.

At lower levels of tethering density (60%, 40%) there were clear signs of deterioration of bilayer quality after being dried out and rehydrated. The addition of polyelectrolytes to these bilayers was shown to decrease the amount of deterioration that occurred. Extremely low tethering density (10%) bilayers were also investigated, however did not appear suitable for further analysis with poor levels of impedance.

Addition of cholesterol into the formation of bilayers appeared to have minimal change to the quality and functionality of 80%-tethered bilayers even after being dried out and rehydrated. At lower density of tethering (60%) bilayers were not of the same level of impedance as non-cholesterol bilayers with the same tethering density, likely due to the increased effect of cholesterol on membrane fluidity compared to 80%-tethered samples. However, they were still able to show some functionality after drying out and rehydrating.

Table 3-1: Initial electrical sealing quality of DPhyPC bilayers at different DPhyTL tethering lipid densities in the inner leaflet as well as changes in electrical sealing when dried out and rehydrated both with and without the presence of polyelectrolyte coating layers. Addition of 10% cholesterol refers to the percentage of cholesterol making up the DPhyPC lipid solution added to complete the bilayer.

Tethering Density	**Basic Function**	**Rehydration + Valinomycin**	**Polyelectrolyte + Rehydration + Valinomycin**
100%	Excellent	Minimal change	Minimal change
80%	Good	Minimal change	Minimal change
60%	Good	Deterioration	Minimal change
40%	Poor	Deterioration	Minimal change
10%	Unusable	N/A	N/A
80% (+ 10% cholesterol)	Good	Minimal change	N/A
60% (+ 10% cholesterol)	Poor	Minimal change	N/A

3.2 Methods

3.2.1 Standard EIS Methods

For all experiments in this chapter bilayers were formed using DPhyTL as the anchorlipid which also made up the inner leaflet of the bilayer. For tethering densities below 100% 2-mercaptoethanol was used as a spacer lipid. The outer leaflet for each bilayer was made using DPhyPC lipid. For 100% tethering density vesicle extrusion was used to form the outer leaflet. For all other tethering densities rapid solvent exchange was used. Both methods are outlined above in chapter 2.5.1.

For verification of basic function, bilayers were initially formed using the methods described in chapter 2.5.1. Initial EIS measurements were made in 100 mM NaCl solution, before the addition of 5 µl valinomycin solution (1 mg/ml in EtOH). For ion transport measurements, bilayers were left for 1-2 hours after valinomycin addition to allow for the peptide to incorporate into the bilayer. To test valinomycin incorporation and ion transport function, EIS measurements of bilayer samples were then taken in alternating 100 mM NaCl and 100 mM KCl solution. The bilayer was flushed with 5 cell volumes of the corresponding 100 mM salt solution before each measurement.

To investigate the effects of dehydration and rehydration, bilayers were again formed using the methods described in chapter 2.5.1. After taking initial EIS measurements of the bilayer samples in 100 mM NaCl solution, the solution was then drained from the samples, and the samples were left for 4 days to dry out in air, mimicking a potential biosensor environment.

Following the 4-day drying period bilayers were rehydrated in 100 mM NaCl and a further EIS measurement taken after 1 hour post-rehydration. After this, their basic function was tested with the incorporation of 5 µl valinomycin solution as for basic function testing.

3.2.2 Neutron Reflectometry Methods

For each bilayer, 3 different measurements were taken in 3 different solvent mixtures to fully characterise the membranes. These mixtures were D_2O, H_2O and a mixture of D_2O and H_2O designed to match the SLD of gold, CM 4.5.

After obtaining an initial rough fit using differential evolution modelling, final values and errors were modelled using a Monte Carlo Markov Chain multisampling algorithm with 10000 steps, 200 walkers and burning and thinning by 400. For both bilayers, these measurements were performed for an initial bilayer profile, as well as after dehydrating and rehydrating the bilayers. Bilayers were dehydrated by pumping nitrogen gas into the wet cells that made up the bilayer to replace 100 mM NaCl solution and left for 2 days before being rehydrated for final measurements. Only 2 days of dehydration were possible due to unforeseen neutron beamtime restrictions.

3.2.3 Polyelectrolyte Methods

Polyelectrolyte solutions were made using 10 mg/ml polyelectrolyte from bulk solution in a 10 mM NaCl solution. Bulk polyelectrolyte solutions were 35 wt. % in H_2O PDADMAC (Sigma-Aldrich, Australia) (average M_w < 100 000) and 30 wt. % in H_2O PSS (Sigma-Aldrich, Australia) (average M_w ~ 70 000).

Initially DPhyPC bilayers were formed at 80, 60 and 40% tethering density using previously described methods and measuring with EIS before addition of polyelectrolytes. Further EIS measurements were made after addition of each of three layers of PDADMAC, PSS and a second layer of PDADMAC, with 3 ml of each polyelectrolyte solution flushed through the sample environment. After measurement of the third layer of polyelectrolyte, samples were dried as described previously and left for a period of 4 days. Upon rehydration measurements were made in the same form as in 3.2.1. For each tethering density measurements were also made of bilayers with valinomycin incorporated after polyelectrolyte addition both with and without the rehydration process. This was done to determine any effects the presence of polyelectrolyte might have on incorporation of other compounds into the membrane, and to verify that bilayers retained functionality after rehydration with polyelectrolyte addition.

3.2.4 Cholesterol Incorporation Methods

Cholesterol was incorporated into DPhyPC tBLMs during the formation of the outer leaflet. With monolayer formation proceeding as described previously, 10% w/w of the DPhyPC in the rapid solvent exchange solutions was replaced with cholesterol.

3.3 Effect of Dehydration and Rehydration on DPhyPC Lipid Bilayers

For the experiments involved in this sub-chapter, bilayers were formed using DPhyPC as well as different tethering densities of DPhyTL. For each tethering density of DPhyTL, the remainder of the tethering solution was made up to 0.2 mM with 2-mercaptoethanol as a spacer molecule to compete with DPhyTL for space on the gold substrate. As outlined in figure 3-2, the experimental process for each bilayer sample involved a 2-day formation of the bilayer, with measurements occurring over the following 2-3 days. For bilayers that were dried out and then rehydrated after 4 days, this extended the process to 8-9 days.

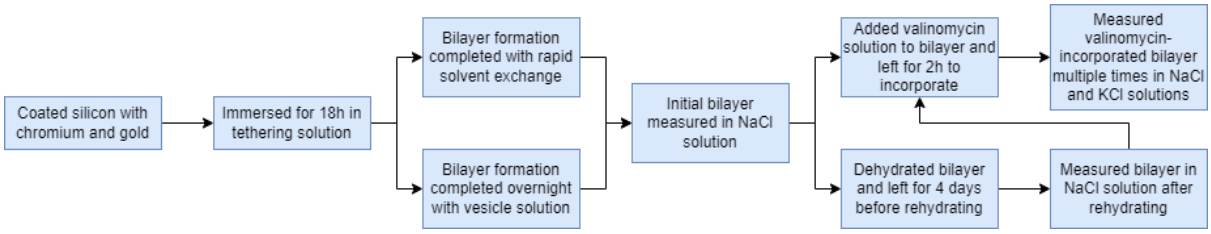

Figure 3-2: Flow diagram of the experimental steps involved in bilayer formation and impedance measurement throughout sub-chapter 3.3.

5 different tethering densities were utilised – 100%, 80%, 60%, 40% and 10%. For study in fields such as ion channels, membrane impedance of at least 1 MΩ is desirable. The use of 100%-tethered bilayers was primarily as a baseline of the highest quality bilayers that could be achieved and analysed. However, decreased tethering creates a more realistic membrane environment and so is of more significant interest. The use of tethering densities between 40-80% was hence also implemented. At this

level of tethering density not all types of tBLM are able to be formed to adequate electrical sealing quality.

Notably, bacterial analogues such as LPS-based tBLMs have not produced promising results at tethering densities of 60%, however this has not been an issue for exclusively DPhyPC-based bilayers.[137] Alternative tBLM systems have produced bilayers with tethering densities as low as 1-10%.[191] Investigations of a 10%-tethered DPhyPC bilayer were hence also investigated here to provide a lower bound for the experiments shown in this chapter.

3.3.1 100%-Tethered Lipid Bilayers

Fully tethered DPhyPC bilayers tend to be of exceptionally high electrical sealing quality, so the basic function of these bilayers would be expected to be exceptional. This is due to the high level of anchoring between the gold substrate and the DPhyTL lipid making up the inner leaflet of the bilayer. Previous studies have found that such tethering set ups can produce bilayers with resistance modelled at up to gigaohm levels with DPhyPC in the outer leaflet[129], so the initial bilayers producing resistances of tens of megaohms is not surprising and indeed expected.

Initial formation of 100% tethered DPhyTL bilayers involves the use purely of the DPhyTL anchorlipid in the inner leaflet with no addition of spacer lipids (figure 3-3). Vesicle extrusion of DPhyPC can be used for these samples as there is no requirement for DPhyPC to fill any of the inner leaflet, so the vesicles breaking open to form the outer leaflet is satisfactory to form a high electrically sealing bilayer with strong resistance and capacitance.

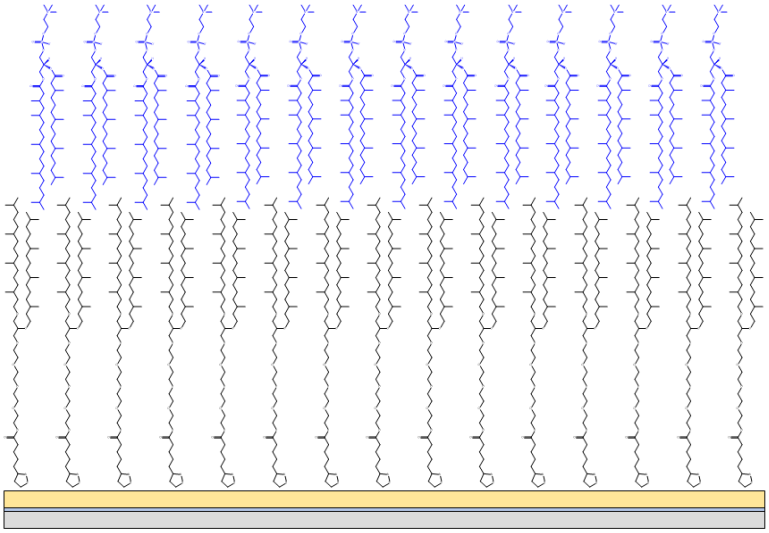

Figure 3-3: Schematic of the lipid composition of a 100% tethered DPhyPC tBLM. The tethering DPhyTL anchorlipid (back) also makes up the initial monolayer, whilst DPhyPC (blue) then forms the outer leaflet of the bilayer on top.

To determine the structural qualities of the resulting bilayers they are analysed utilising EIS with the resulting data fitted using an equivalent circuit with resistive and capacitive components. For high quality bilayers with modelled resistances of greater than a couple of megaohms it is usually sufficient to use model A from chapter 2.2. The high level of bilayer resistance means that an additional capacitive element is not necessary as the sub-membrane spacing region is not visible in the frequency spectrum that the measurements are taken in.

Initial measurements of 100% tethered DPhyPC bilayers showed results consistent with literature, providing resistances greater than 10 MΩcm^2 for most bilayer samples (figure 3-4). Capacitance values of lower than 1 µFcm^{-2} are also consistent with these results.[131]

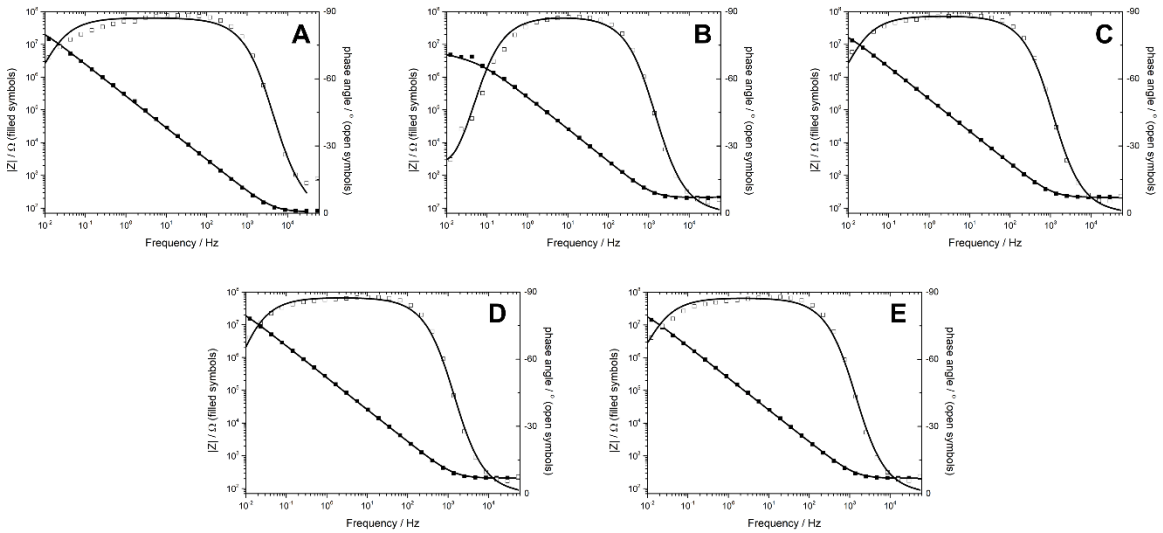

Sample	Impedance (MΩcm^2)	Capacitance (μFcm^{-2})
Bilayer 100% 1	30 ± 3	0.84 ± 0.03
Bilayer 100% 2	5.9 ± 0.2	0.86 ± 0.02
Bilayer 100% 3	23 ± 2	1.1 ± 0.03
Bilayer 100% 4	35 ± 1	0.81 ± 0.01
Bilayer 100% 5	25 ± 2	0.96 ± 0.03

Figure 3-4: Bode plots of impedance (closed squares) and phase angle (open squares) for five different 100% tethered DPhyPC bilayer samples in 100 mM NaCl. Table shows impedance and capacitance values of the lipid bilayers. Data and errors were determined using the ZView equivalent circuit fitting tool and only fitted data relevant to the lipid bilayer is shown.

When valinomycin was initially added to the membranes a slight decrease in resistance was modelled, however at high levels of impedance a change from 30 to 22 MΩcm^2 is not especially large (figure 3-5). When modelling high levels of impedance above 10 MΩcm^2 slight changes in modelling at low frequency can result in sizeable changes in resistance. Observing figure 3-5 there is very little change in the data itself. However, it is also sometimes the case that addition of valinomycin on its own can lead to a decrease in bilayer impedance. This is potentially due to minor disruption of the bilayer by valinomycin itself, or the presence of traces of K^+ ions left in the valinomycin.[127]

Exchange of electrolyte solution from NaCl to KCl provided a decrease in bilayer resistance from 22 to 8 MΩcm^2, which represents a notable decrease to just over ¼ the resistance of the initial bilayer.

This, as well as the return to almost the same level of impedance as the initial bilayer when solution was exchanged for NaCl again, suggests that valinomycin was successfully incorporated into the lipid bilayer. This process can be repeated multiple times in a stable lipid bilayer and indeed further cycling followed a similar trajectory of impedance changes.

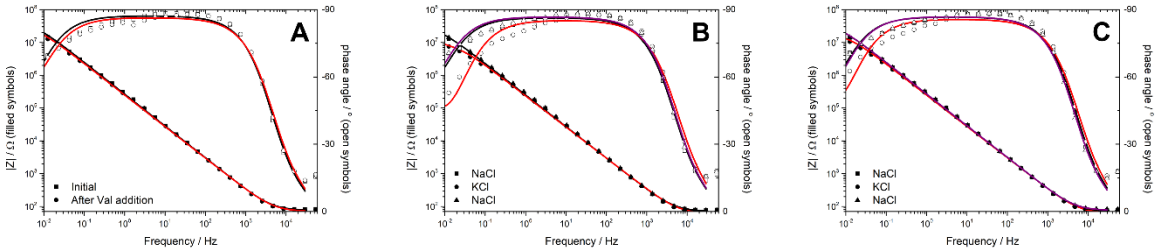

Bilayer 100% 1	Impedance (MΩcm^2)	Capacitance (μFcm^{-2})	Change in Impedance
Initial Bilayer	30 ± 3	0.84 ± 0.03	
After Val Addition	22 ± 2	0.91 ± 0.03	-27%
KCl	8.0 ± 0.5	0.88 ± 0.02	-73%
NaCl	26 ± 2	0.86 ± 0.03	-13%
KCl	15 ± 1	0.85 ± 0.02	-50%
NaCl	27 ± 2	0.83 ± 0.02	-10%

Figure 3-5: Bode plots of impedance (closed shapes) and phase angle (open shapes) for a 100% tethered DPhyPC bilayer sample. A) Before (black) and after (red) addition of valinomycin. B & C) Cycling electrolyte twice consecutively between NaCl (black), KCl (red) and NaCl (purple) with valinomycin incorporated. Table shows impedance and capacitance values of the lipid bilayer. Also shown is percentage difference between each impedance value and the initial bilayer impedance.

Rehydration of lipid bilayers involved removal of the NaCl electrolyte, before leaving the samples for a period of four days for complete dryness to occur. For fully tethered samples, it would be assumed that barring any additional disruption the monolayer would be able to maintain its full integrity as the surface binding between gold and sulphur groups is independent of the presence of electrolyte solution. However, the secondary layer of DPhyPC lipids is initially self-assembled due to the amphiphilic interactions between the head and tail sections of the lipids with water. Thus, it could be assumed that there would be some degree of structural deterioration in the outer leaflet from removal of electrolyte solution.

This did not eventuate however, with fully tethered samples showing minimal change in bilayer quality (figure 3-6). This could be due to several factors such as the hydrophobic interactions and packing density between lipids being strong enough to counteract a lack of electrolyte solution or due to interactions between lipids and the outer wall of the bilayer samples creating anchoring points for the lipids. It is also possible that lipids disorganised themselves from the outer leaflet but were then able to re-assemble to the same level of packing density and charge insulation when electrolyte solution was re-added to the sample.

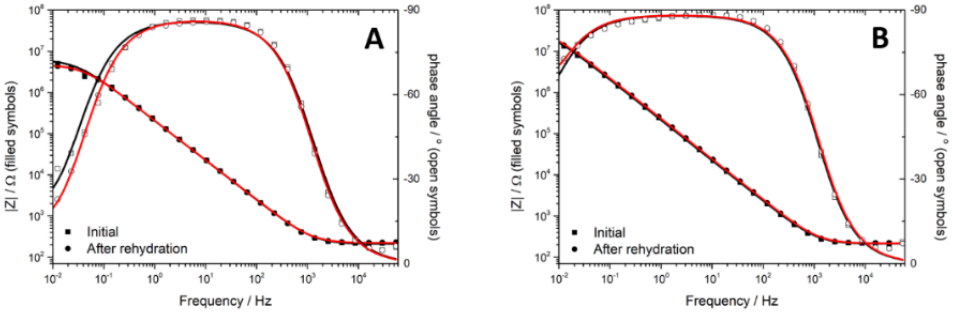

		Impedance (MΩcm^2)	Capacitance (μFcm^{-2})	Change in Impedance
Bilayer 100% 2	**Initial**	5.9 ± 0.2	0.86 ± 0.02	
	After Rehydration	4.5 ± 0.2	0.84 ± 0.02	-24%
Bilayer 100% 3	**Initial**	23 ± 2	1.1 ± 0.03	
	After Rehydration	18 ± 1	1.2 ± 0.03	-22%

Figure 3-6: Bode plots of impedance (closed shapes) and phase angle (open shapes) for two different 100% tethered DPhyPC bilayer samples before (black) and after (red) drying out over a period of four days and rehydrating before allowing them to sit for an hour prior to measurement. Table shows impedance and capacitance values of the lipid bilayers. Also shown is percentage difference between each impedance value and the initial bilayer impedance.

As with samples used without drying and rehydrating valinomycin was shown to have no major effect on the quality of membrane bilayers, with change in impedance less than ¼ and not observable on the modelled data (figure 3-7). Exchange of electrolyte solution from NaCl to KCl showed a noticeable change in the recorded data points and a decrease in modelled bilayer impedance up to around 90% in both samples to below 10 MΩcm^2. Most of this change was also observed to be reversible with an increase back up to above 20 MΩcm^2 for all measured samples.

The main difference between the two sample types was that the rehydrated samples showed slightly more of an increase in capacitance when in KCl solution.

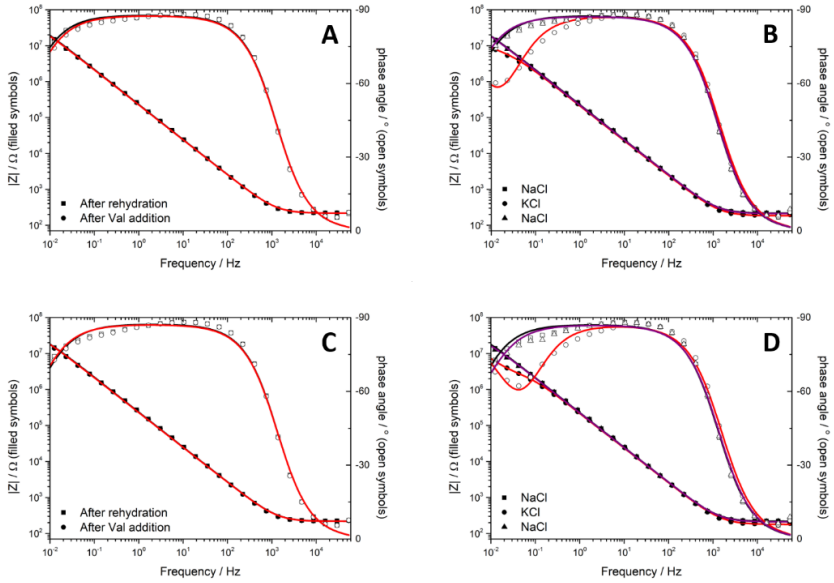

		Impedance ($M\Omega cm^2$)	Capacitance ($\mu F cm^{-2}$)	Change in Impedance
Bilayer 100% 4	**Initial**	35 ± 1	0.81 ± 0.01	
	After Rehydration	48 ± 4	0.95 ± 0.03	
	After Val Addition	41 ± 3	0.97 ± 0.03	-15%
	KCl	5.6 ± 0.3	1.1 ± 0.03	-88%
	NaCl	53 ± 6	0.94 ± 0.03	$+10\%$
Bilayer 100% 5	**Initial**	25 ± 2	0.96 ± 0.03	
	After Rehydration	31 ± 2	0.95 ± 0.02	
	After Val Addition	36 ± 3	0.94 ± 0.03	$+16\%$
	KCl	1.7 ± 0.2	1.3 ± 0.07	-95%
	NaCl	23 ± 2	1.0 ± 0.03	-26%

Figure 3-7: Bode plots of impedance (closed shapes) and phase angle (open shapes) for two different 100% tethered DPhyPC bilayer samples. A & C) Before (black) and after (red) addition of valinomycin. B & D) Cycling electrolyte between NaCl (black), KCl (red) and NaCl (purple) with valinomycin incorporated. Table shows impedance and capacitance values of the lipid bilayers. Also shown is percentage difference between each impedance value and the initial bilayer impedance after rehydration.

The results suggest that for fully tethered systems it is possible to temporarily remove the electrolyte solution without compromising the quality or function of the bilayer. Fully tethered bilayers are highly stable systems especially in the inner leaflet.

However, this stability is not realistic to the qualities of membranes found in biological species, and it can be difficult to fully incorporate many proteins and other molecules into them due to the heavily anchored tethering region below the inner leaflet, so investigating more realistic sparsely tethered bilayers is of importance.[126, 136]

3.3.2 80%-Tethered Lipid Bilayers

The use of 2-mercaptoethanol in the tethering solution allows for the formation of tBLMs with lower densities of DPhyTL tethering. This is due to the SH groups on 2-mercaptoethanol and the disulphide component of DPhyTL entering a competitive adsorption process with the gold surface, creating less space for DPhyTL. This likely results in a more fluid inner leaflet of the bilayer as some DPhyPC from the outer leaflet becomes a part of the inner leaflet potentially either through the initial assembly process or by being able to flip and fill in the spaces created (figure 3-8). As DPhyPC is not anchored to the substrate it is able to move around more, creating an environment more realistic to a biological membrane where phospholipids shift around constantly.[4]

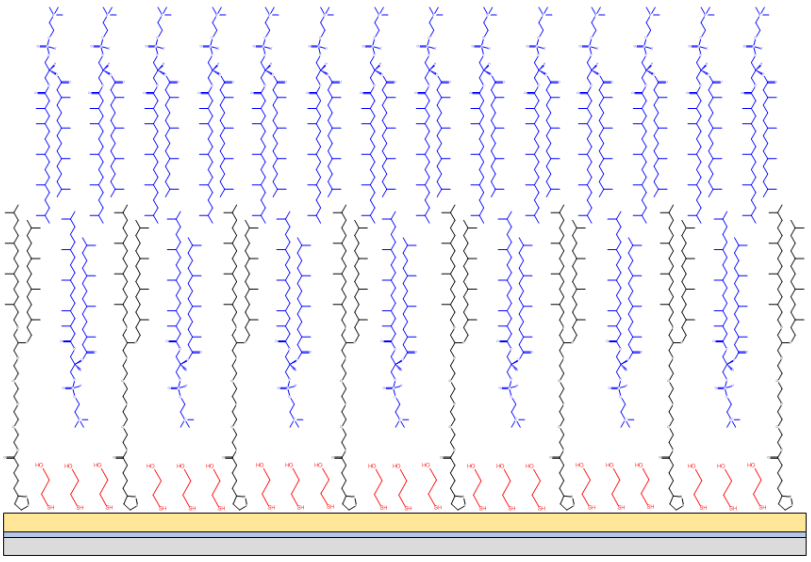

Figure 3-8: Schematic of the lipid composition of an 80% tethered DPhyPC tBLM. The tethering DPhyTL anchorlipid (black) also makes up the initial monolayer, whilst DPhyPC (blue) then forms the outer leaflet of the bilayer on top as well as filling in spaces in the initial monolayer. The spaces are caused by the presence of 2-mercaptoethanol (red) adhering to the gold surface.

A decreased density of tethering also results in lower impedance and higher capacitance for sparsely tethered bilayers, with decreasing stability as tethering density decreases. Whilst monolayers of DPhyTL for all bilayer samples were formed using the same methodology, bilayers with 80% tethering density and below were formed using rapid solvent exchange instead of vesicle fusion for self-assembly of the outer leaflet. It is more effective than vesicle fusion for allowing some DPhyPC to flip and fill spaces in the inner leaflet of the membrane left by the decreased DPhyTL content present due to lower tethering density.[192] This is due to the greater intensity of the transfer event from ethanol to ionic water solvent as compared to the slow process of vesicle fusion. Rapid solvent exchange is a much quicker process than vesicle fusion, which requires vesicles to be left for 16-20 hours on the surface of the monolayer. In comparison, rapid solvent exchange can be performed within a one-hour period and is ideal for lipids with low steric bulk such as DPhyPC.

It was found that the initial impedance of bilayers formed using tethering densities below 100% was more inconsistent. For 80% tethered bilayers the formation of stable systems was still achievable, however initial impedance modelling ranged from between 0.5-10 $M\Omega cm^2$, with capacitance trending slightly higher than fully tethered bilayers (figure 3-9). The inconsistency in initial impedance between samples makes taking the average results from a variety of different bilayers very difficult to do. Thus, it is more informative to observe overall trends in the modelled results rather than the specific numbers themselves.

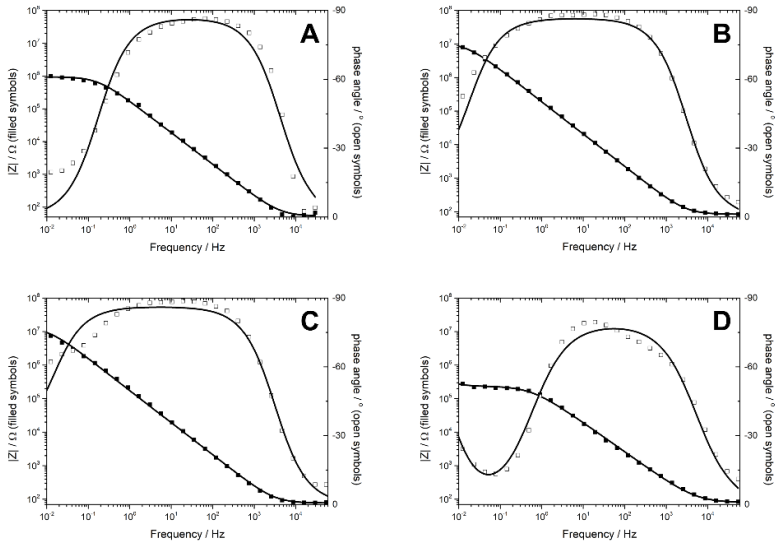

Sample	Impedance (MΩcm^2)	Capacitance (μFcm^{-2})
Bilayer 80% 1	0.94 ± 0.05	0.99 ± 0.05
Bilayer 80% 2	10 ± 0.5	0.94 ± 0.02
Bilayer 80% 3	12 ± 0.9	1.1 ± 0.04
Bilayer 80% 4	0.24 ± 0.006	1.4 ± 0.05

Figure 3-9: Bode plots of impedance (closed squares) and phase angle (open squares) for four different 80% tethered DPhyPC bilayer samples in 100 mM NaCl. Table shows impedance and capacitance values of the four different DPhyPC lipid bilayers.

Addition of valinomycin to partially tethered samples can sometimes cause a sizeable change in bilayer resistance due to the presence of some potassium ions as mentioned previously. However, a large decrease and subsequent recovery when exchanging between NaCl and KCl electrolyte is a clear indicator that a bilayer is functioning properly. An example of this can be seen in figure 3-10. Addition of valinomycin resulted in a small increase in bilayer resistance initially from 0.94 to 2.4 MΩcm^2. However, when solvent was exchanged from NaCl to KCl a decrease of several orders of magnitude was observed and modelled, with a large dip in phase angle and impedance clearly observable. This was fully reversible on return to NaCl solvent with impedance returning to the MΩcm^2 level.

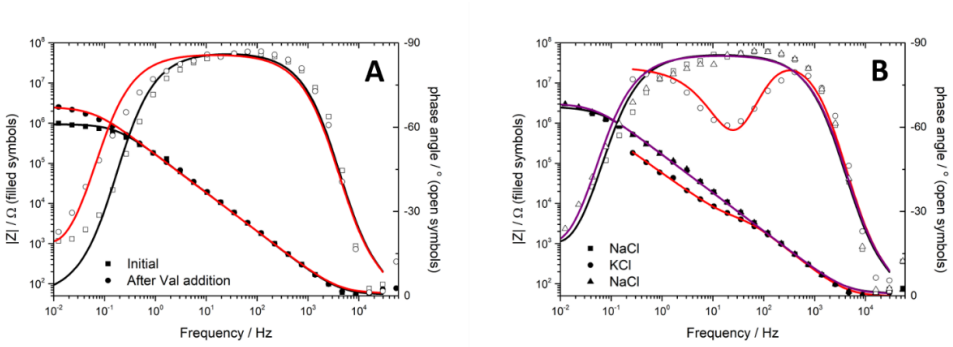

Bilayer 80% 1	Impedance (MΩcm^2)	Capacitance (μFcm^{-2})	Change in Impedance
Initial Bilayer	0.94 ± 0.05	0.99 ± 0.05	
After Val Addition	2.4 ± 0.3	1.1 ± 0.05	$+155\%$
KCl	0.0024 ± 0.0005	0.85 ± 0.2	-99.7%
NaCl	2.9 ± 0.5	1.1 ± 0.07	$+209\%$

Figure 3-10: Bode plots of impedance (closed shapes) and phase angle (open shapes) for an 80% tethered DPhyPC bilayer sample. A) Before (black) and after (red) addition of valinomycin. B) Cycling electrolyte between NaCl (black), KCl (red) and NaCl (purple) with valinomycin incorporated. Table shows impedance and capacitance values of the lipid bilayer. Also shown is percentage difference between each impedance value and the initial bilayer impedance.

Whilst rehydration of fully tethered bilayer models resulted in minimal change in sealing quality and functionality, this was not always the case with the 80% tethered models (figure 3-11). One sample saw a decrease in resistance from 10 to 1 MΩcm^2, however the other two showed very little difference in sealing quality. Interestingly this does not suggest any correlation between the initial quality of the bilayer and how effectively it will maintain its quality on drying out and rehydration, as bilayers 3 and 4 had quite different initial impedance but were both able to maintain sealing quality through the rehydration process.

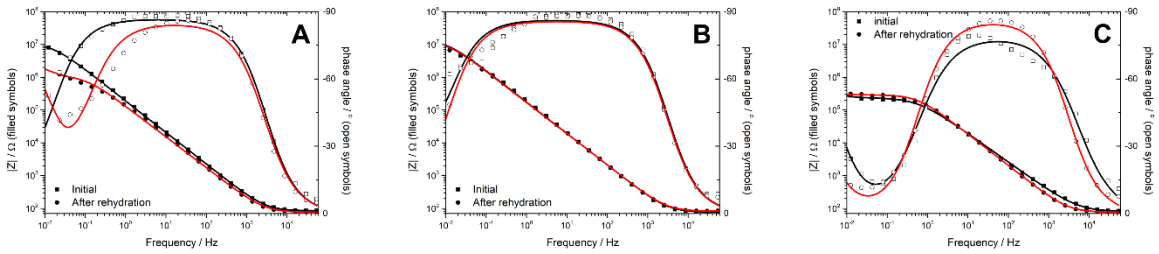

	Sample	Impedance ($M\Omega cm^2$)	Capacitance ($\mu F cm^{-2}$)	Change in Impedance
Bilayer 80% 2	**Initial**	10 ± 0.5	0.94 ± 0.02	
	After Rehydration	0.98 ± 0.08	1.5 ± 0.08	-90%
Bilayer 80% 3	**Initial**	12 ± 0.9	1.1 ± 0.04	
	After Rehydration	13 ± 0.5	1.0 ± 0.02	$+8.3\%$
Bilayer 80% 4	**Initial**	0.24 ± 0.006	1.4 ± 0.05	
	After Rehydration	0.29 ± 0.006	1.0 ± 0.03	$+21\%$

Figure 3-11: Bode plots of impedance (closed shapes) and phase angle (open shapes) for three different 80% tethered DPhyPC bilayer samples before (black) and after (red) drying out over a period of four days and rehydrating before allowing them to sit for an hour prior to measurement. Table shows impedance and capacitance values of the lipid bilayers. Also shown is percentage difference between each impedance value and the initial bilayer impedance.

Further variation between sample sets occurred when valinomycin was introduced and subsequent exchanging of electrolyte solutions was performed. Addition of valinomycin to bilayer 80% 2, which had already had a strong decrease in impedance following the rehydration process, resulted in a further drop from 0.98 $M\Omega cm^2$ to only 3.6 $K\Omega cm^2$ (figure 3-12). There was also a noticeable increase in capacitance of this sample both after rehydration and after exchange of solvent that was only partially reversible. This increase in capacitance is suggestive of an increase in the hydration of the membrane, which could be expected in a membrane with decreased sealing properties and suggests a degree of damage to the membrane. Exchange of electrolyte to KCl showed that there was still a decrease in impedance from 3.6 to 1.1 $K\Omega cm^2$, and recovery to a slightly higher level of resistance when solvent was exchanged to NaCl, however this sample was clearly no longer a high-quality bilayer.

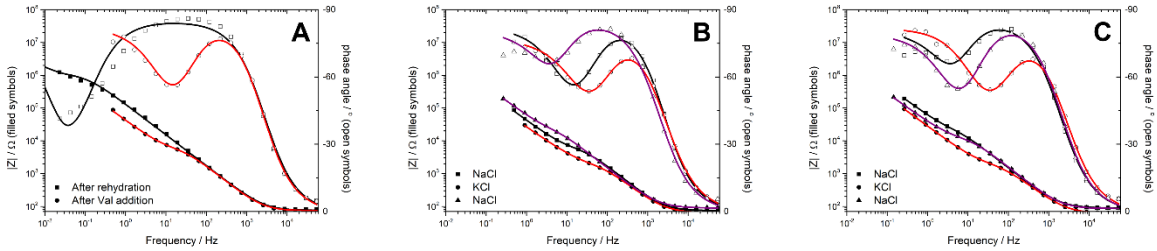

Bilayer 80% 2	Impedance (MΩcm^2)	Capacitance (μFcm^{-2})	Change in Impedance
Initial Bilayer	10 ± 0.5	0.94 ± 0.02	
After Rehydration	0.98 ± 0.08	1.5 ± 0.08	
After Val Addition	0.0036 ± 0.0002	1.5 ± 0.1	-99.6%
KCl	0.0011 ± 0.00005	2.1 ± 0.1	-99.9%
NaCl	0.0090 ± 0.002	2.2 ± 0.3	-99.1%
KCl	0.0013 ± 0.00005	2.6 ± 0.2	-99.9%
NaCl	0.0073 ± 0.0004	1.6 ± 0.1	-99.3%

Figure 3-12: Bode plots of impedance (closed shapes) and phase angle (open shapes) for a rehydrated 80% tethered DPhyPC bilayer sample. A) Before (black) and after (red) addition of valinomycin. B & C) Cycling electrolyte twice consecutively between NaCl (black), KCl (red) and NaCl (purple) with valinomycin incorporated. Table shows impedance and capacitance values of the lipid bilayer. Also shown is percentage difference between each impedance value and the bilayer impedance after rehydration.

In the case of bilayer 80% 3, introduction of valinomycin also caused a decrease in membrane resistance, from 13 MΩcm^2 to 0.18 MΩcm^2 (figure 3-13). However, this was still multiple orders of magnitude above the impedance that the first bilayer sample dropped to. Swapping to KCl electrolyte produced a further 100 times drop in bilayer resistance to a similar level seen in bilayer 80% 2, however in this instance returning to NaCl electrolyte showed a far greater degree of recovery to 2.8 MΩcm^2, suggesting that this bilayer was able to incorporate valinomycin successfully whilst still retaining reasonable electrical sealing properties after drying out and rehydrating. There was also minimal change in the membrane capacitance unlike the previous bilayer, suggesting that its hydration and lipid packing was not heavily affected.

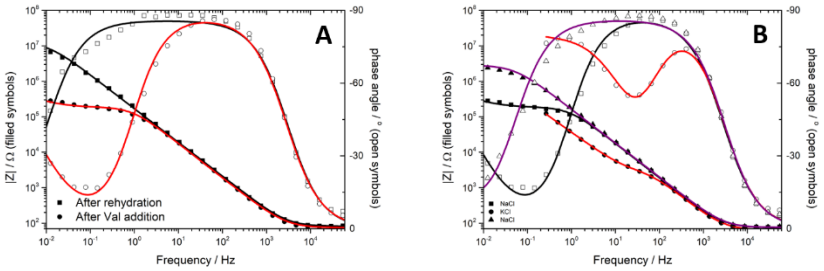

Bilayer 80% 3	Impedance (MΩcm^2)	Capacitance (μFcm^{-2})	Change in Impedance
Initial Bilayer	12 ± 0.9	1.1 ± 0.04	
After Rehydration	13 ± 0.5	1.0 ± 0.02	
After Val Addition	0.18 ± 0.006	1.0 ± 0.04	-99.3%
KCl	0.0019 ± 0.0002	1.3 ± 0.2	-99.99%
NaCl	2.8 ± 0.1	1.1 ± 0.03	-78%

Figure 3-13: Bode plots of impedance (closed shapes) and phase angle (open shapes) for a rehydrated 80% tethered DPhyPC bilayer sample. A) Before (black) and after (red) addition of valinomycin. B) Cycling electrolyte between NaCl (black), KCl (red) and NaCl (purple) with valinomycin incorporated. Table shows impedance and capacitance values of the lipid bilayer. Also shown is percentage difference between each impedance value and the bilayer impedance after rehydration.

Addition of valinomycin to bilayer 80% 4 after drying out and rehydration saw minimal change in the quality of the bilayer (figure 3-14). In fact, a small increased was observed from 0.29 to 0.5 MΩcm^2. Exchange of solvent between NaCl and KCl showed two magnitudes of decrease whilst KCl was present, with full recovery of the bilayer's resistance on return to NaCl electrolyte through multiple solvent cycles.

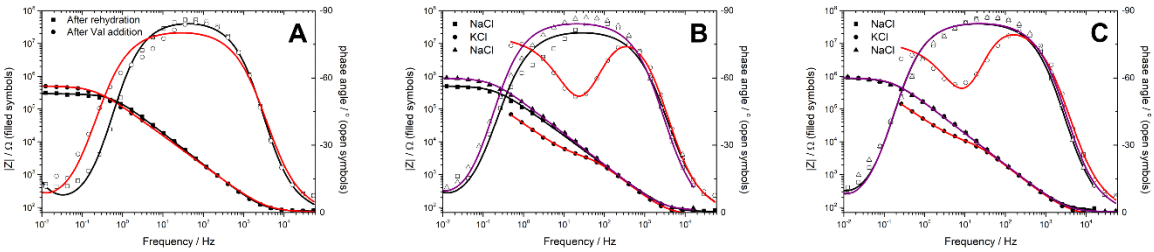

Bilayer 80% 4	Impedance (MΩcm^2)	Capacitance (μFcm^{-2})	Change in Impedance
Initial Bilayer	0.24 ± 0.006	1.4 ± 0.05	
After Rehydration	0.29 ± 0.006	1.0 ± 0.03	
After Val Addition	0.50 ± 0.02	1.5 ± 0.06	$+72\%$
KCl	0.0024 ± 0.0001	1.2 ± 0.1	-99.2%
NaCl	0.84 ± 0.04	1.1 ± 0.04	$+190\%$
KCl	0.0056 ± 0.0007	1.1 ± 0.2	-98%
NaCl	0.87 ± 0.04	1.1 ± 0.04	$+200\%$

Figure 3-14: Bode plots of impedance (closed shapes) and phase angle (open shapes) for a rehydrated 80% tethered DPhyPC bilayer sample. A) Before (black) and after (red) addition of valinomycin. B & C) Cycling electrolyte twice consecutively between NaCl (black), KCl (red) and NaCl (purple) with valinomycin incorporated. Table shows impedance and capacitance values of the lipid bilayer. Also shown is percentage difference between each impedance value and the bilayer impedance after rehydration.

The results here suggest that whilst in some cases it is possible for the drying out and rehydration process to cause some change in bilayer quality, it is possible for partially tethered bilayer systems to recover enough to have functionality with antibiotics like valinomycin. Comparing the functionality of the bilayers that were and were not subject to the rehydration process it appears that the rehydrated bilayers are potentially less stable than the initial bilayers as the effects of valinomycin addition were generally more pronounced, however the ability for most bilayers to recover after multiple solvent cycles was highly encouraging.

3.3.3 60%-Tethered Lipid Bilayers

Lower densities of tethering were achieved by increasing the ratio of 2-mercaptoethanol to DPhyTL during the tethering process. A lower density of tethering can increase the space under the inner bilayer leaflet for molecule incorporation, though it will also decrease the stability of the bilayer. With less DPhyTL present even more of the inner leaflet will be made up of DPhyPC. Initial measurements of DPhyPC bilayers showed similar levels of resistance to 80% tethered samples, and in some cases higher, but with an increase in average capacitance from around 1 μF up to around 1.2 (figure 3-15).

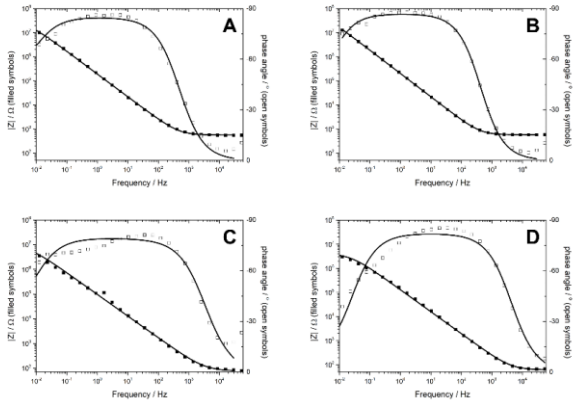

Sample	Impedance (MΩcm^2)	Capacitance (μFcm^{-2})
Bilayer 60% 1	16 ± 2	1.3 ± 0.05
Bilayer 60% 2	54 ± 6	0.83 ± 0.008
Bilayer 60% 3	8.0 ± 2	2.3 ± 0.1
Bilayer 60% 4	3.9 ± 0.2	1.5 ± 0.04

Figure 3-15: Bode plots of impedance (closed squares) and phase angle (open squares) for four different 60% tethered DPhyPC bilayer samples in 100 mM NaCl. Table shows impedance and capacitance values of the four different DPhyPC lipid bilayers.

Similarly, functionality of 60% tethered bilayers with valinomycin incorporated was fully intact (figures 3-16 and 3-17). In these samples there was a decrease in impedance on addition of valinomycin of one order of magnitude. Transition to KCl solvent saw a decrease of 3-4 orders of magnitude, which was reversible on return to NaCl. This is consistent with the functionality shown in 80% tethered samples.

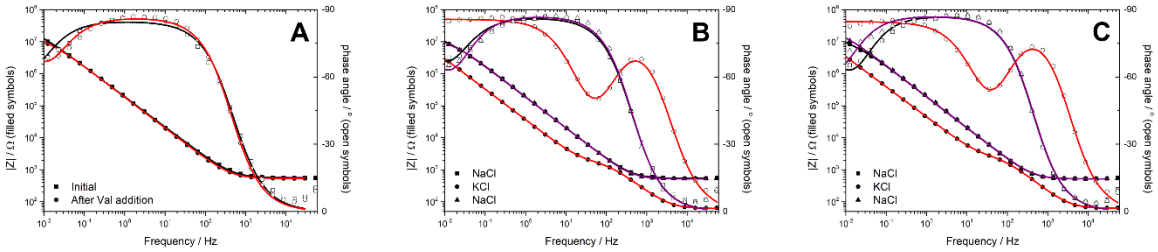

Bilayer 60% 1	Impedance (MΩcm^2)	Capacitance (μFcm^{-2})	Change in Impedance
Initial Bilayer	16 ± 2	1.3 ± 0.05	
After Val Addition	6.1 ± 0.39	1.5 ± 0.03	-62%
KCl	0.0013 ± 0.00003	1.5 ± 0.1	-99.99%
NaCl	4.8 ± 0.8	1.5 ± 0.2	-70%
KCl	0.0018 ± 0.00006	1.3 ± 0.08	-99.99%
NaCl	12 ± 4	1.4 ± 0.4	-25%

Figure 3-16: Bode plots of impedance (closed shapes) and phase angle (open shapes) for a 60% tethered DPhyPC bilayer sample. A) Before (black) and after (red) addition of valinomycin. B & C) Cycling electrolyte twice consecutively between NaCl (black), KCl (red) and NaCl (purple) with valinomycin incorporated. Table shows impedance and capacitance values of the lipid bilayer. Also shown is percentage difference between each impedance value and the initial bilayer impedance.

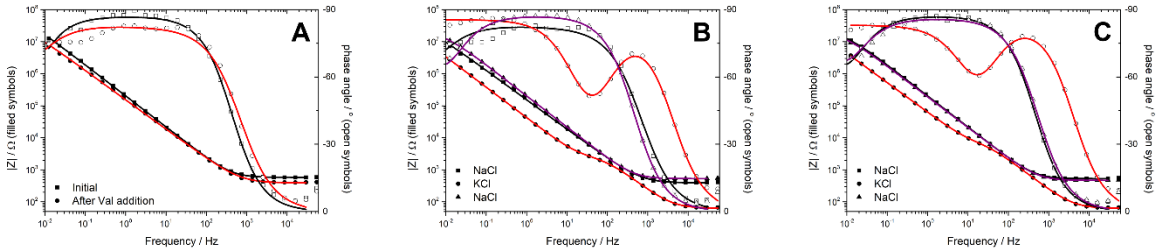

Bilayer 60% 2	Impedance (MΩcm²)	Capacitance (μFcm⁻²)	Change in Impedance
Initial Bilayer	54 ± 6	0.83 ± 0.008	
After Val Addition	15 ± 2	1.8 ± 0.07	-72%
KCl	0.0019 ± 0.00005	1.5 ± 0.09	-99.99%
NaCl	9.6 ± 1	1.3 ± 0.1	-82%
KCl	0.0041 ± 0.0002	1.5 ± 0.07	-99.99%
NaCl	8.2 ± 0.5	1.5 ± 0.03	-85%

Figure 3-17: Bode plots of impedance (closed shapes) and phase angle (open shapes) for a 60% tethered DPhyPC bilayer sample. A) Before (black) and after (red) addition of valinomycin. B & C) Cycling electrolyte twice consecutively between NaCl (black), KCl (red) and NaCl (purple) with valinomycin incorporated. Table shows impedance and capacitance values of the lipid bilayer. Also shown is percentage difference between each impedance value and the initial bilayer impedance.

Rehydration of 60% tethered samples showed a drop of multiple magnitudes of resistance in one sample, whilst a second appeared to be relatively intact with a small increase in impedance (figure 3-18). The drop in resistance of bilayer 60% 3 was much greater than that seen in any of the 80% tethered samples, whilst bilayer 60% 4 was more consistent with the results seen for a majority of the 80% tethered bilayers for which drying out and rehydrating did not appear to cause much deviance in bilayer impedance. Bilayer 60% 3 also had an initially higher level of capacitance than most other samples that increased further after the drying out and rehydrating process which suggests a greater degree of membrane hydration than bilayer 60% 4. It is possible that this influenced the effect that the rehydration process had on the membrane and why it was so different to the second sample.

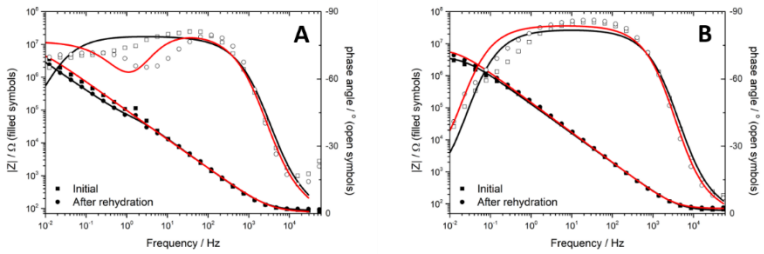

	Sample	Impedance ($M\Omega cm^2$)	Capacitance ($\mu F cm^{-2}$)	Change in Impedance
Bilayer 60% 3	**Initial**	8.0 ± 2	2.3 ± 0.1	
	After Rehydration	0.026 ± 0.009	3.1 ± 0.07	-99.7%
Bilayer 60% 4	**Initial**	3.9 ± 0.2	1.5 ± 0.04	
	After Rehydration	6.5 ± 0.4	1.3 ± 0.04	$+67\%$

Figure 3-18: Bode plots of impedance (closed shapes) and phase angle (open shapes) for two different 60% tethered DPhyPC bilayer samples before (black) and after (red) drying out over a period of four days and rehydrating before allowing them to sit for an hour prior to measurement. Table shows impedance and capacitance values of the lipid bilayers. Also shown is percentage difference between each impedance value and the initial bilayer impedance.

Addition of valinomycin to bilayer 60% 4, which maintained a high level of impedance after rehydration, resulted in an extreme decrease in resistance from 6.5 $M\Omega cm^2$ to only 9.2 $K\Omega cm^2$ (figure 3-19). Whilst this result also occurred for one of the 80% tethered samples, in that case the bilayer had already been impacted by the rehydration process. Swapping between NaCl and KCl solvents was able to show some changes in the impedance. However, there was only recovery back to initial valinomycin-inclusive NaCl levels, and not to anything above that approaching the initial bilayer impedance after rehydration. Increase in capacitance was also observed on addition of valinomycin, however this reverted to initial capacitance after a couple of rinses. This suggests that there was temporary destabilisation of the membrane structure on addition of valinomycin, with some return to a more ordered state shown by the return of the capacitance to its original value.

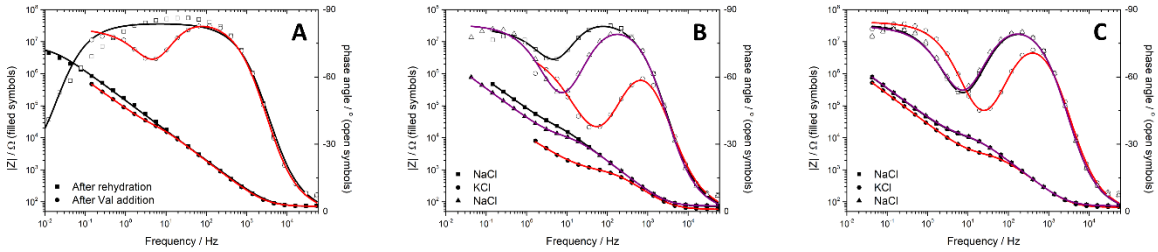

Bilayer 60% 4	Impedance (MΩcm²)	Capacitance (μFcm⁻²)	Change in Impedance
Initial Bilayer	3.9 ± 0.2	1.5 ± 0.04	
After Rehydration	6.5 ± 0.4	1.3 ± 0.04	
After Val Addition	0.0092 ± 0.0008	1.7 ± 0.1	-99.9%
KCl	0.00072 ± 0.00004	1.8 ± 0.02	-99.99%
NaCl	0.0081 ± 0.0003	1.3 ± 0.06	-99.9%
KCl	0.0025 ± 0.00005	1.3 ± 0.06	-99.96%
NaCl	0.0082 ± 0.0003	1.3 ± 0.06	-99.9%

Figure 3-19: Bode plots of impedance (closed shapes) and phase angle (open shapes) for a rehydrated 60% tethered DPhyPC bilayer sample. A) Before (black) and after (red) addition of valinomycin. B & C) Cycling electrolyte twice consecutively between NaCl (black), KCl (red) and NaCl (purple) with valinomycin incorporated. Table shows impedance and capacitance values of the lipid bilayer. Also shown is percentage difference between each impedance value and the bilayer impedance after rehydration.

The results for 60% bilayers suggest that whilst they are still able to recover from the drying out and rehydration process in some cases, it is possible that they are not as able to maintain their structure afterwards with the introduction of further molecules to their structure such as valinomycin. This would limit their functionality as testing or sensing structures after rehydration in comparison to more densely tethered bilayers.

3.3.4 40%-Tethered Lipid Bilayers

At 40% tethering density, the stability of the bilayer is heavily compromised in comparison to fully tethered bilayers. With over half of the gold surface connected to 2-mercaptoethanol instead of DPhyTL, there is a much-decreased number of anchoring points for the bilayer. This means that over half of the inner bilayer leaflet would be made up of DPhyPC that has been introduced during the rapid solvent exchange process. This greater proportion of DPhyPC means a further increase in the fluidity of the tBLM, however it could create difficulty in the bilayers having adequate electrical sealing properties and being resilient against the rehydration process.

For the bilayer samples created and modelled, a low level of initial impedance was observed (figure 3-20). The highest level of initial impedance measured for any of the samples was only 2.5 MΩcm^2 as compared to tens of MΩcm^2 for even the 60% tethered samples. It was also the case that most samples had initial resistances of below 1 MΩcm^2.

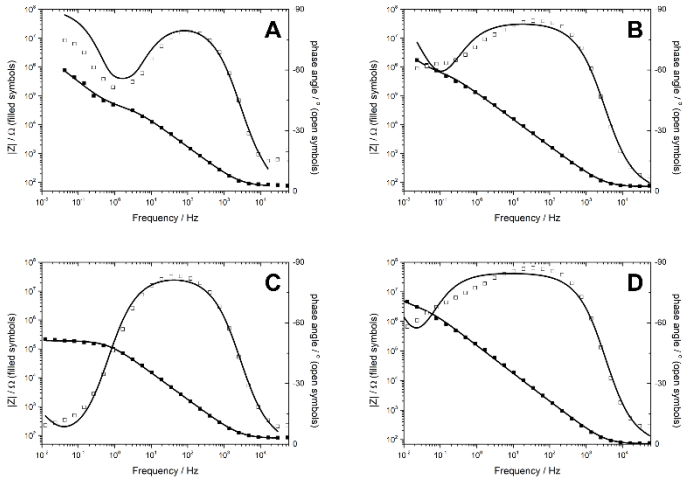

Sample	Impedance (MΩcm^2)	Capacitance (μFcm^{-2})
Bilayer 40% 1	0.035 ± 0.004	1.9 ± 0.2
Bilayer 40% 2	0.51 ± 0.04	1.9 ± 0.08
Bilayer 40% 3	0.19 ± 0.004	1.4 ± 0.04
Bilayer 40% 4	2.5 ± 0.3	1.5 ± 0.2

Figure 3-20: Bode plots of impedance (closed squares) and phase angle (open squares) for four different 40% tethered DPhyPC bilayer samples in 100 mM NaCl. Table shows impedance and capacitance values of the four different lipid bilayers.

For bilayer 40% 1 and bilayer 40% 2, a 1-2 magnitude decrease in resistance was observed on addition of valinomycin (figures 3-21 and 3-22). For bilayer 40% 1 a further decrease in resistance was observed when switching to KCl from NaCl, however return to NaCl showed recovery back to the bilayer's initial impedance level with repeated washes continuing this trend. For bilayer 40% 2 this was not the case as impedance level did not recover to that of the initial bilayer, however there was still an overall recovery after multiple washes to an impedance one magnitude higher than on the initial addition of valinomycin.

The low levels of impedance observed throughout these sample suggest that the 40% tethered bilayer samples were not as resilient or initially as well sealed as those for higher tethering densities. This is also supported by the increased levels of capacitance observed in the samples throughout the incorporated valinomycin testing process.

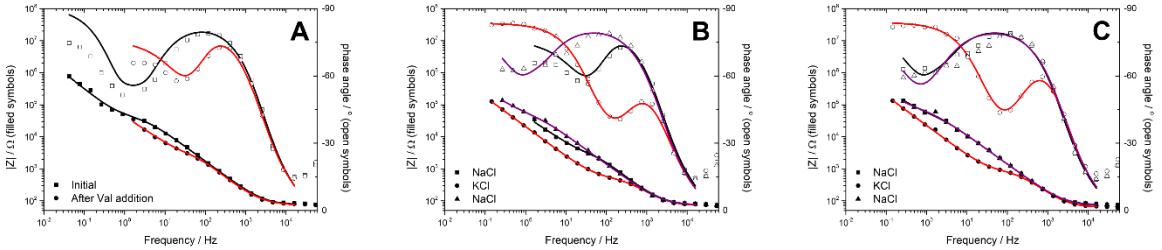

Bilayer 40% 1	Impedance (MΩcm^2)	Capacitance (μFcm^{-2})	Change in Impedance
Initial Bilayer	0.035 ± 0.004	1.9 ± 0.2	
After Val Addition	0.0012 ± 0.0004	1.1 ± 0.6	-96.6%
KCl	0.00037 ± 0.00001	2.2 ± 0.3	-99%
NaCl	0.035 ± 0.02	3.2 ± 0.2	-0%
KCl	0.00063 ± 0.00004	1.8 ± 0.3	-98%
NaCl	0.052 ± 0.04	3.0 ± 0.7	$+49\%$

Figure 3-21: Bode plots of impedance (closed shapes) and phase angle (open shapes) for a 40% tethered DPhyPC bilayer sample, Bilayer 1. A) Before (black) and after (red) addition of valinomycin. B & C) Cycling electrolyte twice consecutively between NaCl (black), KCl (red) and NaCl (purple) with valinomycin incorporated. Table shows impedance and capacitance values of the lipid bilayer. Also shown is percentage difference between each impedance value and the initial bilayer impedance.

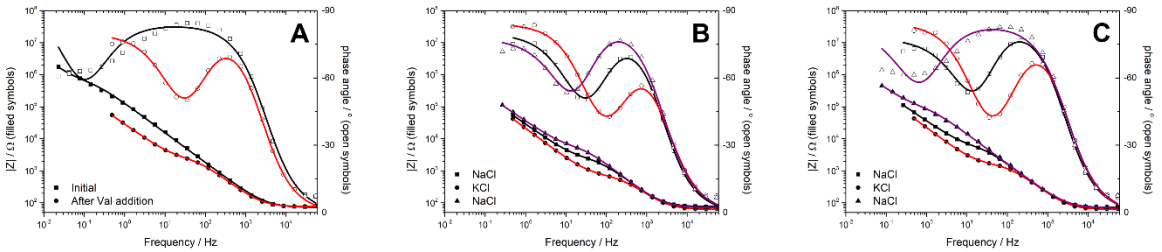

Bilayer 40% 2	Impedance (MΩcm^2)	Capacitance (μFcm^{-2})	Change in Impedance
Initial Bilayer	0.51 ± 0.04	1.9 ± 0.08	
After Val Addition	0.0016 ± 0.00007	1.6 ± 0.1	-99.7%
KCl	0.00054 ± 0.00001	1.9 ± 0.2	-99.9%
NaCl	0.0033 ± 0.0002	1.4 ± 0.1	-99.4%
KCl	0.0013 ± 0.00003	1.4 ± 0.07	-99.7%
NaCl	0.063 ± 0.01	2.2 ± 0.2	-88%

Figure 3-22: Bode plots of impedance (closed shapes) and phase angle (open shapes) for a 40% tethered DPhyPC bilayer sample, Bilayer 2. A) Before (black) and after (red) addition of valinomycin. B & C) Cycling electrolyte twice consecutively between NaCl (black), KCl (red) and NaCl (purple) with valinomycin incorporated. Table shows impedance and capacitance values of the lipid bilayer. Also shown is percentage difference between each impedance value and the initial bilayer impedance.

Rehydration of 40% tethered samples had mixed results (figure 3-23). Whilst bilayer 40% 3 was modelled with a minimal decrease in resistance after drying out and rehydrating, bilayer 40% 4 showed a decrease of multiple magnitudes of impedance. However, both samples had increases in capacitance from around 1.5 to around 4, greater than for any of the more highly tethered samples. This suggests a far higher degree of hydration in the membrane which could be due to far less efficient lipid packing after rehydration.

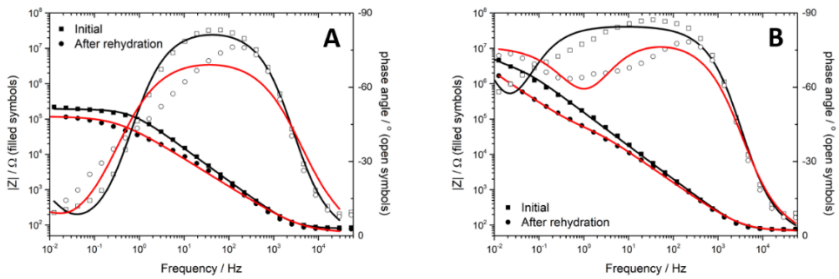

	Sample	Impedance ($M\Omega cm^2$)	Capacitance ($\mu F cm^{-2}$)	Change in Impedance
Bilayer 40% 3	**Initial**	0.19 ± 0.004	1.4 ± 0.04	
	After Rehydration	0.12 ± 0.006	4.8 ± 0.4	-37%
Bilayer 40% 4	**Initial**	2.5 ± 0.3	1.5 ± 0.2	
	After Rehydration	0.029 ± 0.007	3.7 ± 0.5	-99%

Figure 3-23: Bode plots of impedance (closed shapes) and phase angle (open shapes) for two different 40% tethered DPhyPC bilayer samples before (black) and after (red) drying out over a period of four days and rehydrating before allowing them to sit for an hour prior to measurement. Table shows impedance and capacitance values of the two lipid bilayers. Also shown is percentage difference between each impedance value and the initial bilayer impedance.

Both bilayer samples decreased to single $k\Omega cm^2$ levels of resistance on addition of valinomycin irrespective of the change incurred from the rehydration process (figures 3-24 and 3-25). Additionally, whilst a small degree of change in impedance through swapping between NaCl and KCl was observed, neither sample had any appreciable recovery beyond that. This suggests that these bilayers were unlikely to be able to regain the levels of impedance modelled before addition of valinomycin. The high level of capacitance for both samples reverted to similar levels observed initially however, on addition of valinomycin.

Whilst the addition of valinomycin decreased the bilayer impedance, it may also have helped re-organise the lipid structure a little better. However, it could also be the case that it would have happened after time without addition of the valinomycin, and that the lower density tethering samples needed more time to recover from the rehydration process.

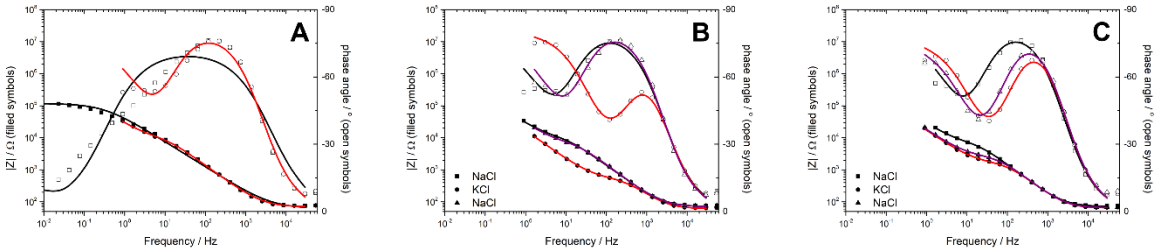

Bilayer 40% 3	Impedance (MΩcm^2)	Capacitance (μFcm^{-2})	Change in Impedance
Initial Bilayer	0.19 ± 0.004	1.4 ± 0.04	
After Rehydration	0.12 ± 0.006	4.8 ± 0.4	
After Val Addition	0.0069 ± 0.002	2.4 ± 0.4	-94%
KCl	0.00039 ± 0.00001	1.9 ± 0.2	-99.7%
NaCl	0.0048 ± 0.0006	1.8 ± 0.2	-96%
KCl	0.0013 ± 0.00005	1.4 ± 0.1	-99%
NaCl	0.0020 ± 0.00008	1.4 ± 0.09	-98%

Figure 3-24: Bode plots of impedance (closed shapes) and phase angle (open shapes) for a rehydrated 40% tethered DPhyPC bilayer sample. A) Before (black) and after (red) addition of valinomycin. B & C) Cycling electrolyte twice consecutively between NaCl (black), KCl (red) and NaCl (purple) with valinomycin incorporated. Table shows impedance and capacitance values of the lipid bilayer. Also shown is percentage difference between each impedance value and the bilayer impedance after rehydration.

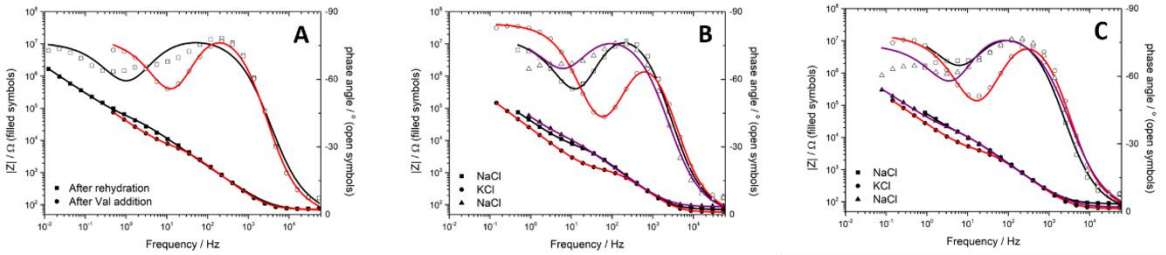

Bilayer 40% 4	Impedance (MΩcm^2)	Capacitance (μFcm^{-2})	Change in Impedance
Initial Bilayer	2.5 ± 0.3	1.5 ± 0.2	
After Rehydration	0.029 ± 0.007	3.7 ± 0.5	
After Val Addition	0.0038 ± 0.0003	1.5 ± 0.1	-87%
KCl	0.00099 ± 0.00002	1.5 ± 0.08	-97%
NaCl	0.0057 ± 0.003	3.2 ± 0.8	-80%
KCl	0.0028 ± 0.0001	1.8 ± 0.1	-90%
NaCl	0.0085 ± 0.002	2.6 ± 0.7	-71%

Figure 3-25: Bode plots of impedance (closed shapes) and phase angle (open shapes) for a rehydrated 40% tethered DPhyPC bilayer sample. A) Before (black) and after (red) addition of valinomycin. B & C) Cycling electrolyte twice consecutively between NaCl (black), KCl (red) and NaCl (purple) with valinomycin incorporated. Table shows impedance and capacitance values of the lipid bilayer. Also shown is percentage difference between each impedance value and the bilayer impedance after rehydration.

The results suggest that the 40% tethered bilayers are still able to retain a degree of functionality after the drying out and rehydration process, but that compared to other higher tethering density samples this functionality is greatly reduced. With impedance values consistently around the 1-10 KΩcm^2 range the quality of results they could provide for any sensing or testing purposes would be questionable.

3.3.5 10%-Tethered Lipid Bilayers

For completeness, bilayers with only 10% tethering density of DPhyTL with 90% 2-mercaptoethanol were prepared. With only 10% DPhyTL in solution, DPhyPC would need to be able to make up a majority of the inner leaflet of the bilayer, with little to tether it in place and prevent it from floating in solution or forming free-standing vesicles instead. Bilayers made using 10% tethering were found to have exceptionally poor impedance, with addition of valinomycin decreasing the impedance further (figure 3-26). With such poor impedance and phase angles being modelled it is possible that these were either incomplete bilayers with many defects or more likely a collection of lipids scattered on the surface amongst the monolayer DPhyTL. As such, no further experiments were performed using these samples.

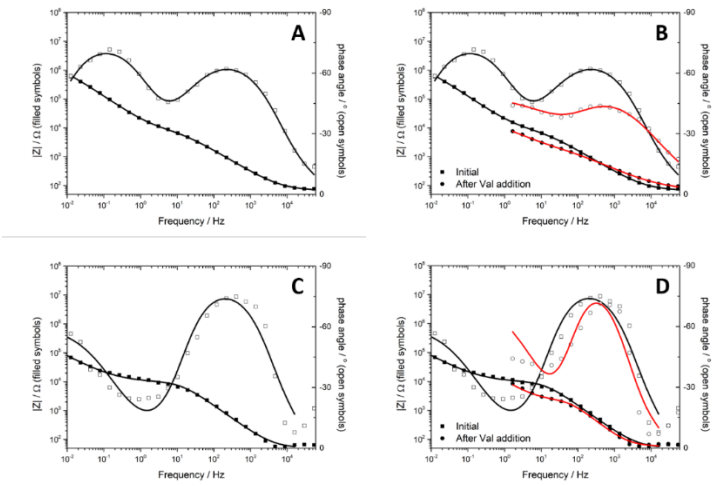

Figure 3-26: Bode plots of impedance (closed shapes) and phase angle (open shapes) for two different 10% tethered DPhyPC bilayer samples in 100 mM NaCl. A & C) Initial bilayers. B & D) Before (black) and after (red) addition of valinomycin.

3.3.6 Neutron Reflectometry of DPhyPC tBLMs

The use of EIS showed that bilayers at high tethering density were able to maintain a high level of impedance after dehydrating them and rehydrating for further measurements. The use of neutron reflectometry for 80% and 60% tethered bilayers provides a further indication of the quality of bilayers before and after rehydration. Neutron reflectometry requires the use of bilayers with a larger surface area, which means that results are averaged over a much greater range than the 0.283 cm^2 of the EIS, where the effects of small defects are exaggerated. It also allows for analysis of the different components of the bilayer to determine if there are any more specific structural changes occurring throughout the rehydration process, by providing sub-nanometre vertical resolution.

For each component of bilayer samples 4 things can be modelled – thickness, SLD, roughness and hydration. For components that make up the substrate, these values are usually fixed. This is because there is minimal chemical change occurring to the silicon substrate, with the same being true for the deposited chromium and gold binding layers. For measurements of interactions between lipid bilayers and other molecules it is also unusual for any major changes to occur to the tethering region, however such changes could occur for these experiments due to the dehydration process effecting the entirety of the bilayer. Changes in thickness and SLD of layers can be due to a change in the structural makeup of the lipid bilayer. Changes in hydration suggest that there is an increase in fluidity of the bilayer caused by formation of defects or otherwise an increase in bilayer disorder, which can also be observed through changes in layer roughness.

Measurements were taken on two different DPhyPC wafers. One with a bilayer tethered at 80% density and one with a bilayer tethered at 60% density. For each bilayer, 3 different measurements were taken in 3 different solvent mixtures to fully characterise the membranes. These mixtures were D_2O, H_2O and a mixture of D_2O and H_2O designed to match the SLD of gold, CM 4.5. For each bilayer, dehydration was performed through pumping of nitrogen through the wet cells holding the bilayers. Bilayers were stored for a period of 2 days under nitrogen before being rehydrated for final measurements.

For the bilayer at 80% tethering density, the initial and final fit before and after drying out and rehydrating are shown in figure 3-27. The values for the initial fit were in good agreement with values previously determined in literature, suggesting that bilayers of good quality had been formed.[126, 137] After obtaining a fit for the initial bilayer, values were fixed for the silicon, silicon oxide, chromium, and gold layers as these would be unaffected by the drying out and rehydrating process. Thus, changes were only modelled in the bilayer for the tethers, hydrocarbon tails and head group region and no MCMC uncertainty is present for the silicon, chromium, and gold layers.

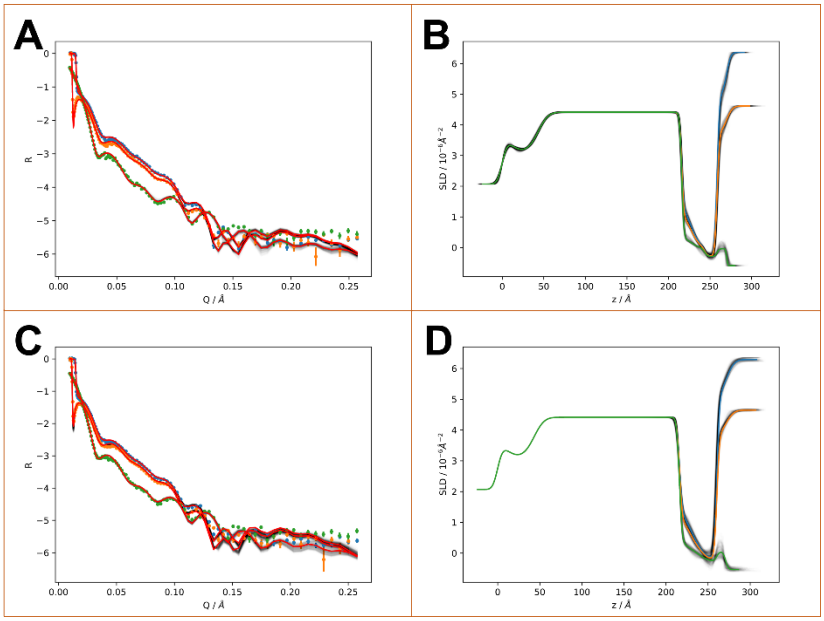

Figure 3-27: Comparison in reflectivity and SLD for an 80%-tethered DPhyPC bilayer before and after drying out and rehydrating 2 days later. A & B show the reflectivity and SLD plots for the initial bilayer. C & D show the final reflectivity and SLD plots after rehydration. Coloured lines show the modelled median values of MCMC sampling, faded lines show MCMC uncertainty. Blue represents the data gathered in D_2O, orange CM 4.5 and green H_2O.

The initial and final values for the 80%-tethered, with errors provided by MCMC sampling, are shown in table 3-2. NR data is averaged over a large area, so small defects do not have such a large effect on the overall profile of the bilayer. Thus, any large changes modelled between samples are quite impactful. In the case of the DPhyPC bilayers at 80% tethering density formed for EIS experiments, there was often minimal change in their quality after undergoing the dehydration and rehydration process. This is shown in the neutron reflectometry data as well.

Table 3-2: Modelled NR data for 80%-tethered DPhyPC bilayer. Thickness and roughness provided in Å, SLD in 10^{-6} Å^{-2} and hydration in %. See Tables 1 and 2 in Appendix for full data set.

	Initial Bilayer	**After Rehydration**
Tether Region		
Thickness	11.4 ± 2.4	13.4 ± 2.3
SLD	0.520 ± 0.033	0.542 ± 0.079
Roughness	2.08 ± 0.093	2.70 ± 0.40
Hydration	15.1 ± 3.5	15.6 ± 2.3
Inner Hydrocarbons		
Thickness	16.3 ± 2.1	15.3 ± 2.0
SLD	-0.023 ± 0.092	-0.0722 ± 0.085
Roughness	8.14 ± 0.79	9.14 ± 0.86
Hydration	0.511 ± 0.53	2.36 ± 2.2
Outer Hydrocarbons		
Thickness	14.9 ± 1.5	15.9 ± 2.6
SLD	-0.290 ± 0.058	-0.242 ± 0.16
Roughness	2.83 ± 1.7	5.31 ± 2.9
Hydration	0.250 ± 0.38	1.16 ± 1.4
Outer Head Groups		
Thickness	11.5 ± 1.3	10.3 ± 1.6
SLD	1.38 ± 0.28	1.48 ± 0.26
Roughness	2.33 ± 0.37	2.51 ± 0.37
Hydration	72.0 ± 5.9	71.1 ± 6.5

There was a small increase in the thickness of the tether region from 11.4 to 13.4 Å, however this is within the error range provided by modelling. Otherwise, there was minimal change in the tether region of the bilayer. An increase was modelled in the roughness of the hydrocarbon tails, particularly in the outer layer where it increased from 2.83 to 5.31 Å. This suggests that the dehydration and rehydration process may have resulted in a small increase in the disorder of the outer leaflet of the bilayer. However, minimal change could be observed in these regions otherwise with only a very small increase in hydration, and minimal change in the outer head group region as well. Overall, this suggests that the bilayer remained intact after being dehydrated and rehydrated, with only a minor increase in outer leaflet disorder.

The initial and final fit before and after drying out and rehydrating for the second sample at 60%-tethering density are shown in figure 3-28. As with the 80%-tethered bilayer values for the silicon, chromium and gold regions were fixed after determining initial fit values from the first set of measurements.

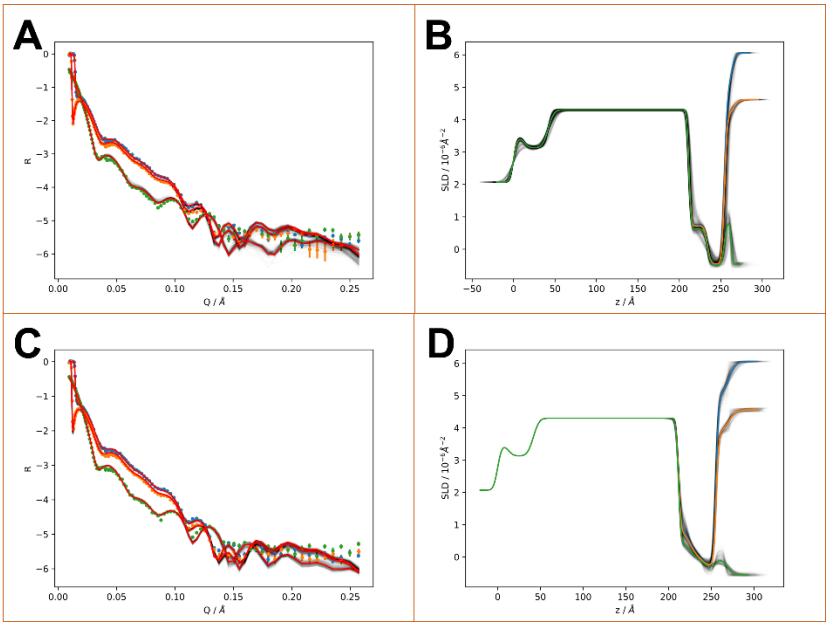

Figure 3-28: Comparison in reflectivity and SLD for a 60%-tethered DPhyPC bilayer before and after drying out and rehydrating 2 days later. A & B show the reflectivity and SLD plots for the initial bilayer. C & D show the final reflectivity and SLD plots after rehydration. Coloured lines show the modelled median values of MCMC sampling, faded lines show MCMC uncertainty. Blue represents the data gathered in D_2O, orange CM 4.5 and green H_2O.

The initial and final values for the second bilayer, with errors provided by MCMC sampling, are shown in the table below. Unlike the 80%-tethered samples, 60%-tethered bilayers were often highly disrupted in EIS measurements after drying out and being rehydrated. This would be supported by clear changes in the neutron modelling between samples, which is indeed the case in some parts of the bilayer.

Table 3-3: Modelled NR data for 60%-tethered DPhyPC bilayer. Thickness and roughness provided in Å, SLD in 10^{-6} $Å^{-2}$ and hydration in %. See tables 3 and 4 in appendix for full data set.

	Initial Bilayer	**After Rehydration**
Tether		
Thickness	22.3 ± 1.6	13.1 ± 2.9
SLD	0.648 ± 0.11	0.589 ± 0.094
Roughness	2.17 ± 0.26	2.36 ± 0.23
Hydration	1.76 ± 2.1	7.39 ± 6.2
Inner HC		
Thickness	10.2 ± 0.20	15.7 ± 2.2
SLD	-0.481 ± 0.069	-0.0763 ± 0.070
Roughness	3.16 ± 3.1	7.58 ± 1.5
Hydration	0.677 ± 0.82	0.607 ± 0.61
Outer HC		
Thickness	10.4 ± 2.0	15.6 ± 2.5
SLD	-0.479 ± 0.12	-0.296 ± 0.12
Roughness	6.66 ± 2.7	4.51 ± 2.8
Hydration	0.350 ± 0.55	0.846 ± 0.89
Outer HG		
Thickness	8.28 ± 0.37	14.0 ± 2.0
SLD	2.87 ± 0.44	1.34 ± 0.20
Roughness	2.66 ± 0.46	2.47 ± 0.35
Hydration	60.6 ± 13	76.1 ± 5.2

A large decrease in the tethering region's thickness was modelled, changing from 22.3 Å to 13.1 Å. The initial tethering region thickness was unusually high – despite a difference in tethering density between the 80 and 60% tethered samples there was no fundamental change to the material making up this region. As such it is difficult to draw any conclusions from this specific change as the final value after drying out and rehydrating is purely in line with what would be expected initially of the tethering region thickness.

An increase in hydration was also modelled from 1.76% to 7.39%. This suggests that there was some disruption in the tethering region of the bilayer, as it became more condensed after the dehydration and rehydration process.

The opposite occurred in the hydrocarbon chain layers where both inner leaflet and outer leaflet hydrocarbons were modelled with an increase of ~50% in thickness, whilst an increase of inner chain roughness occurred from 3.16 to 7.58 Å. Disruption of the outer head group area was also apparent from the increase in thickness from 8.28 to 14 Å, decrease in SLD from 2.87 to 1.34 and hydration percentage increasing from 60.6 to 76.1.

These results suggest that unlike the 80%-tethered sample where only a small amount of disruption occurred, much more change was apparent in the 60%-tethered sample after being dehydrated and rehydrated. It is not possible using neutron reflectometry to determine exactly what is happening to each part of the bilayer, however the implication from the data is that whilst the membrane disorder has likely increased, it is still intact as a functional bilayer. This is consistent with EIS samples which often experienced sizeable impedance decreases suggesting bilayer perturbation but were still successfully able to be functionalised with valinomycin.

3.4 Effect of Polyelectrolyte on Dehydration and Rehydration on DPhyPC Lipid Bilayers

Whilst results from the previous section indicated that at full tethering density there was minimal impact from the rehydration process on bilayer quality, at lower tethering densities there was an increasingly stronger effect. Lower tethering densities make for more realistic membrane models. Thus, it is important to determine if there are non-destructive ways to improve bilayer resilience to the drying out process. In this sub-chapter two different polyelectrolytes, PDADMAC and PSS (figure 3-29), were investigated to determine their effect on addition to DPhyPC bilayers at different tethering density, and whether their presence improved stability of the bilayers through the rehydration process.

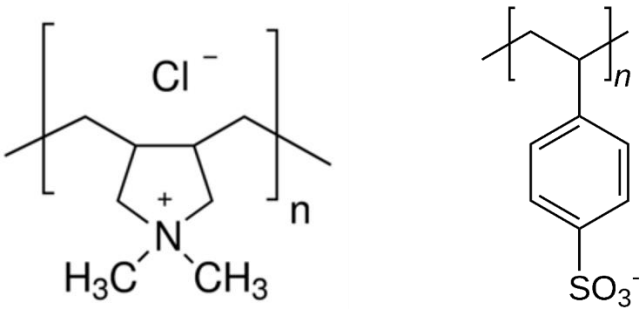

Figure 3-29: Structure of the 2 polyelectrolytes used throughout this sub-chapter, PDADMAC (left) and PSS (right).

For the experiments involved in this sub-chapter, bilayers were initially formed in the same way outlined for chapter 3.3. The experimental process for each bilayer sample is shown in figure 3-30, with the additional polyelectrolyte-coating steps shown in yellow. The procedure involved a 2-day formation of the bilayer, followed by an initial measurement of the bilayer quality. Following this, addition of polyelectrolyte and further measurements were taken over the next following 3-4 days. For bilayers that were dried out and then rehydrated after 4 days, this extended the process to 9-10 days for each sample.

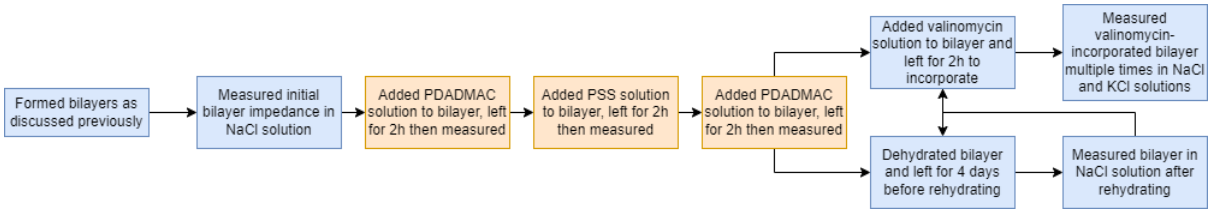

Figure 3-30: Flow diagram of the experimental steps involved in bilayer formation and impedance measurement throughout sub-chapter 3.4.

As a water soluble and high charge density cationic polymer, it was expected that PDADMAC would have some affinity to the zwitterionic head groups of the DPhyPC lipid making up the surface of the bilayer. This electrostatic attraction would result in the build-up of PDADMAC on the surface of the bilayer. Addition of the anionic PSS polyelectrolyte would then form a second layer as the PSS would be attracted to the cationic nature of PDADMAC, allowing the formation of a secondary layer and then a third layer on addition of more PDADMAC (figure 3-31). Whilst the layered structure shown in figure 3-31 is speculative, it could be confirmed by performing a neutron scattering experiment with deuterated polyelectrolyte samples being introduced to the lipid bilayers and modelling structural changes in solution.

Formation of polyelectrolyte multilayers has been previously observed on solid substrates where the charge of the polyelectrolyte layer overcomes the charge of the material beneath in a process known as charge overcompensation, allowing addition of a new oppositely charged layer.[193]

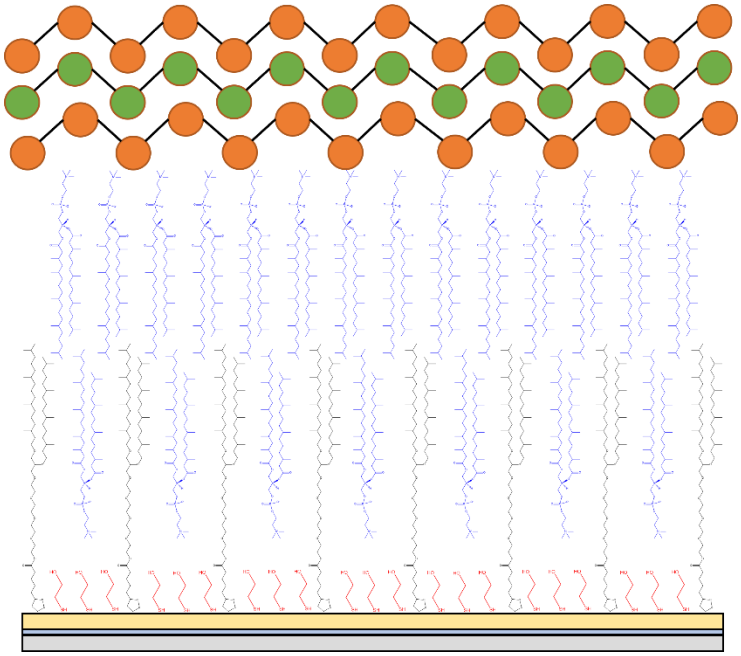

Figure 3-31: Schematic of proposed polyelectrolyte coating over sparsely tethered DPhyPC lipid bilayer. PDADMAC (orange, first and third layer) and PSS (green, second layer) would form a multi-layered protective element over the bilayer.

3.4.1 80%-Tethered Lipid Bilayers with Polyelectrolyte

Upon addition of polyelectrolytes to bilayer samples there was a phase shift in the impedance and phase angle graphs due to an increased level of resistance in the modelled resistivity R_1, which relates to the resistance of the electrolyte solution. This shift is due to the presence of the lower-conductivity polyelectrolyte floating in solution increasing the resistivity of the electrolyte. This phase shift was reversible with impedance reverted to normal levels of electrolyte resistance upon flushing of the solution after polyelectrolyte coating. For 80% tethered bilayers, the addition of polyelectrolytes had somewhat inconsistent effects on impedance. In all cases, the initial addition of PDADMAC resulted in an increase in impedance. However, addition of PSS and further addition of PDADMAC did not cause uniform changes in impedance.

For most samples the final impedance after addition of all 3 polyelectrolyte solutions was very similar to the initial impedance (figures 3-32 and 3-33). For bilayer PE 80% 1, the overall impedance increased from 2.9 to 12 MΩcm^2, with increases on addition of each layer of polyelectrolyte. This consistent increase from the initial bilayer impedance to 4 times its original level suggests that the polyelectrolyte could be filling over gaps in the bilayer's outer layer to improve its overall sealing capacity. In the case of bilayer PE 80% 2 an overall decrease of 40% is observed, which is not enough to suggest that the bilayer's overall quality has changed. This was the only sample found to have a decrease in impedance after addition of all 3 polyelectrolyte layers. Before the final layer addition, the increase in impedance is again over 4 times. This suggests that the first- and second-layer addition of polyelectrolyte has insulated the bilayer very strongly, but not in a permanent capacity due to the decrease of resistance afterwards.

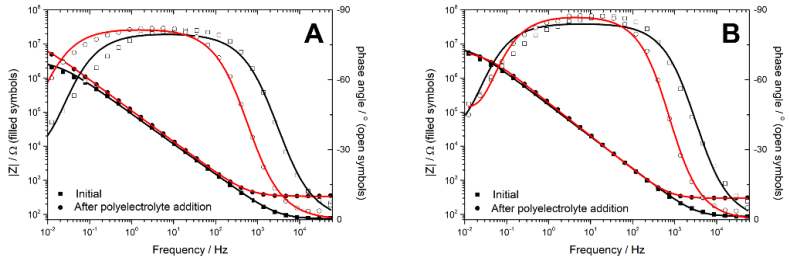

	Sample	Impedance (MΩcm^2)	Capacitance (μFcm^{-2})	Change in Impedance
Bilayer PE 80% 1	**Initial**	2.9 ± 0.1	2.3 ± 0.06	
	PDADMAC	7.1 ± 0.4	2.2 ± 0.03	$+145\%$
	PSS	8.1 ± 0.3	1.9 ± 0.02	$+179\%$
	PDADMAC	12 ± 0.5	1.9 ± 0.02	$+314\%$
Bilayer PE 80% 2	**Initial**	6.8 ± 0.4	1.2 ± 0.04	
	PDADMAC	25 ± 4	1.2 ± 0.06	$+268\%$
	PSS	21 ± 4	1.4 ± 0.07	$+209\%$
	PDADMAC	4.1 ± 0.2	1.1 ± 0.02	-40%

Figure 3-32: Bode plots of impedance (closed shapes) and phase angle (open shapes) for two different 80% tethered DPhyPC bilayer samples in 100 mM NaCl before (black) and after (red) addition of three polyelectrolyte layers. Table shows impedance and capacitance values of the two different lipid bilayers. Also shown is percentage difference between each impedance value and the initial bilayer impedance.

For bilayers PE 80% 3 and 4 there was an overall increase in the final impedance after addition of 3 polyelectrolyte solutions, however a large amount of variance in the impedance changes after addition of each layer (figure 3-33). This could have been due to different amounts of polyelectrolyte settling on the bilayer surfaces resulting in different amounts of improved bilayer sealing.

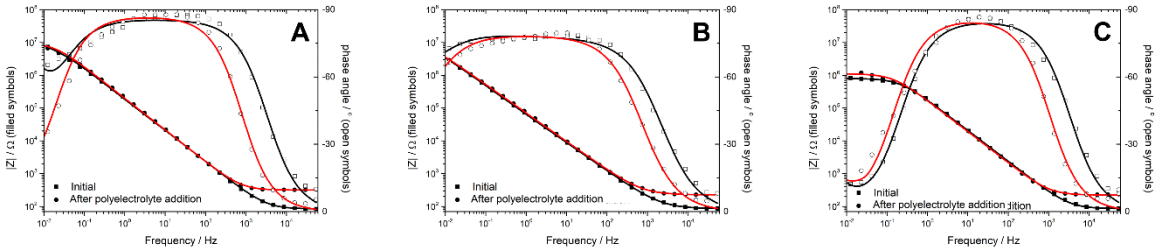

Sample	Sample	Impedance ($M\Omega cm^2$)	Capacitance ($\mu F cm^{-2}$)	Change in Impedance
Bilayer PE 80% 3	**Initial**	4.7 ± 0.4	1.4 ± 0.04	
	PDADMAC	11 ± 1	1.4 ± 0.05	$+134\%$
	PSS	3.8 ± 0.4	1.4 ± 0.05	-19%
	PDADMAC	9.4 ± 0.3	0.88 ± 0.02	$+100\%$
Bilayer PE 80% 4	**Initial**	7.8 ± 2	3.8 ± 0.1	
	PDADMAC	18 ± 6	3.1 ± 0.2	$+131\%$
	PSS	8.7 ± 0.6	2.9 ± 0.05	$+12\%$
	PDADMAC	10 ± 1	3.2 ± 0.06	$+28\%$
Bilayer PE 80% 5	**Initial**	0.79 ± 0.02	0.96 ± 0.02	
	PDADMAC	1.3 ± 0.04	1.1 ± 0.03	$+65\%$
	PSS	4.7 ± 0.3	1.2 ± 0.05	$+495\%$
	PDADMAC	1.1 ± 0.03	1.0 ± 0.03	$+39\%$

Figure 3-33: Bode plots of impedance (closed shapes) and phase angle (open shapes) for three different 80% tethered DPhyPC bilayer samples in 100 mM NaCl before (black) and after (red) addition of three polyelectrolyte layers. Table shows impedance and capacitance values of the three lipid bilayers. Also shown is percentage difference between each impedance value and the initial bilayer impedance.

Valinomycin was added to bilayers PE 80% 1 and 2 to determine whether the presence of polyelectrolytes would impede the incorporation of valinomycin into bilayers and its function as a selective carrier of potassium ions. This is important because even if bilayer quality after rehydration would be improved by addition of polyelectrolytes, this could be detrimental if it limits what bilayers could be used for.

For bilayer PE 80% 1 addition of valinomycin resulted in a small decrease in resistance (figure 3-34). When switching from NaCl to KCl, impedance dropped from 8 MΩcm^2 to only 1.2 kΩcm^2. This suggests that valinomycin was successfully incorporated to allow flow of ions across the bilayer. This was further supported by a strong recovery back to 5.6 MΩcm^2 after exchanging solution back to NaCl.

This bilayer had a higher than usual capacitance reading to begin with, so it is possible that there was inconsistent lipid packing in this sample resulting in an increased level of bilayer hydration. It did not appear to affect the impedance quality and functionality of the bilayer, however. Repetition of cycling between NaCl and KCl process provided consistent drops in resistance to kΩcm^2 levels and increases back to the original MΩcm^2 level, consistent with full functionality of 80% tethered bilayers without polyelectrolyte present.

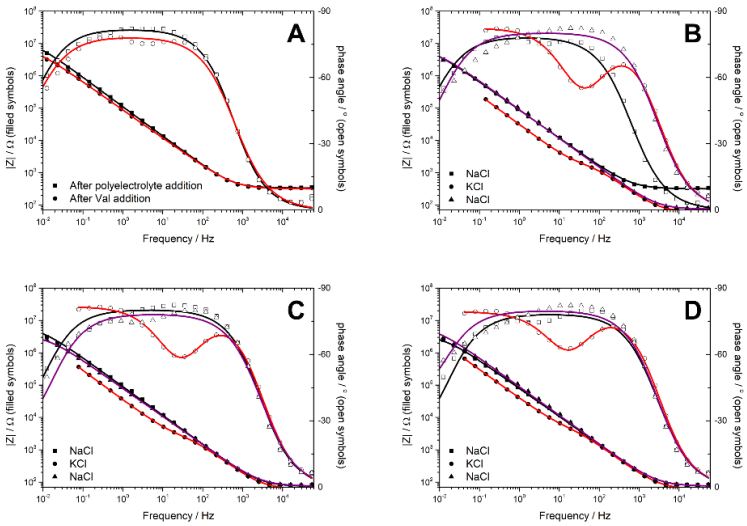

Bilayer PE 80% 1	Impedance ($M\Omega cm^2$)	Capacitance ($\mu F cm^{-2}$)	Change in Impedance
Initial Bilayer	2.9 ± 0.1	2.3 ± 0.06	
After Polyelectrolyte Addition	12 ± 0.5	1.9 ± 0.02	
After Val Addition	8.0 ± 0.4	2.5 ± 0.03	-33%
KCl	0.0012 ± 0.00006	3.1 ± 0.3	-99.99%
NaCl	5.6 ± 3	2.4 ± 0.9	-53%
KCl	0.0017 ± 0.00007	3.3 ± 0.2	-99.99%
NaCl	3.2 ± 0.6	2.7 ± 0.3	-73%
KCl	0.0024 ± 0.0001	3.6 ± 0.2	-99.98%
NaCl	4.5 ± 3	2.8 ± 1	-63%

Figure 3-34: Bode plots of impedance (closed shapes) and phase angle (open shapes) for an 80% tethered DPhyPC bilayer sample. A) Before (black) and after (red) addition of valinomycin following addition of three polyelectrolyte layers. B, C & D) Cycling electrolyte thrice consecutively between NaCl (black), KCl (red) and NaCl (purple) with valinomycin incorporated. Table shows impedance and capacitance values of the lipid bilayer. Also shown is percentage difference between each impedance value and the bilayer impedance after addition of polyelectrolyte layers.

Bilayer PE 80% 2, which was more inconsistent in impedance during the polyelectrolyte addition process, had a large drop in resistance on addition of valinomycin (figure 3-35). This could have been due to the bilayer being less stable than the first one, or due to the presence of some potassium ions in solution.

Switching solvents to KCl caused minor further decrease in resistance, but not enough to conclude valinomycin was functioning effectively. By cycling solution to NaCl again, a recovery to $M\Omega cm^2$ resistance levels was observed.

This suggests that the initial drop in impedance from addition of valinomycin was caused by potassium ions present in solution that were removed after flushing with NaCl. Further cycling of KCl and NaCl provided similar results to bilayer PE 80% 1, suggesting that functionality of bilayer PE 80% 2 was intact after addition of polyelectrolyte.

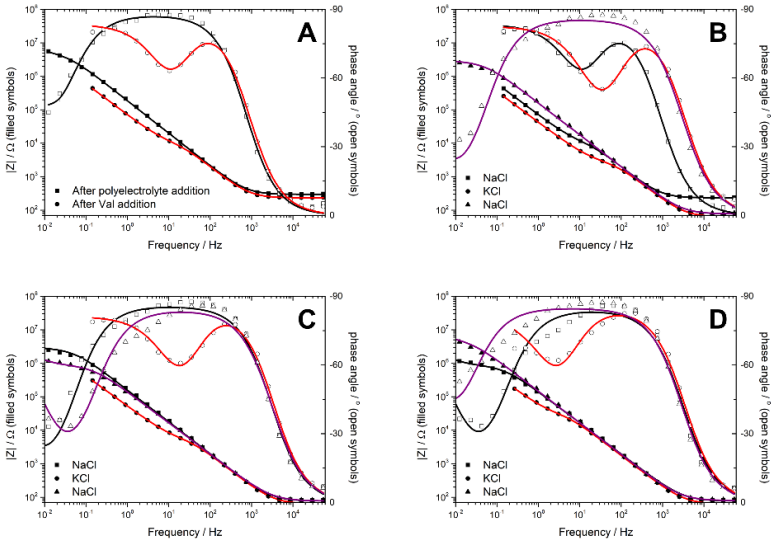

Bilayer PE 80% 2	Impedance ($M\Omega cm^2$)	Capacitance ($\mu F cm^{-2}$)	Change in Impedance
Initial Bilayer	6.8 ± 0.4	1.2 ± 0.04	
After Polyelectrolyte Addition	4.1 ± 0.2	1.1 ± 0.02	
After Val Addition	0.0053 ± 0.0003	1.5 ± 0.08	-99.9%
KCl	0.0019 ± 0.00007	1.3 ± 0.1	-99.95%
NaCl	2.6 ± 0.2	1.2 ± 0.04	-37%
KCl	0.0031 ± 0.0002	1.4 ± 0.1	-99.9%
NaCl	0.78 ± 0.08	1.4 ± 0.05	-81%
KCl	0.018 ± 0.003	1.8 ± 0.2	-99.6%
NaCl	4.3 ± 1	1.5 ± 0.2	$+4.9\%$

Figure 3-35: Bode plots of impedance (closed shapes) and phase angle (open shapes) for an 80% tethered DPhyPC bilayer sample. A) Before (black) and after (red) addition of valinomycin following addition of three polyelectrolyte layers. B, C & D) Cycling electrolyte thrice consecutively between NaCl (black), KCl (red) and NaCl (purple) with valinomycin incorporated. Table shows impedance and capacitance values of the lipid bilayer. Also shown is percentage difference between each impedance value and the bilayer impedance after addition of polyelectrolyte layers.

Rehydration of three different polyelectrolyte-coated samples (figure 3-36) caused minimal changes in two samples (bilayer PE 80% 4 and bilayer PE 80% 5), whilst one sample saw an almost tenfold decrease in modelled impedance (bilayer PE 80% 5).

This sample also had a relatively large change in impedance on addition of polyelectrolyte. Impedance of these samples after rehydration was higher compared to the uncoated samples of comparable tethering density. Rehydration of uncoated samples also resulted in 2 bilayers with minimal impedance change and one with a decrease in impedance of 90%.

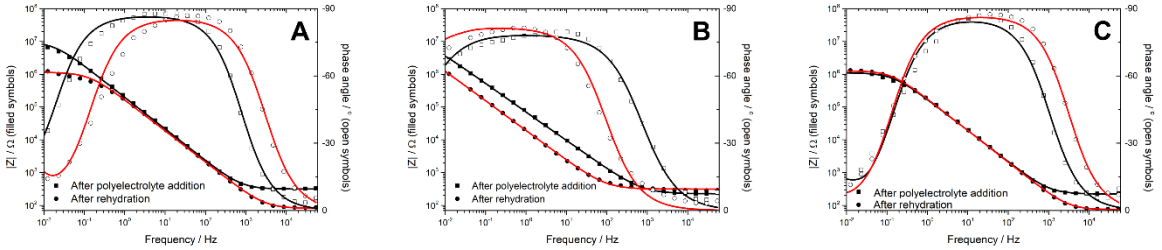

Sample	Sample	Impedance ($M\Omega cm^2$)	Capacitance ($\mu F cm^{-2}$)	Change in Impedance
Bilayer PE 80% 3	**Initial**	4.7 ± 0.4	1.4 ± 0.04	
	After Polyelectrolyte Addition	9.4 ± 0.3	0.88 ± 0.02	
	After Rehydration	1.1 ± 0.05	1.1 ± 0.05	-88%
Bilayer PE 80% 4	**Initial**	7.8 ± 2	3.8 ± 0.1	
	After Polyelectrolyte Addition	10 ± 1	3.2 ± 0.06	
	After Rehydration	7.2 ± 4	12 ± 2	-28%
Bilayer PE 80% 5	**Initial**	0.79 ± 0.02	0.96 ± 0.02	
	After Polyelectrolyte Addition	1.1 ± 0.03	1.0 ± 0.03	
	After Rehydration	1.3 ± 0.02	1.0 ± 0.02	$+18\%$

Figure 3-36: Bode plots of impedance (closed shapes) and phase angle (open shapes) for three different 80% tethered DPhyPC bilayer samples in 100 mM NaCl before (black) and after (red) rehydration following addition of three polyelectrolyte layers. Table shows impedance and capacitance values of the lipid bilayers. Also shown is percentage difference between each impedance value and the bilayer impedance after addition of polyelectrolyte layers.

For bilayer PE 80% 3, which had an 88% decrease in resistance after the rehydration process, the addition of valinomycin caused an impedance decrease of 3 orders of magnitude which was only partially reversible (figure 3-37). The decrease from 1.1 $M\Omega cm^2$ to 2.4 $k\Omega cm^2$ on addition of valinomycin suggests either the presence of additional KCl ions during this step or some disruption to the bilayer. When electrolyte solution was changed to KCl only a small decrease was modelled, down to 1.6 $k\Omega cm^2$. This was somewhat reversible when exchanging back to NaCl, with an increase to 20.1 $k\Omega cm^2$.

Such a large decrease from the original bilayer resistance suggests that the bilayer had been permanently perturbed during the addition of valinomycin, or that the initial higher level of resistance after rehydration and before addition of valinomycin was due to settling of material on the surface that was not a properly formed bilayer.

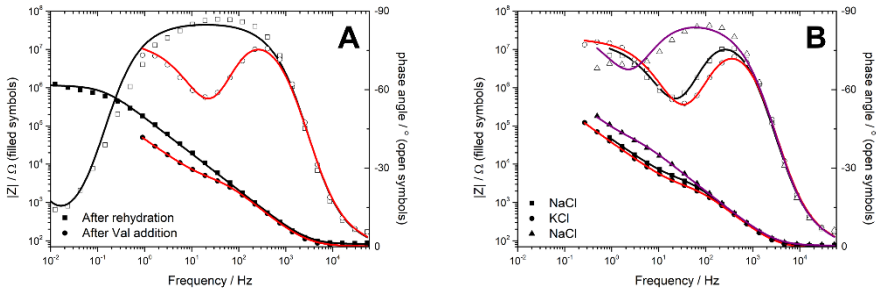

Bilayer 80% 3	Impedance ($M\Omega cm^2$)	Capacitance ($\mu F cm^{-2}$)	Change in Impedance
Initial Bilayer	4.7 ± 0.4	1.4 ± 0.04	
After Polyelectrolyte Addition	9.4 ± 0.3	0.88 ± 0.02	
After Rehydration	1.1 ± 0.05	1.1 ± 0.05	
After Val Addition	0.0024 ± 0.0002	1.1 ± 0.1	-99.8%
KCl	0.0016 ± 0.00008	1.4 ± 0.1	-99.9%
NaCl	0.021 ± 0.007	1.8 ± 0.4	-98%

Figure 3-37: Bode plots of impedance (closed shapes) and phase angle (open shapes) for a rehydrated 80% tethered DPhyPC bilayer sample. A) Before (black) and after (red) addition of valinomycin following addition of three polyelectrolyte layers. B) Cycling electrolyte between NaCl (black), KCl (red) and NaCl (purple) with valinomycin incorporated. Table shows impedance and capacitance values of the lipid bilayer. Also shown is percentage difference between each impedance value and the bilayer impedance after rehydration.

Addition of valinomycin to bilayer PE 80% 4 resulted only in a minor decrease to membrane resistance, with the bilayer retaining an impedance in the $M\Omega cm^2$ range (figure 3-38). Cycling of electrolyte to KCl resulted in a further decrease to less than 10% of the original post-rehydration impedance, reversible to the same level as valinomycin addition on cycling back to NaCl. The decrease in impedance in the presence of valinomycin was far less for this sample than for uncoated samples where bilayers were reduced to $k\Omega cm^2$ levels of impedance when KCl solvent was present. This suggests that the polyelectrolyte coating may have been more effectively maintaining bilayer stability for this sample.

This sample also showed a dramatically increased capacitance after the drying out and rehydration process. It could be the case that for this sample in particular a thicker polyelectrolyte film was able to form over the bilayer when it was dried out. This film would have been able to accumulate charge more effectively on the surface of the bilayer, increasing the capacitance.

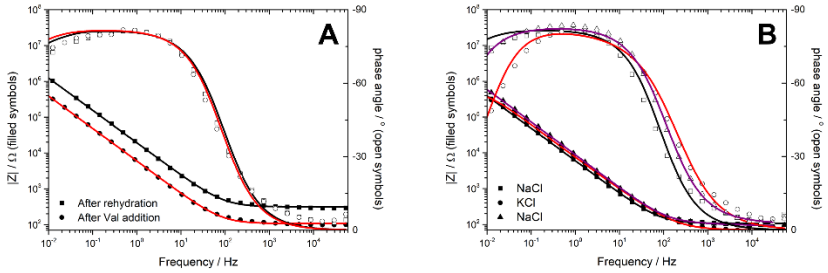

Bilayer PE 80% 4	Impedance ($M\Omega cm^2$)	Capacitance ($\mu F cm^{-2}$)	Change in Impedance
Initial Bilayer	7.8 ± 2	3.8 ± 0.1	
After Polyelectrolyte Addition	10 ± 1	3.2 ± 0.06	
After Rehydration	7.2 ± 4	12 ± 2	
After Val Addition	3.5 ± 3	37 ± 10	-51%
KCl	0.50 ± 0.04	29 ± 1	-93%
NaCl	3.1 ± 0.1	21 ± 0.2	-57%

Figure 3-38: Bode plots of impedance (closed shapes) and phase angle (open shapes) for a rehydrated 80% tethered DPhyPC bilayer sample. A) Before (black) and after (red) addition of valinomycin following addition of three polyelectrolyte layers. B) Cycling electrolyte between NaCl (black), KCl (red) and NaCl (purple) with valinomycin incorporated. Table shows impedance and capacitance values of the lipid bilayer. Also shown is percentage difference between each impedance value and the bilayer impedance after rehydration.

Addition of valinomycin to bilayer PE 80% 5 resulted in minimal decrease in impedance (figure 3-39). By transitioning electrolyte from NaCl to KCl a decrease from 1 $M\Omega cm^2$ to 1.8 $k\Omega cm^2$ was modelled, which is more in line with results for uncoated samples. Similarly, cycling between electrolyte solutions showed recovery to almost $M\Omega cm^2$-level resistance in the presence of NaCl and a return to $k\Omega cm^2$-level resistance in presence of KCl.

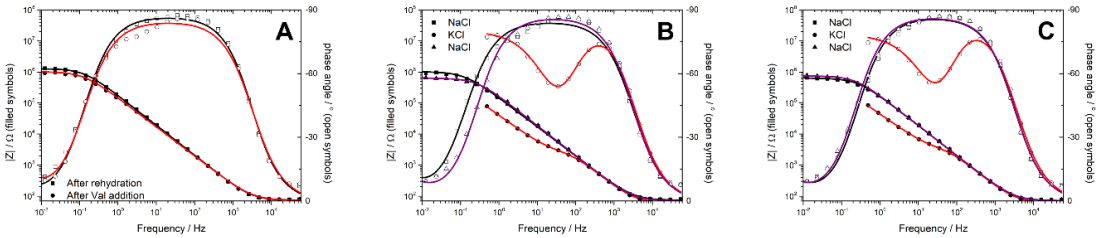

Bilayer PE 80% 5	Impedance ($M\Omega cm^2$)	Capacitance ($\mu F cm^{-2}$)	Change in Impedance
Initial Bilayer	0.79 ± 0.02	0.96 ± 0.02	
After Polyelectrolyte Addition	1.1 ± 0.03	1.0 ± 0.03	
After Rehydration	1.3 ± 0.02	1.0 ± 0.02	
After Val Addition	1.0 ± 0.02	1.2 ± 0.03	-23%
KCl	0.0018 ± 0.00009	1.2 ± 0.1	-99.9%
NaCl	0.61 ± 0.02	1.0 ± 0.03	-53%
KCl	0.0020 ± 0.0002	1.0 ± 0.1	-99.8%
NaCl	0.73 ± 0.02	1.0 ± 0.02	-44%

Figure 3-39: Bode plots of impedance (closed shapes) and phase angle (open shapes) for a rehydrated 80% tethered DPhyPC bilayer sample. A) Before (black) and after (red) addition of valinomycin following addition of three polyelectrolyte layers. B & C) Cycling electrolyte twice consecutively between NaCl (black), KCl (red) and NaCl (purple) with valinomycin incorporated. Table shows impedance and capacitance values of the lipid bilayer. Also shown is percentage difference between each impedance value and the bilayer impedance after rehydration.

Whilst the mixed results for these samples make it difficult to draw a conclusion on the interactions between the bilayers and polyelectrolyte coating post-rehydration, in all cases addition of polyelectrolyte itself did not cause major perturbation of bilayers, and in some cases improved their electrical sealing. Rehydration of bilayers with polyelectrolyte coating provided similar results to uncoated samples as well. However, post-rehydration there was some variance between samples in the interaction with valinomycin. In all cases there was variance in resistance in the presence of different electrolyte solutions indicative of successful incorporation of valinomycin, but the degree of variance was inconsistent.

3.4.2 60%-Tethered Lipid Bilayers with Polyelectrolyte

Addition of polyelectrolyte to 60% tethered bilayers provided similar results to 80% tethered bilayers. For bilayers of higher initial impedance, a small resistance drop after addition of three polyelectrolyte layers was observed (bilayer PE 60% 1 and bilayer PE 60% 2), whilst for the other 3 bilayer samples no change or a small increase was observed. In all cases it appeared that the addition of polyelectrolyte did not negatively affect the quality of the bilayers as the impedance consistently remained above 1 MΩcm^2 (figures 3-40 and 3-41).

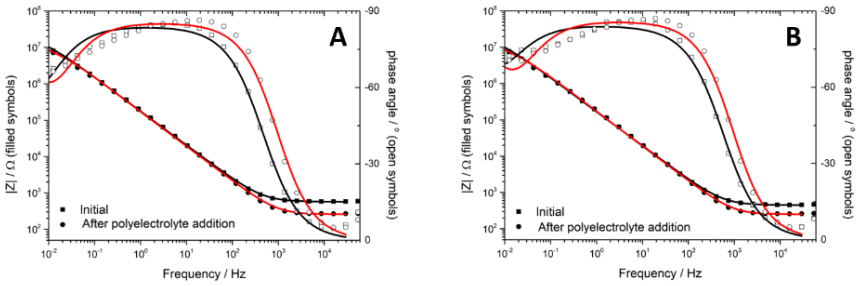

	Sample	Impedance (MΩcm^2)	Capacitance (μFcm^{-2})	Change in Impedance
Bilayer PE 60% 1	**Initial**	13 ± 1	1.4 ± 0.03	
	PDADMAC	10 ± 0.8	1.4 ± 0.04	-23%
	PSS	6.8 ± 0.7	1.4 ± 0.05	-48%
	PDADMAC	6.0 ± 0.5	1.5 ± 0.05	-54%
Bilayer PE 60% 2	**Initial**	8.4 ± 1	1.7 ± 0.06	
	PDADMAC	3.4 ± 0.4	1.8 ± 0.06	-60%
	PSS	9.0 ± 1	1.5 ± 0.06	$+7.1\%$
	PDADMAC	4.3 ± 0.5	1.6 ± 0.07	-49%

Figure 3-40: Bode plots of impedance (closed shapes) and phase angle (open shapes) for two different 60% tethered DPhyPC bilayer samples in 100 mM NaCl before (black) and after (red) addition of three polyelectrolyte layers. Table shows impedance and capacitance values of the lipid bilayers. Also shown is percentage difference between each impedance value and the initial bilayer impedance.

In some cases, the addition of a polyelectrolyte layer caused a large increase in bilayer resistance that was reversed upon addition of the next layer. This was likely due to settling of additional polyelectrolyte on the bilayer surface that was removed on flushing with the solution containing the following polyelectrolyte material.

It was most evident in bilayer PE 60% 4 where addition of polyelectrolyte increased impedance from 6.2 to 16 MΩcm^2 before decreasing back to its original impedance on addition of further polyelectrolyte layers.

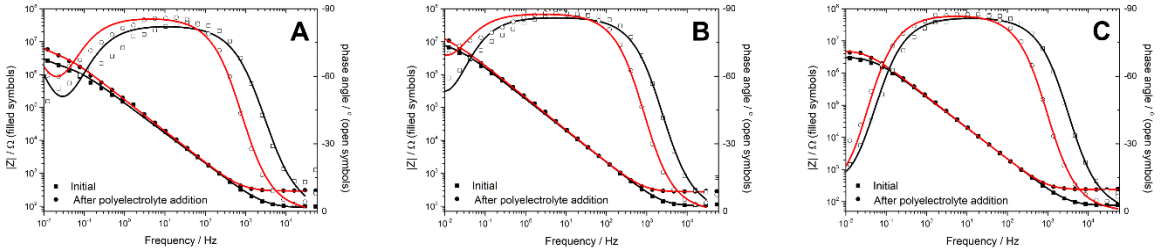

Sample	Sample	Impedance (MΩcm^2)	Capacitance (μFcm^{-2})	Change in Impedance
Bilayer PE 60% 3	**Initial**	1.6 ± 0.2	1.6 ± 0.1	
	PDADMAC	2.1 ± 0.2	1.6 ± 0.08	$+43\%$
	PSS	3.0 ± 0.2	1.3 ± 0.04	-48%
	PDADMAC	3.1 ± 0.2	1.4 ± 0.04	$+48\%$
Bilayer PE 60% 4	**Initial**	6.2 ± 0.4	1.2 ± 0.03	
	PDADMAC	16 ± 1	1.2 ± 0.03	$+158\%$
	PSS	9.4 ± 0.6	1.1 ± 0.02	$+52\%$
	PDADMAC	6.4 ± 0.9	1.5 ± 0.07	$+3.2\%$
Bilayer PE 60% 5	**Initial**	3.2 ± 0.08	0.98 ± 0.02	
	PDADMAC	5.3 ± 0.1	0.92 ± 0.01	$+66\%$
	PSS	5.9 ± 0.2	0.93 ± 0.02	$+84\%$
	PDADMAC	5.2 ± 0.2	0.90 ± 0.02	$+63\%$

Figure 3-41: Bode plots of impedance (closed shapes) and phase angle (open shapes) for three different 60% tethered DPhyPC bilayer samples in 100 mM NaCl before (black) and after (red) addition of three polyelectrolyte layers. Table shows impedance and capacitance values of the lipid bilayers. Also shown is percentage difference between each impedance value and the initial bilayer impedance.

For bilayer PE 60% 1, an initial decrease from 13 to 6 MΩcm^2 was modelled after the addition of polyelectrolyte, however this was still enough resistance to suggest a good quality bilayer (figure 3-42). Addition of valinomycin caused an immediate drop in impedance to 0.83 MΩcm^2, which then decreased further to just 1.3 kΩcm^2. This drop in the presence of KCl ions is consistent with the uncoated 60%-tethered samples. On flushing with NaCl solution, full recovery occurred with the bilayer impedance modelled at a similar level as after initial addition of polyelectrolytes. This suggests that the presence of polyelectrolytes did not impede functionality of the bilayer.

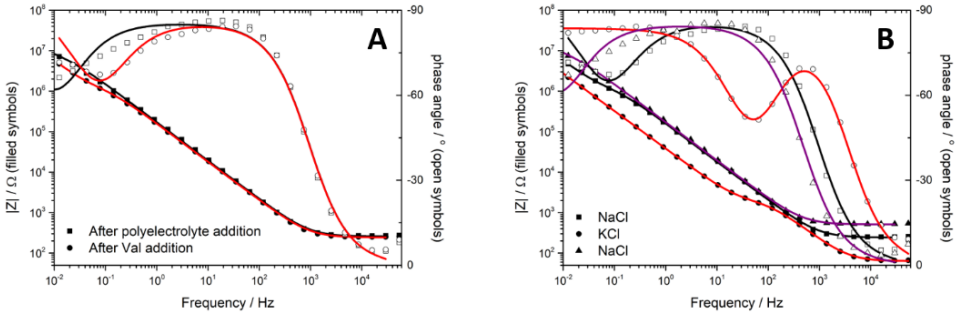

Bilayer PE 60% 1	Impedance ($M\Omega cm^2$)	Capacitance ($\mu F cm^{-2}$)	Change in Impedance
Initial Bilayer	13 ± 1	1.4 ± 0.03	
After Polyelectrolyte Addition	6.0 ± 0.5	1.5 ± 0.05	
After Val Addition	0.83 ± 0.06	1.7 ± 0.05	-86%
KCl	0.0013 ± 0.00004	1.3 ± 0.08	-99.98%
NaCl	6.7 ± 2	1.7 ± 0.04	$+12\%$

Figure 3-42: Bode plots of impedance (closed shapes) and phase angle (open shapes) for a 60% tethered DPhyPC bilayer sample. A) Before (black) and after (red) addition of valinomycin following addition of three polyelectrolyte layers. B) Cycling electrolyte between NaCl (black), KCl (red) and NaCl (purple) with valinomycin incorporated. Table shows impedance and capacitance values of the lipid bilayer. Also shown is percentage difference between each impedance value and the bilayer impedance after polyelectrolyte addition.

Similar results were observed with bilayer PE 60% 2, showing an initial small decrease in bilayer impedance on addition of polyelectrolyte, before a large decrease on addition of valinomycin and a further drop when flushed with KCl solution (figure 3-43). Recovery was again strong with a return to a level of impedance similar to after polyelectrolyte addition. When compared to uncoated 60%-tethered samples there was minimal difference in behaviour between samples. The main difference was the greater initial decrease in impedance for coated samples in the presence of valinomycin, however as previously mentioned this was likely due to the presence of unwanted KCl ions in the added valinomycin solution.

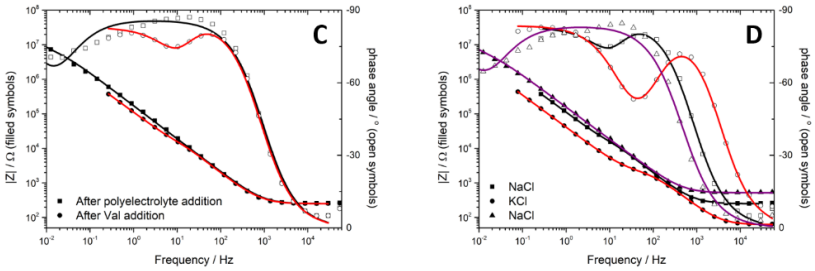

Bilayer PE 60% 2	Impedance ($M\Omega cm^2$)	Capacitance ($\mu F cm^{-2}$)	Change in Impedance
Initial Bilayer	8.4 ± 1	1.7 ± 0.06	
After Polyelectrolyte Addition	4.3 ± 0.5	1.6 ± 0.07	
After Val Addition	0.0034 ± 0.0006	1.7 ± 0.4	-99.92%
KCl	0.0015 ± 0.00004	1.3 ± 0.08	-99.97%
NaCl	3.3 ± 2	2.2 ± 0.9	-23%

Figure 3-43: Bode plots of impedance (closed shapes) and phase angle (open shapes) for a 60% tethered DPhyPC bilayer sample. A) Before (black) and after (red) addition of valinomycin following addition of three polyelectrolyte layers. B) Cycling electrolyte between NaCl (black), KCl (red) and NaCl (purple) with valinomycin incorporated. Table shows impedance and capacitance values of the lipid bilayer. Also shown is percentage difference between each impedance value and the bilayer impedance after polyelectrolyte addition.

The drying out and rehydration of 60%-tethered bilayers coated in polyelectrolyte consistently showed a decrease in bilayer impedance by around half, with 68% for bilayer PE 60% 3 and just under 50% for bilayer PE 60% 4 and bilayer PE 60% 5 (figure 3-44). This consistent decrease suggests that the dehydration process is having a stronger impact than in the case of 80%-tethered samples, where only one of three samples underwent a similar level of degradation. In comparison to uncoated samples, the impedance changes were much more consistent, with uncoated samples exhibiting complete impedance collapse or a minor increase.

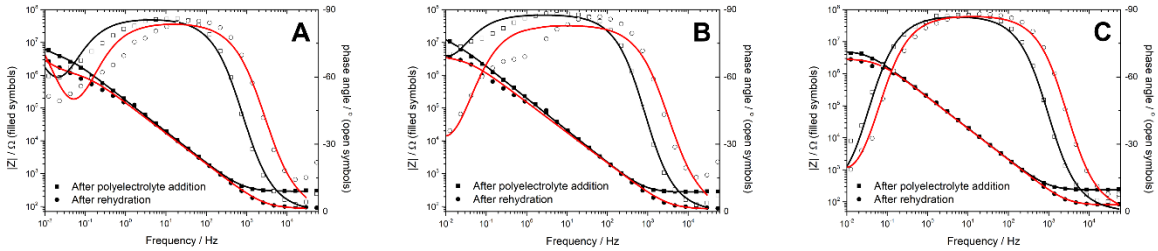

	Sample	Impedance ($M\Omega cm^2$)	Capacitance ($\mu F cm^{-2}$)	Change in Impedance
Bilayer PE 60% 3	**Initial**	1.6 ± 0.2	1.6 ± 0.1	
	After Polyelectrolyte Addition	3.1 ± 0.2	1.4 ± 0.04	
	After Rehydration	0.98 ± 0.1	1.5 ± 0.1	-68%
Bilayer 60% 4	**Initial**	6.2 ± 0.4	1.2 ± 0.03	
	After Polyelectrolyte Addition	6.4 ± 0.9	1.5 ± 0.07	
	After Rehydration	3.3 ± 0.3	1.3 ± 0.08	-48%
Bilayer 60% 5	**Initial**	3.2 ± 0.08	0.98 ± 0.02	
	After Polyelectrolyte Addition	5.2 ± 0.2	0.90 ± 0.02	
	After Rehydration	2.8 ± 0.09	0.93 ± 0.02	-46%

Figure 3-44: Bode plots of impedance (closed shapes) and phase angle (open shapes) for three different 60% tethered DPhyPC bilayer samples in 100 mM NaCl before (black) and after (red) rehydration following addition of three polyelectrolyte layers. Table shows impedance and capacitance values of the lipid bilayers. Also shown is percentage difference between each impedance value and the bilayer impedance after addition of polyelectrolyte layers.

The most significant issue for uncoated samples was the inability to maintain reasonable impedance levels after addition of valinomycin, with resistances modelled consistently below 10 $k\Omega cm^2$ even in the presence of NaCl. For bilayer PE 60% 3 an improvement was observed in this regard (figure 3-45). This sample had the highest impedance decrease of bilayers PE 60% 3, 4 and 5 when dried and rehydrated, with an impedance of 0.98 $M\Omega cm^2$. A further decrease in impedance was modelled on addition of valinomycin, to 0.47 $M\Omega cm^2$, however this was well above the impedance levels of the uncoated sample with the same tethering density. Full valinomycin functionality was also observed with a decrease to only 0.76 $k\Omega cm^2$ in the presence of KCl solution and a recovery to 0.16 $M\Omega cm^2$ when cycled back to NaCl.

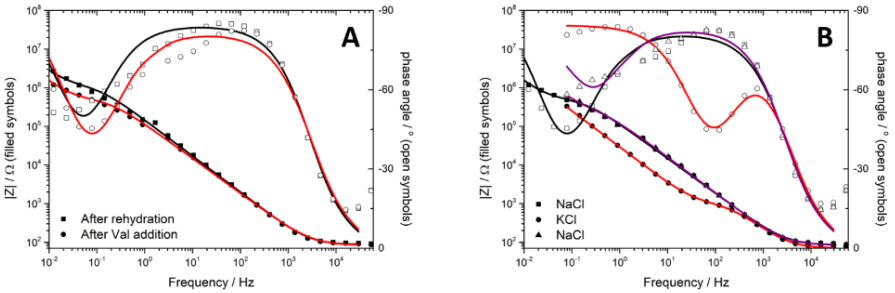

Bilayer PE 60% 3	Impedance ($M\Omega cm^2$)	Capacitance ($\mu F cm^{-2}$)	Change in Impedance
Initial Bilayer	1.6 ± 0.2	1.6 ± 0.1	
After Polyelectrolyte Addition	3.1 ± 0.2	1.4 ± 0.04	
After Rehydration	0.98 ± 0.1	1.5 ± 0.1	
After Val Addition	0.47 ± 0.03	1.8 ± 0.1	-52%
KCl	0.00076 ± 0.00004	1.7 ± 0.3	-99.92%
NaCl	0.16 ± 0.09	2.3 ± 0.3	-84%

Figure 3-45: Bode plots of impedance (closed shapes) and phase angle (open shapes) for a rehydrated 60% tethered DPhyPC bilayer sample. A) Before (black) and after (red) addition of valinomycin following addition of three polyelectrolyte layers. B) Cycling electrolyte between NaCl (black), KCl (red) and NaCl (purple) with valinomycin incorporated. Table shows impedance and capacitance values of the lipid bilayer. Also shown is percentage difference between each impedance value and the bilayer impedance after rehydration.

Unlike the previous sample, bilayer PE 60% 4 showed a large decrease in impedance on addition of valinomycin that was only partially recoverable on cycling of solvents (figure 3-46). Functionality of the bilayer appeared intact with a further resistance decrease when NaCl was swapped with KCl, and a recovery to above 10 $k\Omega cm^2$ impedance when cycled back to NaCl. This is more consistent with the results observed for the uncoated sample.

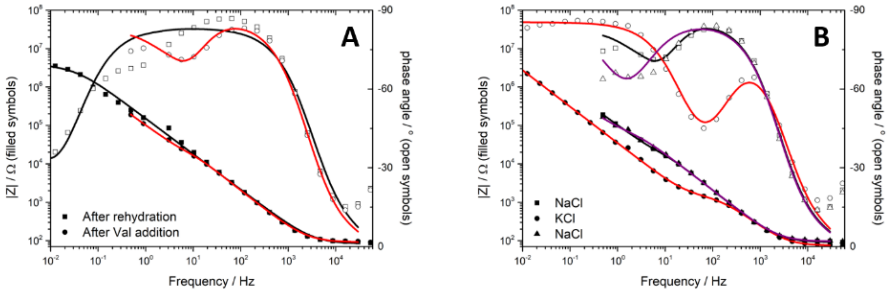

Bilayer PE 60% 4	Impedance ($M\Omega cm^2$)	Capacitance ($\mu F cm^{-2}$)	Change in Impedance
Initial Bilayer	6.2 ± 0.4	1.2 ± 0.03	
After Polyelectrolyte Addition	6.4 ± 0.9	1.5 ± 0.07	
After Rehydration	3.3 ± 0.3	1.3 ± 0.08	
After Val Addition	0.0068 ± 0.002	1.5 ± 0.4	-99.8%
KCl	0.0011 ± 0.00007	1.4 ± 0.3	-99.97%
NaCl	0.041 ± 0.03	1.7 ± 0.2	-99%

Figure 3-46: Bode plots of impedance (closed shapes) and phase angle (open shapes) for a rehydrated 60% tethered DPhyPC bilayer sample. A) Before (black) and after (red) addition of valinomycin following addition of three polyelectrolyte layers. B) Cycling electrolyte between NaCl (black), KCl (red) and NaCl (purple) with valinomycin incorporated. Table shows impedance and capacitance values of the lipid bilayer. Also shown is percentage difference between each impedance value and the bilayer impedance after rehydration.

Addition of valinomycin to bilayer PE 60% 5, unlike bilayers PE 60% 3 and 4, resulted in minimal change to bilayer impedance, though some phase angle disruption was observed (figure 3-47). However, on cycling with NaCl and KCl solvents it was not possible to recover $M\Omega cm^2$ resistance after the decrease to $k\Omega cm^2$ resistance observed on flushing with KCl. Flushing with NaCl was only able to improve impedance to 31 $k\Omega cm^2$.

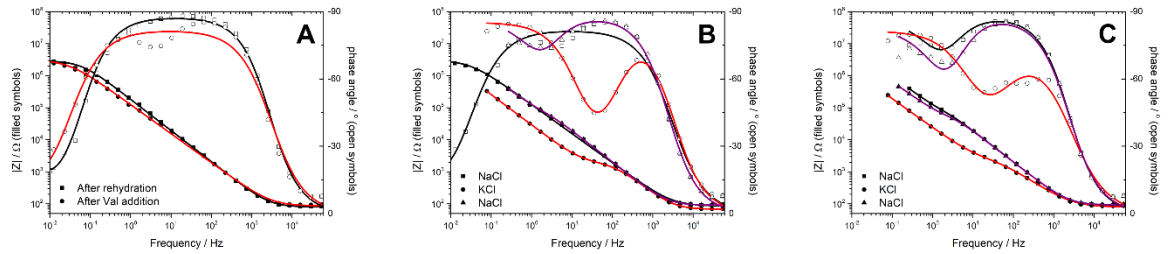

Bilayer PE 60% 5	Impedance ($M\Omega cm^2$)	Capacitance ($\mu F cm^{-2}$)	Change in Impedance
Initial Bilayer	3.2 ± 0.08	0.98 ± 0.02	
After Polyelectrolyte Addition	5.2 ± 0.2	0.90 ± 0.02	
After Rehydration	2.8 ± 0.09	0.93 ± 0.02	
After Val Addition	3.0 ± 0.1	1.5 ± 0.05	$+7.1\%$
KCl	0.0015 ± 0.00003	1.2 ± 0.07	-99.95%
NaCl	0.031 ± 0.008	2.1 ± 0.2	-99%
KCl	0.0019 ± 0.0002	5.1 ± 0.6	-99.93%
NaCl	0.027 ± 0.004	1.4 ± 0.2	-99%

Figure 3-47: Bode plots of impedance (closed shapes) and phase angle (open shapes) for a rehydrated 60% tethered DPhyPC bilayer sample. A) Before (black) and after (red) addition of valinomycin following addition of three polyelectrolyte layers. B & C) Cycling electrolyte twice consecutively between NaCl (black), KCl (red) and NaCl (purple) with valinomycin incorporated. Table shows impedance and capacitance values of the lipid bilayer. Also shown is percentage difference between each impedance value and the bilayer impedance after rehydration.

The bilayers with polyelectrolyte coating were able to consistently maintain a reasonable level of impedance when dried out and rehydrated, which showed a clear improvement over uncoated samples. Some of the coated samples were also able to show a small degree of improvement over an uncoated sample in their capacity to maintain and recover reasonable sealing qualities when valinomycin was incorporated and the samples flushed with multiple solvents.

3.4.3 40%-Tethered Lipid Bilayers with Polyelectrolyte

As shown through the uncoated samples of the same tethering density, at 40%-tethering density there is a much lower level of impedance in the initial quality of most bilayers, with most below 1 $M\Omega cm^2$ and decreasing further on addition of valinomycin or after undergoing the drying out and rehydration process.

Bilayer samples formed using 40% tethering density were consistently of low impedance, with most samples in the region of 0.5-1.5 MΩcm^2 (figures 3-48 and 3-49), which is still enough for studies of ion transport provided the membranes did not degrade too quickly. The addition of polyelectrolyte to these bilayers increased their electrical sealing properties in most cases to more than double the initial resistance, with only one sample, bilayer PE 40% 4, where the change was minimal. Sparse tethering of 40%-tethered samples would have resulted in a much more fluid bilayer, with much of the inner leaflet made up of DPhyPC instead of the DPhyTL tether. This may have made it easier for polyelectrolyte to settle into the bilayer and increase its impedance by increasing the rigidity of both leaflets.

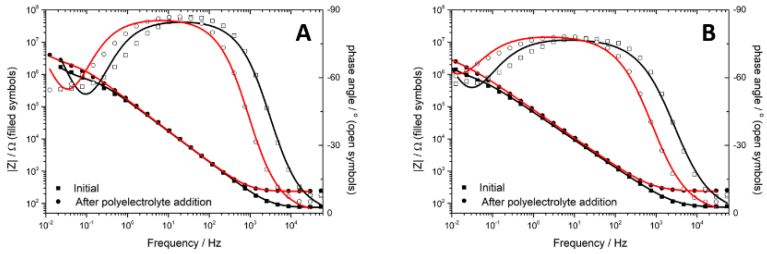

	Sample	Impedance (MΩcm^2)	Capacitance (μFcm^{-2})	Change in Impedance
Bilayer PE 40% 1	**Initial**	0.60 ± 0.04	1.4 ± 0.06	
	PDADMAC	2.0 ± 0.2	1.3 ± 0.06	+233%
	PSS	2.4 ± 0.1	1.2 ± 0.04	+300%
	PDADMAC	1.7 ± 0.1	1.4 ± 0.04	+183%
Bilayer PE 40% 2	**Initial**	0.77 ± 0.06	3.8 ± 0.1	
	PDADMAC	3.6 ± 0.2	3.2 ± 0.07	+368%
	PSS	3.2 ± 0.3	2.9 ± 0.07	+316%
	PDADMAC	1.9 ± 0.1	3.3 ± 0.06	+147%

Figure 3-48: Bode plots of impedance (closed shapes) and phase angle (open shapes) for two different 40% tethered DPhyPC bilayer samples in 100 mM NaCl before (black) and after (red) addition of three polyelectrolyte layers. Table shows impedance and capacitance values of the lipid bilayers. Also shown is percentage difference between each impedance value and the initial bilayer impedance.

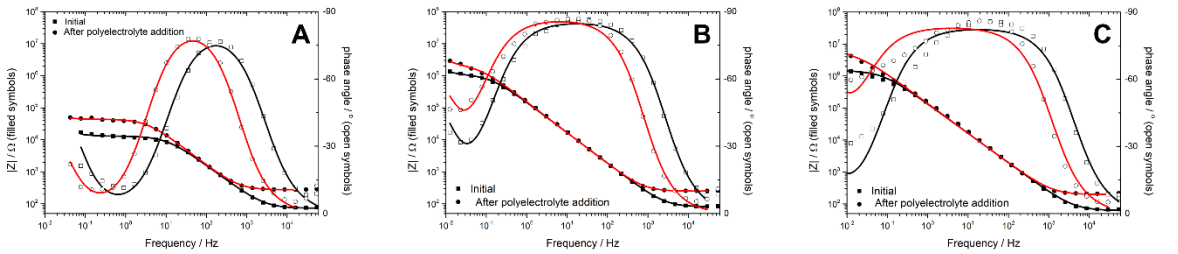

	Sample	Impedance ($M\Omega cm^2$)	Capacitance ($\mu F cm^{-2}$)	Change in Impedance
Bilayer PE 40% 3	**Initial**	0.013 ± 0.0003	1.6 ± 0.1	
	PDADMAC	0.047 ± 0.001	1.4 ± 0.09	$+262\%$
	PSS	0.041 ± 0.0007	1.4 ± 0.06	$+215\%$
	PDADMAC	0.043 ± 0.0005	1.3 ± 0.04	$+231\%$
Bilayer PE 40% 4	**Initial**	1.0 ± 0.02	1.3 ± 0.02	
	PDADMAC	0.75 ± 0.04	1.4 ± 0.05	-25%
	PSS	0.80 ± 0.05	1.4 ± 0.06	-20%
	PDADMAC	1.8 ± 0.08	1.3 ± 0.03	$+80\%$
Bilayer PE 40% 5	**Initial**	1.4 ± 0.06	1.4 ± 0.06	
	PDADMAC	4.3 ± 0.3	1.5 ± 0.05	$+207\%$
	PSS	2.0 ± 0.2	1.5 ± 0.07	$+43\%$
	PDADMAC	3.8 ± 0.4	1.7 ± 0.08	$+171\%$

Figure 3-49: Bode plots of impedance (closed shapes) and phase angle (open shapes) for three different 40% tethered DPhyPC bilayer samples in 100 mM NaCl before (black) and after (red) addition of three polyelectrolyte layers. Table shows impedance and capacitance values of the lipid bilayers. Also shown is percentage difference between each impedance value and the initial bilayer impedance.

Bilayer PE 40% 1 and bilayer PE 40% 2 initially had an impedance just under 1 $M\Omega cm^2$ which doubled to almost 2 $M\Omega cm^2$ on addition of polyelectrolyte layers (figures 46 and 47). Addition of valinomycin to these samples in both cases resulted in a drop in impedance to below 1 MΩ again, with a further level of magnitude decrease for the first bilayer. Both bilayers were able to show functionality with valinomycin incorporated as they decreased to kΩ level impedance on cycling of electrolyte solution from NaCl to KCl. Strong recovery on cycling back to NaCl was also modelled with bilayer impedance returning to the same magnitude of impedance between 0.1 and 1 $M\Omega cm^2$ observed in the initial bilayers, in most cases.

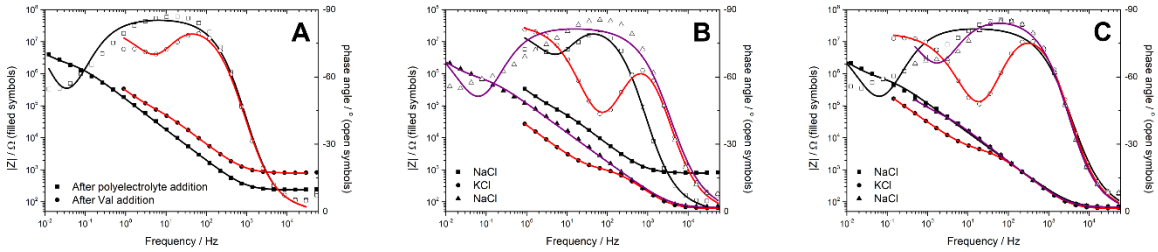

Bilayer PE 40% 1	Impedance ($M\Omega cm^2$)	Capacitance (μFcm^{-2})	Change in Impedance
Initial Bilayer	0.60 ± 0.04	1.4 ± 0.06	
After Polyelectrolyte Addition	1.7 ± 0.1	1.4 ± 0.04	
After Val Addition	0.026 ± 0.005	0.62 ± 0.09	-98%
KCl	0.00080 ± 0.00002	1.4 ± 0.08	-99.95%
NaCl	0.51 ± 0.1	2.2 ± 0.2	-70%
KCl	0.0030 ± 0.00008	1.2 ± 0.05	-99.8%
NaCl	0.031 ± 0.009	2.0 ± 0.2	-98%

Figure 3-50: Bode plots of impedance (closed shapes) and phase angle (open shapes) for a 40% tethered DPhyPC bilayer sample. A) Before (black) and after (red) addition of valinomycin following addition of three polyelectrolyte layers. B & C) Cycling electrolyte twice consecutively between NaCl (black), KCl (red) and NaCl (purple) with valinomycin incorporated. Table shows impedance and capacitance values of the lipid bilayer. Also shown is percentage difference between each impedance value and the bilayer impedance after polyelectrolyte addition.

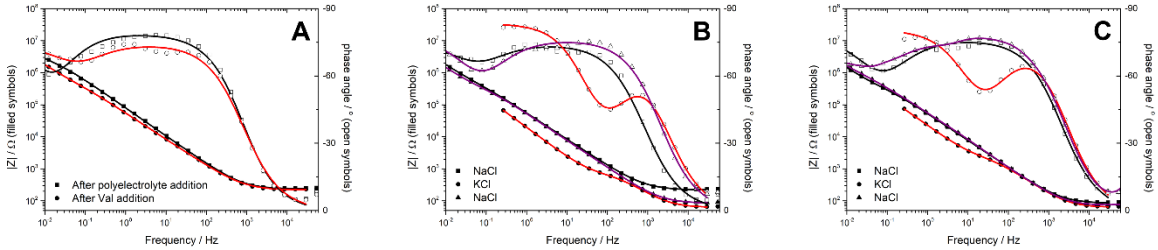

Bilayer PE 40% 2	Impedance ($M\Omega cm^2$)	Capacitance (μFcm^{-2})	Change in Impedance
Initial Bilayer	0.77 ± 0.06	3.8 ± 0.1	
After Polyelectrolyte Addition	1.9 ± 0.1	3.3 ± 0.06	
After Val Addition	0.14 ± 0.08	13 ± 4	-93%
KCl	0.00051 ± 0.000007	4.5 ± 0.2	-99.97%
NaCl	0.18 ± 0.03	7.7 ± 0.5	-91%
KCl	0.0016 ± 0.00006	5.0 ± 0.2	-99.92%
NaCl	0.31 ± 0.07	7.9 ± 0.9	-84%

Figure 3-51: Bode plots of impedance (closed shapes) and phase angle (open shapes) for a 40% tethered DPhyPC bilayer sample. A) Before (black) and after (red) addition of valinomycin following addition of three polyelectrolyte layers. B & C) Cycling electrolyte twice consecutively between NaCl (black), KCl (red) and NaCl (purple) with valinomycin incorporated. Table shows impedance and capacitance values of the lipid bilayer. Also shown is percentage difference between each impedance value and the bilayer impedance after polyelectrolyte addition.

Results for these samples are an improvement over uncoated samples where no samples were able to achieve this degree of recovery in the presence of valinomycin when cycling between solvents.

In this scenario it suggests that the addition of the polyelectrolyte coating to sufficiently sparsely tethered bilayers could improve their longevity.

In subchapter 3.3 it was shown that drying out and rehydration of 40% tethered bilayers that were not coated in polyelectrolyte resulted in irreversible degradation of bilayer sealing either initially or after addition of valinomycin. In the case of coated samples, a degree of electrical sealing quality decrease was also observed, however only in the instance of the sample which was already of very low initial impedance (bilayer PE 40% 3) did the drop off in resistance match that seen in the uncoated sample that degraded immediately (figure 3-52). In the case of bilayer PE 40% 4 a decrease to 37 kΩcm^2 was modelled which represents a poor-quality bilayer, however bilayer PE 40% 5 was able to maintain impedance above 0.1 MΩcm^2.

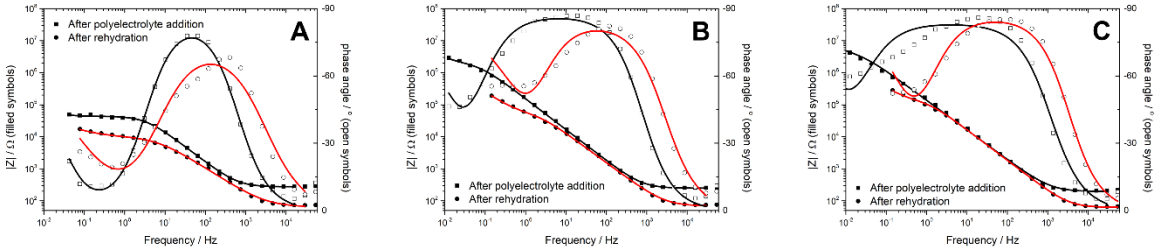

	Sample	Impedance (MΩcm^2)	Capacitance (μFcm^{-2})	Change in Impedance
Bilayer PE 40% 3	**Initial**	0.013 ± 0.0003	1.6 ± 0.1	
	After Polyelectrolyte Addition	0.043 ± 0.0005	1.3 ± 0.04	
	After Rehydration	0.0093 ± 0.001	4.7 ± 0.6	-78%
Bilayer PE 40% 4	**Initial**	1.0 ± 0.02	1.3 ± 0.02	
	After Polyelectrolyte Addition	1.8 ± 0.08	1.3 ± 0.03	
	After Rehydration	0.037 ± 0.009	2.2 ± 0.2	-98%
Bilayer PE 40% 5	**Initial**	1.4 ± 0.06	1.4 ± 0.06	
	After Polyelectrolyte Addition	3.8 ± 0.4	1.7 ± 0.08	
	After Rehydration	0.11 ± 0.02	1.5 ± 0.07	-97%

Figure 3-52: Bode plots of impedance (closed shapes) and phase angle (open shapes) for three different 40% tethered DPhyPC bilayer samples in 100 mM NaCl before (black) and after (red) rehydration following addition of three polyelectrolyte layers. Table shows impedance and capacitance values of the lipid bilayers. Also shown is percentage difference between each impedance value and the bilayer impedance after addition of polyelectrolyte layers.

Addition of valinomycin to bilayer PE 40% 3 did not result in any meaningful change in impedance, however with a starting impedance after rehydration of only 9.3 kΩcm^2 this was still a very low-quality bilayer (figure 3-53). Cycling with different solvents showed that bilayer functionality was still intact, with a decrease to less than 1 kΩcm^2 in both instances of KCl being present and recovery to 10 and 8.2 kΩcm^2 on sequential cycles with NaCl. Despite the low levels of impedance across measurements, this is consistent with uncoated samples after rehydration.

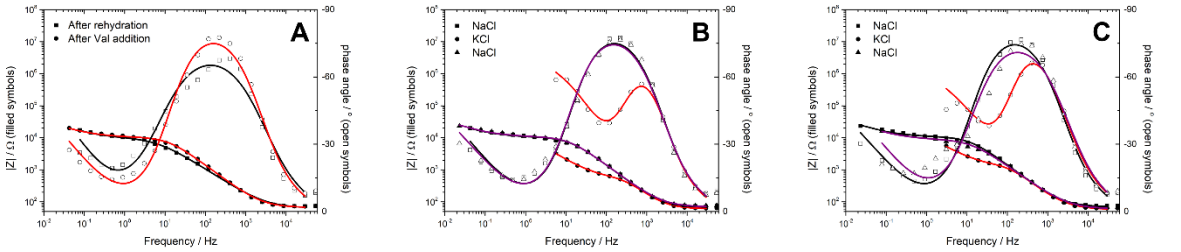

Bilayer PE 40% 3	Impedance (MΩcm^2)	Capacitance (μFcm^{-2})	Change in Impedance
Initial Bilayer	0.013 ± 0.0003	1.6 ± 0.1	
After Polyelectrolyte Addition	0.043 ± 0.0005	1.3 ± 0.04	
After Rehydration	0.0093 ± 0.001	4.7 ± 0.6	
After Val Addition	0.0098 ± 0.0004	1.6 ± 0.1	$+5.4\%$
KCl	0.00037 ± 0.00003	1.1 ± 0.2	-96%
NaCl	0.010 ± 0.0004	1.6 ± 0.1	$+7.5\%$
KCl	0.00090 ± 0.0001	0.94 ± 0.2	-90%
NaCl	0.0082 ± 0.0008	2.2 ± 0.4	-12%

Figure 3-53: Bode plots of impedance (closed shapes) and phase angle (open shapes) for a rehydrated 40% tethered DPhyPC bilayer sample. A) Before (black) and after (red) addition of valinomycin following addition of three polyelectrolyte layers. B & C) Cycling electrolyte twice consecutively between NaCl (black), KCl (red) and NaCl (purple) with valinomycin incorporated. Table shows impedance and capacitance values of the lipid bilayer. Also shown is percentage difference between each impedance value and the bilayer impedance after rehydration.

Bilayer PE 40% 4, which had the largest decrease in impedance after rehydration, also showed a large amount of perturbation on addition of valinomycin (figure 3-54). A decreased was modelled from 37 kΩcm^2 to less than 1 kΩcm^2. Minimal change occurred on cycling to KCl, with some recovery to 4.3 kΩcm^2 after switching back to NaCl. Further cycling suggested some functionality was intact, with a decrease to 2.2 kΩcm^2 and recovery to 6.7 kΩcm^2 on further cycling. This was again consistent with uncoated samples.

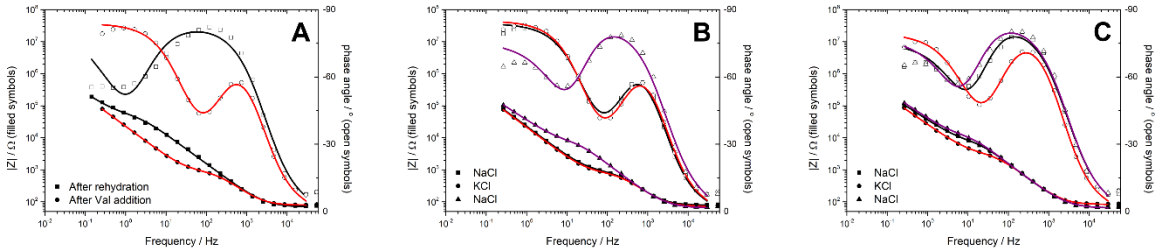

Bilayer PE 40% 4	Impedance ($M\Omega cm^2$)	Capacitance ($\mu F cm^{-2}$)	Change in Impedance
Initial Bilayer	1.0 ± 0.02	1.3 ± 0.02	
After Polyelectrolyte Addition	1.8 ± 0.08	1.3 ± 0.03	
After Rehydration	0.037 ± 0.009	2.2 ± 0.2	
After Val Addition	0.00066 ± 0.00002	1.6 ± 0.1	-98%
KCl	0.00062 ± 0.00001	1.5 ± 0.1	-98%
NaCl	0.0043 ± 0.0005	1.4 ± 0.2	-88%
KCl	0.0022 ± 0.00008	1.4 ± 0.09	-94%
NaCl	0.0067 ± 0.0009	1.5 ± 0.2	-82%

Figure 3-54: Bode plots of impedance (closed shapes) and phase angle (open shapes) for a rehydrated 40% tethered DPhyPC bilayer sample. A) Before (black) and after (red) addition of valinomycin following addition of three polyelectrolyte layers. B & C) Cycling electrolyte twice consecutively between NaCl (black), KCl (red) and NaCl (purple) with valinomycin incorporated. Table shows impedance and capacitance values of the lipid bilayer. Also shown is percentage difference between each impedance value and the bilayer impedance after rehydration.

Bilayer 40% 5, was able to maintain a reasonable level of impedance even after rehydration (figure 3-55). However, addition of valinomycin decreased this from 0.11 $M\Omega cm^2$ to 4.6 $k\Omega cm^2$. Valinomycin functionality was intact, with the biggest change being the improved recovery to above 10 $k\Omega cm^2$ after cycling back to NaCl from KCl solvent. This was not something observed for any of the uncoated samples.

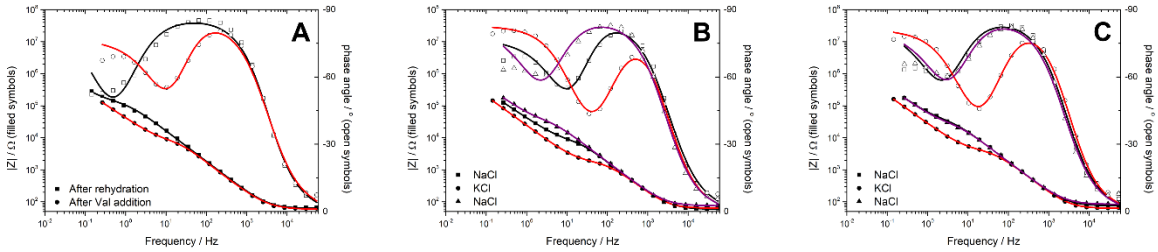

Bilayer PE 40% 5	Impedance ($M\Omega cm^2$)	Capacitance ($\mu F cm^{-2}$)	Change in Impedance
Initial Bilayer	1.4 ± 0.06	1.4 ± 0.06	
After Polyelectrolyte Addition	3.8 ± 0.4	1.7 ± 0.08	
After Rehydration	0.11 ± 0.02	1.5 ± 0.07	
After Val Addition	0.0046 ± 0.0004	1.1 ± 0.2	-96%
KCl	0.0014 ± 0.00003	1.2 ± 0.06	-99%
NaCl	0.021 ± 0.004	1.6 ± 0.2	-81%
KCl	0.0031 ± 0.00008	1.1 ± 0.05	-97%
NaCl	0.016 ± 0.003	1.6 ± 0.2	-85%

Figure 3-55: Bode plots of impedance (closed shapes) and phase angle (open shapes) for a rehydrated 40% tethered DPhyPC bilayer sample. A) Before (black) and after (red) addition of valinomycin following addition of three polyelectrolyte layers. B & C) Cycling electrolyte twice consecutively between NaCl (black), KCl (red) and NaCl (purple) with valinomycin incorporated. Table shows impedance and capacitance values of the lipid bilayer. Also shown is percentage difference between each impedance value and the bilayer impedance after rehydration.

The bilayers at 40% tethering density were able to recover from the rehydration process more consistently when coated with polyelectrolyte. Once valinomycin was incorporated into the bilayers, there was also evidence of improved functionality with polyelectrolyte incorporated, however this improvement was inconsistent and relatively small.

3.5 Effect of Cholesterol on Dehydration and Rehydration on DPhyPC Lipid Bilayers

Whilst tBLMs provide an important testing mechanism far simpler than true lipid membranes, there is much value in adding further complexity to them to better simulate the biological membrane environment. Cholesterol is a major component of mammalian cell membranes. It acts to modulate membrane fluidity and permeability, preventing crystallisation by separating phospholipid tails.

Whilst bilayers were able to successfully be dried out and rehydrated with minimal change at high tethering density when only the tethering monolayer and DPhyPC lipids were present, it is of interest to also determine whether the introduction of another chemical species affects this.

Cholesterol was added as part of the DPhyPC solution making up the bilayer outer leaflet and the spaces left by the tethering lipid in the inner leaflet. The addition of cholesterol in this solution was performed at 10%, with the remaining 90% being DPhyPC as used in previous experiments. Too much cholesterol can cause phase separation in the bilayer, whilst it has been documented that a typical lipid bilayer is 10-15% made up by proteins.[194, 195] Thus, 10% was considered an adequate percentage of cholesterol to include. Future experiments could be performed to investigate any differences that could arise from alternate ratios.

3.5.1 80%-Tethered Lipid Bilayers with 10% Cholesterol in DPhyPC Outer Layer

Formation of 80%-tethered samples resulted in bilayers that consistently had a lower level of impedance than most cholesterol-free bilayers modelled previously. Whilst one sample was modelled with an impedance of 38 MΩcm^2, the others were modelled between 0.78 and 2.3 MΩcm^2 (figures 3-56 and 3-57). However, despite the slightly lower initial impedance, membranes still appeared to be formed.

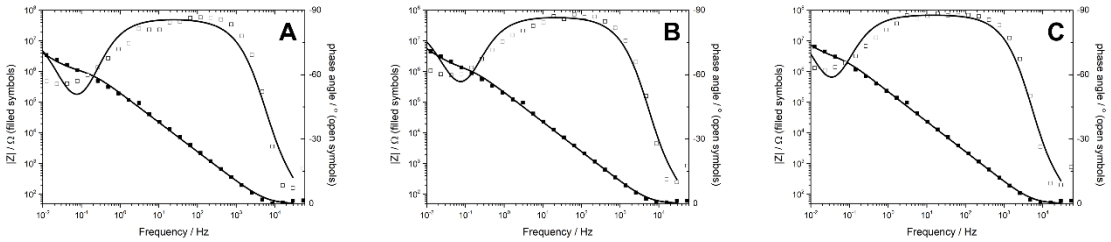

Sample	Impedance (MΩcm^2)	Capacitance (μFcm^{-2})
Bilayer Chol 80% 1	0.82 ± 0.3	1.1 ± 0.1
Bilayer Chol 80% 2	0.95 ± 0.3	1.1 ± 0.1
Bilayer Chol 80% 3	2.3 ± 0.8	1.1 ± 0.2

Figure 3-56: Bode plots of impedance (closed squares) and phase angle (open squares) for three different 80% tethered DPhyPC bilayer samples in 100 mM NaCl with 10% cholesterol in the outer leaflet of the bilayer. Table shows impedance and capacitance values of the four different lipid bilayers.

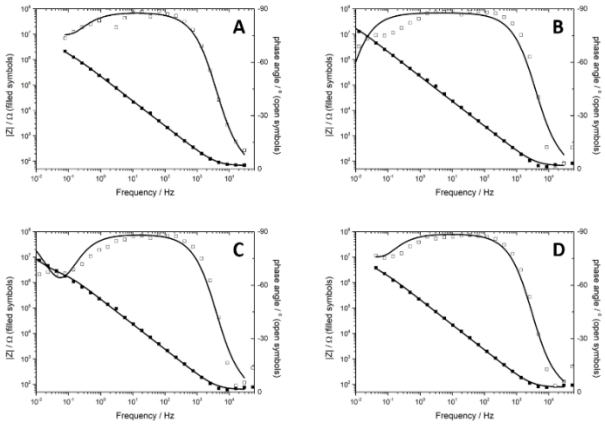

Sample	Impedance (MΩcm^2)	Capacitance (μFcm^{-2})
Bilayer Chol 80% 4	0.78 ± 0.2	1.8 ± 0.2
Bilayer Chol 80% 5	38 ± 6	0.76 ± 0.02
Bilayer Chol 80% 6	1.6 ± 0.3	1.2 ± 0.09
Bilayer Chol 80% 7	1.2 ± 0.3	1.8 ± 0.2

Figure 3-57: Bode plots of impedance (closed squares) and phase angle (open squares) for four different 80% tethered DPhyPC bilayer samples in 100 mM NaCl with 10% cholesterol in the outer leaflet of the bilayer. Table shows impedance and capacitance values of the four different lipid bilayers.

Addition of valinomycin to cholesterol-incorporated bilayers showed functionality was intact in all cases (figures 3-58, 3-59 and 3-60). Valinomycin addition resulted in some impedance decrease across samples ranging from 50% decrease for one sample to almost 2 orders of magnitude for another. For all samples there was consistently a further decrease to less than 10 kΩcm^2 on cycling to KCl. Recovery on return to NaCl occurred for all samples, with variation in magnitude, and further cycling producing similar results. These results suggest that the presence of cholesterol did not affect the functionality of 80%-tethered bilayers.

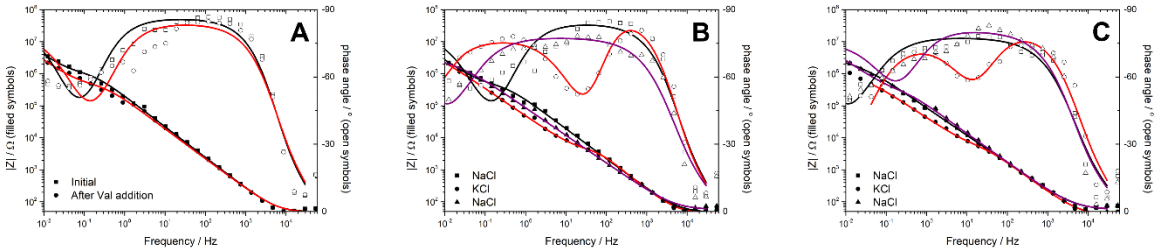

Bilayer Chol 80% 1	Impedance (MΩcm^2)	Capacitance (μFcm^{-2})	Change in Impedance
Initial Bilayer	0.82 ± 0.3	1.1 ± 0.1	
After Val Addition	0.34 ± 0.1	1.4 ± 0.2	-59%
KCl	0.0026 ± 0.0004	0.53 ± 0.2	-99.7%
NaCl	2.0 ± 0.3	2.7 ± 0.1	$+144\%$
KCl	0.0031 ± 0.0008	2.2 ± 0.6	-99.6%
NaCl	0.16 ± 0.07	2.9 ± 0.5	-80%

Figure 3-58: Bode plots of impedance (closed shapes) and phase angle (open shapes) for an 80% tethered DPhyPC bilayer sample with 10% cholesterol in the outer leaflet. A) Before (black) and after (red) addition of valinomycin. B & C) Cycling electrolyte twice consecutively between NaCl (black), KCl (red) and NaCl (purple) with valinomycin incorporated. Table shows impedance and capacitance values of the lipid bilayer. Also shown is percentage difference between each impedance value and the initial bilayer impedance.

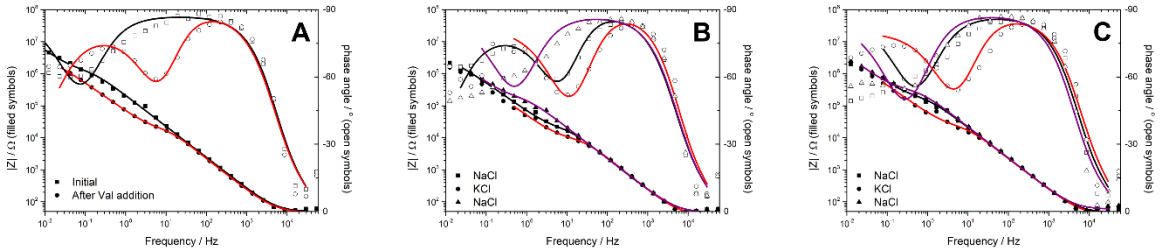

Bilayer Chol 80% 2	Impedance (MΩcm^2)	Capacitance (μFcm^{-2})	Change in Impedance
Initial Bilayer	0.95 ± 0.3	1.1 ± 0.1	
After Val Addition	0.011 ± 0.002	0.83 ± 0.2	-99%
KCl	0.0065 ± 0.001	0.70 ± 0.2	-99.3%
NaCl	0.13 ± 0.05	1.2 ± 0.1	-86%
KCl	0.015 ± 0.004	0.96 ± 0.3	-98%
NaCl	0.24 ± 0.05	1.0 ± 0.1	-75%

Figure 3-59: Bode plots of impedance (closed shapes) and phase angle (open shapes) for an 80% tethered DPhyPC bilayer sample with 10% cholesterol in the outer leaflet. A) Before (black) and after (red) addition of valinomycin. B & C) Cycling electrolyte twice consecutively between NaCl (black), KCl (red) and NaCl (purple) with valinomycin incorporated. Table shows impedance and capacitance values of the lipid bilayer. Also shown is percentage difference between each impedance value and the initial bilayer impedance.

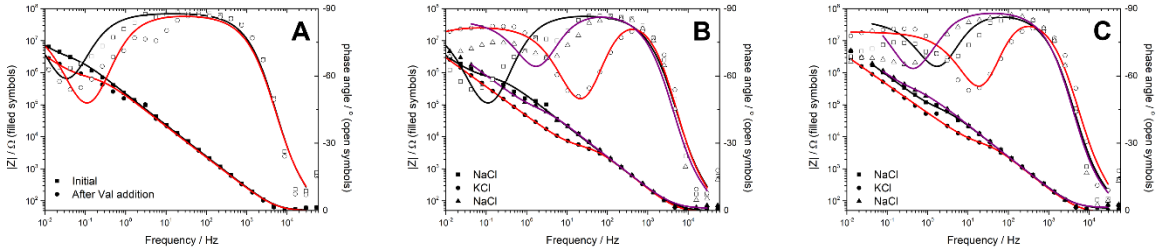

Bilayer Chol 80% 3	Impedance (MΩcm^2)	Capacitance (μFcm^{-2})	Change in Impedance
Initial Bilayer	2.3 ± 0.8	1.1 ± 0.2	
After Val Addition	0.56 ± 0.1	1.1 ± 0.1	-76%
KCl	0.0035 ± 0.0003	0.67 ± 0.1	-99.8%
NaCl	0.042 ± 0.01	1.2 ± 0.2	-98%
KCl	0.0036 ± 0.0006	0.67 ± 0.2	-99.8%
NaCl	0.19 ± 0.08	1.1 ± 0.1	-92%

Figure 3-60: Bode plots of impedance (closed shapes) and phase angle (open shapes) for an 80% tethered DPhyPC bilayer sample with 10% cholesterol in the outer leaflet. A) Before (black) and after (red) addition of valinomycin. B & C) Cycling electrolyte twice consecutively between NaCl (black), KCl (red) and NaCl (purple) with valinomycin incorporated. Table shows impedance and capacitance values of the lipid bilayer. Also shown is percentage difference between each impedance value and the initial bilayer impedance.

The dehydration and subsequent rehydration of 80%-tethered cholesterol-incorporated samples showed minimal change in impedance, with less than 25% change for two of the samples (figure 3-61). Bilayer Chol 80% 7 showed a small degree of degradation from 1.2 to 0.63 MΩcm^2, whilst the decrease seen for bilayer Chol 80% 5 from 38 to 5.4 MΩcm^2 still resulted in a bilayer of good impedance compared to the other samples.

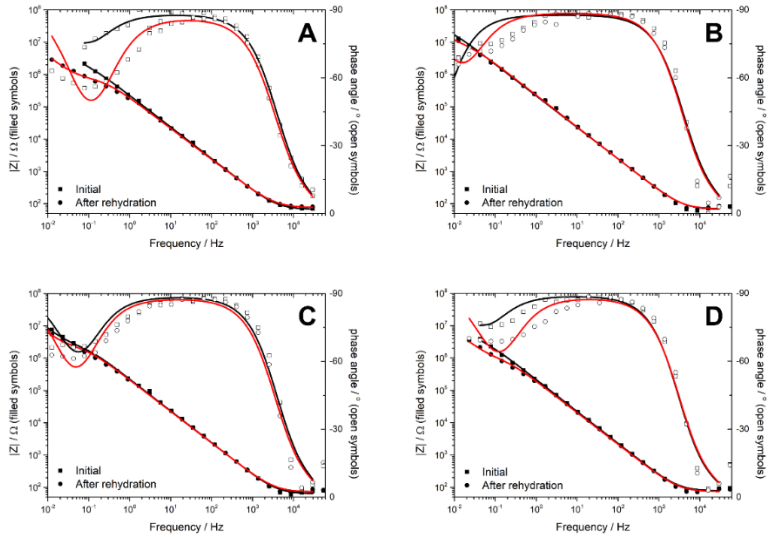

Sample	Sample	Impedance ($M\Omega cm^2$)	Capacitance ($\mu F cm^{-2}$)	Change in Impedance
Bilayer Chol 80% 4	**Initial**	0.78 ± 0.2	1.8 ± 0.2	
	After Rehydration	0.62 ± 0.05	1.1 ± 0.05	-21%
Bilayer Chol 80% 5	**Initial**	38 ± 6	0.76 ± 0.02	
	After Rehydration	5.4 ± 1	1.2 ± 0.09	-86%
Bilayer Chol 80% 6	**Initial**	1.6 ± 0.3	1.2 ± 0.09	
	After Rehydration	1.7 ± 0.2	1.1 ± 0.06	$+6.3\%$
Bilayer Chol 80% 7	**Initial**	1.2 ± 0.3	1.8 ± 0.2	
	After Rehydration	0.63 ± 0.1	1.4 ± 0.1	-48%

Figure 3-61: Bode plots of impedance (closed shapes) and phase angle (open shapes) for four different 80% tethered DPhyPC bilayer samples in 100 mM NaCl with 10% cholesterol in the outer leaflet before (black) and after (red) rehydration. Table shows impedance and capacitance values of the lipid bilayers. Also shown is percentage difference between each impedance value and the initial bilayer impedance.

Addition of valinomycin to bilayer Chol 80% 4 resulted in a decrease in impedance from 0.62 $M\Omega cm^2$ to only 6.9 $k\Omega cm^2$ (figure 3-62). A further decrease to 3.7 $k\Omega cm^2$ in the presence of KCl and recovery to 54 $k\Omega cm^2$ suggested that the bilayer had successfully incorporated valinomycin, with further cycling resulting in a decrease to below 10 $k\Omega cm^2$ again before recovery to 53 $k\Omega cm^2$.

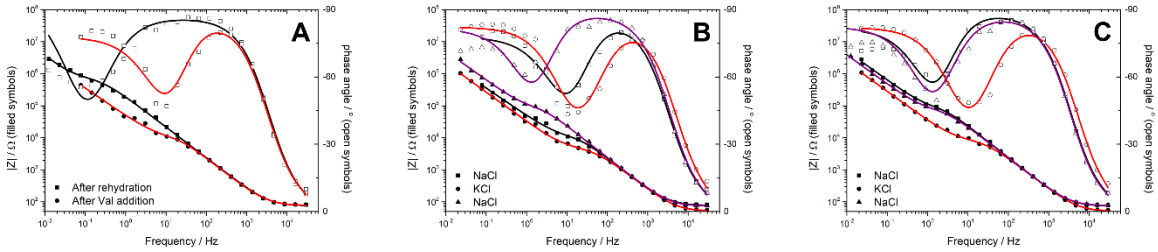

Bilayer Chol 80% 4	Impedance (MΩcm^2)	Capacitance (μFcm^{-2})	Change in Impedance
Initial Bilayer	0.78 ± 0.2	1.8 ± 0.2	
After Rehydration	0.62 ± 0.05	1.1 ± 0.05	
After Val Addition	0.0069 ± 0.001	0.88 ± 0.2	-99%
KCl	0.0037 ± 0.0002	1.1 ± 0.1	-99.4%
NaCl	0.054 ± 0.007	0.92 ± 0.1	-91%
KCl	0.0066 ± 0.0003	1.0 ± 0.08	-99%
NaCl	0.053 ± 0.005	1.0 ± 0.09	-91%

Figure 3-62: Bode plots of impedance (closed shapes) and phase angle (open shapes) for a rehydrated 80% tethered DPhyPC bilayer sample with 10% cholesterol in the outer leaflet. A) Before (black) and after (red) addition of valinomycin. B & C) Cycling electrolyte twice consecutively between NaCl (black), KCl (red) and NaCl (purple) with valinomycin incorporated. Table shows impedance and capacitance values of the lipid bilayer. Also shown is percentage difference between each impedance value and the bilayer impedance after rehydration.

Rehydration of bilayer Chol 80% 5 resulted in the highest impedance of all rehydrated bilayers with cholesterol incorporated, however addition of valinomycin caused a huge decrease in impedance to just 27 kΩcm^2 (figure 3-63). A further decrease then occurred on cycling to KCl with a modelled impedance of 9.5 kΩcm^2. Strong recovery was observed on cycling back to NaCl with a return to the MΩcm^2 level initially observed before rehydration. This suggests the initial perturbation on addition of valinomycin was due to the presence of potassium ions or some other reversible change to the bilayer structure. Continued cycling was able to show decrease to 23 kΩcm^2 and again strong recovery to 3.8 MΩcm^2, only 30% less than the initial-post rehydration impedance.

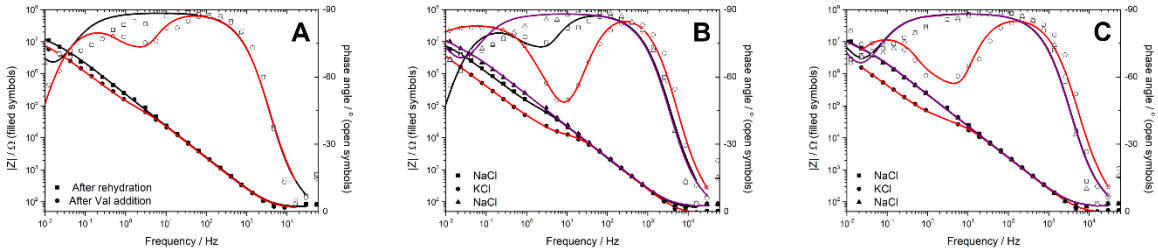

Bilayer Chol 80% 5	Impedance (MΩcm^2)	Capacitance (μFcm^{-2})	Change in Impedance
Initial Bilayer	38 ± 6	0.76 ± 0.02	
After Rehydration	5.4 ± 1	1.2 ± 0.09	
After Val Addition	0.027 ± 0.01	1.4 ± 0.4	-99.5%
KCl	0.0095 ± 0.0006	0.69 ± 0.07	-99.8%
NaCl	3.2 ± 3	1.4 ± 0.07	-41%
KCl	0.023 ± 0.004	0.89 ± 0.1	-99.6%
NaCl	3.8 ± 0.7	1.2 ± 0.1	-30%

Figure 3-63: Bode plots of impedance (closed shapes) and phase angle (open shapes) for a rehydrated 80% tethered DPhyPC bilayer sample with 10% cholesterol in the outer leaflet. A) Before (black) and after (red) addition of valinomycin. B & C) Cycling electrolyte twice consecutively between NaCl (black), KCl (red) and NaCl (purple) with valinomycin incorporated. Table shows impedance and capacitance values of the lipid bilayer. Also shown is percentage difference between each impedance value and the bilayer impedance after rehydration.

Bilayer Chol 80% 6 showed minimal no change after rehydration, and addition of valinomycin also did not result in much impedance shift (figure 3-64). Cycling to KCl produced a dramatic decrease in resistance to 2.8 kΩcm^2, with good recovery to an impedance still above 1 MΩcm^2. Further exchange of solvent solutions showed continued functionality of valinomycin incorporated within the bilayer.

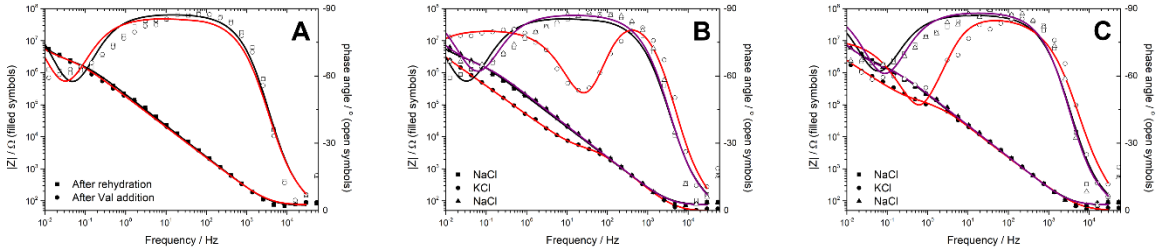

Bilayer 6	Impedance (MΩcm^2)	Capacitance (μFcm^{-2})	Change
Initial Bilayer	1.6 ± 0.3	1.2 ± 0.09	
After Rehydration	1.7 ± 0.2	1.1 ± 0.06	
After Val Addition	2.1 ± 0.3	1.3 ± 0.09	$+24\%$
KCl	0.0028 ± 0.0002	0.63 ± 0.1	-99.8%
NaCl	1.3 ± 0.2	1.2 ± 0.09	-24%
KCl	0.086 ± 0.015	0.97 ± 0.2	-95%
NaCl	0.98 ± 0.15	1.1 ± 0.09	-42%

Figure 3-64: Bode plots of impedance (closed shapes) and phase angle (open shapes) for a rehydrated 80% tethered DPhyPC bilayer sample with 10% cholesterol in the outer leaflet. A) Before (black) and after (red) addition of valinomycin. B & C) Cycling electrolyte twice consecutively between NaCl (black), KCl (red) and NaCl (purple) with valinomycin incorporated. Table shows impedance and capacitance values of the lipid bilayer. Also shown is percentage difference between each impedance value and the bilayer impedance after rehydration.

Bilayer Chol 80% 7 showed some decrease in impedance after rehydration (figure 3-65), and further decrease like that modelled in bilayer Chol 80% 4 on addition of valinomycin. Further decrease on electrolyte exchange to KCl and recovery to above 0.1 MΩcm^2 suggested that valinomycin functionality was intact, however the bilayer was not able to recover completely to the level of impedance initially modelled after rehydration.

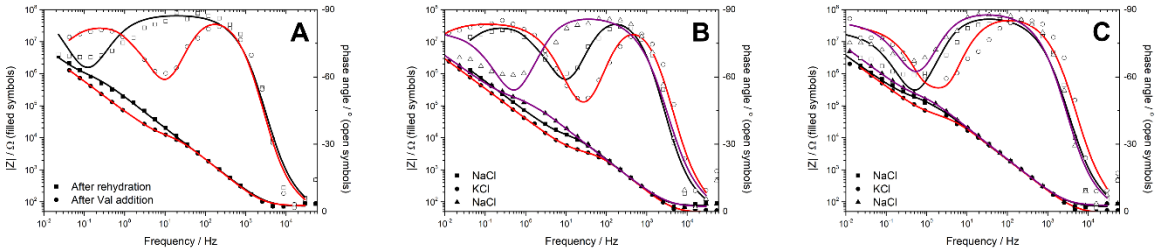

Bilayer Chol 80% 7	Impedance (MΩcm^2)	Capacitance (μFcm^{-2})	Change in Impedance
Initial Bilayer	1.2 ± 0.3	1.8 ± 0.2	
After Rehydration	0.63 ± 0.1	1.4 ± 0.1	
After Val Addition	0.0074 ± 0.001	0.087 ± 0.2	-99%
KCl	0.0026 ± 0.0001	0.075 ± 0.09	-99.6%
NaCl	0.11 ± 0.03	1.2 ± 0.2	-83%
KCl	0.035 ± 0.005	1.1 ± 0.1	-94%
NaCl	0.12 ± 0.03	1.2 ± 0.1	-81%

Figure 3-65: Bode plots of impedance (closed shapes) and phase angle (open shapes) for a rehydrated 80% tethered DPhyPC bilayer sample with 10% cholesterol in the outer leaflet. A) Before (black) and after (red) addition of valinomycin. B & C) Cycling electrolyte twice consecutively between NaCl (black), KCl (red) and NaCl (purple) with valinomycin incorporated. Table shows impedance and capacitance values of the lipid bilayer. Also shown is percentage difference between each impedance value and the bilayer impedance after rehydration.

The results for these bilayers show that cholesterol-DPhyPC samples with 80% DPhyTL tethering density were still able to be dried out and rehydrated, with valinomycin functionality also remaining intact. The degree of bilayer degradation after rehydration was inconsistent, however most samples were able to show functionality and recovery in presence of different solvents with valinomycin incorporated at similar levels to 80%-tethered bilayers without cholesterol present.

The main difference between samples was the lower level of initial bilayer impedance compared to samples without cholesterol incorporated. Bilayer samples in 3.2.2 and 3.3.1 with 80% tethering density and no cholesterol incorporated were regularly able to provide initial impedance levels comfortably above 1 MΩ, whilst most cholesterol-incorporated samples were only able to achieve initial levels of impedance around 1 MΩ. This may have been to do with cholesterol affecting the bilayer's initial level of fluidity by preventing lipids from stiffening and becoming more electrically sealing. Regardless, such levels of impedance are still reasonable for undertaking of ion transport studies.

3.5.2 60%-Tethered Lipid Bilayers with 10% Cholesterol in DPhyPC Outer Layer

The decrease in tethering density afforded by a greater proportion of 2-mercaptoethanol in tethering solution results in an increased amount of space in the bilayer's inner leaflet that is taken up by DPhyPC. The inclusion of cholesterol in the DPhyPC solution that is used to form the outer layer of the membrane bilayer could play a role not only in how the bilayer itself forms initially, but how resistant it is to degradation upon drying out and rehydration. Thus, it was important to investigate the formation and rehydration of DPhyPC bilayers at a decreased tethering density.

The impedance modelled for 60% tethered bilayers was less than 1 MΩcm^2 in most cases, with two samples slightly above at 1.2 and 1.3 MΩcm^2 (figures 3-66 and 3-67). This was lower than the impedance initially modelled for most of the bilayers at 60% tethering density without cholesterol incorporated.

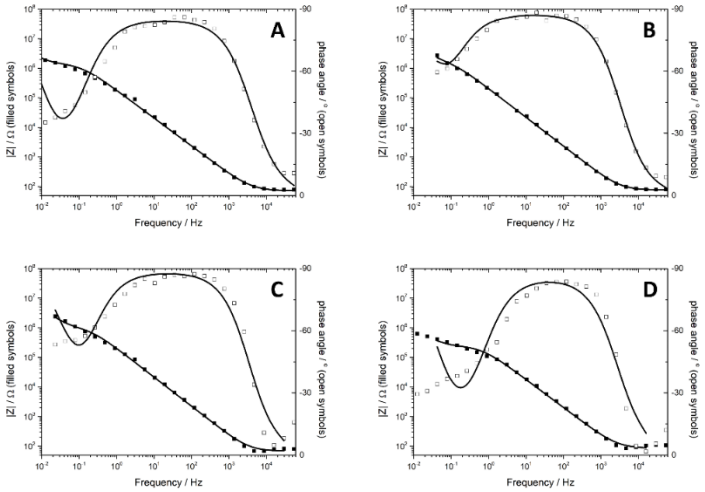

Sample	Impedance (MΩcm^2)	Capacitance (μFcm^{-2})
Bilayer Chol 60% 1	1.3 ± 0.1	1.1 ± 0.07
Bilayer Chol 60% 2	1.2 ± 0.1	1.3 ± 0.06
Bilayer Chol 60% 3	0.78 ± 0.09	1.0 ± 0.07
Bilayer Chol 60% 4	0.23 ± 0.02	1.2 ± 0.1

Figure 3-66: Bode plots of impedance (closed squares) and phase angle (open squares) for four different 60% tethered DPhyPC bilayer samples in 100 mM NaCl with 10% cholesterol in the outer leaflet of the bilayer. Table shows impedance and capacitance values of the four different lipid bilayers.

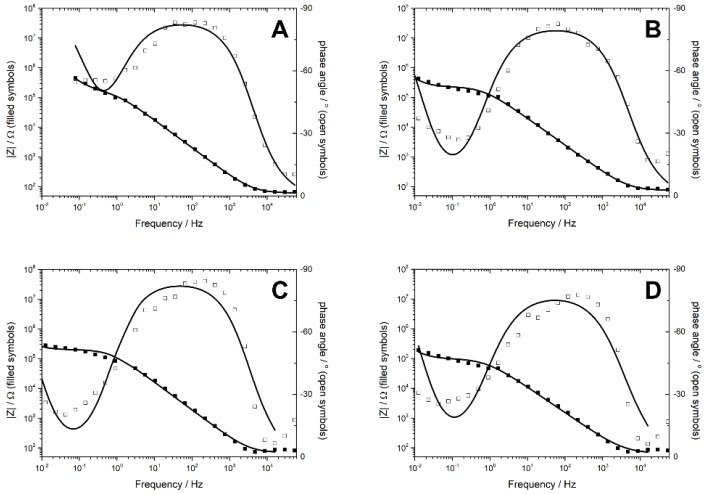

Sample	Impedance (MΩcm^2)	Capacitance (μFcm^{-2})
Bilayer Chol 60% 5	0.14 ± 0.01	1.5 ± 0.09
Bilayer Chol 60% 6	0.23 ± 0.01	1.2 ± 0.09
Bilayer Chol 60% 7	0.20 ± 0.01	1.3 ± 0.1
Bilayer Chol 60% 8	0.10 ± 0.007	2.5 ± 0.3

Figure 3-67: Bode plots of impedance (closed squares) and phase angle (open squares) for four different 60% tethered DPhyPC bilayer samples in 100 mM NaCl with 10% cholesterol in the outer leaflet of the bilayer. Table shows impedance and capacitance values of the four different lipid bilayers.

All bilayers formed with 10% w/w cholesterol at 60% tethering density were able to function well with valinomycin incorporated, with varying levels of impedance drop and recovery. Bilayer Chol 60% 1 had very little change in impedance on addition of valinomycin, with a modelled decrease of only 25% (figure 3-68). The cycling of solvents to KCl showed a drop to 1.6 kΩcm^2. Cycling to NaCl resulted in only a small increase of impedance to 6.5 kΩcm^2, however further cycling of solvents resulted in almost full recovery to above 1 MΩcm^2. This delayed recovery may have been due to potassium ions still present in solution that had not been properly removed, or a temporary defect in the bilayer.

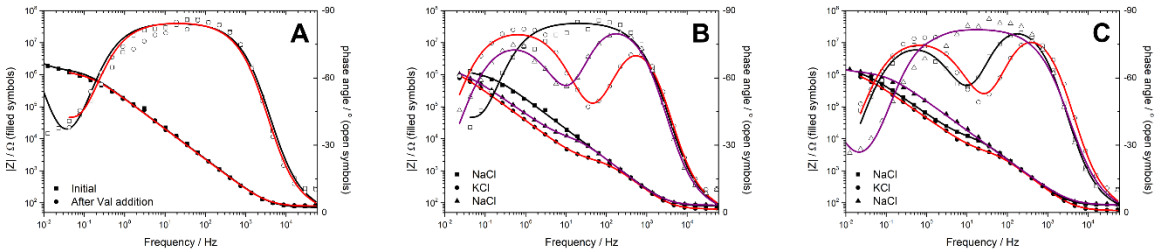

Bilayer Chol 60% 1	Impedance (MΩcm^2)	Capacitance (μFcm^{-2})	Change in Impedance
Initial Bilayer	1.3 ± 0.1	1.1 ± 0.07	
After Val Addition	0.97 ± 0.08	1.1 ± 0.05	-25%
KCl	0.0016 ± 0.0001	1.0 ± 0.1	-99.9%
NaCl	0.0065 ± 0.0005	0.95 ± 0.09	-99.5%
KCl	0.0026 ± 0.0002	0.95 ± 0.1	-99.8%
NaCl	1.1 ± 0.2	1.3 ± 0.07	-15%

Figure 3-68: Bode plots of impedance (closed shapes) and phase angle (open shapes) for a 60% tethered DPhyPC bilayer sample with 10% cholesterol in the outer leaflet. A) Before (black) and after (red) addition of valinomycin. B & C) Cycling electrolyte twice consecutively between NaCl (black), KCl (red) and NaCl (purple) with valinomycin incorporated. Table shows impedance and capacitance values of the lipid bilayer. Also shown is percentage difference between each impedance value and the initial bilayer impedance.

Addition of valinomycin to bilayer Chol 60% 2 resulted in an increase in impedance, however with a high amount of modelling error this is not possible to draw any conclusions from (figure 3-69). Transition to KCl solvent showed a decrease to below 5 kΩin both instances which could only be recovered to 110 and 86 kΩcm^2 after each cycle back to NaCl. This is still evidence of functionality, but not with the degree of recovery observed for bilayer Chol 60% 1.

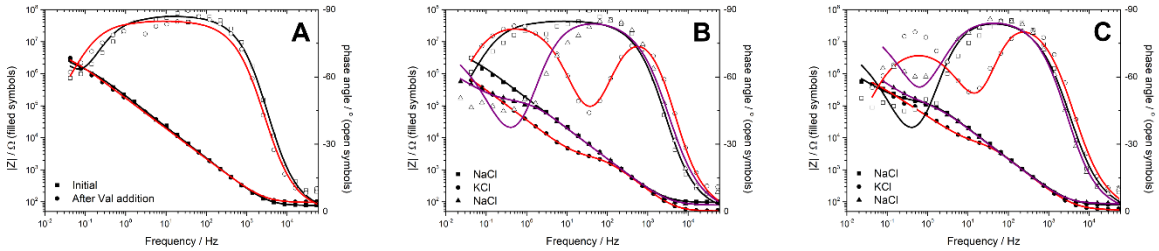

Bilayer Chol 60% 2	Impedance (MΩcm^2)	Capacitance (μFcm^{-2})	Change in Impedance
Initial Bilayer	1.2 ± 0.1	1.3 ± 0.06	
After Val Addition	3.0 ± 6	1.4 ± 1.9	$+150\%$
KCl	0.0020 ± 0.00006	0.93 ± 0.06	-99.8%
NaCl	0.11 ± 0.01	0.99 ± 0.1	-91%
KCl	0.0040 ± 0.0007	0.70 ± 0.2	-99.7%
NaCl	0.086 ± 0.01	1.3 ± 0.1	-93%

Figure 3-69: Bode plots of impedance (closed shapes) and phase angle (open shapes) for a 60% tethered DPhyPC bilayer sample with 10% cholesterol in the outer leaflet. A) Before (black) and after (red) addition of valinomycin. B & C) Cycling electrolyte twice consecutively between NaCl (black), KCl (red) and NaCl (purple) with valinomycin incorporated. Table shows impedance and capacitance values of the lipid bilayer. Also shown is percentage difference between each impedance value and the initial bilayer impedance.

The third bilayer again showed a small increase in bilayer impedance on addition of valinomycin (figure 3-70). There was also an improved degree of recovery on cycling of solvents when compared to the second bilayer. After cycling to KCl a decrease to 1.9 kΩcm^2 was modelled which then increased to 0.75 MΩcm^2 on return to NaCl. Further cycling provided similar results.

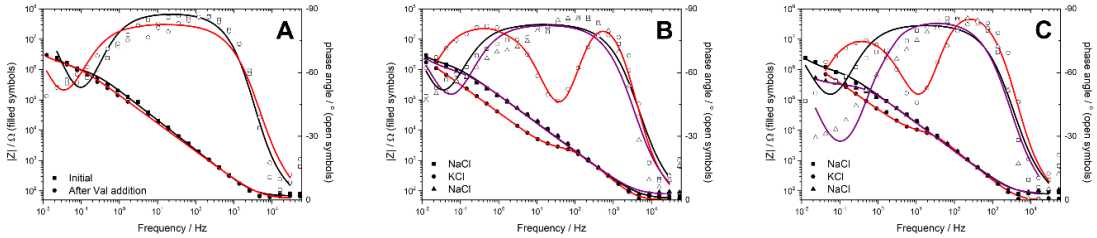

Bilayer Chol 60% 3	Impedance (MΩcm^2)	Capacitance (μFcm^{-2})	Change in Impedance
Initial Bilayer	0.78 ± 0.09	1.0 ± 0.07	
After Val Addition	1.4 ± 0.2	1.6 ± 0.1	$+80\%$
KCl	0.0019 ± 0.0001	0.49 ± 0.08	-99.8%
NaCl	0.75 ± 0.4	1.6 ± 0.3	-3.8%
KCl	0.0062 ± 0.0007	0.55 ± 0.1	-99.2%
NaCl	0.30 ± 0.07	1.2 ± 0.1	-62%

Figure 3-70: Bode plots of impedance (closed shapes) and phase angle (open shapes) for a 60% tethered DPhyPC bilayer sample with 10% cholesterol in the outer leaflet. A) Before (black) and after (red) addition of valinomycin. B & C) Cycling electrolyte twice consecutively between NaCl (black), KCl (red) and NaCl (purple) with valinomycin incorporated. Table shows impedance and capacitance values of the lipid bilayer. Also shown is percentage difference between each impedance value and the initial bilayer impedance.

Bilayer 60% 4 had a decrease from a low starting impedance of 0.23 MΩcm^2 to 18 kΩcm^2 on addition of valinomycin (figure 3-71). On cycling with KCl and NaCl solvents the same decrease to below 10 kΩcm^2 was observed in KCl whilst in NaCl recovery to above 0.1 MΩcm^2 was modelled, similarly to bilayer Chol 60% 3.

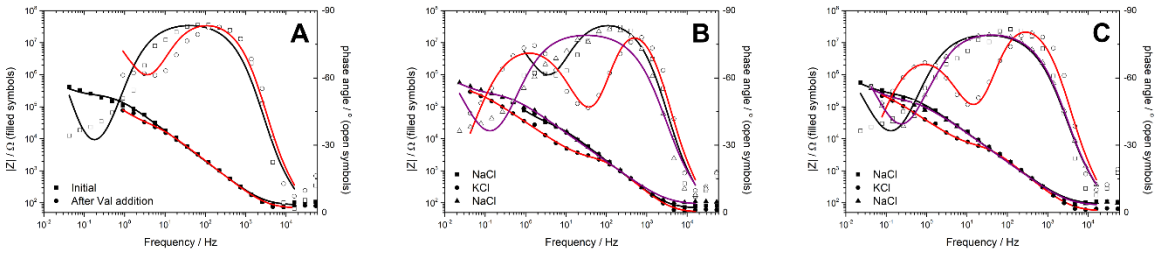

Bilayer Chol 60% 4	Impedance (MΩcm^2)	Capacitance (μFcm^{-2})	Change in Impedance
Initial Bilayer	0.23 ± 0.02	1.2 ± 0.1	
After Val Addition	0.018 ± 0.01	1.4 ± 0.3	-92%
KCl	0.0017 ± 0.0002	0.51 ± 0.1	-99.3%
NaCl	0.22 ± 0.05	1.8 ± 0.2	-4.3%
KCl	0.0041 ± 0.0005	0.69 ± 0.1	-98%
NaCl	0.14 ± 0.05	1.8 ± 0.2	-39%

Figure 3-71: Bode plots of impedance (closed shapes) and phase angle (open shapes) for a 60% tethered DPhyPC bilayer sample with 10% cholesterol in the outer leaflet. A) Before (black) and after (red) addition of valinomycin. B & C) Cycling electrolyte twice consecutively between NaCl (black), KCl (red) and NaCl (purple) with valinomycin incorporated. Table shows impedance and capacitance values of the lipid bilayer. Also shown is percentage difference between each impedance value and the initial bilayer impedance.

Across all samples the functionality of valinomycin was intact. For most there was also a reasonable degree of recovery in impedance when comparing resistance in KCl and NaCl after valinomycin was incorporated. Behaviourally this was consistent with bilayers formed without incorporation of cholesterol, with the main difference remaining the weaker initial bilayer impedance of the samples.

The dehydration and rehydration of 60%-tethered samples with cholesterol incorporated showed consistent decreases in bilayer impedance with all samples decreasing between 60 and 90% of their initial resistance (figure 3-72). No bilayers were able to maintain a reasonable level of quality after rehydration, with the highest modelled impedance for any sample being only 81 kΩcm^2.

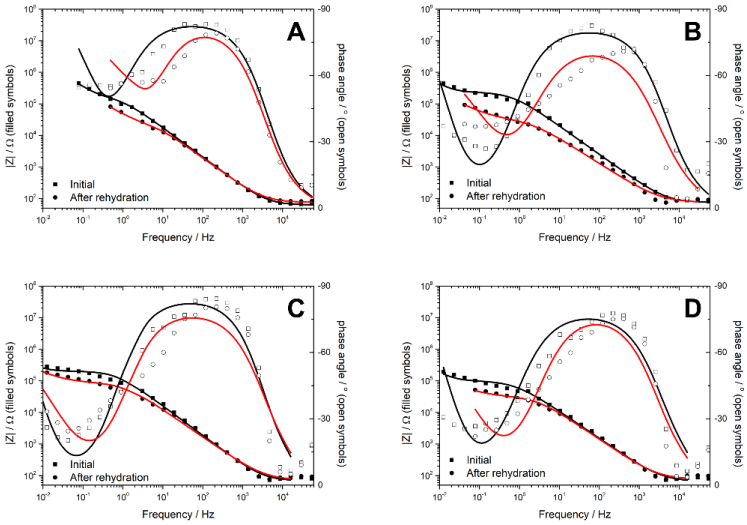

Sample	Sample	Impedance ($M\Omega cm^2$)	Capacitance ($\mu F cm^{-2}$)	Change in Impedance
Bilayer Chol 60% 5	**Initial**	0.14 ± 0.01	1.5 ± 0.09	
	After Rehydration	0.014 ± 0.004	1.8 ± 0.4	-90%
Bilayer Chol 60% 6	**Initial**	0.23 ± 0.01	1.2 ± 0.09	
	After Rehydration	0.027 ± 0.009	4.4 ± 0.8	-88%
Bilayer Chol 60% 7	**Initial**	0.20 ± 0.01	1.3 ± 0.1	
	After Rehydration	0.081 ± 0.01	2.2 ± 0.4	-60%
Bilayer Chol 60% 8	**Initial**	0.099 ± 0.007	2.5 ± 0.3	
	After Rehydration	0.030 ± 0.007	2.7 ± 0.4	-70%

Figure 3-72: Bode plots of impedance (closed shapes) and phase angle (open shapes) for four different 60% tethered DPhyPC bilayer samples in 100 mM NaCl with 10% cholesterol in the outer leaflet before (black) and after (red) rehydration. Table shows impedance and capacitance values of the lipid bilayers. Also shown is percentage difference between each impedance value and the initial bilayer impedance.

Further decrease in impedance was observed in bilayer Chol 60% 5 after the addition of valinomycin to solution, however further cycling with KCl and NaCl still showed a difference in impedance between solution presence (figure 3-73). There was also some recovery back to a value above the impedance values determined immediately after rehydration for the sample with a final impedance of 62 $k\Omega cm^2$.

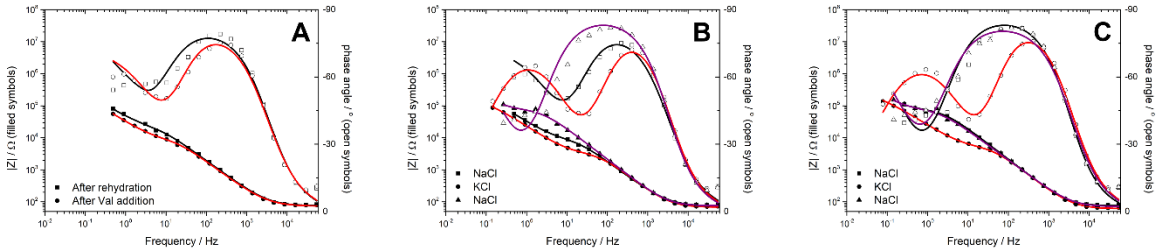

Bilayer Chol 60% 5	Impedance (MΩcm^2)	Capacitance (μFcm^{-2})	Change in Impedance
Initial Bilayer	0.14 ± 0.01	1.5 ± 0.09	
After Rehydration	0.014 ± 0.004	1.8 ± 0.4	
After Val Addition	0.0054 ± 0.0007	1.5 ± 0.3	-61%
KCl	0.0024 ± 0.0001	1.1 ± 0.09	-83%
NaCl	0.065 ± 0.01	1.0 ± 0.1	$+364\%$
KCl	0.0036 ± 0.0002	0.92 ± 0.09	-74%
NaCl	0.062 ± 0.01	1.4 ± 0.1	$+343\%$

Figure 3-73: Bode plots of impedance (closed shapes) and phase angle (open shapes) for a rehydrated 60% tethered DPhyPC bilayer sample with 10% cholesterol in the outer leaflet. A) Before (black) and after (red) addition of valinomycin. B & C) Cycling electrolyte twice consecutively between NaCl (black), KCl (red) and NaCl (purple) with valinomycin incorporated. Table shows impedance and capacitance values of the lipid bilayer. Also shown is percentage difference between each impedance value and the bilayer impedance after rehydration.

Addition of valinomycin to bilayer Chol 60% 6 after rehydration resulted in only a small change in impedance (figure 3-74). A more dramatic shift occurred when exchanging solvents to KCl and some recovery was observed on cycling back to NaCl with a final impedance of 10 kΩcm^2. This suggested some functionality with valinomycin incorporated, but in a bilayer of very poor electrical sealing quality.

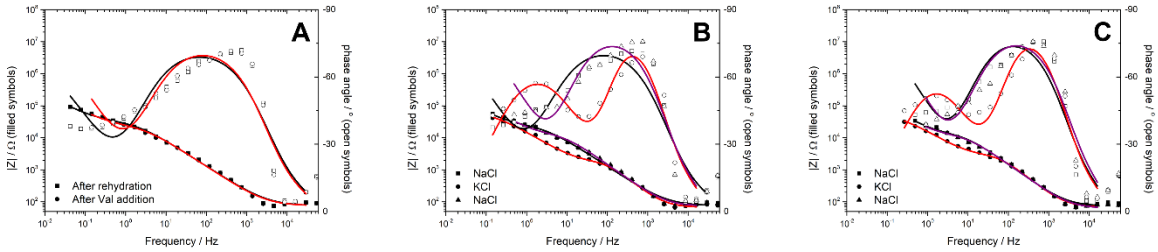

Bilayer Chol 60% 6	Impedance (MΩcm^2)	Capacitance (μFcm^{-2})	Change in Impedance
Initial Bilayer	0.23 ± 0.01	1.2 ± 0.09	
After Rehydration	0.027 ± 0.009	4.4 ± 0.8	
After Val Addition	0.021 ± 0.009	4.1 ± 0.8	-22%
KCl	0.0013 ± 0.0002	0.84 ± 0.3	-95%
NaCl	0.011 ± 0.005	2.3 ± 0.7	-59%
KCl	0.0022 ± 0.0005	0.93 ± 0.4	-92%
NaCl	0.010 ± 0.006	2.3 ± 0.7	-63%

Figure 3-74: Bode plots of impedance (closed shapes) and phase angle (open shapes) for a rehydrated 60% tethered DPhyPC bilayer sample with 10% cholesterol in the outer leaflet. A) Before (black) and after (red) addition of valinomycin. B & C) Cycling electrolyte twice consecutively between NaCl (black), KCl (red) and NaCl (purple) with valinomycin incorporated. Table shows impedance and capacitance values of the lipid bilayer. Also shown is percentage difference between each impedance value and the bilayer impedance after rehydration.

Bilayer Chol 60% 7 also showed minimal change in impedance on addition of valinomycin (figure 3-75), with larger impedance changes through the cycling process than in the case of the lower quality bilayer Chol 60% 6. Impedance was initially able to recover completely to the initial post-rehydration level when cycled through KCl and NaCl initially. Some drop off in recovery was modelled through the second cycle with bilayer resistance recovering to only 25% of the initial level.

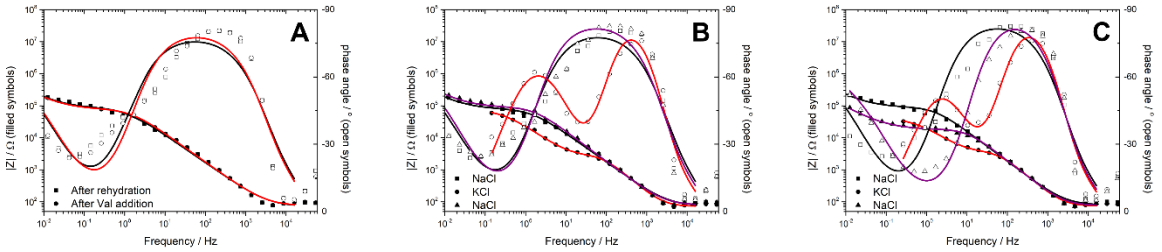

Bilayer Chol 60% 7	Impedance (MΩcm^2)	Capacitance (μFcm^{-2})	Change in Impedance
Initial Bilayer	0.20 ± 0.01	1.3 ± 0.1	
After Rehydration	0.081 ± 0.01	2.2 ± 0.4	
After Val Addition	0.075 ± 0.01	1.7 ± 0.2	-7%
KCl	0.0022 ± 0.0002	0.51 ± 0.1	-97%
NaCl	0.086 ± 0.01	1.2 ± 0.2	$+6\%$
KCl	0.0029 ± 0.0004	0.58 ± 0.1	-96%
NaCl	0.018 ± 0.001	0.85 ± 0.1	-78%

Figure 3-75: Bode plots of impedance (closed shapes) and phase angle (open shapes) for a rehydrated 60% tethered DPhyPC bilayer sample with 10% cholesterol in the outer leaflet. A) Before (black) and after (red) addition of valinomycin. B & C) Cycling electrolyte twice consecutively between NaCl (black), KCl (red) and NaCl (purple) with valinomycin incorporated. Table shows impedance and capacitance values of the lipid bilayer. Also shown is percentage difference between each impedance value and the bilayer impedance after rehydration.

Bilayer Chol 60% 8 began with a very low level of initial impedance, which decreased from 99 kΩcm^2 to 30 kΩcm^2 after rehydration, with an increase to 50 kΩcm^2 on addition of valinomycin (figure 3-76). Whilst this bilayer was of poor electrical sealing quality to begin with, it was still able to show valinomycin functionality with a decrease in impedance by an order of magnitude when electrolyte was changed to KCl. There was also recovery on cycling to NaCl with the impedance returning to above 10 kΩcm^2.

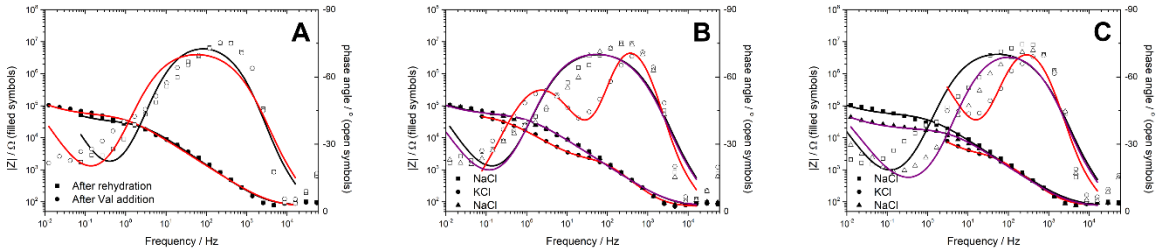

Bilayer Chol 60% 8	Impedance (MΩcm^2)	Capacitance (μFcm^{-2})	Change in Impedance
Initial Bilayer	0.099 ± 0.007	2.5 ± 0.3	
After Rehydration	0.030 ± 0.007	2.7 ± 0.4	
After Val Addition	0.050 ± 0.01	3.8 ± 0.6	$+67\%$
KCl	0.0015 ± 0.0002	0.78 ± 0.3	-95%
NaCl	0.051 ± 0.009	3.8 ± 0.6	$+70\%$
KCl	0.0024 ± 0.0007	1.4 ± 0.5	-92%
NaCl	0.018 ± 0.002	3.5 ± 0.6	-40%

Figure 3-76: Bode plots of impedance (closed shapes) and phase angle (open shapes) for a rehydrated 60% tethered DPhyPC bilayer sample with 10% cholesterol in the outer leaflet. A) Before (black) and after (red) addition of valinomycin. B & C) Cycling electrolyte twice consecutively between NaCl (black), KCl (red) and NaCl (purple) with valinomycin incorporated. Table shows impedance and capacitance values of the lipid bilayer. Also shown is percentage difference between each impedance value and the bilayer impedance after rehydration.

Across all samples, the introduction of cholesterol to the lipid bilayer did not affect whether the bilayers were able to recover from the drying out and rehydration process, even with a poor level of initial impedance. The major difference between cholesterol and cholesterol-free samples was the decrease in average initial impedance of the bilayer samples, with only 2 samples providing an initial impedance value above 1 MΩ.

3.6 Summary

The results from this chapter highlighted important new information about tBLMs. Firstly, it was shown that at especially high tethering density, tBLMs are able to retain their electrical sealing properties after being dried out and rehydrated. Secondly, at lower tethering densities in particular the addition of polyelectrolytes was able to improve bilayer resilience to being dried out and rehydrated. Finally, the addition of cholesterol to the outer leaflet of the bilayer did not greatly reduce the ability of tBLMs to recover from being dried out and rehydrated.

Chapter 4 - Biomedical Applications of tethered-Bilayer Lipid Membranes

This chapter highlights biomedical applications of tBLMs. The first sub-chapter, published in Langmuir, details the use of tBLMs as a testing platform for improvement of drug delivery platforms. Specifically, it focuses on the use of gold nanoparticles to improve the efficacy of colistin, a cationic polypeptide antibiotic, on bacterial cells. This is performed using tBLMs designed to mimic the outer cell membrane of bacteria using LPS extracted from *E. coli* as the primary component of the bilayer's outer leaflet.

The second sub-chapter highlights a novel way to create tBLMs that are more analogous to bacterial membranes by using lipid mixtures extracted directly from *A. baumannii*. The tBLMs created using these lipid extracts were used to help determine whether DHA incorporation resulted in ion leakage, part of a wider study examining the efflux activities of AdeB and AdeJ in *A. Baumannii*.

4.1 The Use of Cationic Gold Nanoparticles in Gram-Negative Bacterial Membrane Models

This sub-chapter has been published as:

Increasing Antibiotic Susceptibility: The Use of Cationic Gold Nanoparticles in Gram-Negative Bacterial Membrane Models, Jakob Andersson, Melanie Fuller, Alex Ashenden, Stephen A. Holt and Ingo Koeper, Langmuir 2021

Abstract

Antibiotic resistance will be one of the most prominent challenges to health-care systems in the coming decades, with the OECD predicting that up to 2.4 million deaths will be caused between 2015 and 2050 by drug-resistant bacterial infections in first-world countries alone, with infections costing health-care systems billions of dollars each year. Developing new methods to increase bacterial susceptibility toward drugs is an important step in treating resistant infections. Here, the synergistic effects of gold nanoparticles and the antibiotic drug colistin sulfate have been examined. A tethered lipid bilayer membrane was used to mimic a Gram-negative bacterial cell membrane. Exposing the membrane to gold nanoparticles prior to adding the antibiotic significantly increased the effect of the antibiotic on the membrane. Cationic gold nanoparticles could thus be used to enhance bacterial susceptibility to antibiotics, leading to a more potent treatment.

4.1.1 Introduction

With the rapid emergence of antibiotic resistance in the last few decades, existing antibiotic treatments have become significantly less effective, causing an increase in hospitalization rates, treatment costs, and mortality.[196-198]

Modelling released by the OECD in 2018 estimates that up to 2.4 million deaths will be caused between 2015 and 2050 by drug-resistant bacterial infections in first-world countries alone,[199] with infections costing health-care systems billions of dollars each year. The impact is even worse for countries with less sophisticated health-care infrastructure such as third world and emerging economies where at present around half of all bacterial infections are already resistant to one or more antibiotics.[200] Health-care systems in these countries are unlikely to be able to fund newly developed antibacterial therapies. Thus, increasing the efficacy of currently available antibiotics may be a better option. Various methods of increasing antibiotic efficacy have been proposed or explored, for example, combining antibiotics with nonantibiotic drugs,[201] inhibiting the function of bacterial proteins conferring resistance,[202] and combining antibiotics with phytochemicals.[203] However, these methods require the use of additional chemicals, which may place an additional burden on the patient or cause increased side effects. Alternatively, inert substances such as nanoparticles could be used to increase antibiotic efficacy, which, ideally, only target the pathogen without affecting the patient, reducing the required dosages for successful treatment.

Due to the unique structure of their cell membranes, Gram-negative bacteria are particularly resistant to traditional antibiotics. The cell walls of these bacteria consist of an inner and outer membrane with a layer of peptidoglycans and lipoproteins between the two membrane layers.[198] The outer membrane is asymmetric, with an outer leaflet comprised largely of lipopolysaccharide molecules that act as a shield, impeding antibiotic penetration into the membrane.[137, 204] Several of the currently used antibiotics target the bacterial cell membrane, including the last-resort drug colistin, which has also been used here.

Colistin is a cationic polypeptide antibiotic, which electrostatically interacts with the negatively charged phosphate groups of the lipopolysaccharides (LPS) in the outer membrane.[205, 206] This interaction leads to the formation of defects in the membrane, causing permeability and leakage of cellular contents, which ultimately leads to cell death.[206] Although colistin is a powerful drug, it also causes severe side effects,[207] and use of the drug was largely stopped in the 1970s. However, due to the increasing prevalence of multidrug-resistant bacterial infections, particularly by Gram-negative strains such as *Pseudomonas aeruginosa*, *Acinetobacter baumannii*, and *Klebsiella pneumoniae*, it is now increasingly used often[208] despite its toxicity. All of these pathogens have been listed in the highest priority category for the development of new antibiotic treatments by the World Health Organization.[209] A better understanding of the pharmacokinetics of colistin has increased its safety (Li Colistin), but it is one of the few remaining antibiotics with any effect on multidrug-resistant Gram-negative infections. Moreover, resistance against the drug has begun to emerge.[210-212] As there are few antibiotics ready to enter the market (in 2019, only eight drugs in total were in phase III clinical trials,[213] five of which are targeted toward Gram-negative bacteria[214]), enhancement of existing treatments is one of the best routes toward improved treatment methods. The exact mechanism of colistin resistance is not yet clear and several mechanisms likely exist, but it is suspected that some pathways include chemical modification of the lipid A component of LPS in the outer membrane.[215, 216] Antibiotic efficacy against changes in LPS structure can easily be tested using model systems.

To further reduce toxicity and increase effectiveness in case resistance emerges, it would be desirable to improve the efficacy of the antibiotic to achieve the same treatment effect at a lower concentration or to avoid increasing antibiotic concentration in case of resistance. Although gold nanoparticles, particularly positively charged particles, can pass through the cell membrane, they do not cause significant cytotoxicity[217, 218] and could therefore be a good solution. Previous research has shown that 3 nm diameter cationic gold nanoparticles can form defects in the membrane of both Gram-positive and Gram-negative bacteria.[219] These defects can cause a significant increase in cell permeability for *Escherichia coli* from 5% for untreated control cells compared to 73% for cells treated with gold nanoparticles. As colistin also targets the bacterial membrane, it should have an increased effect on membranes already damaged from pre-treatment with gold nanoparticles.

Here, the formation of defects caused by the binding of colistin to the membrane was enhanced through the addition of cationic gold nanoparticles. To simplify experiments, a model lipopolysaccharide-tethered bilayer lipid membrane (LPS-tBLM) system has been used to explore the effects of nanoparticle pre-treatment (figure 4-1). This model membrane system was developed to simplify the bacterial membrane structure and to allow a better understanding of how drugs and nanoparticles interact with the cell membrane.[123, 137] The membrane consists of a tethered lipid monolayer attached to a gold substrate, which is fused with LPS vesicles to mimic a bacterial membrane. The inner membrane leaflet is formed from an anchor-lipid mixed with a small thiol, mercaptoethanol, resulting in a sparsely tethered monolayer.

Although the model does not contain embedded membrane proteins, transporters, or peptides, it does replicate the fundamental chemical and physical properties of the bacterial membrane and therefore allows the qualitative observation of fundamental interactions between the cellular membrane and antibiotics.[201] In this manner, the most promising treatment methods can be identified and further investigated using other tools such as cell cultures, which are more realistic but also more time consuming and challenging to handle. Electrochemical impedance spectroscopy (EIS) and neutron reflectometry are well-established complementary methods to gain a detailed understanding of model membrane systems[130] and are the primary methods used here to monitor the interactions of the model membrane with the antibiotic and nanoparticles. These techniques are sensitive to small changes in the membrane structure and can provide detailed insight into the interaction between the membrane and drugs or nanoparticles.

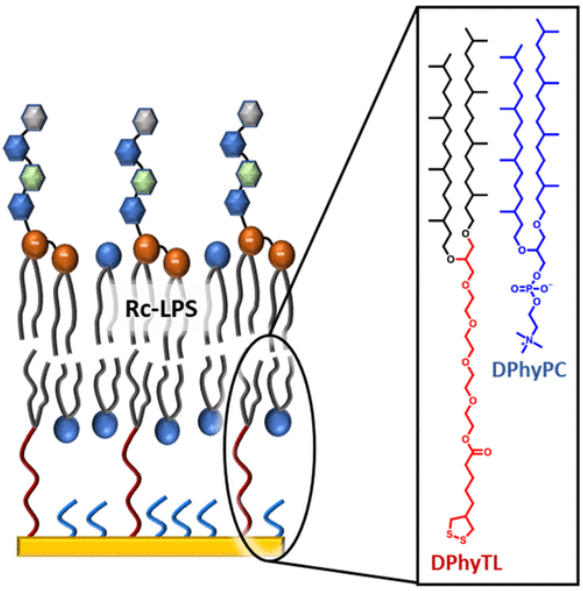

Figure 4-0-1: LPS-tBLM system with an inner leaflet comprised of DPhyTL (red/grey) and mercaptoethanol and an outer leaflet comprised of DPhyPC (blue) and Rc-strain LPS.

While EIS investigates the electrical properties of the membrane, neutron reflectivity allows determination of structural features at the sub-nanometre level.

This allows small defects or changes in the structure of the membrane, which do not result in significant changes in the electrical properties of the bilayer to be observed. Neutron reflectivity measures scattered neutron intensity as a function of scattering angle, affording vertically resolved structural information of the bilayer system. Experimental data is fitted to a previously established model[137] describing the membrane as an eight-layer system with each layer being fitted with thickness (Å), scattering length density (SLD) (10^{-6} Å^{-2}), hydration (vol %), and roughness (Å) (see figure 4-2).

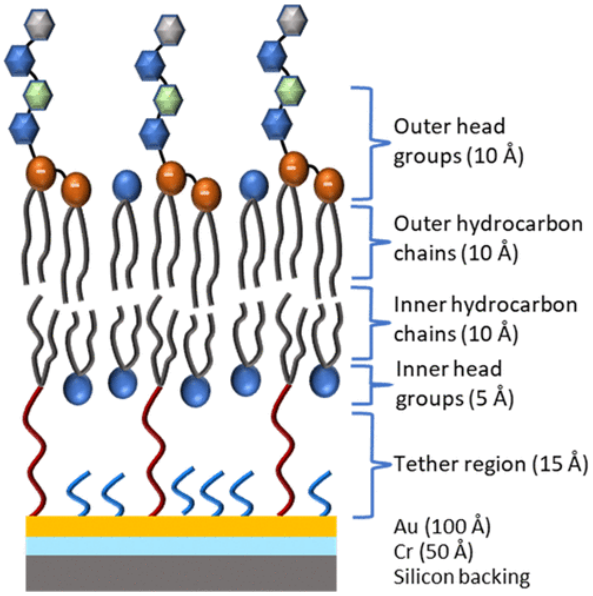

Figure 4-0-2: Schematic of a sparsely tethered tBLM separated into layers used to fit the neutron data as well as the approximate typical thickness of each layer.

In previous studies, we have shown that the addition of colistin to sparsely tethered LPS membranes causes structural changes to the outer leaflet, observed as an increase in roughness of the outer hydrocarbon chains and a change in hydration of the head groups.[137]

Using this information, we compared the roughness and hydration of the membrane before and after the addition of gold nanoparticles as well as determined whether the pre-treatment of the cationic nanoparticles before the addition of colistin causes a larger disruption to the membrane than the addition of nanoparticles and colistin together.

4.1.2 Materials and Methods

4.1.2.1 Chemicals

Colistin sulfate and Rc-strain lipopolysaccharides (Rc-LPS) obtained from the J5 mutant of *E. coli* (Sigma-Aldrich, Australia) were used without further purification. Ultrapure water obtained from a WaterPro PS reverse osmosis system (18.2 MΩcm resistance, Labconco) was used for all experiments. D_2O was obtained from the Australian Centre for Neutron Scattering at the Australian Nuclear Science and Technology Organisation (New South Wales, Australia).

4.1.2.2 Cationic Gold Nanoparticle Synthesis

Citrate-capped gold nanoparticles (AuNPs; 5 nm diameter) at a concentration of 8.4×10^{13} particles/mL were purchased from Nanocomposix. Gold nanoparticle solution (2 mL) was mixed with 3 mL of 5 mg/mL polydiallyldimethylammonium chloride (PDADMAC) (Sigma-Aldrich, Australia) (average M_w < 100 000) in 1 mM NaCl. The AuNP/PDADMAC solution was stirred overnight before centrifuging at 27 000*g* for 40 min to remove excess PDADMAC. The supernatant was removed, and the pellet was resuspended in ultrapure water. This washing step was repeated twice to ensure no excess PDADMAC remained. The characterization of the polyelectrolyte-coated gold nanoparticles can be found elsewhere.[220]

Prior to using the AuNPs for neutron studies, they were centrifuged and resuspended in D_2O at a concentration of approximately 3×10^{13} particles/mL.

4.1.2.3 Bilayer Formation

For all EIS experiments, membranes were assembled as described previously.[137] Briefly, clean silicon substrates were coated with layers of 5 nm chromium and 20 nm gold. Once coated, the substrates were rinsed with ethanol before being inserted into a solution of 80 μM DPhyTL and 20 μM mercaptoethanol for 18 h to allow the formation of the tethered monolayer. After monolayer formation, the substrates were removed from the ethanolic solution and rinsed thoroughly with ethanol before being dried under nitrogen. The bilayers were then formed by vesicle fusion with the already formed monolayer. Vesicles with 6% DPhyPC (Sigma-Aldrich, Australia) and 94% Rc-LPS at a lipid concentration of 1 mg/mL were used. Vesicles were prepared by mixing lipids in chloroform, evaporating the solvent, and rehydrating the lipids in water. The lipid–water mixture was extruded 31 times through a 200 nm track-etched polycarbonate filter membrane. All vesicle solutions were extruded just prior to use. The extruded vesicle solution (10 μL/mL) was added to the monolayer in 100 mM $CaCl_2$. The bilayers were left to form for 18 h at ambient temperature, and the resulting bilayers were rinsed with 5 cell volumes of $CaCl_2$.

To study the interaction of gold nanoparticles with the bilayers, 100 μL of cationic nanoparticles were either added simultaneously with 10 mg/mL colistin sulfate solution or the nanoparticles were added and left on the membrane for 18 h before being rinsed off, and then 10 mg/mL colistin sulfate solution was added to the membrane.

4.1.2.4 Electrochemical Impedance Spectroscopy

Electrochemical impedance spectroscopy was performed using a Metrohm Autolab potentiostat with a three-electrode setup using a platinum wire as a counter electrode and a Ag/AgCl reference electrode. For each spectrum, 30 data points were collected in the range from 100 kHz to 5 mHz with an amplitude of ±10 mV. All measurements were carried out in 100 mM NaCl or $CaCl_2$ electrolyte.

EIS data were analysed using ZView2 (Scribner Associates). All spectra were area-normalized using a surface area of 0.283 cm^2. The data were fitted to one of four equivalent circuits shown below. The error is the range of values that can be fitted for the respective parameter without decreasing the quality of the fit (evaluated by least-squares fitting).

4.1.2.5 Neutron Scattering

All neutron experiments were performed at the Australian Nuclear Science and Technology Organisation (ANSTO) at the 20 MW OPAL reactor (Lucas Heights, Sydney, Australia). Neutron reflectometry (NR) measurements were conducted using the PLATYPUS time-of-flight neutron reflectometer.[221] Cold neutrons with wavelengths from 2.5 to 18 Å were used. The reflected intensity of the neutrons was measured at glancing angles of 0.5, 0.9, and 5° under D_2O, H_2O, and CM4.5 (a mixture of 76% D_2O and 24% H_2O). All measurements were completed in 100 mM $CaCl_2$ for approximately 2 h per contrast unless otherwise stated. Preparation of the substrates was conducted at the South Australian node of the ANFF. Briefly, 10 cm diameter by 1 cm thickness polished circular crystal silicon disks were cleaned using a 1:1:5 mixture of NH_3/H_2O_2/MilliQ for 1 h at 70 °C. They were then rinsed with ultrapure water and ethanol (Sigma-Aldrich, Australia) and dried with nitrogen.

The substrates were then coated with 5 nm chromium (100 mA current) and 20 nm gold (10 mA) via sputter coating. Monolayers and bilayers were formed as described for the EIS experiments.

For neutron scattering, three different bilayers were produced. The first bilayer was pre-treated with 100 µL of cationic nanoparticles for 18 h and rinsed, and then 10 mg/mL colistin was added. The second bilayer was exposed for 18 h to a mixture of 100 µL of nanoparticles and 10 mg/mL colistin sulfate. The third bilayer was exposed to 1 mL of AuNPs for 18 h, rinsed, and then exposed to colistin sulfate for an additional 18 h.

Neutron data were fitted to a multilayer model (see figure 4-2). Each layer is fitted with a thickness, roughness (with respect to the preceding layer), scattering length density, and hydration level (in vol %). Data was fitted using the Python-based Refnx program.[222] Data were fitted using a differential evolution algorithm using 100 iterations. Parameters set to the expected values for each layer were allowed to vary within a reasonable range. The model used to fit the data was a slab-based model used previously.[201]

4.1.3 Results and Discussion

4.1.3.1 Addition of Gold Nanoparticles to the Membrane

Initially, the addition of the AuNPs to the LPS-tBLMs was monitored by EIS measurements (see figure 4-3, table 4-1). The nanoparticle stock solution used had a concentration of 3.46×10^{12} particles/mL. For convenience, the volume of the nanoparticles used will be stated rather than the concentration.

Impedance data was collected from 100 kHz to 5 mHz and fitted to an equivalent circuit describing the membrane as a combination of resistive and capacitive elements.[137] A decrease in the impedance of the membrane indicates the formation of defects, allowing ions to cross the lipid bilayer. Upon initial exposure to nanoparticles for 18 h, there was a small change in membrane resistance, which can be attributed to distortions created in the outer leaflet of the membrane due to electrostatic interactions between the cationic nanoparticles and the negatively charged LPS head groups. The small decrease in resistance makes the submembrane space more visible in the EIS data. To fit the low-frequency region accurately, a capacitive element had to be fitted to take this into account (circuit 2 vs circuit 1), in good agreement with previous experiments. The capacitance of the membrane increased by 50% from ca. 1 to 1.5 $\mu F/cm^2$, indicating the presence of additional charged species on the surface as well as an increase in surface area resulting from the additional roughness due to nanoparticle adsorption. However, neither an increase in nanoparticle concentration nor prolonged exposure caused further damage. This could indicate that the bilayer was already saturated with nanoparticles and no additional particles could bind, either due to steric reasons or electrostatic repulsion. The lack of further changes in membrane capacitance further supports this hypothesis. The effects of nanoparticle binding to the membrane could not be reversed by rinsing (see Supporting Information figure S1 and table S1).

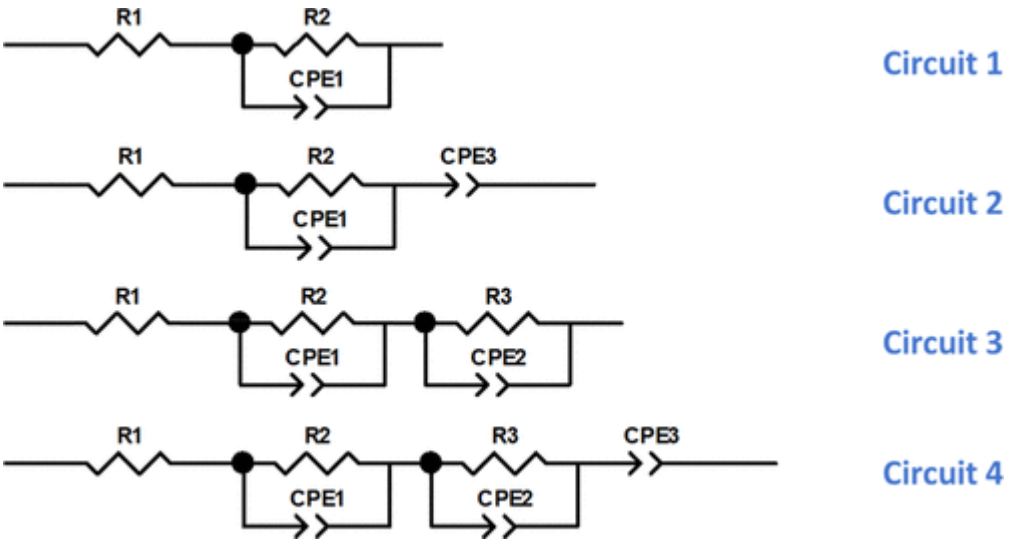

Figure 4-0-3: Equivalent circuits used to fit the EIS data. R: resistor and CPE: constant phase element. R1 represents the electrolyte. R2 and CPE1 represent the resistance and capacitance of the lipid bilayer, respectively. R3 and CPE2 represent the resistance and capacitance of conductive defects in the membrane, respectively. CPE3 represents the Helmholtz double-layer capacitance of the interface between the submembrane space and the gold electrode.

Table 4-1: Electrical Data of an LPS-tBLM Exposed to Increasing Concentrations of Gold Nanoparticles.

	Impedance ($M\Omega cm^2$)	**Capacitance ($\mu F cm^{-2}$)**	**Circuit used to fit data (figure 4-3)**
Bilayer	12.5 ± 0.39	0.99 ± 0.01	1
50 µL/mL AuNPs (18 h)	2.02 ± 0.45	1.58 ± 0.19	2
300 µL/mL AuNPs (48 h)	1.88 ± 0.37	1.45 ± 0.16	2
300 µL/mL AuNPs (96 h)	3.49 ± 1.22	1.18 ± 0.21	2

4.1.3.2 Simultaneous Addition of Colistin and Gold Nanoparticles

Upon incubation of the membrane with 50 µL of AuNPs for 18 h, the membrane resistance was reduced by around 80% from 12 to 2 $M\Omega cm^2$. No further reduction in membrane resistance occurred with increases in either incubation time or nanoparticle concentration. Rinsing the membranes with a buffer solution did not improve the membrane resistance (see table S2). The concentration of 50 µL AuNPs was therefore used to study the combination of nanoparticles with the antibiotic colistin sulfate. This combination did not result in any additional membrane damage over a period of up to 96 h.

In fact, membrane resistance increased slightly upon exposure of the membrane to the mixture of nanoparticles and the antibiotic. Rinsing the bilayer slightly reduced the membrane resistance (see figure 4-4 and table 4-2).

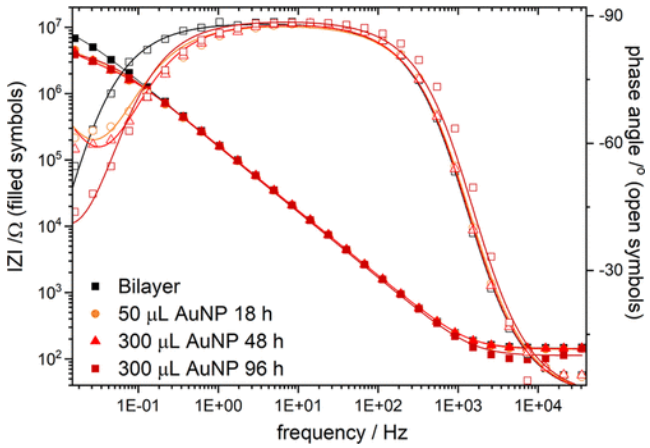

Figure 4-0-4: Bode plots of an LPS-tBLM before exposure to gold nanoparticles (black) and after exposure to increasing concentrations of nanoparticles for increasing periods of time. Symbols represent experimental data, and lines represent fits. The equivalent circuits used to fit the impedance data are shown in figure 2.

Table 4-4: Electrical Properties of an LPS-tBLM Treated with a Combination of 50 and 100 µL/mL Gold Nanoparticles and 10 mg/mL Colistin Sulfate for up to 96 h.

	Impedance ($M\Omega cm^2$)	**Capacitance ($\mu F cm^{-2}$)**	**Circuit used to fit data (figure 4-3)**
50 µL/mL AuNPs			
Bilayer	5.29 ± 1.21	1.55 ± 0.26	1
50 µL/mL AuNPs + 10 mg/mL colistin; 18 h	17.6 ± 4.72	1.34 ± 0.34	2
50 µL/mL AuNPs + 10 mg/mL colistin; 48 h	17.3 ± 5.20	1.37 ± 0.36	2
Rinse	3.61 ± 1.18	1.83 ± 0.40	2
100 µL/mL AuNPs			
Bilayer	0.84 ± 0.13	1.93 ± 0.11	2
100 µL/mL AuNPs + 10 mg/mL colistin; 18 h	4.02 ± 0.39	1.40 ± 0.08	2
100 µL/mL AuNPs + 10 mg/mL colistin; 48 h	0.05 ± 0.03	2.42 ± 0.30	4
Rinse	0.62 ± 0.08	1.73 ± 0.19	4
Bilayer	0.63 ± 0.08	1.68 ± 0.07	2
200 µL/mL AuNPs + 10 mg/mL colistin; 18 h	0.02 ± 0.001	1.79 ± 0.07	2
$CaCl_2$ rinse	1.98 ± 0.29	1.47 ± 0.11	4

The lack of any additional membrane damage when colistin was combined with gold nanoparticles suggests that colistin was not able to disturb the membrane structure, even with lesions that appear to form upon nanoparticle binding to the bilayer.

Instead, the slight increase in membrane resistance suggests that colistin binds to the lesions formed in the membrane, blocking charge transport through these defect sites. Upon rinsing, the membrane resistance decreased slightly, which could be attributed to the removal of some lipids from the membrane as they were solubilized by the integration of colistin into the bilayer structure, at the sites where the membrane was prestressed due to nanoparticle binding.

A doubling of the nanoparticle concentration resulted in an unexpected initial increase in membrane resistance. It is possible that this increase in resistance was a result of colistin penetrating into the membrane at the sites perturbed by nanoparticle binding but in insufficient quantities to solubilize and remove LPS molecules and cause permanent defects. We continued to observe the membrane for an additional 24 h to determine whether bilayer resistance would increase further. However, during this period, we observed a significant reduction in membrane resistance by two orders of magnitude instead, possibly caused by the penetration of the additional colistin molecules. However, the amount of colistin appeared to be insufficient to solubilize and remove membrane components, as rinsing the bilayer with calcium chloride restored its initial properties.

Doubling the nanoparticle concentration to 200 µL/mL did not cause any additional reductions in membrane resistance compared to incubation with 100 µL/mL. However, unlike the incubation with 100 µL/mL AuNPs, membrane damage occurred immediately rather than after an initial increase in resistance. Thus, we observed the bilayer only for a period of 24 h before rinsing with calcium chloride to determine whether membrane damage was reversible.

It is possible that extending the incubation time would cause additional membrane damage, but an increase in antibiotic efficacy only after 48 h or more is of limited clinical use, and therefore we chose not to test this. Membrane properties could be restored by rinsing the bilayer and incubating it for 72 h with 100 mM $CaCl_2$. The reversal of the damage caused to the membrane could be attributed to restabilization of the bilayer after removal of the gold nanoparticles.

4.1.3.3 Pre-treating with Gold Nanoparticles before Colistin Addition

Incubating the membrane with gold nanoparticles for 18 h prior to the addition of colistin resulted in a much more significant reduction in membrane resistance compared to the simultaneous addition of nanoparticles and the antibiotic (see figure 4-5, table 4-3). Pre-treatment of the membrane with 100 µL/mL gold nanoparticles and subsequent exposure to colistin sulfate resulted in a reduction in membrane resistance by two orders of magnitude, which was partially reversible. Incubation with 200 µL/mL gold nanoparticles before exposure to the antibiotic caused irreversible membrane damage. In fact, the membrane quality deteriorated further over time after rinsing of the lipid bilayer with $CaCl_2$. Thus, significant amounts of lipid were likely solubilized by colistin and removed upon rinsing, severely destabilizing the membrane (see figure 4-6).

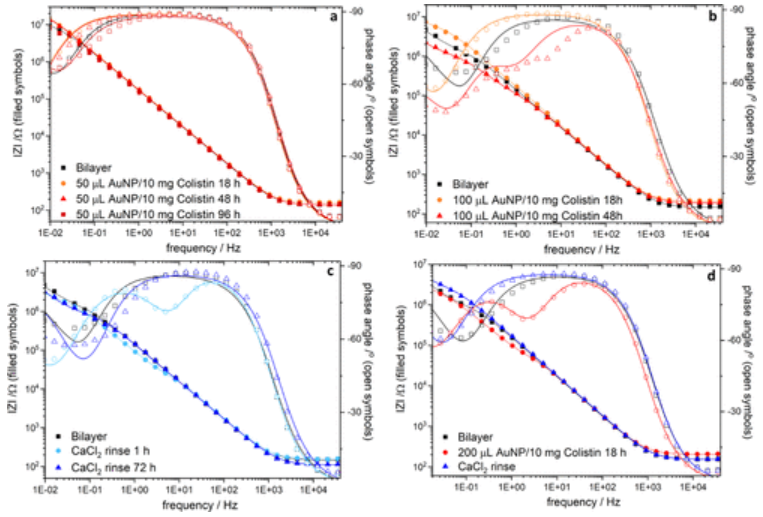

Figure 4-0-5: Bode plots of an LPS-tBLM treated with various colistin–nanoparticle mixtures. (a) Combination of 50 µL/mL gold nanoparticles and 10 mg/mL colistin sulfate for up to 96 h. (b) Gold nanoparticles (100 µL/mL) and colistin (10 mg/mL) for 48 h. (c) Rinsing and incubating the bilayer (b) with $CaCl_2$ could reverse membrane damage. (d) Incubating the membrane with 200 µL gold nanoparticles and 10 mg/mL colistin for 18 h and subsequent rinse.

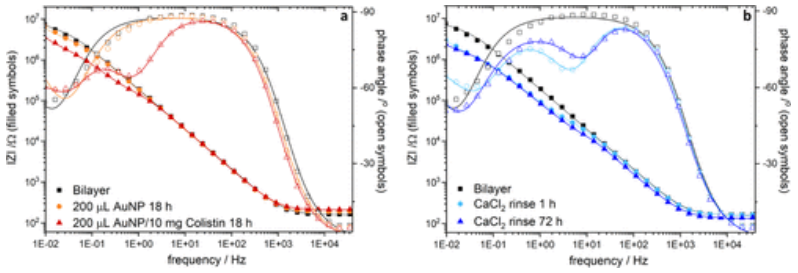

Figure 4-0-6: Bode plots of an LPS-tBLM pre-treated with 200 µL/mL gold nanoparticles: (a) prior to the addition of 10 mg/mL colistin sulfate and (b) subsequent rinsing of the membrane. As the effects of 100 and 200 mL of nanoparticles were highly similar, we only show data from the treatment with 200 µL of AuNPs here.

Table 4-5: Electrical Data of an LPS-tBLM Pre-treated with 100 and 200 µL/mL Gold Nanoparticles Prior to the Addition of 10 mg/mL Colistin Sulfate.

	Impedance ($M\Omega cm^2$)	**Capacitance ($\mu F cm^{-2}$)**	**Circuit used to fit data (figure 4-3)**
Bilayer	0.98 ± 0.22	2.03 ± 0.20	2
100 µL/mL AuNPs; 18 h	0.49 ± 0.07	1.84 ± 0.08	2
100 µL/mL AuNPs + 10 mg/mL colistin; 18 h	0.002 ± 0.0003	2.22 ± 0.32	4
$CaCl_2$ rinse 1 h	0.01 ± 0.0007	1.80 ± 0.19	4
$CaCl_2$ rinse 72 h	0.14 ± 0.01	1.50 ± 0.04	4
Bilayer	4.48 ± 0.67	1.17 ± 0.09	2
200 µL/mL AuNPs; 18 h	2.45 ± 0.37	1.27 ± 0.09	2
200 µL/mL AuNPs + 10 mg/mL colistin; 48 h	0.08 ± 0.01	1.43 ± 0.04	4
$CaCl_2$ 1 h	0.01 ± 0.001	1.25 ± 0.10	4
$CaCl_2$ 72 h	0.003 ± 0.001	1.45 ± 0.35	4

The pre-treatment of the lipid bilayers with gold nanoparticles was further investigated with neutron scattering, which allows the structural investigation of lipid bilayers with a sub-nanometre vertical resolution. A challenging aspect of these experiments is that to fully characterize membrane properties, three solvent contrasts are required, necessitating a flush with the new solvent contrast after each incubation step. It is therefore not possible to exactly replicate the experimental conditions used to collect the EIS data. Instead, neutron scattering can only show permanent changes to membrane structure that remain even after rinsing the membrane. Scattering plots of a lipid bilayer are shown in figure 4-7 and selected fitted parameters are shown in table 4-4.

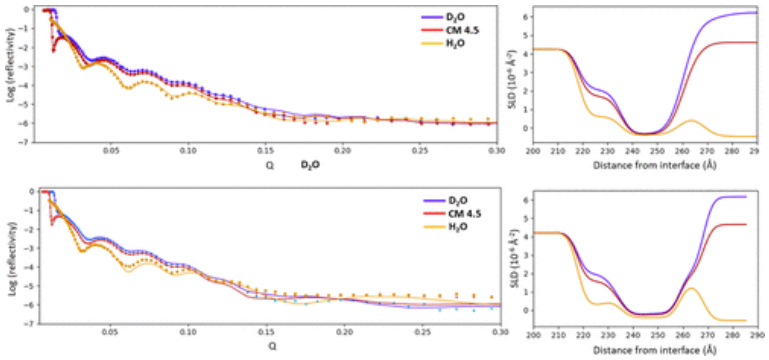

Figure 4-0-7: Scattering plots, fits, and SLD values based on the fit of an LPS-tBLM before (top graphs) and after (bottom graphs) pre-treatment with gold nanoparticles followed by exposure to colistin sulfate. Points show experimental data and lines show fits.

Table 4-6: Selected Structural Parameters of an LPS-tBLM before and after Incubation with Gold Nanoparticles and Colistin Sulfate[a]

	Initial bilayer	After AuNP/Colistin Treatment
Tether thickness	12.00 ± 0.07	12.00
Tether SLD	0.53 ± 0.16	0.53
Tether roughness	3.01 ± 0.53	3.01
Tether hydration	25.2 ± 5.1	25.2
Inner HG thickness	5.01 ± 0.23	5.01
Inner HG SLD	0.81 ± 0.04	0.81
Inner HG roughness	3.19 ± 1.36	3.19
Inner HG hydration	10.1 ± 2.3	10.1
Inner HC thickness	12.01 ± 0.42	12.01
Inner HC SLD	-0.40 ± 0.01	-0.40
Inner HC roughness	3.43 ± 0.54	3.43
Inner HC hydration	0.05 ± 0.01	0.05
Outer HC thickness	12.12 ± 0.13	12.03
Outer HC SLD	-0.38 ± 0.03	-0.38
Outer HC roughness	6.94 ± 2.05	18.77 ± 1.98
Outer HC hydration	3.4 ± 2.02	5.2 ± 1.3
Outer HG thickness	7.81 ± 0.50	9.55 ± 0.05
Outer HG SLD	3.14 ± 0.30	1.63 ± 0.04
Outer HG roughness	3.09 ± 0.07	3.02 ± 0.04
Outer HG hydration	64.1 ± 2.8	10.0 ± 0.8

[a]SLD: scattering length density, HC: hydrocarbon chains, and HG: head groups.

No changes in the scattering plot could be seen during nanoparticle incubation over a period of 2 h; therefore, we do not include the data here. Measurements taken during nanoparticle incubation can be found in the Supporting Information (see figure S6). Errors were estimated using a Monte Carlo Markov chain multisampling algorithm using a minimum of 10 000 steps and 200 walkers. Please see tables S4 and S5 in the Supporting Information for the full set of fitted parameters. Only the parameters describing the outer membrane leaflet were allowed to vary when fitting the data obtained after AuNP/colistin treatment as we expect that changes could only occur there.

The data obtained after AuNP/colistin exposure could not be fitted with the same precision as the data of the initial bilayer, likely because the treatment caused a significant increase in heterogeneity that was no longer efficiently described by the slab-based model. We retained this model to be able to make meaningful comparisons between the experiments.

After the addition of colistin sulfate to the pre-treated membrane, there was a significant increase in the roughness of the inner hydrocarbon chains, which is in good agreement with previously reported effects of colistin sulfate on LPS-tBLMs.[137] In addition to the change in outer carbon chain roughness, there was also a significant reduction in SLD of the outer head groups that is not observed when treating bilayers with only colistin sulfate. This suggests that the outer leaflet becomes significantly disordered and likely partially stripped due to the rinsing process, which explains the strong irreversible reduction in membrane resistance observed in EIS experiments. Given that colistin resistance can be facilitated by adaptations in the lipid A structure,[215, 216] it is possible that the negative charge of the phosphate backbone is reduced or the thickness of the membrane increases. The former would reduce the affinity of both colistin and nanoparticles to the membrane and would require a completely new approach to disrupt the membrane, while the latter would likely decrease the susceptibility of the membrane to disruption (by both nanoparticles and colistin). This would likely require either increased concentrations of drugs or nanoparticles. A model in which the layer thickness is increased by changing either the structure of the inner leaflet or the composition of the outer leaflet could be used to test the effects of these changes.

4.1.4 Conclusions

The addition of AuNPs caused concentration-dependent defects in the membrane as determined via EIS. In neutron reflectometry, disruption to the membrane was not observed upon addition of 100 µL of cationic AuNPs; however, the addition of 1 mL of AuNPs led to significant disruption in the outer membrane. Therefore, the concentration of nanoparticles is important in defect formation. The addition of nanoparticles and colistin simultaneously to the membrane caused small membrane defects only after washing; however, the most significant damage was observed when the membrane was pre-treated with nanoparticles prior to introducing colistin. The pre-treatment led to permanent damage to the membrane, which could not be recovered even after rinsing. The pre-treatment of 100 µL of cationic AuNPs led to significantly increased damage compared to both the addition of colistin alone and simultaneous addition of colistin and AuNPs in neutron reflectometry. This finding suggests that antibiotic susceptibility could be increased with pre-treatment of cationic gold nanoparticles. As nanoparticles are already approved for some clinical uses (i.e., silver in adhesive bandages for sterilization), the findings we report could present an accessible means of improving topical antibiotic treatment, for example, in burn victims and diabetics. As one of the main pathways of resistance against colistin is via changes in the structure of LPS, follow-up studies should assemble model membrane systems with lipids extracted from colistin-resistant species to develop new treatment strategies.

The Supporting Information is available free of charge at https://pubs.acs.org/doi/10.1021/acs.langmuir.1c01150.

4.2 Analysis of the Effects of DHA Incorporation on Model *A. baumannii* Membranes

The work in this sub-chapter was carried out in collaboration with Ashley B. Carey. Some results from this chapter have been published as a part of:

The Membrane Composition Defines the Spatial Organization and Function of a Major Acinetobacter baumannii Drug Efflux System, Maoge Zang et. al., mBio 2021

The author of this thesis was not involved in extraction or analysis of phospholipid samples and was focused specifically on their use in the formation of novel bacterial model membrane systems.

Abstract

The paper this work forms a part of showed that PUFA treatment impacts AdeB-mediated antibiotic resistance. This was done in part through studying the efflux activities of AdeB and AdeJ in *A. Baumannii* with and without omega 3 PUFA enrichment. It was determined that the specific roles of AdeB in resistance to gentamicin and pentamidine were affected by DHA treatment. However, it was still possible that AdeB dysfunction was only due to the incorporation of DHA compromising proton motive force across the membrane, which efflux systems rely upon. To determine if DHA incorporation resulted in ion leakage in *A. baumannii* membranes lipid samples were extracted from actively growing *A. baumannii* cells and used to make tBLMs both with and without DHA incorporated.

4.2.1 Introduction

Resistance of bacterial to antibacterial treatments is a rising problem throughout the world. *Acinetobacter baumannii* is an opportunistic pathogen that is particularly prevalent in hospital settings.

Nosocomial infections it can cause include meningitis, bacteraemia, pneumonia and urinary tract infections.[223, 224] The WHO has labelled *A. baumannii* as an urgent threat and one of the most dangerous of the ESKAPE pathogens, a group of six of the most highly virulent and antibiotic resistant bacterial pathogens.[225, 226] The commonality of outbreaks caused by *A. baumannii* as well as its ability to rapidly mutate its genomic characteristics has allowed it to become multi-drug resistant, meaning few antibiotics can effectively combat it.[223, 227] This increases the importance in understanding its pathogenesis and antibiotic resistant pathways.

Whilst current clinical treatment options are minimal, there has also been a very limited number of new ones developed.[228-230] Gram-negative bacteria like *A. baumannii* have been adapting faster than antimicrobial treatment research, with very few new antibiotic classes developed in the last 20 years, and none of them able to effectively treat multi-drug resistant gram-negative bacteria.[228] Current development of antimicrobial agents do however include some that target *A. baumannii*, however they all fall within the purview of existing classes of antibiotic mechanisms.[228] Deriving new treatments from mechanistic classes similar to the ones bacteria have already developed a resistance to risks such treatments having only short-term efficacy before evolution of further resistance mechanisms occurs.[229] As such, it is important to also develop novel antimicrobial agents that are able to demonstrate effective activity against multi-drug resistant strains.

One of the primary barriers *A. baumannii* and other pathogens have against antibiotic stress is the bacterial membrane. There is currently minimal understanding of *A. baumannii* membrane composition and how it connects to its antibiotic resistance.

It has previously been reported that A. baumannii is susceptible to host-derived omega-3 polyunsaturated fatty acids (PUFAs) including docosahexaenoic acid (DHA).[231, 232] DHA has kinked cis-bond conformation within its hydrocarbon chain that has been shown to prevent the tight packing of phospholipids within the *A. baumannii* membrane. Poorer phospholipid packing is associated with a decrease in bacterial growth as well as an increase in permeability of the membrane.[232, 233] Additionally, DHA has been proposed to be able to facilitate resistance-nodulation division (RND) efflux systems such as $AdeB_3$. This is due to evidence suggesting that phospholipids play a role in the folding and structure - and hence functionality - of RND efflux systems and other similar membrane proteins.[234, 235] The use of DHA as an antimicrobial agent has not been given much attention up to this point, despite its clear antibacterial potential.[232, 236, 237] It is proposed that this could be rectified by gaining a deeper biophysical understanding of its impact on membrane functionality during incorporation into the *A. baumannii* membrane.

Previous investigations into the biophysical properties of DHA using model membranes are limited, and none have been performed using model membranes directly mimicking the behaviour of gram-negative bacteria.[238-240] The effects of DHA on viscoelastic changes in the membrane after incorporation have been investigated using 1-palmitoyl-2-oleyl-sn-glycero-3-phsophocholine (POPC).[239] The addition of DHA showed an increased in rigidity of the membrane, however these experiments utilised model membranes deposited directly onto a silicon dioxide surface. Such solid-supported systems are inherently very inflexible and are less useful for long-term studies due to their decreased stability when compared with model systems that utilise tethering anchor lipids such as those discussed in this thesis.[71, 136]

A major limitation in the study of antimicrobial agents using tBLMs is determining whether experimental findings accurately reflect what happens in true systems.[241] The function of tBLMs to act as simplified models means that they are usually far less complex than biological membranes. This is a necessity for determining the impact of specific membrane-based interactions, however for many membrane functions it is not ideal. Most tBLMs are created using only a couple of different lipid species, much of the time in the form of synthetic analogues.[123] *A. baumannii* however has more than 20 different phospholipid species among other lipophilic material.[242] In order to counteract this deficiency, some complexity needs to be returned to the outer phospholipid layer of tBLMs in order to determine the biophysical impact that antimicrobial agents such as DHA can have on phospholipid membrane behaviour.

To overcome the aforementioned limitations of tBLMs, the existing architecture was adapted to better reflect the outer membrane environment of *A. baumannii*. This was done by using phospholipids extracted directly from actively growing *A. baumannii* with and without incorporated DHA to investigate the antimicrobial effects of substituting DHA into the external tBLM leaflet. The structural and functional properties of membranes both untreated and with DHA incorporated were then analysed using electrochemical impedance spectroscopy.

4.2.2 Chemicals

Valinomycin (≥99%), chloroform ($CHCl_3$, ≥99.5%), sodium chloride (NaCl, ≥99%), docosahexaenoic acid (DHA, ≥98%), phosphate buffered saline tablets (PBS, 10 mM, pH 7.4) and potassium chloride (KCl, ≥99%) were purchased from Sigma Aldrich, Australia. Ethanol (C_2H_5OH, 100%), hydrogen peroxide (H_2O_2, 30% w/w), methanol (CH_3OH, ≥99.9%) and ammonia solution (NH_3, 30 wt%) were obtained from Chem-Supply, Australia. For biological sample extraction, phosphate buffered saline (PBS, 10 mM, pH 7.5) was sourced from University of Adelaide Laboratory Supplies. All purchased chemicals used were of analytical grade and utilised without further purification. Ultrapure water obtained from a WaterPro PS reverse osmosis system (18.2 MΩcm resistance, Labconco) was used for all aqueous solutions.

4.2.3 Materials and Methods

A. Baumannii strain AB5075_UW (Manoil Laboratory, University of Washington) was cultured and provided by Ashley B. Carey in collaboration with members of the Eijkelkamp group. Strains were grown in 20 mL LB media with and without 0.25 mM DHA supplementation. Sample purity, quantity of DHA and species verification of extracted phospholipids was determined via gas chromatography-mass spectrometry and liquid chromatography-mass spectrometry prior to model membrane formation.

For all EIS experiments, membranes were assembled as described previously with some minor differences.[137] Clean silicon substrates were coated with layers of 5 nm chromium and 20 nm gold. Once coated, the substrates were rinsed with ethanol before being inserted into a solution of 0.1 mM DPhyTL for 18 h to allow the formation of the tethered monolayer.

After monolayer formation, the substrates were removed from the ethanolic solution and rinsed thoroughly with ethanol before being dried under nitrogen.

The bilayers were then formed by vesicle fusion with the already formed monolayer. Vesicles with phospholipid species extracted from A. *baumannii* were used with a lipid concentration of 1.5 mg/mL. Vesicles were prepared by mixing lipids in an aqueous solution. The lipid–water mixture was extruded 31 times through a 100 nm track-etched polycarbonate filter membrane. All vesicle solutions were extruded just prior to use. The extruded vesicle solution (10 µL/mL) was added to the monolayer in 500 µL PBS solution for a final concentration of 30 µg/mL. The bilayers were left to form for 18 h at ambient temperature, and the resulting bilayers were rinsed with 5 cell volumes of PBS.

For ion transport measurements using valinomycin, bilayers were first flushed with 5 cell volumes of 100 mM NaCl solution, before addition of 5 µL of valinomycin (10 mg/mL in ethanol). Valinomycin was allowed to incorporate for 1-2 hours before measurement. Bilayers were then flushed with 5 cell volumes of KCl and then 5 cell volumes of NaCl with measurements performed between each flush in the different ionic solutions to ascertain changes in membrane resistance.

Electrochemical impedance spectroscopy was performed using a Metrohm Autolab potentiostat with a three-electrode setup using a platinum wire as a counter electrode and a Ag/AgCl reference electrode. For each spectrum, data points were collected in the range from 100 kHz to 5 mHz with an amplitude of ±10 mV. All measurements were carried out in PBS solution unless stated otherwise.

EIS data were analysed using ZView2 (Scribner Associates). All spectra were area-normalized using a surface area of 0.283 cm^2. The data were fitted to one of four equivalent circuits shown previously. The error is the range of values that can be fitted for the respective parameter without decreasing the quality of the fit (evaluated by least-squares fitting).

4.2.4 Results and Discussion

Initial formation of monolayers was the same for all samples and involved the self-assembly of DPhyTL onto a chromium and gold-coated silicon surface. The formation of tBLMs mimicking *A. baumannii* involved the addition of two different vesicle samples to the monolayers, one with untreated phospholipids and one with DHA incorporated into live culture beforehand. It was verified using GC-MS methods described by Jiang et. al[232] that successful DHA incorporation resulted in DHA comprising approximately 20% of the total phospholipid content.

To create an ion gradient between the inside and outside of vesicle samples the vesicles were assembled in ultrapure water then added to the monolayers in a PBS solution. This difference in ionic environment helps to create a driving force for the disruption of vesicles to aid in self-assembly of the bilayer's outer leaflet. Vesicles were generated by both sonicating and extruding the phospholipid mixture. Purely sonicating samples has been reported to result in a variable size distribution of vesicle structures, which if added to a monolayer may result in additional unwanted multilayers.[137] By extruding through 100 nm filters after sonication, more consistent bilayers can be formed with more readily reproducible properties.

To investigate the structural quality of the resulting bilayers they were analysed using EIS (see figure 4-8 and table 4-5). Both untreated and DHA-incorporated samples were fitted using an equivalent circuit with resistive and capacitive components.[130, 173] A resistive component was used to represent the baseline electrolyte resistivity, whilst the bilayers themselves were represented by a resistor and capacitor in parallel. The circuit model components for the bilayer can be impacted by a number of factors including formation of defects, increased surface roughness, or attachment/removal of additional molecules to the surface of the bilayer. Defects in the membrane can greatly facilitate ion transport across the bilayer, which results in a dramatic decrease in the modelled bilayer's resistance. Thus, any increase in defects or a general lowering of the bilayer's electrical sealing capabilities results in a decline in modelled resistance.

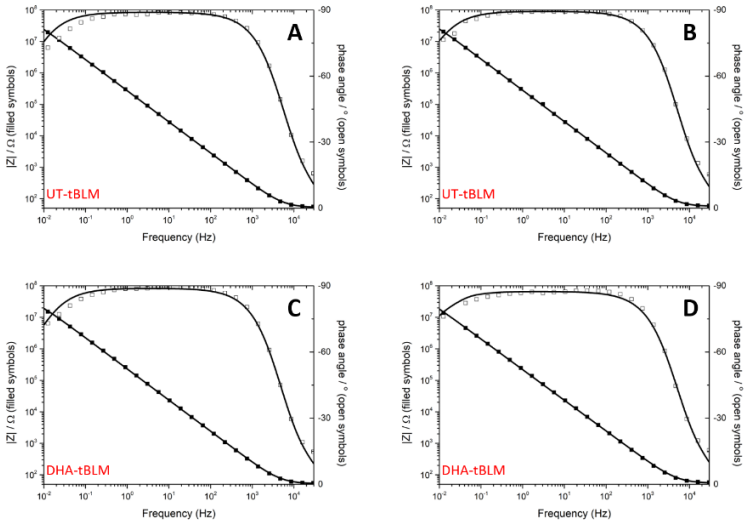

Figure 4-8: Bode plots of impedance (filled squares) and phase angle (empty squares) for 4 different bilayer samples in 10 mM PBS – two formed using untreated lipid extract (A & B) and two formed using DHA-incorporated lipid extract (C & D).

Table 4-5: Impedance and capacitance values of 4 different A. baumannii lipid bilayers created with and without incorporation of DHA in 10 mM PBS solution. Data and errors were determined using the ZView equivalent circuit fitting tool and only fitted data relevant to the lipid bilayer is shown.

Sample	Impedance ($M\Omega cm^2$)	Capacitance ($\mu F cm^{-2}$)
UT-tBLM 1	47 ± 4	0.86 ± 0.03
UT-tBLM 2	32 ± 3	1.0 ± 0.03
DHA-tBLM 1	25 ± 2	1.1 ± 0.03
DHA tBLM 2	50 ± 5	1.0 ± 0.04

Traditionally, fully tethered systems are able to consistently generate resistances of 20-60 $M\Omega cm^2$.[135, 136] Both untreated and DHA-treated bilayer samples had resistances within that range, demonstrating exceptional electrical sealing. This level of electrical sealing is the result of the rigidity of fully tethered membrane systems, which tend towards having very few defects. Incorporation of DHA into the phospholipid mixture had no discernable impact on the electrical sealing properties of the fully tethered bilayers. This suggests that both phospholipid mixtures are able to generate high quality membrane models and that DHA does not inherently destabilise the phospholipid mixture.

Capacitance of the bilayer samples was also modelled alongside resistance modelling. Changes in membrane capacitance can signify a change in hydration or thickness of the membrane.[153] This is due to the capacitance being dependent upon the bilayer's dielectric constant, thickness and area. The untreated bilayer samples were found on average to have a slightly lower capacitance than untreated samples. This is consistent with computational studies that suggest a decrease in membrane thickness when DHA is added.[243] Membrane thinning was suspected to be due to an increase in disorder of phospholipid tails, membrane packing changes and lipid organisation changes on addition of DHA. However, the difference in capacitance in this instance was only of minor statistical significance.

These findings suggest that both untreated and DHA-incorporated tBLMs made from *A. baumannii* phospholipids are able to form stable membranes with strong electrical sealing properties. Due to this, it is unlikely that the dysfunction of RND efflux systems in drug-resistant *A. baumannii* is due to a loss in membrane potential and more likely to be due to the induction of conformational changes. The paper this work is a part of found that the accumulation of incorporated DHA in the central cavity of $AdeB_3$ trimer was responsible for the protein-protein interface between transmembrane domains of $AdeB_3$ being lost. This change in protein conformation was proposed to cause disruption of the conformational cycling mechanism critical for efflux activity.[243]

As well as analysing the initial structural aspects of *A. baumannii* model systems, it is also important to determine their behaviour in response to the addition of antibiotics. By understanding the way antibiotics effect model bacterial systems, it is possible to gain a greater picture of the mechanisms of antimicrobial activity when interacting with phospholipids. The use of species-specific model platforms such as *A. baumannii* models may also provide new information for further development of species-specific screening of potential new drug candidates.

Ionophores such as valinomycin are lipid-soluble molecules capable of providing a transport mechanisms for ions to move across phospholipid membranes.[148] Some ionophores also have antibiotic properties that allow them to kill or inhibit growth of bacteria. Valinomycin, a cyclic peptide, selectively transports potassium ions (K^+) across the phospholipid bilayer. The affinity of valinomycin for K^+ is 1000 times faster than for sodium (Na^+).

This affinity for K^+ ions means that valinomycin is able to disrupt the K^+ gradient across the bacterial cell membrane by greatly increasing the flux of K^+ into the cell. This can ultimately lead to cell death. Valinomycin has six ester carbonyl groups that K^+ is able to form a complex with. The exterior of valinomycin is hydrophobic and forms a ring shielding cationic charge whilst providing solubility through the bilayer's hydrophobic interior.[148]

Investigating the changes in tBLMs in the presence of valinomycin once again involves the use of EIS (see figure 4-9 and table 4-6). Addition of valinomycin was accompanied by a change in solvent from PBS to 100 mM NaCl. This addition of valinomycin was not seen to cause a major change in resistance or capacitance in most samples, apart from one of the two DHA-incorporated samples. The cause of such change was unlikely due to alterations in membrane structure, and more likely to be due to an increased ability of ions to transverse the membrane interior with the increase in electrolyte concentration. At full tethering density in the lower leaflet of the bilayers, phospholipid rearrangement between internal and external leaflets is unlikely.[137]

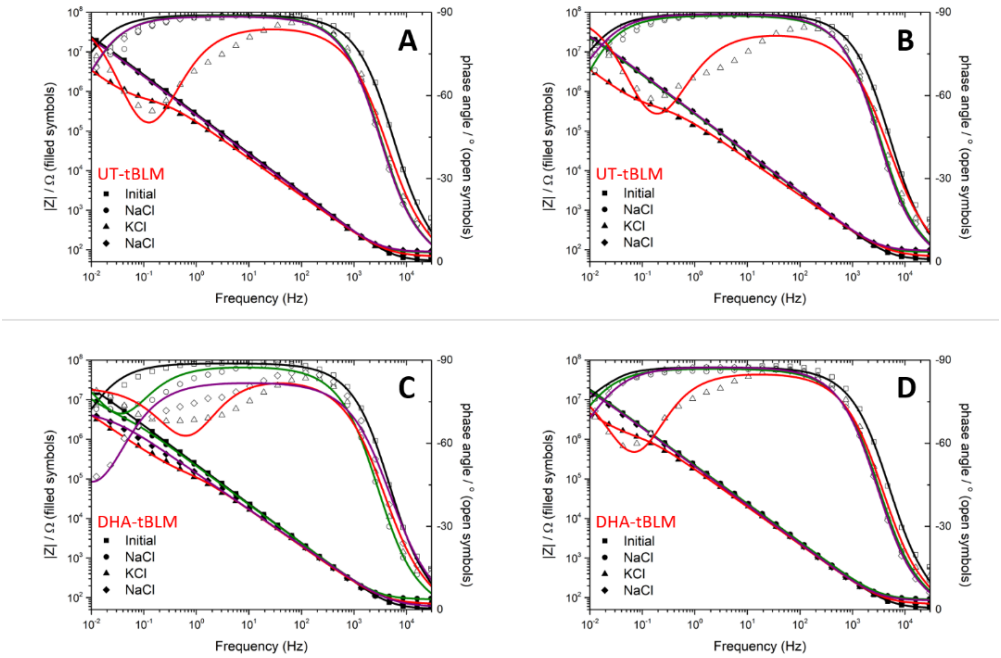

Figure 4-9: Bode plots of impedance (filled shapes) and phase angle (empty shapes) for 4 different bilayer samples showing the effects of valinomycin incorporation on bilayer resistance and capacitance – two formed using untreated lipid extract (A & B) and two formed using DHA-incorporated lipid extract (C & D). For all samples the impedance and capacitance are shown initially in PBS (black), in NaCl with valinomycin added (green), in KCl with valinomycin present (red) and in NaCl again with valinomycin present (purple).

Table 4-6: Impedance and capacitance values of 4 different A. baumannii lipid bilayers created with and without incorporation of DHA, showing the changes associated with the addition of valinomycin and changes in electrolyte. Data and errors were determined using the ZView equivalent circuit fitting tool and only fitted data relevant to the lipid bilayer is shown.

Sample	Sample	Impedance ($M\Omega cm^2$)	Capacitance ($\mu F cm^{-2}$)
UT-tBLM 1	**Initial**	47 ± 4	0.86 ± 0.03
	After Val Addition	27 ± 2	0.93 ± 0.02
	KCl	0.53 ± 0.03	1.2 ± 0.05
	NaCl	32 ± 2	0.88 ± 0.02
UT-tBLM 2	**Initial**	32 ± 3	1.0 ± 0.03
	After Val Addition	37 ± 2	0.80 ± 0.02
	KCl	0.34 ± 0.03	1.4 ± 0.08
	NaCl	27 ± 2	0.96 ± 0.03
DHA-tBLM 1	**Initial**	25 ± 2	1.1 ± 0.03
	After Val Addition	2.2 ± 0.2	1.5 ± 0.06
	KCl	0.070 ± 0.01	2.2 ± 0.2
	NaCl	3.3 ± 3	1.7 ± 0.9
DHA-tBLM 2	**Initial**	50 ± 5	1.0 ± 0.04
	After Val Addition	32 ± 2	1.1 ± 0.03
	KCl	0.81 ± 0.08	1.5 ± 0.06
	NaCl	19 ± 3	1.2 ± 0.07

When NaCl was exchanged for 100 mM KCl electrolyte, a decrease in resistance was observed across all samples. In the case of three samples of the 4, resistance dropped from between 20-40 MΩcm^2 to less than 1 MΩcm^2, whilst in the case of the sample with initial resistance of 2.2 MΩcm^2, a drop to below 0.1 MΩcm^2 was modelled. This resistance drop can be seen visibly in the figure, with an obvious dip in phase angle and flattening of the impedance curve at around 1 Hz. Such a large decrease was expected due to the ability of valinomycin to complex with K^+ ion and increase ion transport across the membrane of both bilayer types. This movement of K^+ across the membrane allows formation of temporary defect-like regions in the membrane that cause a decrease in membrane resistance.

Similarly, an increase of capacitance was also observed across all samples, likely due to an increase in the relative permittivity and decrease in membrane thickness. Increased charge transport and defect density is facilitated by the valinomycin diffusion decreasing the quality of phospholipid packing. This indicates both that valinomycin is functioning as intended and previously observed in other studies of different model systems. It also suggests that the model A. baumannii systems are behaving much as would be expected of a typical tBLM system. If multilayers had been formed instead of bilayers, then such a large decrease in charge capacity would not be expected due to the reduced efficiency of charge transport across a multilayered structure.

Restoration of the original membrane environment through the replacement of KCl with 100 mM NaCl resulted in an increase in resistance and decrease of capacitance approximately back to the levels observed before addition of KCl.

This is also considered to be typical model membrane behaviour for a fully functioning fully tethered system. Removal of K^+ ions likely allowed defect density to decrease back to previous levels and improve packing of phospholipids. The reversibility of this process confirms that the decrease of membrane resistance and capacitance was due to the transport of K^+ ions being mediated by valinomycin and not due to permanent structural damage to the membrane.

4.2.5 Conclusion

This work was able to develop a novel tethered bilayer lipid membrane architecture using phospholipids from *A. baumannii* to mimic the external *A. baumannii* lipid membrane both with and without DHA incorporation. At full tethering density these models were found to be highly stable with strong electrical sealing properties. Minor membrane thinning was observed in DHA-incorporated samples, however otherwise both model systems were fully functional with incorporation of the valinomycin ionophore. Thus, it is posited that RND efflux dysfunction is a more likely antimicrobial mechanism of DHA rather than membrane potential loss. Development of species-specific model membranes such as those in this study provide a unique opportunity for the further creation of bacterial model membrane systems more biologically accurate than existing membrane models. This could provide a more effective screening platform for potential drug candidates and more specialised studies of resistance or transport mechanisms in bacterial species.

Chapter 5 - Conclusions and Future Directions

The research presented in this thesis has showcased three key findings across three different use cases. Firstly, a deeper of the understanding of the resilience of membranes in the sorts of environments they might need to be able to withstand for practical uses. Secondly, an example of how they can be used to develop improvements in the biomedical field through analysis and improvement of antibiotic function. Thirdly, new platforms of model membrane that can be used to mimic their bacterial counterparts more closely were developed.

In chapter 3, it was determined that at high tethering density, traditionally designed DPhyPC tBLMs could withstand being dehydrated for several days before being rehydrated for further measurements, with some improvement in membrane resilience at lower tethering densities when coated with polyelectrolytes. This suggests that membranes designed in this way could be used in real-world situations as components in biosensing devices.

Further research into this area could involve the investigation of different types of membrane lipids to determine differences in resilience to dehydration between them, as well as a deeper investigation into alternative coatings such as hydrogels to improve their resilience without affecting their functionality. tBLMs designed to mimic bacterial outer membranes such as those described in the first part of chapter 4 of this thesis are less stable than those constructed using DPhyPC and tend towards having comparatively lower initial levels of impedance. Thus, it would be of interest to compare their dehydration resilience to the eukaryotic mimics presented in chapter 3 to determine any differences in behaviour.

In the first part of chapter 4, it was determined that polyelectrolyte-coated gold nanoparticles were able to improve the efficacy of last-line antibiotic colistin on *E. coli* bacterial membrane models. This was done by first exposing bilayers to gold nanoparticles before flushing the system and adding colistin. This was both a good example of how tBLMs can be used in a more traditional sense to observe membrane interaction with other materials, as well as the growing trend of gold nanoparticles being used in biomedical settings.

The formation of novel tBLM structures designed using extracts taken directly from bacterial samples was explored in the second half of chapter 4. This research has far-reaching implications in the fundamental design of model membranes. It is still important to be able to create a simplified model to test purely the interactions between materials and the basic lipids used to make traditional tBLMs. However, the ability to create similarly stratified membrane models at a degree of complexity not only similar to biological membranes, but directly proportional to their complexity is an exciting development.

At these early stages there are still a few unknowns as to the exact makeup of the outer leaflet of the bilayers, as well as what could flip and become present in the inner leaflet as well. This is due to the difficulty in analysing specifically which lipids and other chemicals are present in the bilayer once it has been formed. Just because they are present in the extracted solution does not necessarily mean that they carry all the way through the vesicle extrusion and membrane formation process.

Nonetheless, it was promising to be able to create stable bilayer models using extracted lipids from *A. baumannii* samples.

Further analysis has since been performed to further understand the structure of the lipid membranes designed using not only A. baumannii extracts, but extracts also from S. aureus, another of the highly important ESKAPE pathogens. Bilayers for neutron reflectometry were created in the same ways discussed earlier in the thesis, with extracted lipid samples used to form the outer layer on top of a monolayer of DPhyTL (figures 5-1 & 5-2).

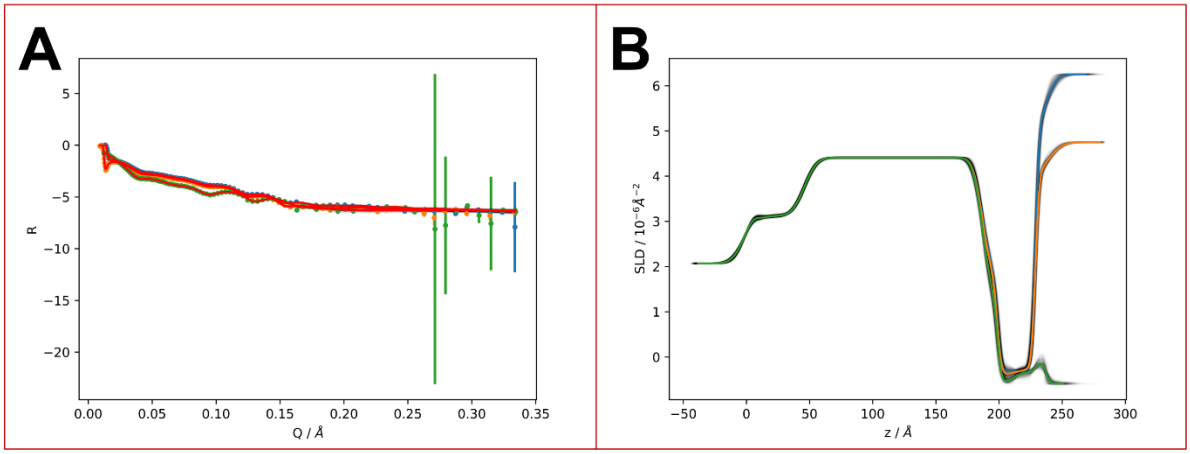

Figure 51: Reflectivity (A) and SLD (B) plots for a 80%-tethered A. baumannii bilayer. Coloured lines show the modelled median values of MCMC sampling, faded lines show MCMC uncertainty. Blue represents the data gathered in D_2O, orange CM 4.5 and green H_2O.

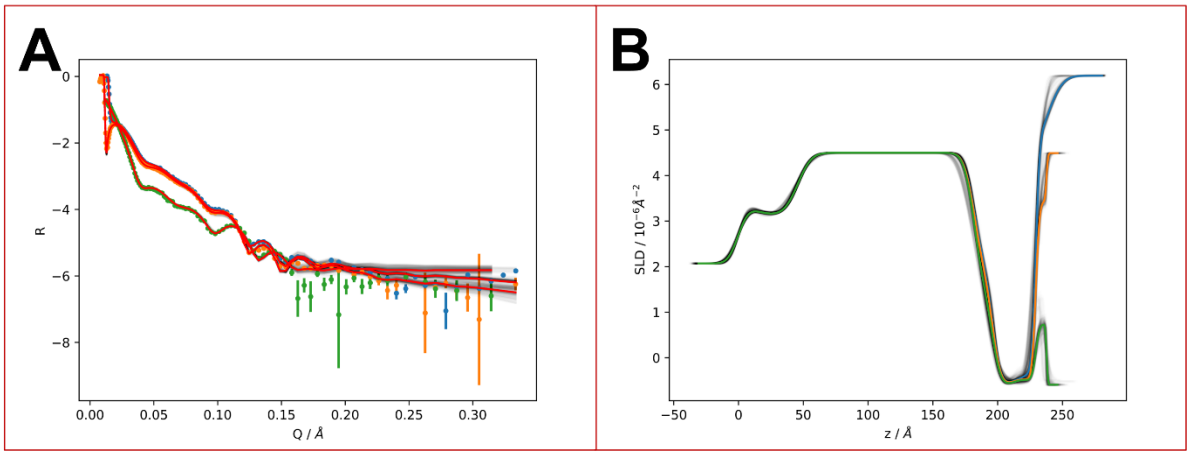

Figure 52: Reflectivity (A) and SLD (B) plots for a 100%-tethered S. aureus bilayer. Coloured lines show the modelled median values of MCMC sampling, faded lines show MCMC uncertainty. Blue represents the data gathered in D_2O, orange CM 4.5 and green H_2O.

For both A. baumannii and S. aureus it was possible to create bilayers with the wafers used for neutron reflectometry. Bilayers were modelled for the thickness, SLD, roughness and hydration of the tether, hydrocarbon and outer head group regions (tables 5-1 & 5-2). In both samples, values determined for each component were consistent with the formation of tBLMs. The increased hydration in the outer head group region of the *baumannii* membrane compared to the *aureus* one suggests that there could be a greater packing density of material in the *aureus* bilayer, however the differing tethering densities may also have played a role here.

Table 5-1: Modelled NR data for 80%-tethered A. baumannii bilayer. Thickness and roughness provided in Å, SLD in 10^{-6} $Å^{-2}$ and hydration in %. See table A5 in appendix for full data set.

	Initial Bilayer
Tether	
Thickness	11.7 ± 0.76
SLD	1.42 ± 0.28
Roughness	6.04 ± 0.58
Hydration	7.50 ± 1.4
Inner HC	
Thickness	13.3 ± 1.3
SLD	-0.565 ± 0.048
Roughness	2.61 ± 0.54
Hydration	3.42 ± 1.2
Outer HC	
Thickness	16.9 ± 1.0
SLD	-0.337 ± 0.057
Roughness	4.97 ± 2.4
Hydration	0.475 ± 0.49
Outer HG	
Thickness	8.6 ± 0.56
SLD	1.22 ± 0.22
Roughness	2.44 ± 0.46
Hydration	74.6 ± 3.8

Table 5-2: Modelled NR data for 100%-tethered S. aureus bilayer. Thickness and roughness provided in Å, SLD in 10^{-6} $Å^{-2}$ and hydration in %. See table A6 in appendix for full data set.

	Initial Bilayer
Tether	
Thickness	14.3 ± 0.46
SLD	1.48 ± 0.47
Roughness	6.53 ± 0.82
Hydration	8.28 ± 2.7
Inner HC	
Thickness	16.0 ± 1.1
SLD	-0.585 ± 0.015
Roughness	4.80 ± 0.99
Hydration	0.284 ± 0.51
Outer HC	
Thickness	17.0 ± 0.79
SLD	-0.487 ± 0.61
Roughness	4.25 ± 1.8
Hydration	0.285 ± 0.65
Outer HG	
Thickness	8.34 ± 0.32
SLD	2.24 ± 0.58
Roughness	2.36 ± 0.75
Hydration	53.1 ± 6.0

Further EIS experiments to determine the consistent quality of the various membranes formed from extracted lipids would be required to better ascertain the differences between these extracted samples and samples created from a more controlled variety of lipids. Ideally, methods would also be identified or created to better determine the makeup of the leaflets of these bilayers.

The work shown throughout this thesis highlights ways in which model tBLMs can be used to help advance understanding in the biomedical area, as well as providing a platform for further enhancement of both the form and function of these membrane devices going forward into the future, with many more exciting developments on the horizon in this field.

Reference List

1. Watson, H., *Biological membranes.* Essays In Biochemistry, 2015. **59**: p. 43-69.
2. Guidotti, G., *The composition of biological membranes.* Archives of Internal Medicine, 1972. **129**(2): p. 194-201.
3. Nickels, J.D., J.C. Smith, and X. Cheng, *Lateral organization, bilayer asymmetry, and inter-leaflet coupling of biological membranes.* Chemistry and Physics of Lipids, 2015. **192**: p. 87-99.
4. Singer, S.J. and G.L. Nicolson, *The Fluid Mosaic Model of the Structure of Cell Membranes.* Science, 1972. **175**(4023): p. 720.
5. Uzman, A., *Essential Cell Biology, Third Edition.* Biochemistry and Molecular Biology Education, 2010. **38**(1): p. 59-59.
6. Alberts, B., et al., *Molecular Biology Of The Cell*. 4 ed. 2002, New York: Garland Science.
7. Li, J., et al., *A review on phospholipids and their main applications in drug delivery systems.* Asian Journal of Pharmaceutical Sciences, 2015. **10**(2): p. 81-98.
8. Strahl, H. and J. Errington, *Bacterial Membranes: Structure, Domains, and Function.* Annual Review of Microbiology, 2017. **71**(1): p. 519-538.
9. Andersson, J., *Mimicking Microbial Membranes*, in *Chemical and Physical Sciences*. 2018, Flinders University: South Australia.
10. Lodish, H., et al., *Molecular Cell Biology*. 4 ed. 2000, New York: W. H. Freeman.
11. Prabudiansyah, I., et al., *Characterization of the annular lipid shell of the Sec translocon.* Biochim Biophys Acta, 2015. **1848**(10 Pt A): p. 2050-6.
12. Forrest, L.R., R. Krämer, and C. Ziegler, *The structural basis of secondary active transport mechanisms.* Biochimica et Biophysica Acta (BBA) - Bioenergetics, 2011. **1807**(2): p. 167-188.
13. Perland, E., et al., *Characteristics of 29 novel atypical solute carriers of major facilitator superfamily type: evolutionary conservation, predicted structure and neuronal co-expression.* Open Biology, 2017. **7**(9).
14. Rebaud, S., O. Maniti, and A.P. Girard-Egrot, *Tethered bilayer lipid membranes (tBLMs): Interest and applications for biological membrane investigations.* Biochimie, 2014. **107**: p. 135-142.
15. Salehi-Reyhani, A., O. Ces, and Y. Elani, *Artificial cell mimics as simplified models for the study of cell biology.* Experimental Biology and Medicine, 2017. **242**(13): p. 1309-1317.
16. Cameron, D.E., C.J. Bashor, and J.J. Collins, *A brief history of synthetic biology.* Nature Reviews Microbiology, 2014. **12**: p. 381.
17. Khalil, A.S. and J.J. Collins, *Synthetic biology: applications come of age.* Nature Reviews Genetics, 2010. **11**: p. 367+.
18. Ezkurdia, I., et al., *Multiple evidence strands suggest that there may be as few as 19 000 human protein-coding genes.* Human Molecular Genetics, 2014. **23**(22): p. 5866-5878.
19. Spector, A.A. and M.A. Yorek, *Membrane lipid composition and cellular function.* Journal of Lipid Research, 1985. **26**(9): p. 1015-35.
20. Booth, P.J., *Sane in the membrane: designing systems to modulate membrane proteins.* Current Opinion in Structural Biology, 2005. **15**(4): p. 435-440.
21. Attard, G.S., et al., *Modulation of CTP:phosphocholine cytidylyltransferase by membrane curvature elastic stress.* Proceedings of the National Academy of Sciences, 2000. **97**(16): p. 9032.
22. Pinot, M., et al., *Effects of Confinement on the Self-Organization of Microtubules and Motors.* Current Biology, 2009. **19**(11): p. 954-960.

23. Robinson, M.M., et al., *Modeling Biological Membranes with Circuit Boards and Measuring Electrical Signals in Axons: Student Laboratory Exercises.* Journal of Visualized Experiments : JoVE, 2011(47): p. 2325.
24. McAdams, H.H. and L. Shapiro, *Circuit simulation of genetic networks.* Science, 1995. **269**(5224): p. 650.
25. Neher, E., B. Sakmann, and J.H. Steinbach, *The extracellular patch clamp: A method for resolving currents through individual open channels in biological membranes.* Pflügers Archiv, 1978. **375**(2): p. 219-228.
26. Neher, E. and B. Sakmann, *Single-channel currents recorded from membrane of denervated frog muscle fibres.* Nature, 1976. **260**: p. 799.
27. Sakmann, B. and E. Neher, *Patch Clamp Techniques for Studying Ionic Channels in Excitable Membranes.* Annual Review of Physiology, 1984. **46**(1): p. 455-472.
28. Yajuan, X., L. Xin, and L. Zhiyuan, *A Comparison of the Performance and Application Differences Between Manual and Automated Patch-Clamp Techniques.* Current Chemical Genomics, 2012. **6**: p. 87-92.
29. Maki, B.A., et al., *One-channel Cell-attached Patch-clamp Recording.* Journal of Visualized Experiments : JoVE, 2014(88): p. 51629.
30. Morgan, D. and T.E. DeCoursey, *Analysis of electrophysiological properties and responses of neutrophils.* Methods in molecular biology (Clifton, N.J.), 2014. **1124**: p. 121-158.
31. Linley, J.E., *Perforated Whole-Cell Patch-Clamp Recording*, in *Ion Channels: Methods and Protocols*, N. Gamper, Editor. 2013, Humana Press: Totowa, NJ. p. 149-157.
32. Griffin, J.D. and J.A. Boulant, *Temperature effects on membrane potential and input resistance in rat hypothalamic neurones.* The Journal of physiology, 1995. **488 (Pt 2)**(Pt 2): p. 407-418.
33. Shibasaki, K., et al., *Effects of Body Temperature on Neural Activity in the Hippocampus: Regulation of Resting Membrane Potentials by Transient Receptor Potential Vanilloid 4.* The Journal of Neuroscience, 2007. **27**(7): p. 1566.
34. Ubl, J., H. Murer, and H.A. Kolb, *Ion channels activated by osmotic and mechanical stress in membranes of opossum kidney cells.* The Journal of Membrane Biology, 1988. **104**(3): p. 223-232.
35. Wang, X. and M. Li, *Automated Electrophysiology: High Throughput of Art.* ASSAY and Drug Development Technologies, 2003. **1**(5): p. 695-708.
36. Mueller, P., et al., *Reconstitution of Cell Membrane Structure in vitro and its Transformation into an Excitable System.* Nature, 1962. **194**: p. 979.
37. Ries, R.S., et al., *Black Lipid Membranes: Visualizing the Structure, Dynamics, and Substrate Dependence of Membranes.* The Journal of Physical Chemistry B, 2004. **108**(41): p. 16040-16049.
38. White, S.H., *Analysis of the Torus Surrounding Planar Lipid Bilayer Membranes.* Biophysical Journal, 1972. **12**(4): p. 432-445.
39. Winterhalter, M., *Black lipid membranes.* Current Opinion in Colloid & Interface Science, 2000. **5**(3): p. 250-255.
40. Dugger, M.E. and C.A. Baker, *Automated formation of black lipid membranes within a microfluidic device via confocal fluorescence feedback-controlled hydrostatic pressure manipulations.* Analytical and Bioanalytical Chemistry, 2019. **411**(19): p. 4605-4614.
41. Montal, M. and P. Mueller, *Formation of Bimolecular Membranes from Lipid Monolayers and a Study of Their Electrical Properties.* Proceedings of the National Academy of Sciences of the United States of America, 1972. **69**(12): p. 3561-3566.
42. Pantoja, R., et al., *Bilayer Reconstitution of Voltage-Dependent Ion Channels using a Microfabricated Silicon Chip.* Biophysical Journal, 2001. **81**(4): p. 2389-2394.
43. Ti Tien, H., *Black Lipid Membranes at Bifaces : Formation characteristics, optical and some thermodynamic properties.* The Journal of General Physiology, 1968. **52**(1): p. 125-144.

44. Zakharian, E., *Recording of Ion Channel Activity in Planar Lipid Bilayer Experiments.* Methods in molecular biology (Clifton, N.J.), 2013. **998**: p. 109-118.
45. Saffman, P.G. and M. Delbrück, *Brownian motion in biological membranes.* Proceedings of the National Academy of Sciences, 1975. **72**(8): p. 3111.
46. Andersson, J., I. Köper, and W. Knoll, *Tethered Membrane Architectures—Design and Applications.* Frontiers in Materials, 2018. **5**(55).
47. Beerlink, A., et al., *X-ray Structure Analysis of Free-Standing Lipid Membranes Facilitated by Micromachined Apertures.* Langmuir, 2008. **24**(9): p. 4952-4958.
48. Malmstadt, N., T.J. Jeon, and J.J. Schmidt, *Long-Lived Planar Lipid Bilayer Membranes Anchored to an In Situ Polymerized Hydrogel.* Advanced Materials, 2007. **20**(1): p. 84-89.
49. Jeon, T.-J., J.L. Poulos, and J.J. Schmidt, *Long-term storable and shippable lipid bilayer membrane platform.* Lab on a Chip, 2008. **8**(10): p. 1742-1744.
50. Poulos, J.L., T.-J. Jeon, and J.J. Schmidt, *Automatable production of shippable bilayer chips by pin tool deposition for an ion channel measurement platform.* Biotechnology Journal, 2010. **5**(5): p. 511-514.
51. Lu, B., G. Kocharyan, and J.J. Schmidt, *Lipid bilayer arrays: Cyclically formed and measured.* Biotechnology Journal, 2014. **9**(3): p. 446-451.
52. Jeon, T.-J., N. Malmstadt, and J.J. Schmidt, *Hydrogel-Encapsulated Lipid Membranes.* Journal of the American Chemical Society, 2006. **128**(1): p. 42-43.
53. Ryu, H., et al., *Automated Lipid Membrane Formation Using a Polydimethylsiloxane Film for Ion Channel Measurements.* Analytical Chemistry, 2014. **86**(18): p. 8910-8915.
54. Lasic, D.D., *The mechanism of vesicle formation.* Biochemical Journal, 1988. **256**(1): p. 1-11.
55. Szoka, F. and D. Papahadjopoulos, *Comparative Properties and Methods of Preparation of Lipid Vesicles (Liposomes).* Annual Review of Biophysics and Bioengineering, 1980. **9**(1): p. 467-508.
56. Frisken, B.J., C. Asman, and P.J. Patty, *Studies of Vesicle Extrusion.* Langmuir, 2000. **16**(3): p. 928-933.
57. Mayer, L.D., M.J. Hope, and P.R. Cullis, *Vesicles of variable sizes produced by a rapid extrusion procedure.* Biochimica et Biophysica Acta (BBA) - Biomembranes, 1986. **858**(1): p. 161-168.
58. Kölchens, S., et al., *Quasi-elastic light scattering determination of the size distribution of extruded vesicles.* Chemistry and Physics of Lipids, 1993. **65**(1): p. 1-10.
59. Popplewell, J.F., et al., *Quantifying the effects of melittin on liposomes.* Biochimica et Biophysica Acta (BBA) - Biomembranes, 2007. **1768**(1): p. 13-20.
60. Alavi, M., N. Karimi, and M. Safaei, *Application of Various Types of Liposomes in Drug Delivery Systems.* Advanced Pharmaceutical Bulletin, 2017. **7**(1): p. 3-9.
61. Bhatia, T., et al., *Preparing giant unilamellar vesicles (GUVs) of complex lipid mixtures on demand: Mixing small unilamellar vesicles of compositionally heterogeneous mixtures.* Biochimica et Biophysica Acta (BBA) - Biomembranes, 2015. **1848**(12): p. 3175-3180.
62. Biner, O., et al., *Delivery of membrane proteins into small and giant unilamellar vesicles by charge-mediated fusion.* FEBS Letters, 2016. **590**(14): p. 2051-2062.
63. Morales-Penningston, N.F., et al., *GUV Preparation and Imaging: Minimizing artifacts.* Biochimica et biophysica acta, 2010. **1798**(7): p. 1324-1332.
64. Baykal-Caglar, E., et al., *Preparation of giant unilamellar vesicles from damp lipid film for better lipid compositional uniformity.* Biochimica et Biophysica Acta (BBA) - Biomembranes, 2012. **1818**(11): p. 2598-2604.
65. Akashi, K., et al., *Preparation of giant liposomes in physiological conditions and their characterization under an optical microscope.* Biophysical Journal, 1996. **71**(6): p. 3242-3250.

66. Breton, M., et al., *Transport of siRNA through Lipid Membranes Driven by Nanosecond Electric Pulses: An Experimental and Computational Study.* Journal of the American Chemical Society, 2012. **134**(34): p. 13938-13941.
67. Tamba, Y., et al., *Stability of giant unilamellar vesicles and large unilamellar vesicles of liquid-ordered phase membranes in the presence of Triton X-100.* Biochimica et Biophysica Acta (BBA) - Biomembranes, 2004. **1667**(1): p. 1-6.
68. Sobral, C.N.C., M.A. Soto, and A.M. Carmona-Ribeiro, *Characterization of DODAB/DPPC vesicles.* Chemistry and Physics of Lipids, 2008. **152**(1): p. 38-45.
69. Armengol, X. and J. Estelrich, *Physical stability of different liposome compositions obtained by extrusion method.* Journal of Microencapsulation, 1995. **12**(5): p. 525-535.
70. Tamm, L.K. and H.M. McConnell, *Supported phospholipid bilayers.* Biophysical Journal, 1985. **47**(1): p. 105-113.
71. Castellana, E.T. and P.S. Cremer, *Solid supported lipid bilayers: From biophysical studies to sensor design.* Surface Science Reports, 2006. **61**(10): p. 429-444.
72. Wittenberg, N.J., et al., *Applications of SPR for the characterization of molecules important in the pathogenesis and treatment of neurodegenerative diseases.* Expert Review of Neurotherapeutics, 2014. **14**(4): p. 449-463.
73. Lin, W.-C., et al., *Lipid Asymmetry in DLPC/DSPC-Supported Lipid Bilayers: A Combined AFM and Fluorescence Microscopy Study.* Biophysical Journal, 2006. **90**(1): p. 228-237.
74. Steltenkamp, S., et al., *Mechanical Properties of Pore-Spanning Lipid Bilayers Probed by Atomic Force Microscopy.* Biophysical Journal, 2006. **91**(1): p. 217-226.
75. Ebara, Y. and Y. Okahata, *A Kinetic Study of Concanavalin A Binding to Glycolipid Monolayers by Using a Quartz-Crystal Microbalance.* Journal of the American Chemical Society, 1994. **116**(25): p. 11209-11212.
76. Tampé, R., et al., *Nanofabrication and Biosystems: Integrating Materials Science, Engineering, and Biology*. 1996, Cambridge. p. 201.
77. Richter, R.P., J.L.K. Him, and A. Brisson, *Supported lipid membranes.* Materials Today, 2003. **6**(11): p. 32-37.
78. Tero, R., *Substrate Effects on the Formation Process, Structure and Physicochemical Properties of Supported Lipid Bilayers.* Materials, 2012. **5**(12): p. 2658-2680.
79. Richter, R., A. Mukhopadhyay, and A. Brisson, *Pathways of Lipid Vesicle Deposition on Solid Surfaces: A Combined QCM-D and AFM Study.* Biophysical Journal, 2003. **85**(5): p. 3035-3047.
80. Ekeroth, J., P. Konradsson, and F. Höök, *Bivalent-Ion-Mediated Vesicle Adsorption and Controlled Supported Phospholipid Bilayer Formation on Molecular Phosphate and Sulfate Layers on Gold.* Langmuir, 2002. **18**(21): p. 7923-7929.
81. Charitat, T., et al., *Adsorbed and free lipid bilayers at the solid-liquid interface.* The European Physical Journal B - Condensed Matter and Complex Systems, 1999. **8**(4): p. 583-593.
82. Andree, H.A., et al., *Clustering of lipid-bound annexin V may explain its anticoagulant effect.* Journal of Biological Chemistry, 1992. **267**(25): p. 17907-17912.
83. Grandbois, M., H. Clausen-Schaumann, and H. Gaub, *Atomic force microscope imaging of phospholipid bilayer degradation by phospholipase A2.* Biophysical Journal, 1998. **74**(5): p. 2398-2404.
84. Milhiet, P.-E., et al., *Spontaneous insertion and partitioning of alkaline phosphatase into model lipid rafts.* EMBO Reports, 2002. **3**(5): p. 485-490.
85. Thompson, J.R., et al., *Enhanced Stability and Fluidity in Droplet on Hydrogel Bilayers for Measuring Membrane Protein Diffusion.* Nano Letters, 2007. **7**(12): p. 3875-3878.
86. Zhao, J. and L.K. Tamm, *FTIR and Fluorescence Studies of Interactions of Synaptic Fusion Proteins in Polymer-Supported Bilayers.* Langmuir, 2003. **19**(5): p. 1838-1846.

87. Mazur, F., et al., *Liposomes and lipid bilayers in biosensors.* Advances in Colloid and Interface Science, 2017. **249**: p. 88-99.
88. Yee, C.K., M.L. Amweg, and A.N. Parikh, *Membrane Photolithography: Direct Micropatterning and Manipulation of Fluid Phospholipid Membranes in the Aqueous Phase Using Deep-UV Light.* Advanced Materials, 2004. **16**(14): p. 1184-1189.
89. Bally, M., et al., *Liposome and Lipid Bilayer Arrays Towards Biosensing Applications.* Small, 2010. **6**(22): p. 2481-2497.
90. Seifert, K., K. Fendler, and E. Bamberg, *Charge transport by ion translocating membrane proteins on solid supported membranes.* Biophysical Journal, 1993. **64**(2): p. 384-391.
91. Pintschovius, J. and K. Fendler, *Charge Translocation by the Na+/K+-ATPase Investigated on Solid Supported Membranes: Rapid Solution Exchange with a New Technique.* Biophysical Journal, 1999. **76**(2): p. 814-826.
92. Buoninsegni, F.T., et al., *Time-Resolved Charge Translocation by Sarcoplasmic Reticulum Ca-ATPase Measured on a Solid Supported Membrane.* Biophysical Journal, 2004. **86**(6): p. 3671-3686.
93. Khan, M.S., et al., *Electrophysiology of Epithelial Sodium Channel (ENaC) Embedded in Supported Lipid Bilayer Using a Single Nanopore Chip.* Langmuir, 2017. **33**(47): p. 13680-13688.
94. Dhoke, M.A., et al., *Porous membranes for reconstitution of ion channels.* Biochimica et Biophysica Acta (BBA) - Biomembranes, 2005. **1716**(2): p. 117-125.
95. Jing, W., Z. Wu, and E. Wang, *Electrochemical study of gramicidin D forming ion-permeable channels in the bilayer lipid membranes.* Electrochimica Acta, 1998. **44**(1): p. 99-102.
96. Steinem, C., et al., *Impedance analysis of ion transport through gramicidin channels incorporated in solid supported lipid bilayers.* Bioelectrochemistry and Bioenergetics, 1997. **42**(2): p. 213-220.
97. Möller, I. and S. Seeger, *Solid supported lipid bilayers from artificial and natural lipid mixtures – long-term stable, homogeneous and reproducible.* Journal of Materials Chemistry B, 2015. **3**(29): p. 6046-6056.
98. Andersson, J. and W. Knoll, *Tethered Lipid Membranes as Platforms for Biophysical Studies and Advanced Biosensors*, in *Biomimetic Lipid Membranes: Fundamentals, Applications, and Commercialization*, F.N. Kök, A. Arslan Yildiz, and F. Inci, Editors. 2019, Springer International Publishing: Cham. p. 183-191.
99. Naumann, C.A., et al., *The Polymer-Supported Phospholipid Bilayer: Tethering as a New Approach to Substrate−Membrane Stabilization.* Biomacromolecules, 2002. **3**(1): p. 27-35.
100. Holden, M.A., et al., *Creating Fluid and Air-Stable Solid Supported Lipid Bilayers.* Journal of the American Chemical Society, 2004. **126**(21): p. 6512-6513.
101. Chiantia, S., N. Kahya, and P. Schwille, *Dehydration Damage of Domain-Exhibiting Supported Bilayers: An AFM Study on the Protective Effects of Disaccharides and Other Stabilizing Substances.* Langmuir, 2005. **21**(14): p. 6317-6323.
102. Han, C.-T. and L. Chao, *Creating Air-Stable Supported Lipid Bilayers by Physical Confinement Induced by Phospholipase A2.* ACS Applied Materials & Interfaces, 2014. **6**(9): p. 6378-6383.
103. Kühner, M., R. Tampé, and E. Sackmann, *Lipid mono- and bilayer supported on polymer films: composite polymer-lipid films on solid substrates.* Biophysical journal, 1994. **67**(1): p. 217-226.
104. Hillebrandt, H., et al., *High Electric Resistance Polymer/Lipid Composite Films on Indium−Tin−Oxide Electrodes.* Langmuir, 1999. **15**(24): p. 8451-8459.
105. Wagner, M.L. and L.K. Tamm, *Tethered Polymer-Supported Planar Lipid Bilayers for Reconstitution of Integral Membrane Proteins: Silane-Polyethyleneglycol-Lipid as a Cushion and Covalent Linker.* Biophysical Journal, 2000. **79**(3): p. 1400-1414.
106. Sackmann, E., *Supported Membranes: Scientific and Practical Applications.* Science, 1996. **271**(5245): p. 43.

107. Pace, H., et al., *Preserved Transmembrane Protein Mobility in Polymer-Supported Lipid Bilayers Derived from Cell Membranes.* Analytical Chemistry, 2015. **87**(18): p. 9194-9203.
108. Bello, J., et al., *Lipid bilayer membrane technologies: A review on single-molecule studies of DNA sequencing by using membrane nanopores.* Microchimica Acta, 2017. **184**(7): p. 1883-1897.
109. Berkelaar, R.P., et al., *Water-Induced Blister Formation in a Thin Film Polymer.* Langmuir, 2015. **31**(3): p. 1017-1025.
110. Seimei, A., D. Saeki, and H. Matsuyama, *Effect of polyelectrolyte structure on formation of supported lipid bilayers on polyelectrolyte multilayers prepared using the layer-by-layer method.* Journal of Colloid and Interface Science, 2020. **569**: p. 211-218.
111. Kügler, R. and W. Knoll, *Polyelectrolyte-supported lipid membranes.* Bioelectrochemistry, 2002. **56**(1): p. 175-178.
112. Wong, J.Y., et al., *Polymer-Cushioned Bilayers. I. A Structural Study of Various Preparation Methods Using Neutron Reflectometry.* Biophysical Journal, 1999. **77**(3): p. 1445-1457.
113. Seitz, M., et al., *Formation of Tethered Supported Bilayers by Vesicle Fusion onto Lipopolymer Monolayers Promoted by Osmotic Stress.* Langmuir, 2000. **16**(14): p. 6067-6070.
114. Xue, Y., et al., *Quantifying thiol–gold interactions towards the efficient strength control.* Nature Communications, 2014. **5**: p. 4348.
115. Zhang, L., M.L. Longo, and P. Stroeve, *Mobile Phospholipid Bilayers Supported on a Polyion/Alkylthiol Layer Pair.* Langmuir, 2000. **16**(11): p. 5093-5099.
116. Mitsuhiko, O., et al., *Molecularly Flat Films of Linear Polyions and Proteins Obtained by the Alternate Adsorption Method.* Japanese Journal of Applied Physics, 1997. **36**(12A): p. L1608.
117. Blakeston, A.C., et al., *New Poly(amino acid methacrylate) Brush Supports the Formation of Well-Defined Lipid Membranes.* Langmuir, 2015. **31**(12): p. 3668-3677.
118. Hertrich, S., et al., *Highly Hydrated Deformable Polyethylene Glycol-Tethered Lipid Bilayers.* Langmuir, 2014. **30**(31): p. 9442-9447.
119. Ahmed, E.M., *Hydrogel: Preparation, characterization, and applications: A review.* Journal of Advanced Research, 2015. **6**(2): p. 105-121.
120. Kibrom, A., et al., *Hydrogel-supported protein-tethered bilayer lipid membranes: a new approach toward polymer-supported lipid membranes.* Soft Matter, 2011. **7**(1): p. 237-246.
121. Acharya, S.A., et al., *Hydrogel-stabilized droplet bilayers for high speed solution exchange.* Scientific reports, 2013. **3**: p. 3139-3139.
122. Tanaka, M., *Polymer-Supported Membranes: Physical Models of Cell Surfaces.* MRS Bulletin, 2011. **31**(7): p. 513-520.
123. Andersson, J. and I. Koper, *Tethered and Polymer Supported Bilayer Lipid Membranes: Structure and Function.* Membranes (Basel), 2016. **6**(2).
124. Wiegand, G., et al., *Electrical Properties of Supported Lipid Bilayer Membranes.* The Journal of Physical Chemistry B, 2002. **106**(16): p. 4245-4254.
125. Förtig, A., et al., *Solid-supported biomimetic membranes with tailored lipopolymer tethers.* Macromolecular Symposia, 2004. **210**(1): p. 329-338.
126. McGillivray, D.J., et al., *Molecular-scale structural and functional characterization of sparsely tethered bilayer lipid membranes.* Biointerphases, 2007. **2**(1): p. 21-33.
127. Atanasov, V., et al., *Membrane on a Chip: A Functional Tethered Lipid Bilayer Membrane on Silicon Oxide Surfaces.* Biophysical Journal, 2005. **89**(3): p. 1780-1788.
128. Cornell, B.A., et al., *A biosensor that uses ion-channel switches.* Nature, 1997. **387**: p. 580.
129. Vockenroth, I.K., et al., *Tethered bilayer lipid membranes with giga-ohm resistances.* Electrochemistry Communications, 2008. **10**(2): p. 323-328.

130. Junghans, A. and I. Köper, *Structural Analysis of Tethered Bilayer Lipid Membranes.* Langmuir, 2010. **26**(13): p. 11035-11040.
131. Vockenroth, I.K., et al., *Stable insulating tethered bilayer lipid membranes.* Biointerphases, 2008. **3**(2): p. FA68-FA73.
132. Onaizi, S.A., M.S. Nasser, and F. Twaiq, *Lysozyme binding to tethered bilayer lipid membranes prepared by rapid solvent exchange and vesicle fusion methods.* European Biophysics Journal, 2014. **43**(4): p. 191-198.
133. Vockenroth, I.K., et al., *Incorporation of α-Hemolysin in Different Tethered Bilayer Lipid Membrane Architectures.* Langmuir, 2008. **24**(2): p. 496-502.
134. Buboltz, J.T. and G.W. Feigenson, *A novel strategy for the preparation of liposomes: rapid solvent exchange.* Biochimica et Biophysica Acta (BBA) - Biomembranes, 1999. **1417**(2): p. 232-245.
135. Koper, I., *Insulating tethered bilayer lipid membranes to study membrane proteins.* Molecular BioSystems, 2007. **3**(10): p. 651-657.
136. Andersson, J., et al., *Synthesis and Characterization of Novel Anchorlipids for Tethered Bilayer Lipid Membranes.* Langmuir, 2017.
137. Andersson, J., et al., *A tethered bilayer lipid membrane that mimics microbial membranes.* Physical Chemistry Chemical Physics, 2018.
138. Shenoy, S., et al., *In-plane homogeneity and lipid dynamics in tethered bilayer lipid membranes (tBLMs).* Soft Matter, 2010. **6**(6): p. 1263-1274.
139. Lindsey, H., N.O. Petersen, and S.I. Chan, *Physicochemical characterization of 1,2-diphytanoyl-sn-glycero-3-phosphocholine in model membrane systems.* Biochimica et Biophysica Acta (BBA) - Biomembranes, 1979. **555**(1): p. 147-167.
140. Atanasov, V., et al., *A Molecular Toolkit for Highly Insulating Tethered Bilayer Lipid Membranes on Various Substrates.* Bioconjugate Chemistry, 2006. **17**(3): p. 631-637.
141. Schiller, S.M., et al., *Archaea Analogue Thiolipids for Tethered Bilayer Lipid Membranes on Ultrasmooth Gold Surfaces.* Angewandte Chemie International Edition, 2003. **42**(2): p. 208-211.
142. Naumann, R., et al., *Kinetics of valinomycin-mediated K+ ion transport through tethered bilayer lipid membranes.* Journal of Electroanalytical Chemistry, 2003. **550-551**: p. 241-252.
143. Attwood, S.J., Y. Choi, and Z. Leonenko, *Preparation of DOPC and DPPC Supported Planar Lipid Bilayers for Atomic Force Microscopy and Atomic Force Spectroscopy.* International journal of molecular sciences, 2013. **14**(2): p. 3514-3539.
144. Zhang, G., T.C. Meredith, and D. Kahne, *On the essentiality of lipopolysaccharide to Gram-negative bacteria.* Current opinion in microbiology, 2013. **16**(6): p. 779-785.
145. Tsujimoto, H., N. Gotoh, and T. Nishino, *Diffusion of macrolide antibiotics through the outer membrane of Moraxella catarrhalis.* Journal of Infection and Chemotherapy, 1999. **5**(4): p. 196-200.
146. Thomas, C.J., N. Surolia, and A. Surolia, *Surface Plasmon Resonance Studies Resolve the Enigmatic Endotoxin Neutralizing Activity of Polymyxin B.* Journal of Biological Chemistry, 1999. **274**(42): p. 29624-29627.
147. Bakker, E., P. Bühlmann, and E. Pretsch, *Carrier-Based Ion-Selective Electrodes and Bulk Optodes. 1. General Characteristics.* Chemical Reviews, 1997. **97**(8): p. 3083-3132.
148. Kendall, J.K.R., et al., *Effect of the Structure of Cholesterol-Based Tethered Bilayer Lipid Membranes on Ionophore Activity.* ChemPhysChem, 2010. **11**(10): p. 2191-2198.
149. Su, Z., et al., *Gramicidin A ion channel formation in model phospholipid bilayers tethered to gold (111) electrode surfaces.* Electrochimica Acta, 2017. **243**: p. 364-373.
150. Kozuch, J., et al., *Combined Electrochemistry and Surface-Enhanced Infrared Absorption Spectroscopy of Gramicidin A Incorporated into Tethered Bilayer Lipid Membranes.* Angewandte Chemie International Edition, 2012. **51**(32): p. 8114-8117.

151. Becucci, L., et al., *Potassium ion transport by gramicidin and valinomycin across a Ag(111)-supported tethered bilayer lipid membrane.* Electrochimica Acta, 2008. **53**(22): p. 6372-6379.
152. Vockenroth, I.K., et al. *Functional tethered bilayer membranes as a biosensor platform*. in *IEEE Sensors, 2005.* 2005.
153. Alghalayini, A., et al., *The Use of Tethered Bilayer Lipid Membranes to Identify the Mechanisms of Antimicrobial Peptide Interactions with Lipid Bilayers.* Antibiotics (Basel, Switzerland), 2019. **8**(1): p. 12.
154. Andersson, M., et al., *Detection of Single Ion Channel Activity on a Chip Using Tethered Bilayer Membranes.* Langmuir, 2007. **23**(6): p. 2924-2927.
155. Becucci, L. and R. Guidelli, *Kinetics of Channel Formation in Bilayer Lipid Membranes (BLMs) and Tethered BLMs: Monazomycin and Melittin.* Langmuir, 2007. **23**(10): p. 5601-5608.
156. Zieleniecki, J., *Drug-Membrane and Protein Interactions in tethered Bilayer Lipid Membranes Studied by Surface Analytical Methods*, in *School Of Chemical And Physical Sciences*. 2017, Flinders University: Bedford Park, SA. p. 236.
157. Stora, T., J.H. Lakey, and H. Vogel, *Ion-Channel Gating in Transmembrane Receptor Proteins: Functional Activity in Tethered Lipid Membranes.* Angewandte Chemie International Edition, 1999. **38**(3): p. 389-392.
158. Terrettaz, S., M. Mayer, and H. Vogel, *Highly Electrically Insulating Tethered Lipid Bilayers for Probing the Function of Ion Channel Proteins.* Langmuir, 2003. **19**(14): p. 5567-5569.
159. Bezrukov, S.M. and J.J. Kasianowicz, *Current noise reveals protonation kinetics and number of ionizable sites in an open protein ion channel.* Physical Review Letters, 1993. **70**(15): p. 2352-2355.
160. Valincius, G., et al., *Enzyme Activity to Augment the Characterization of Tethered Bilayer Membranes.* The Journal of Physical Chemistry B, 2006. **110**(21): p. 10213-10216.
161. Kasianowicz, J.J., et al., *Characterization of individual polynucleotide molecules using a membrane channel.* Proceedings of the National Academy of Sciences of the United States of America, 1996. **93**(24): p. 13770-13773.
162. Penkauskas, T. and G. Preta, *Biological applications of tethered bilayer lipid membranes.* Biochimie, 2019. **157**: p. 131-141.
163. Salomoni, R., et al., *Antibacterial effect of silver nanoparticles in Pseudomonas aeruginosa.* Nanotechnology, science and applications, 2017. **10**: p. 115-121.
164. Shahverdi, A.R., et al., *Synthesis and effect of silver nanoparticles on the antibacterial activity of different antibiotics against Staphylococcus aureus and Escherichia coli.* Nanomedicine: Nanotechnology, Biology and Medicine, 2007. **3**(2): p. 168-171.
165. Goreham, R.V., et al., *Interaction of Silver Nanoparticles with Tethered Bilayer Lipid Membranes.* Langmuir, 2015. **31**(21): p. 5868-5874.
166. Liu, Y., et al., *Biomembrane disruption by silica-core nanoparticles: Effect of surface functional group measured using a tethered bilayer lipid membrane.* Biochimica et Biophysica Acta (BBA) - Biomembranes, 2014. **1838**(1, Part B): p. 429-437.
167. Liu, Y. and R. Mark Worden, *Size dependent disruption of tethered lipid bilayers by functionalized polystyrene nanoparticles.* Biochimica et Biophysica Acta (BBA) - Biomembranes, 2015. **1848**(1, Part A): p. 67-75.
168. Barsoukov, E., et al., *Impedance Spectroscopy Theory, Experiment and Applications*. 2nd Edition ed, ed. E. Barsoukov and J.R. Macdonald. 2005, Hoboken, New Jersey: John Wiley & Sons Inc.
169. Alexander, C.K. and M.N.O. Sadiku, *Fundamentals Of Electric Circuits*. 5th Edition ed. 2013, New York, NY: McGraw-Hill.
170. Choi, W., et al., *Modeling and Applications of Electrochemical Impedance Spectroscopy (EIS) for Lithium-ion Batteries.* J. Electrochem. Sci. Technol, 2020. **11**(1): p. 1-13.

171. Vockenroth, I.K., et al., *Formation of tethered bilayer lipid membranes probed by various surface sensitive techniques.* Biointerphases, 2009. **4**(2): p. 19-26.
172. Guidelli, R. and L. Becucci, *4 Electrochemistry of Biomimetic Membranes*, in *Applications of Electrochemistry and Nanotechnology in Biology and Medicine II*, N. Eliaz, Editor. 2012, Springer US: Boston, MA. p. 147-266.
173. Valincius, G., T. Meškauskas, and F. Ivanauskas, *Electrochemical Impedance Spectroscopy of Tethered Bilayer Membranes.* Langmuir, 2012. **28**(1): p. 977-990.
174. Lasia, A., *Electrochemical Impedance Spectroscopy and its Applications*, in *Modern Aspects of Electrochemistry*, B.E. Conway, J.O.M. Bockris, and R.E. White, Editors. 2002, Springer US: Boston, MA. p. 143-248.
175. Jackson, A.J., *Introduction to Small-Angle Neutron Scattering and Neutron Reflectometry*. 2008, NIST Center For Neutron Research: Gaithersburg, MD.
176. Hollinshead, C.M., et al., *Neutron reflection from a dimyristoylphosphatidylcholine monolayer adsorbed on a hydrophobised silicon support.* Biochimica et Biophysica Acta (BBA) - Biomembranes, 2001. **1511**(1): p. 49-59.
177. Demkowicz, M. and J. Majewski, *Probing Interfaces in Metals Using Neutron Reflectometry.* Metals, 2016. **6**(1): p. 20.
178. Nelson, A., *Co-refinement of multiple-contrast neutron/X-ray reflectivity data using MOTOFIT.* Journal of Applied Crystallography, 2006. **39**(2): p. 273-276.
179. Banc, A., et al., *Small angle neutron scattering contrast variation reveals heterogeneities of interactions in protein gels.* Soft Matter, 2016. **12**(24): p. 5340-5352.
180. Von White, G., F.S. Mohammed, and C.L. Kitchens, *Small-Angle Neutron Scattering Investigation of Gold Nanoparticle Clustering and Ligand Structure Under Antisolvent Conditions.* The Journal of Physical Chemistry C, 2011. **115**(38): p. 18397-18405.
181. Ho, C., S.J. Slater, and C.D. Stubbs, *Hydration and order in lipid bilayers.* Biochemistry, 1995. **34**(18): p. 6188-95.
182. Chattopadhyay, M., et al., *Hydration Layer of Only a Few Molecules Controls Lipid Mobility in Biomimetic Membranes.* Journal of the American Chemical Society, 2021. **143**(36): p. 14551-14562.
183. Beddow, J.A., et al., *Reconstitution of Nicotinic Acetylcholine Receptors into Gel-Protected Lipid Membranes.* Analytical Chemistry, 2004. **76**(8): p. 2261-2265.
184. Kang, X.-f., et al., *A Storable Encapsulated Bilayer Chip Containing a Single Protein Nanopore.* Journal of the American Chemical Society, 2007. **129**(15): p. 4701-4705.
185. Shim, J.W. and L.Q. Gu, *Stochastic Sensing on a Modular Chip Containing a Single-Ion Channel.* Analytical Chemistry, 2007. **79**(6): p. 2207-2213.
186. Cisternas, M.A., et al., *Dry Two-Step Self-Assembly of Stable Supported Lipid Bilayers on Silicon Substrates.* International Journal of Molecular Sciences, 2020. **21**(18): p. 6819.
187. Beule, A.G., *Physiology and pathophysiology of respiratory mucosa of the nose and the paranasal sinuses.* GMS current topics in otorhinolaryngology, head and neck surgery, 2011. **9**: p. Doc07-Doc07.
188. Wilson, W.R. and M.R. Allansmith, *Rapid, Atraumatic Method for Obtaining Nasal Mucus Samples.* Annals of Otology, Rhinology & Laryngology, 1976. **85**(3): p. 391-393.
189. Quraishi, M.S., N.S. Jones, and J. Mason, *The rheology of nasal mucus: a review.* Clinical Otolaryngology & Allied Sciences, 2002. **23**(5): p. 403-413.
190. Stillwell, W., *Chapter 19 - Membrane Transport*, in *An Introduction to Biological Membranes (Second Edition)*. 2016, Elsevier. p. 423-451.
191. Cranfield, Charles G., et al., *Transient Potential Gradients and Impedance Measures of Tethered Bilayer Lipid Membranes: Pore-Forming Peptide Insertion and the Effect of Electroporation.* Biophysical Journal, 2014. **106**(1): p. 182-189.
192. Budvytyte, R., et al., *Modification of Tethered Bilayers by Phospholipid Exchange with Vesicles.* Langmuir, 2013. **29**(13): p. 4320-4327.

193. Sánchez, P.A., et al., *PDADMAC/PSS Oligoelectrolyte Multilayers: Internal Structure and Hydration Properties at Early Growth Stages from Atomistic Simulations.* Molecules, 2020. **25**(8).
194. Heberle, F.A. and G.W. Feigenson, *Phase separation in lipid membranes.* Cold Spring Harb Perspect Biol, 2011. **3**(4).
195. Sheetz, M.P., *Glycoprotein motility and dynamic domains in fluid plasma membranes.* Annu Rev Biophys Biomol Struct, 1993. **22**: p. 417-31.
196. Friedman, N.D., E. Temkin, and Y. Carmeli, *The negative impact of antibiotic resistance.* Clin Microbiol Infect, 2016. **22**(5): p. 416-22.
197. Cosgrove, S.E. and Y. Carmeli, *The impact of antimicrobial resistance on health and economic outcomes.* Clin Infect Dis, 2003. **36**(11): p. 1433-7.
198. Exner, M., et al., *Antibiotic resistance: What is so special about multidrug-resistant Gram-negative bacteria?* GMS hygiene and infection control, 2017. **12**: p. Doc05-Doc05.
199. OECD, *Stemming the Superbug Tide: Just A Few Dollars More*, in *Health Policy Studies*. 2018, OECD Publishing: Paris.
200. Hofer, U., *The cost of antimicrobial resistance.* Nature Reviews Microbiology, 2019. **17**(1): p. 3-3.
201. Ejim, L., et al., *Combinations of antibiotics and nonantibiotic drugs enhance antimicrobial efficacy.* Nature Chemical Biology, 2011. **7**(6): p. 348-350.
202. Ayhan, D.H., et al., *Sequence-Specific Targeting of Bacterial Resistance Genes Increases Antibiotic Efficacy.* PLOS Biology, 2016. **14**(9): p. e1002552.
203. Abreu, A.C., et al., *Combinatorial approaches with selected phytochemicals to increase antibiotic efficacy against Staphylococcus aureus biofilms.* Biofouling, 2016. **32**(9): p. 1103-1114.
204. Fuller, M.A., et al., *Nanoparticles in an antibiotic-loaded nanomesh for drug delivery.* RSC Advances, 2019. **9**(52): p. 30064-30070.
205. Gurjar, M., *Colistin for lung infection: an update.* Journal of Intensive Care, 2015. **3**(1): p. 3.
206. Martis, N., S. Leroy, and V. Blanc, *Colistin in multi-drug resistant Pseudomonas aeruginosa blood-stream infections: A narrative review for the clinician.* Journal of Infection, 2014. **69**(1): p. 1-12.
207. Spapen, H., et al., *Renal and neurological side effects of colistin in critically ill patients.* Annals of Intensive Care, 2011. **1**(1): p. 14.
208. Li, J., et al., *Colistin: the re-emerging antibiotic for multidrug-resistant Gram-negative bacterial infections.* The Lancet Infectious Diseases, 2006. **6**(9): p. 589-601.
209. Asokan, G.V., et al., *WHO Global Priority Pathogens List: A Bibliometric Analysis of Medline-PubMed for Knowledge Mobilization to Infection Prevention and Control Practices in Bahrain.* Oman Med J, 2019. **34**(3): p. 184-193.
210. Ah, Y.-M., A.-J. Kim, and J.-Y. Lee, *Colistin resistance in Klebsiella pneumoniae.* International Journal of Antimicrobial Agents, 2014. **44**(1): p. 8-15.
211. Sun, J., et al., *Towards Understanding MCR-like Colistin Resistance.* Trends in Microbiology, 2018. **26**(9): p. 794-808.
212. Cai, Y., et al., *Colistin resistance of Acinetobacter baumannii: clinical reports, mechanisms and antimicrobial strategies.* Journal of Antimicrobial Chemotherapy, 2012. **67**(7): p. 1607-1615.
213. Butler, M.S. and D.L. Paterson, *Antibiotics in the clinical pipeline in October 2019.* The Journal of Antibiotics, 2020. **73**(6): p. 329-364.
214. Koulenti, D., et al., *Infections by multidrug-resistant Gram-negative Bacteria: What's new in our arsenal and what's in the pipeline?* International Journal of Antimicrobial Agents, 2019. **53**(3): p. 211-224.
215. Breazeale, S.D., A.A. Ribeiro, and C.R.H. Raetz, *Origin of Lipid A Species Modified with 4-Amino-4-deoxy-l-arabinose in Polymyxin-resistant Mutants of Escherichia coli: AN AMINOTRANSFERASE (ArnB) THAT GENERATES UDP-4-AMINO-4-DEOXY-l-ARABINOSE*.* Journal of Biological Chemistry, 2003. **278**(27): p. 24731-24739.

216. Gunn, J.S. and S.I. Miller, *PhoP-PhoQ activates transcription of pmrAB, encoding a two-component regulatory system involved in Salmonella typhimurium antimicrobial peptide resistance.* Journal of Bacteriology, 1996. **178**(23): p. 6857-6864.
217. Kong, W.H., et al., *Cationic Lipid-Coated Gold Nanoparticles as Efficient and Non-Cytotoxic Intracellular siRNA Delivery Vehicles.* Pharmaceutical Research, 2012. **29**(2): p. 362-374.
218. Connor, E.E., et al., *Gold Nanoparticles Are Taken Up by Human Cells but Do Not Cause Acute Cytotoxicity.* Small, 2005. **1**(3): p. 325-327.
219. Zhao, Y., et al., *Small Molecule-Capped Gold Nanoparticles as Potent Antibacterial Agents That Target Gram-Negative Bacteria.* Journal of the American Chemical Society, 2010. **132**(35): p. 12349-12356.
220. Fuller, M. and I. Köper, *Polyelectrolyte-Coated Gold Nanoparticles: The Effect of Salt and Polyelectrolyte Concentration on Colloidal Stability.* Polymers, 2018. **10**(12): p. 1336.
221. James, M., et al., *Platypus: a time-of-flight neutron reflectometer at Australia's new research reactor.* Journal of Neutron Research, 2006. **14**: p. 91-108.
222. Nelson, A.R.J. and S.W. Prescott, *refnx: neutron and X-ray reflectometry analysis in Python.* J Appl Crystallogr, 2019. **52**(Pt 1): p. 193-200.
223. Lee, C.-R., et al., *Biology of Acinetobacter baumannii: Pathogenesis, Antibiotic Resistance Mechanisms, and Prospective Treatment Options.* Frontiers in Cellular and Infection Microbiology, 2017. **7**(55).
224. Sato, Y., et al., *Multidrug-resistant Acinetobacter baumannii resists reactive oxygen species and survives in macrophages.* Scientific Reports, 2019. **9**(1): p. 17462.
225. Shrivastava, S., P. Shrivastava, and J. Ramasamy, *World health organization releases global priority list of antibiotic-resistant bacteria to guide research, discovery, and development of new antibiotics.* Journal of Medical Society, 2018. **32**(1): p. 76-77.
226. WHO. *WHO publishes list of bacteria for which new antibiotics are urgently needed*. 2017; Available from: https://www.who.int/news/item/27-02-2017-who-publishes-list-of-bacteria-for-which-new-antibiotics-are-urgently-needed.
227. Solomon, S.L. and K.B. Oliver, *Antibiotic resistance threats in the United States: stepping back from the brink.* Am Fam Physician, 2014. **89**(12): p. 938-41.
228. Chilambi, G.S., et al., *Membrane adaptation limitations in Enterococcus faecalis underlie sensitivity and the inability to develop significant resistance to conjugated oligoelectrolytes.* RSC Advances, 2018. **8**(19): p. 10284-10293.
229. Renwick, M.J., V. Simpkin, and E. Mossialos, *European Observatory Health Policy Series*, in *Targeting innovation in antibiotic drug discovery and development: The need for a One Health – One Europe – One World Framework*. 2016, European Observatory on Health Systems and Policies
© World Health Organization 2016 (acting as the host organization for, and secretariat of, the European Observatory on Health Systems and Policies). Copenhagen (Denmark).
230. Ventola, C.L., *The antibiotic resistance crisis: part 1: causes and threats.* P t, 2015. **40**(4): p. 277-83.
231. Eder, A.E., et al., *Exogenous polyunsaturated fatty acids (PUFAs) alter phospholipid composition, membrane permeability, biofilm formation and motility in Acinetobacter baumannii.* Microbiology, 2017. **163**(11): p. 1626-1636.
232. Jiang, J.-H., et al., *Identification of Novel Acinetobacter baumannii Host Fatty Acid Stress Adaptation Strategies.* mBio, 2019. **10**(1): p. e02056-18.
233. Calder, P.C., *Docosahexaenoic Acid.* Annals of Nutrition and Metabolism, 2016. **69(suppl 1)**(Suppl. 1): p. 8-21.
234. Nikaido, H., *Structure and mechanism of RND-type multidrug efflux pumps.* Adv Enzymol Relat Areas Mol Biol, 2011. **77**: p. 1-60.
235. Nikaido, H. and Y. Takatsuka, *Mechanisms of RND multidrug efflux pumps.* Biochim Biophys Acta, 2009. **1794**(5): p. 769-81.

236. Churchward, C.P., R.G. Alany, and L.A.S. Snyder, *Alternative antimicrobials: the properties of fatty acids and monoglycerides.* Crit Rev Microbiol, 2018. **44**(5): p. 561-570.
237. Chanda, W., et al., *Effectiveness of omega-3 polyunsaturated fatty acids against microbial pathogens.* J Zhejiang Univ Sci B, 2018. **19**(4): p. 253-262.
238. Sherratt, S.C.R. and R.P. Mason, *Eicosapentaenoic acid and docosahexaenoic acid have distinct membrane locations and lipid interactions as determined by X-ray diffraction.* Chem Phys Lipids, 2018. **212**: p. 73-79.
239. Thid, D., et al., *DHA-induced changes of supported lipid membrane morphology.* Langmuir, 2007. **23**(11): p. 5878-81.
240. Clifton, L.A., et al., *An Accurate In Vitro Model of the E. coli Envelope.* Angewandte Chemie International Edition, 2015. **54**(41): p. 11952-11955.
241. Vestergaard, M., T. Hamada, and M. Takagi, *Using model membranes for the study of amyloid beta:lipid interactions and neurotoxicity.* Biotechnol Bioeng, 2008. **99**(4): p. 753-63.
242. van Meer, G., D.R. Voelker, and G.W. Feigenson, *Membrane lipids: where they are and how they behave.* Nature Reviews Molecular Cell Biology, 2008. **9**: p. 112.
243. Zang, M., et al., *The Membrane Composition Defines the Spatial Organization and Function of a Major Acinetobacter baumannii Drug Efflux System.* mBio, 2021. **12**(3): p. e01070-21.

Appendix

Table A1: Full modelled NR data for 80%-tethered DPhyPC bilayer. Thickness and roughness provided in Å, SLD in 10^{-6} $Å^{-2}$ and hydration in %.

Values	Result	Error	Error (%)
Scale - D2O	0.989161	0.0045492	0.46
Background – D2O	4.50885e-07	5.56458e-08	12
Scale – CM 4.5	1.03846	0.00601411	0.58
Background – CM 4.5	4.72381e-07	3.11344e-08	6.6
Scale - H2O	0.964099	0.00737098	0.76
Background – H2O	4.86736e-07	2.06802e-08	4.3
SiO2			
Thickness	12.5212	1.263	10
SLD	3.47	Fixed	
Roughness	4.71729	0.669506	14
Hydration	0	Fixed	
Cr			
Thickness	30.8043	1.78057	5.8
SLD	3.15393	0.0384715	1.2
Roughness	7.74862	2.12631	27
Hydration	0	Fixed	
Au			
Thickness	172.581	0.639734	0.37
SLD	4.4139	0.00738839	0.17
Roughness	9.50414	0.750981	7.9
Hydration	0	Fixed	
Tethers			
Thickness	11.3813	2.40886	21
SLD	0.52012	0.032551	6.3
Roughness	2.07593	0.0934446	4.5
Hydration	0.150647	0.0348842	23
Inner HC			
Thickness	16.3024	2.11761	13
SLD	-0.022735	0.0922413	406
Roughness	8.14051	0.786753	9.7
Hydration	0.00510638	0.00534784	105
Outer HC			
Thickness	14.9139	1.45532	9.8
SLD	-0.289937	0.0580484	20
Roughness	2.82802	1.65465	59
Hydration	0.00249884	0.00379459	152
Outer HG			
Thickness	11.468	1.27714	11
SLD	1.38474	0.28313	20
Roughness	2.32892	0.370365	16
Hydration	0.720083	0.0593844	8.3
Backing			
SLD – D2O	6.36365	0.00198998	0.031
Roughness – D2O	3.97874	1.49479	38
SLD – CM 4.5	4.61632	0.00270215	0.059

Roughness – CM 4.5	5.66057	1.41836	25
SLD – H2O	-0.591184	0.00824424	1.4
Roughness – H2O	1.17144	0.930101	79

Table A2: *Full modelled NR data for 80%-tethered DPhyPC bilayer after being dehydrated and rehydrated. Thickness and roughness provided in Å, SLD in 10^{-6} $Å^{-2}$ and hydration in %.*

Values	**Result**	**Error**	**Error (%)**
Scale - D2O	0.982589	0.0102354	1.0
Background – D2O	4.02912e-07	7.23579e-08	18
Scale – CM 4.5	1.03516	0.00873879	0.84
Background – CM 4.5	3.88082e-07	6.79029e-08	17
Scale - H2O	0.974513	0.00994116	1.0
Background – H2O	4.40784e-07	5.07075e-08	12
SiO2			
Thickness	12.5212	Fixed	
SLD	3.47	Fixed	
Roughness	4.71729	Fixed	
Hydration	0	Fixed	
Cr			
Thickness	30.8043	Fixed	
SLD	3.15393	Fixed	
Roughness	7.74862	Fixed	
Hydration	0	Fixed	
Au			
Thickness	172.581	Fixed	
SLD	4.4139	Fixed	
Roughness	9.50414	Fixed	
Hydration	0	Fixed	
Tethers			
Thickness	13.3719	2.30854	17
SLD	0.541628	0.0792895	15
Roughness	2.69691	0.395948	15
Hydration	0.156429	0.0232145	15
Inner HC			
Thickness	15.257	1.98034	13
SLD	-0.0721956	0.0849514	118
Roughness	9.13769	0.860529	9.4
Hydration	0.0235508	0.0216166	92
Outer HC			
Thickness	15.9204	2.57216	16
SLD	-0.242426	0.155781	64
Roughness	5.30954	2.86923	54
Hydration	0.0116045	0.0139217	120
Outer HG			
Thickness	10.3277	1.57425	15
SLD	1.47947	0.256406	17
Roughness	2.51348	0.366539	15
Hydration	0.711471	0.0652521	9.2

Backing			
SLD – D2O	6.29171	0.0434024	0.69
Roughness – D2O	7.94212	1.3671	17
SLD – CM 4.5	4.64608	0.0222801	0.48
Roughness – CM 4.5	7.67118	1.59624	21
SLD – H2O	-0.532546	0.0454203	8.5
Roughness – H2O	2.59108	1.53188	59

Table A3: Full modelled NR data for 60%-tethered DPhyPC bilayer. Thickness and roughness provided in Å, SLD in 10^{-6} $Å^{-2}$ and hydration in %.

Values	**Result**	**Error**	**Error (%)**
Scale - D2O	0.953161	0.00386149	0.41
Background – D2O	3.13728e-07	1.67673e-07	53
Scale – CM 4.5	1.04336	0.0105821	1.01
Background – CM 4.5	2.14644e-07	1.22035e-07	57
Scale - H2O	0.960744	0.0146417	1.5
Background – H2O	4.51441e-07	4.03863e-08	8.9
SiO2			
Thickness	12.5798	1.8409	14.6
SLD	3.47	Fixed	
Roughness	3.8838	0.821237	21
Hydration	0	Fixed	
Cr			
Thickness	29.1805	2.44809	8.4
SLD	3.13275	0.0328754	1.0
Roughness	4.60531	2.11439	46
Hydration	0	Fixed	
Au			
Thickness	169.758	0.743793	0.44
SLD	4.2999	0.0143405	0.33
Roughness	5.51667	1.50972	27
Hydration	0	Fixed	
Tethers			
Thickness	22.2541	1.5844	7.1
SLD	0.64831	0.109477	17
Roughness	2.16727	0.25513	12
Hydration	0.0175829	0.0210608	120
Inner HC			
Thickness	10.2439	0.203707	2.0
SLD	-0.480724	0.0689541	14
Roughness	3.15939	3.09051	98
Hydration	0.00677166	0.00817466	121
Outer HC			
Thickness	10.4152	1.97145	19
SLD	-0.479167	0.119922	-25
Roughness	6.6648	2.67042	40
Hydration	0.00350129	0.00552539	158
Outer HG			
Thickness	8.27946	0.371156	4.5
SLD	2.87339	0.444264	15

Roughness	2.65637	0.455618	17
Hydration	0.605517	0.127041	21
Backing			
SLD – D2O	6.0615	0.00338432	0.056
Roughness – D2O	3.80298	1.09636	29
SLD – CM 4.5	4.61708	0.00256051	0.055
Roughness – CM 4.5	6.84627	1.34117	20
SLD – H2O	-0.470445	0.0512574	11
Roughness – H2O	1.54722	0.686114	44

Table A4: Full modelled NR data for 60%-tethered DPhyPC bilayer after being dehydrated and rehydrated. Thickness and roughness provided in Å, SLD in 10^{-6} $Å^{-2}$ and hydration in %.

Values	**Result**	**Error**	**Error (%)**
Scale - D2O	1.00271	0.0143198	1.4
Background – D2O	2.92533e-07	8.87489e-08	30
Scale – CM 4.5	1.03934	0.00816308	0.79
Background – CM 4.5	3.76016e-07	9.05706e-08	24
Scale - H2O	0.99718	0.0175986	1.8
Background – H2O	4.54906e-07	3.95585e-08	8.7
SiO2			
Thickness	12.5798	Fixed	
SLD	3.47	Fixed	
Roughness	3.8838	Fixed	
Hydration	0	Fixed	
Cr			
Thickness	29.1805	Fixed	
SLD	3.13275	Fixed	
Roughness	4.60531	Fixed	
Hydration	0	Fixed	
Au			
Thickness	169.758	Fixed	
SLD	4.2999	Fixed	
Roughness	5.51667	Fixed	
Hydration	0	Fixed	
Tethers			
Thickness	13.1134	2.87614	22
SLD	0.589157	0.0936609	16
Roughness	2.35969	0.230073	9.8
Hydration	0.0739159	0.0621438	84
Inner HC			
Thickness	15.6774	2.15645	14
SLD	-0.076333	0.0695893	91
Roughness	7.58023	1.48508	20
Hydration	0.00607076	0.00612684	101
Outer HC			
Thickness	15.3533	2.48274	16
SLD	-0.295852	0.118154	40
Roughness	4.50652	2.77723	61
Hydration	0.00846086	0.00886003	105

Outer HG			
Thickness	14.0366	1.96048	14
SLD	1.34147	0.204766	15
Roughness	2.47252	0.349153	14
Hydration	0.761084	0.0519971	6.8
Backing			
SLD – D2O	6.0571	0.0100624	0.17
Roughness – D2O	6.92092	2.12727	31
SLD – CM 4.5	4.56273	0.0385825	0.85
Roughness – CM 4.5	7.4149	3.28817	44
SLD – H2O	-0.559617	0.0304745	5.4
Roughness – H2O	4.45612	2.66312	60

Table A5: Full modelled NR data for 80%-tethered A. baumannii bilayer. Thickness and roughness provided in Å, SLD in 10^{-6} $Å^{-2}$ and hydration in %.

Values	**Result**	**Error**	**Error (%)**
Scale - D2O	0.950924	0.00205056	0.22
Background – D2O	1.53836e-07	8.4229e-08	55
Scale – CM 4.5	0.965068	0.00464731	0.48
Background – CM 4.5	1.75456e-07	6.30308e-08	36
Scale - H2O	1.0188	0.00574783	0.56
Background – H2O	4.8727e-07	3.38313e-08	6.9
SiO2			
Thickness	8.18745	1.5766	19
SLD	3.47	Fixed	
Roughness	8.31891	0.705187	8.5
Hydration	0	Fixed	
Cr			
Thickness	37.7283	2.06842	5.5
SLD	3.12108	0.0166551	0.53
Roughness	4.22663	0.991892	23
Hydration	0	Fixed	
Au			
Thickness	141.017	0.7949	0.56
SLD	4.40643	0.00515517	0.12
Roughness	7.82685	0.369092	4.7
Hydration	0	Fixed	
Tethers			
Thickness	11.7357	0.761117	6.5
SLD	1.41762	0.27974	20
Roughness	6.04493	0.577627	9.6
Hydration	0.0750148	0.0144775	19
Inner HC			
Thickness	13.2702	1.25114	9.4
SLD	-0.56506	0.0480128	8.5
Roughness	2.61129	0.541396	21
Hydration	0.0341629	0.0124511	36
Outer HC			
Thickness	16.8814	1.02717	6.1
SLD	-0.336994	0.0573419	17

Roughness	4.96916	2.42361	49
Hydration	0.00474774	0.0048979	103
Outer HG			
Thickness	8.5566	0.557962	6.5
SLD	1.21611	0.220407	18
Roughness	2.44092	0.460101	19
Hydration	0.74624	0.0380281	5.1
Backing			
SLD – D2O	6.25177	0.00236575	0.038
Roughness – D2O	6.53609	1.38639	21
SLD – CM 4.5	4.74999	0.0014733	0.031
Roughness – CM 4.5	9.47196	0.715346	7.6
SLD – H2O	-0.587479	0.0158208	2.7
Roughness – H2O	2.13354	1.36245	64

Table A6: Full modelled NR data for 100%-tethered S. aureus bilayer. Thickness and roughness provided in Å, SLD in 10^{-6} $Å^{-2}$ and hydration in %.

Values	**Result**	**Error**	**Error (%)**
Scale - D2O	0.950842	0.00415881	0.44
Background – D2O	4.58172e-07	7.76173e-08	17
Scale – CM 4.5	1.09879	0.00196948	0.18
Background – CM 4.5	2.47055e-07	3.29678e-07	133
Scale - H2O	0.98825	0.0070671	0.72
Background – H2O	1.3651e-06	2.76271e-07	20
SiO2			
Thickness	7.70214	3.17954	41
SLD	3.47	Fixed	
Roughness	6.469	0.611815	9.5
Hydration	0	Fixed	
Cr			
Thickness	38.193	3.95376	10
SLD	3.14203	0.0282064	0.90
Roughness	10.3648	1.54101	15
Hydration	0	Fixed	
Au			
Thickness	136.273	1.67196	1.2
SLD	4.49768	0.0023112	0.051
Roughness	8.30632	0.482204	5.8
Hydration	0	Fixed	
Tethers			
Thickness	14.3164	0.462671	3.2
SLD	1.4773	0.473575	32
Roughness	6.52998	0.822506	13
Hydration	0.0827623	0.0269418	33
Inner HC			
Thickness	15.9859	1.14553	7.2
SLD	-0.584844	0.0150543	2.6
Roughness	4.79797	0.989878	21
Hydration	0.00284111	0.00512763	180
Outer HC			

Thickness	16.982	0.790566	4.7
SLD	-0.486668	0.609679	125
Roughness	4.2469	1.83674	43
Hydration	0.00285177	0.00651447	228
Outer HG			
Thickness	8.34027	0.324019	3.9
SLD	2.24311	0.578653	26
Roughness	2.35754	0.753295	32
Hydration	0.530923	0.05982	11
Backing			
SLD – D2O	6.19102	0.00471992	0.076
Roughness – D2O	9.45228	2.84581	30
SLD – CM 4.5	4.49143	0.00170246	0.038
Roughness – CM 4.5	0.882463	0.649088	74
SLD – H2O	-0.593969	0.0119072	2.0
Roughness – H2O	0.849787	0.691468	81